From Mathematical Models to Quantum Chemistry in Cluster Science

A thesis presented in partial fulfilment of the
requirements for the degree of

Doctor of Philosophy
in
Chemistry

at
Massey University, Albany
New Zealand

Lukas Trombach

2019

Abstract

The structures and stabilities of hollow gold clusters are investigated by means of density functional theory (DFT) as topological duals of carbon fullerenes. Fullerenes can be constructed by taking a graphene sheet and wrapping it around a sphere, which requires the introduction of exactly 12 pentagons. In the dual case, a (111) face-centred cubic (fcc) gold sheet can be deformed in the same way, introducing 12 vertices of degree five, to create hollow gold nano-cages. This one-to-one relationship follows trivially from Euler's polyhedral formula and there are as many golden dual fullerene isomers as there are carbon fullerenes. Photoelectron spectra of the clusters are simulated and compared to experimental results to investigate the possibility of detecting other dual fullerene isomers. The stability of the hollow gold cages is compared to compact structures and a clear energy convergence towards the (111) fcc sheet of gold is observed.

The relationship between the Lennard-Jones (LJ) and sticky-hard-sphere (SHS) potential is investigated by means of geometry optimisations starting from the SHS clusters. It is shown that the number of non-isomorphic structures resulting from this procedure depends strongly on the exponents of the LJ potential. Not all LJ minima, that have been discovered in previous work, can be retrieved this way and the mapping from the SHS to the LJ structures is therefore non-injective and non-surjective. The number of missing structures is small and they correspond to energetically unfavourable minima on the energy landscape. The optimisations are also carried out for an extended Lennard-Jones potential derived from coupled-cluster calculations for the xenon dimer, and, although the shape of the potential is not too different from a regular (6,12)-LJ potential, the number of minima increases substantially.

Gregory-Newton clusters, which are clusters where 12 spheres surround and touch a central sphere, are obtained from the complete set of SHS clusters. All 737 structures result in an icosahedron, when optimised with a (6,12)-LJ potential. Furthermore, the contact graphs, consisting only of atoms from the outer shell of the clusters, are all edge-induced sub-graphs of the icosahedral graph. For higher LJ exponents the symmetry of the potential energy surface breaks away from the icosahedral motif towards the SHS landscape, which does not support a perfect icosahedron for energetic reasons. This symmetry breaking is mainly governed by the shape of the potential in the repulsive region, with the long-range attractive region having little influence.

Acknowledgements

With the conclusion of this thesis another chapter of my life is coming to an end, and there are many people who supported me in one way or another along my path and I would like to express my sincere gratitude to all of them.

First and foremost, I have to thank my supervisor Peter for all the support and assistance he gave me during the four years I spent as a member of his research group. The selection of research projects and the way he directed me towards the interesting questions that needed to be answered were both excellent. I would also like to thank Elke for taking on co-supervision and always helping me with any questions I had.

My time in the Schwerdtfeger group has been filled with countless great memories, all due to the people that I shared our premises with. Lukas_0, Lukas_1 and Jayson were always available for a competitive round of table tennis and helped me tremendously with all kinds of scientific questions and problems. I want to thank Lukas_0, Jayson, Paul and Morten specifically for being great office mates and for all the interesting and fruitful discussions we had. Furthermore, thanks for all the conversations about "crypto" and stock markets to Antony and for all the discussions about writing a good PhD thesis and life in general to Odile. A special thanks goes out to Vesna for keeping the group up and running in the first place.

I am very grateful for all the moral and financial support I received from my parents, my grandparents and my brother. The certainty that there was always someone who would stand by me no matter what happened contributed immensely to the way I was able to approach this degree. Although, there were around 18,000 km and probably ten time zones separating us, Susi was always ready for a phone call when I needed it, and I'm very grateful to have her as a friend. I also wish to thank Emma and Victor for helping me to stay active and for being amazing friends and climbing buddies.

And last but not least, I would like to thank Bali for making my last couple of months a little bit more special. Helping me to take my mind of all the work that was lying ahead of me made finishing this thesis just so much easier.

Contents

Abstract i

Acknowledgements iii

List of Publications vii

List of Acronyms ix

List of Figures xi

List of Tables xvii

1 Introduction 1
- 1.1 Nanotechnology . . . 1
- 1.2 Cluster Science . . . 2
- 1.3 The Potential Energy Surface . . . 4
- 1.4 Outline . . . 6

I Theoretical Background 9

2 Graph Theory 11
- 2.1 The Definition of a Graph . . . 11
- 2.2 Planar Graphs . . . 14
- 2.3 Graph Matching . . . 17

3 Quantum Chemistry 19
- 3.1 The Schrödinger Equation . . . 19
- 3.2 The Born-Oppenheimer Approximation . . . 20
- 3.3 The Hartree-Fock Approximation . . . 21
- 3.4 Density Functional Theory . . . 24
- 3.5 Periodic Boundary Conditions . . . 29
- 3.6 Basis Sets . . . 30
- 3.7 Description of Core Electrons . . . 32

4 Geometry Optimisation 35
- 4.1 General Considerations about Minima . . . 35
- 4.2 Properties of Optimisation Algorithms . . . 37
- 4.3 Quadratic Models . . . 38
- 4.4 Implementation for Two-Body Interaction Potentials . . . 43
- 4.5 Global Optimisation . . . 45

5 Interaction Potentials **51**
5.1 Thermodynamic Considerations 51
5.2 Lennard-Jones Potential 54
5.3 Sticky-Hard-Sphere Potential 57

II Methods **61**

6 Program Package SPHERES **63**
6.1 Structural Optimisation and Analysis 63
6.2 Graph-Theoretical Analysis 67
6.3 Additional Functionalities 68
6.4 Implementations in Detail 69

III Results **73**

7 Golden Dual Fullerenes **75**
7.1 Introduction 75
7.2 Topological Aspects 76
7.3 Computational Details 80
7.4 Structure and Stability 81
7.5 Convergence Towards the Infinite Structure 89
7.6 Simulation of Photoelectron Spectra 90
7.7 Conclusion 92

8 From Sticky-Hard-Sphere to Lennard-Jones-Type Clusters **95**
8.1 Introduction 95
8.2 Computational Details 98
8.3 Exploring the Limits of Lennard-Jones 99
8.4 (6,12)-Lennard-Jones Clusters from Basin-Hopping 105
8.5 Conclusion 108

9 The Gregory-Newton Clusters **111**
9.1 Introduction 111
9.2 Computational Details 113
9.3 The Gregory-Newton Problem for Soft Potentials 113
9.4 Rigid Gregory-Newton Clusters and Corresponding Graphs . 115
9.5 Symmetry-Broken Lennard-Jones Gregory-Newton Clusters . 119
9.6 Adding a 14th Sphere 122
9.7 Conclusion 125

IV Appendix **127**

A List of Gregory-Newton Contact Graphs **129**

Bibliography **149**

List of Publications

The results presented in this thesis have been released previously in the following publications:

[1] L. Trombach, S. Rampino, L.-S. Wang, and P. Schwerdtfeger, "Hollow Gold Cages and Their Topological Relationship to Dual Fullerenes", Chemistry–A European Journal **22**, 8823 (2016).

[2] L. Trombach, R. S. Hoy, D. J. Wales, and P. Schwerdtfeger, "From sticky-hard-sphere to Lennard-Jones-type clusters", Physical Review E **97**, 043309 (2018).

[3] L. Trombach and P. Schwerdtfeger, "Gregory-Newton problem for kissing sticky spheres", Physical Review E **98**, 033311 (2018).

List of Acronyms

AFM	atomic force microscope
BFGS	Broyden-Fletcher-Goldfarb-Shanno
COS	center-to-outer sphere
DFP	Davidon-Fletcher-Powell
DFT	density functional theory
ECP	effective core potential
EDM	Euclidean distance matrix
eLJ	extended Lennard-Jones
fcc	face-centered cubic
FR	Fletcher-Reeves
GDF	golden dual fullerene
GEA	gradient expansion approximation
GGA	generalised gradient approximation
GN	Gregory-Newton
GNC	Gregory-Newton cluster
GTO	Gaussian-type orbital
hcp	hexagonal-closed packed
LCAO	linear combination of atomic orbitals
LDA	local density approximation
LJ	Lennard-Jones
MDS	minimum distance sphere
OMP	Open Multi-Processing

PAW	projector-augmented wave
PES	potential energy surface
RMS	root mean square
SCF	self-consistent field
STM	scanning tunneling microscope
SHS	sticky-hard-sphere
STO	Slater-type orbital

List of Figures

1.1 (a) STM image of a clean gold (100) surface showing atomic resolution. The ridges are a result of surface reconstructions. The image is part of the public domain. (b) STM image of Xenon atoms arranged on a nickel (110) surface in a pattern resembling the IBM logo. Reprinted by permission from Springer Nature Customer Service Centre GmbH: Springer Nature, "Positioning Single Atoms with a Scanning Tunnelling Microscope",[3] ©1990. 2

1.2 Buckminsterfullerene C_{60}. 3

1.3 (a) Example of a two-dimensional potential energy landscape and (b) the same hypersurface represented with contour lines. Red lines mark the boundaries of the basins of attraction around the minima (blue dots) and transition states (green dots). Reprinted figures with permission from the American Physical Society: "Power-Law Distributions for the Areas of the Basins of Attraction on a Potential Energy Landscape",[18] ©2007 by the American Physical Society. 5

2.1 The Königsberg Bridge Problem. (a) Schematic representation of the bridge layout of Königsberg with the river Pregel (blue), landmasses (green) and bridges (red), and (b) respective graph drawing. 11

2.2 Example of one possible (a) trail, (b) walk and (c) path over the bridges of Königsberg. Traversal is in direction of the arrows. Red edges indicate not-traversed bridges. 13

2.3 Example of a disconnected graph with two components. The vertex B has no path to any of the other vertices, therefore the graph is disconnected. Adding one edge from B to any other vertex would make this graph connected. As a result from being disconnected the graph consists of two components (dashed lines; one contains only the vertex B and the other one contains the other three vertices. 14

2.4 Stretching and flattening of a icosahedron surface with one removed face. (a) Icosahedron with on removed face in the centre, (b) stretching of the hole in the surface, (c) fully flattened surface shows a plane graph. 15

2.5 (a) Graph of a cube, (b) triangulation of the internal regions of the same graph, (c) removal of one face and edge. 16

4.1 Hypersurface transformation in the basin-hopping method. The original hypersurface (solid line) is mapped onto the transformed surface (dashed line) by a geometry optimisation. 48

5.1 Examples of Lennard-Jones potential curves for the (6,12)-LJ potential with different values for ε and r_e. 56

6.1 Schematic representation of the optimisation, analysis and matching procedure. Red circles: program input or output, blue ellipses: program executions. 64

7.1 (a) *p3m1*-G graphene and (b) its dual sheet *p3m1*-T adopted in the (111) surface of fcc gold. 76
7.2 (a) $D_{6\mathrm{d}}-\mathrm{C}_{144}$ zig-zag fullerene nanotube and (b) its dual $D_{6\mathrm{d}}-\mathrm{Au}_{74}$. 77
7.3 (a) Schlegel diagram of C_{60} (red vertices) and its dual (blue vertices and dashed edges), (b) the C_{60} structure, and (c) its dual Au_{32} structure. 78
7.4 Mackay icosahedron with 7 shells and 1415 atoms. The outer icosahedral shell is the dual of the halma transform $GC_{7,0}[I_{\mathrm{h}}-\mathrm{C}_{20}]=I_{\mathrm{h}}-\mathrm{C}_{980}$. 79
7.5 Structures of anionic gold clusters (Au_{12}^- to Au_{19}^-). 82
7.6 Structures of anionic gold clusters (Au_{20}^-). 83
7.7 Overview of PBE-D3 optimisation results for the dual fullerene structures. Green: dual fullerene structure, orange: hollow structure, red: non-hollow structure. 87
7.8 Relative energies for the investigated dual fullerene clusters. Energy differences compared to the most stable compact cluster (per atom) are given in eV. 88
7.9 Cohesive energies for (a) the compact gold clusters with cluster size N and convergence toward the bulk fcc structure and (b) for the hollow gold clusters with cluster size N and convergence toward the (111) gold sheet. 90
7.10 Comparison of simulated photoelectron spectra of the three dual fullerene isomers of Au_{17}^- with (2c) and without spin-orbit coupling. 91
7.11 Simulated photoelectron spectra for the negatively charged hollow gold clusters (shifted to the experimental threshold energy). (a) The two possible dual fullerene isomers of Au_{16}^-. The green curve shows a combination of the D_2 and T_{d} spectra with a ratio of 1:1.; (b) The three possible dual fullerene isomers of Au_{17}^-; (c) The six possible dual fullerene isomers of Au_{18}^- (shifted to the experimental threshold energy). 92
7.12 Simulated photoelectron spectra for isomer 32:1812 of Au_{32}^-. 93

8.1 Lennard-Jones potentials for different exponents (m, n) with fixed $n = 2m$. As the exponents grow larger, the well of attraction becomes narrower and its shape approaches the SHS potential. The dashed line shows the extended Lennard-Jones potential for the xenon dimer.[107] 97

8.2 Convergence of the number of distinct LJ local minima $|\mathcal{M}_{\mathrm{SHS}\to\mathrm{LJ}}|$ obtained through geometry optimisations starting from the non-isomorphic SHS structures with increasing LJ exponent n. Permutation-inversion isomers and enantiomers are not distinguished. The dashed line gives the exact SHS limit $|\mathcal{M}_{\mathrm{SHS}}|$. Top panel: $m = n/2$. Bottom panel: fixed $m = 6$. 101

8.3 Growth behaviour of $|\mathcal{M}(N)|$ of SHS and (6,12)-LJ clusters and corresponding asymptotic exponential rise rate parameter α for $N \geq 12$ as defined in equation (8.7). The intercepts $\ln|\mathcal{M}(N = 0)|$ are -17.19 and -6.94 for the SHS and (6,12)-LJ cases, respectively. 102

8.4 Convergence behaviour of the asymptotic exponential rise rate parameter α (equation (8.7)) towards the SHS limit with respect to the LJ exponent n. The inlet shows the ratio of the two quantities $\alpha(|\mathcal{M}_{\mathrm{SHS}\to(n/2,n)-\mathrm{LJ}}(N)|)/\alpha(|\mathcal{M}_{\mathrm{SHS}\to(6,n)-\mathrm{LJ}}(N)|)$. 103

8.5 Histogram of the energies (bin size $\Delta E = 0.1$) of minima $\mathcal{M}_{\mathrm{SHS}\to(n/2,n)-\mathrm{LJ}}(N)$ for $N = 13$ and different exponents n up to the SHS limit. For better visibility, the height of the bars are set to $\Delta|\mathcal{M}|/|\mathcal{M}|$ in the interval $\Delta(E/\epsilon)$. The inlet shows the same data in logarithmic scale. 104

8.6 Histograms of the difference between the longest and shortest bond distances $d_\Delta = d_{\mathrm{max}} - d_{\mathrm{min}}$ for the complete set of distinct LJ minima $\mathcal{M}_{\mathrm{LJ}}(N)$ for $N = \{11, 12, 13\}$. Orange bars give the number of distinct structures not contained in $\mathcal{M}_{\mathrm{LJ}}$ as obtained from the basin-hopping algorithm. 107

8.7 Graphical representations of the structures that are starting new seeds, but are not contained in $\mathcal{M}_{\mathrm{SHS}\to\mathrm{LJ}}$. See table 8.2 and text for more details. 108

9.1 Left: Symmetric realization of $N_k(3) = 12$ for unit hard spheres (icosahedral symmetry, I_h). The minimum distance between the outer spheres is $r = \sin^{-1}\left(\frac{2\pi}{5}\right) = 1.05146222\ldots$, hence they do not touch. Right: The corresponding icosahedral graph. Numbering refers to the respective node index. 112

9.2 Relation of LJ exponents m and n to the difference of largest and smallest COS distances. A value of zero would imply that all surrounding spheres are touching the center sphere. 114

9.3 GN hcp (triangular orthobicupola) and fcc (cuboctahedron) graphs (central sphere removed) as sub-graphs of the icosahedral graph and corresponding rigid GNCs. Red lines indicate the edges that were removed to create the GN graph. The ordinal numbers ω refer to Table A.1 in the appendix. 116
9.4 Illustration of one zig-zag path (light blue spheres) that needs to be deformed such that it aligns with the triangular plane (shown in grey) of the fcc crystal. 117
9.5 Representative GN graphs (central sphere removed) with $|F_3| = 10$ as sub-graphs of the icosahedral graph and corresponding rigid GNCs. The icosahedral motif in the 3D embedding is clearly visible. Red lines indicate the edges that were removed to create the GN graph. The ordinal numbers ω refer to Table A.1 in the appendix. 118
9.6 GN graph (central sphere removed) as sub-graphs of the icosahedral graph and corresponding GN Johnson-like solid (with edges removed). Red lines indicate the edges that were removed from the icosahedral graph to create the GN graph. The ordinal number ω refers to Table A.1 in the appendix. 119
9.7 Number of unique structures resulting from an optimisation with a (a, b)-LJ potential. The lowest contour line shows the point where more than one structure results from the optimisation and the distance between contour lines is 1. 120
9.8 Different types of energy landscapes arising from combinations of the (a, b)-LJ exponents. (1) One single (icosahedral) minimum, (2) more than one minimum with the icosahedron as the global minimum, (3) more than one minimum with the icosahedron becoming a local (and not global) minimum, (4) the icosahedral motif disappears completely. The unshaded small area in the bottom right corner corresponds to $a > b$, which is excluded. The resolution for a is 1.0 and for b 0.25. 121
9.9 Comparison of different shapes of LJ potentials at the phase transition lines shown in figure 9.8 with the traditional (6,12)-LJ potential (black solid line). Dashed lines refer to potentials with low a values (left side of figure 9.8), while solid lines refer to potentials with high a values (right side of figure 9.8). 122
9.10 Hard-sphere radii σ in reduced units for the (a, b)-LJ potentials on the transition lines shown in figure 9.8. 123
9.11 Graphical representations of SHS packings with $N = 14$, where a center sphere is maximally contacting. The orange sphere in each cluster is the 14th outer sphere, not able to touch the center sphere (in black). (a) distorted elongated pentagonal bipyramid (Johnson solid); (b) distorted icosahedron; (c) hcp capped on a square; (d) hcp capped on a triangle. 124

9.12 Frequency of distances from the cluster center to the most distant sphere for all Gregory-Newton-like clusters with $N = 14$ contained in the structures from Holmes-Cerfon.[114] The width of the bars is $0.01\ r_e$. 125

List of Tables

7.1 Topological parameters for the neutral gold clusters. Number of gold atoms and isomer numbers of the corresponding fullerene in canonical order of the pentagon spiral indices,[181] ideal and actual point group symmetry, energy differences ΔE_g to the most stable neutral cluster of same size and binding energy per atom $\Delta E_n = [E(\mathrm{Au}_n) - nE(\mathrm{Au})]/n$ (in eV), shortest and largest bond distance (in Å), pentagon index (PI) N_p, and distortion parameter D (in %) for the initial force-field optimised fullerene structure (F) and the GDF. 85

7.2 Topological parameters for the anionic gold clusters. Number of gold atoms and isomer numbers of the fullerene in canonical order of the pentagon spiral indices,[181] ideal and actual point group symmetry, energy differences ΔE_g to the most stable anionic cluster of same size and binding energy per atom $\Delta E_n = [E(\mathrm{Au}_n) - (n-1)E(\mathrm{Au}) - E(\mathrm{Au}^-)]/n$ (in eV), shortest and largest bond distance (in Å), and distortion parameter D (in %) for the GDF. 86

7.3 Binding energy per atom (in eV) for investigated neutral and anionic compact cluster compounds. For the definition of the binding energy see tables 7.1 and 7.2, and for the definition of the isomers 1 and 10 for Au_{32} see Jalbout et al.[208] 89

8.1 Number of distinct local minima $|\mathcal{M}_{\mathrm{SHS}}|$ for cluster size N (from references [114–116]) and contact number N_c from the exact enumeration, compared to the number of different structures obtained from a geometry optimisation starting from the set $\mathcal{M}_{\mathrm{SHS}}(N, N_c)$ for a (6,12)-LJ potential. The overall number of unique minima $|\mathcal{M}_{\mathrm{SHS}\to\mathrm{LJ}}| = \sum_{N_c} |\mathcal{M}_{\mathrm{SHS}\to\mathrm{LJ}}(N_c)| -$ (# of duplicate structures) is shown in the following column. This result can be compared to the number of unique minima found using the basin-hopping method ($|\mathcal{M}_{\mathrm{LJ}}|$). The difference $\Delta\mathcal{M} = |\mathcal{M}_{\mathrm{LJ}}| - |\mathcal{M}_{\mathrm{SHS}\to\mathrm{LJ}}|$ is also listed. 100

8.2 Number of missing structures after optimisation belonging to the same "seed" (figure 8.7). $N = 8$ is excluded because all LJ minima were found starting from the SHS model. 106

8.3 Range $[E_0 = 0, E_{\max}]$ of the energy spectrum of all LJ minima, position of the second lowest minimum structure E_1 and position of the first unmatched (UM) structure E_0^{UM} relative to the respective global minimum (in reduced units). 106

A.1 List of all GN polyhedral graphs. The ordinal numbers ω in the first column can be used to identify the individual polyhedral graphs. $|E|$ is the number of edges, and the pairs of numbers refer to edges deleted incident vertices (k, l) as defined in the icosahedral graph as shown in figure 9.1 (page 112). Note that $|E| + |\{(k, l)\}| = 30$. . 129

A.2 GN polyhedron grouped by vertex and face degrees. $|N_n|$ is the number of vertices of degree n, $|F_n|$ the number of n-gonal faces. The ordinal numbers ω in the last column identify the polyhedral graphs shown in table A.1. 144

1 Introduction

1.1 Nanotechnology

Not many scientists can claim to have envisioned an entirely new field of physics, but it is not an overstatement to say that the field of *nanotechnology* was developed in large parts due to one of the most brilliant physicists of the 20th century, Richard Feynman. In his talk "There's Plenty of Room at the Bottom—An invitation to enter a new field of physics"[1] he challenges scientists to construct devices and compounds that only consist of a few tens or hundreds of atoms. Such objects usually turn out to be a few nanometres (10^{-9} m) in diameter, giving rise to the field's name. It is astounding to read through the transcript of Feynman's talk from today's perspective, as it is filled with ideas that have become a reality now. For example, he devises the miniaturisation of the computer and even mentions the concept of a facial recognition system. One of the reasons Feynman gives for the usefulness of nanoscience is cost effectiveness. Scaling everything down in size decreases the amount of materials needed drastically. As a side effect one ends up with much smaller and potentially more powerful devices and less waste.

Feynman noted that in order to effectively use nano-scale devices one needs to be able to investigate these small structures down to the atomic level, something that was not possible with the electron microscopy methods available at the time. This became a practical reality with the invention of the scanning tunneling microscope (STM) in 1981,[2] which secured its inventors the Nobel prize in 1986. Figure 1.1a shows an image produced with such a microscope. One problem with STM imaging is that it only works on conductive surfaces. However, this was resolved with the introduction of the atomic force microscope (AFM), which does not rely on a tunnelling current to produce atomic resolution.[4] The technology was perfected to such a degree that it became possible to move individual atoms and arrange them in almost any pattern imaginable (figure 1.1b).[3]

In the last part of his talk, Feynman speaks about how "atoms on a small scale behave like nothing on a large scale, for they satisfy the laws of quantum mechanics". This property has found application in so-called nano-particles, which refers to molecules or chemical compounds in general with the size of a few nanometres. Belonging to this group are for example the *Buckminsterfullerenes* (or short fullerenes) discovered by Kroto[5] or carbon nano-tubes,[6] and their discovery helped fuelling the push for nanotechnology even further.

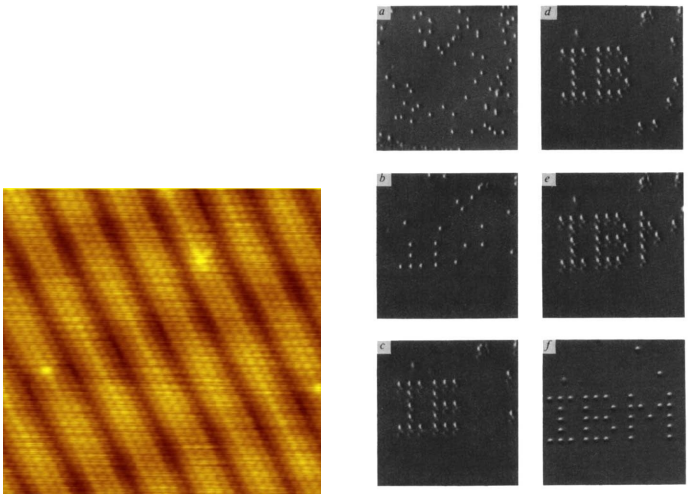

(a) (b)

Figure 1.1 (a) STM image of a clean gold (100) surface showing atomic resolution. The ridges are a result of surface reconstructions. The image is part of the public domain. (b) STM image of Xenon atoms arranged on a nickel (110) surface in a pattern resembling the IBM logo. Reprinted by permission from Springer Nature Customer Service Centre GmbH: Springer Nature, "Positioning Single Atoms with a Scanning Tunnelling Microscope",[3] ©1990.

It was however not until the beginning of the 21st century, that nanotechnology gained traction by securing public funding, e.g. from the National Nanotechnology Initiative, a U.S. American federal government program. This increase in research funding gave rise to many interesting scientific projects like the "Nanocar"[7] or Graphene transistors.[8] Today, the technology is present in many consumer products with over 800 goods reported to contain nanotechnology.[9]

1.2 Cluster Science

A term that is often used for chemical compounds in nanotechnology is *cluster*, but the definition of this term is still debated. Originally, it was proposed as "an appropriate one [term] for a finite group of metal atoms which are held together mainly, or at least to a significant extent, by bonds directly between the metal atoms, even though some non-metal atoms may also be intimately associated with the cluster".[10] However, this definition limits itself only to the fraction of metal atoms in the periodic table and the term is not necessarily used in this form today. The most accurate definition of a cluster is perhaps given through size, as almost any chemical compound with a finite

number of atoms of $2–10^n$ ($n \lessapprox 7$) atoms is referred to as a cluster.[a][11,12] Therefore, clusters are structures, that are of intermediate size, bridging the gap between small molecules and bulk solids, and they appear naturally when discussing nucleation phenomena and nano-particles.

Clusters can be divided into several groups that are characterised by the type of atoms comprising the cluster and therefore its electronic bonding situation. For example, molecular clusters, which, due to their closed electronic shells, mainly interact inter-molecularly via weak van-der-Waals forces. However, the intra-molecular interactions are usually of covalent nature. Such clusters are found for simple molecules, such as water,[13] ammonia[14] or carbon dioxide.[15] Without these attractive intermolecular interactions there would not be a condensed phase. In contrast, semi-conductor clusters are bound much more strongly by covalent interactions. Their name stems from the type of atoms that make up the cluster as they are semi-conductors in the solid state. Most famously, this group includes the already mentioned carbon fullerenes,[5] but also other semi-conductors like silicon[16] and germanium.[17] If a cluster is not monoatomic and the difference in the electronegativity of the atoms is large enough, the covalent bonding situation can change to ionic.

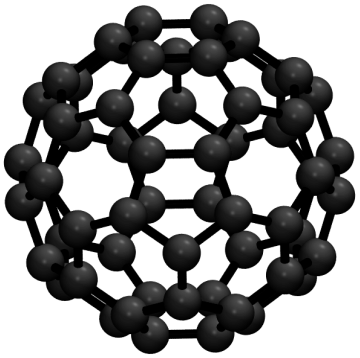

Figure 1.2 Buckminsterfullerene C_{60}.

In this thesis, two types of clusters are considered, monoatomic metal and rare gas clusters. The bonding situation in metal clusters is particularly interesting, because of the high degree of delocalisation and non-directional bonding. To describe this situation, several bonding models have been developed. The most simple one is perhaps the *liquid drop model* which approximates the metal cluster as a uniform conducting sphere, i.e. it is a classical electrostatic model. The liquid drop model does not give rise to an electronic structure,

[a] It should be noted that very large organic compounds like peptides are usually not considered clusters, and should be exempt from this definition.

which is resolved in the *spherical jellium model*. In this model the cluster is modelled as a uniform, positively charged sphere filled with an electron gas, which is solved using the *Schrödinger equation*. This gives rise to quantised electron energy levels and therefore an electronic shell structure. For metal clusters of not too many atoms it is also possible to use accurate quantum chemical methods, which will be introduced in chapter 3.

Rare gas clusters can form at very low temperatures, when the average kinetic energy of the rare gas atoms is smaller than the weak dispersive forces between them. The reason they interact so weakly is because of their closed shell electronic structures, allowing for neither covalent nor ionic bonding. As dispersive interactions are a correlation effect of the electrons, it is difficult to describe them accurately with quantum chemical methods. However, the interaction can be approximated by simple models like, for example, the London formula.

$$V_{\text{disp}} = -\frac{C_6}{r^6}, \quad C_6 = \frac{3\alpha^2 I}{4\left(4\pi\varepsilon_0\right)^2} \tag{1.1}$$

Here, I is the ionisation potential and α is the atomic polarisability. In combination with a term describing the repulsive contribution to the energy, the Lennard-Jones potential can be derived, which agrees well with structural and energetic predictions for rare gas clusters. The Lennard-Jones potential will be explained in more detail in chapter 5.

1.3 The Potential Energy Surface

A question that naturally arises when studying clusters bound by a certain potential is "how many stable structures exist for a given number of atoms N", and related to this "what is the most stable structure". For this, it is useful to investigate this problem from a mathematical point of view. If the movement of the atomic nuclei is decoupled from the electronic movement (Born-Oppenheimer approximation, section 3.2), the nuclei can be said to move on a potential energy hypersurface. This potential energy surface (PES) is a multi-dimensional function of all $3N$ atomic coordinates and it maps each point of configuration space to an energy value depending on the chosen potential. A stable structure on this hypersurface corresponds to a local minimum, with the most stable structure being represented by the global minimum. Thus, the question of how many stable structures there are is equivalent to the question of how many local minima can be supported by the multi-dimensional potential energy surface. An example for such a hypersurface is shown in figure 1.3a. The distribution of the minima on the hypersurface can be investigated by dividing the configuration space into basins of attraction as shown in figure 1.3b. A basin of attraction marks an area (or hyper-area for multi-dimensional PESs) in which the enveloped minimum (blue dots) can be

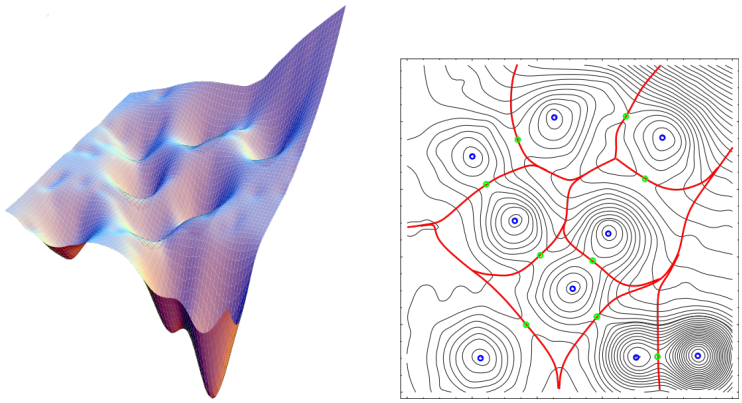

(a) (b)

Figure 1.3 (a) Example of a two-dimensional potential energy landscape and (b) the same hypersurface represented with contour lines. Red lines mark the boundaries of the basins of attraction around the minima (blue dots) and transition states (green dots). Reprinted figures with permission from the American Physical Society: "Power-Law Distributions for the Areas of the Basins of Attraction on a Potential Energy Landscape",[18] ©2007 by the American Physical Society.

reached from any point of configuration within the basin of attraction by following a steepest-descent path. These basins of attraction therefore tile the energy landscape, and it was found that this tiling is very similar to that of Apollonian packings.[18] The results also suggested that this is a universal feature of PESs, independent of the underlying potential. Furthermore, the area of the basins seems to correlate with the depth of the corresponding minimum, which makes finding the global minimum on a PES a little bit easier as it should correspond to the largest basin of attraction by area.

The question of stable structures can also be tackled from a different point of view, namely that of graph theory. Under the assumption that the atoms in a cluster are connected, the question becomes "how many non-isomorphic connected graphs exist for a specific number of vertices N". This problem is also known as the Graph isomorphism problem and no analytic solution is known. However, it can be attempted to derive upper and lower bounds within which the solution must lie. As graphs can be represented by adjacency matrices (chapter 2.1), the maximum number of such matrices can be used as a loose upper bound, i.e. $2^{N(N-1)/2} = \mathcal{O}\left(\exp\left\{N^2\right\}\right)$ different matrices exist.[19] Some observations suggest[20] that the growth is exponential, to be precise asymptotically exponential.[21,22]

Another interesting question with special importance for chemistry is the

number of contacts or bonds a cluster can form. This question is fundamentally linked to the Gregory-Newton problem, which asks "how many spheres can be arranged around a central sphere of the same size such that they all touch the central sphere". As proven by Schütte et al.[23] there can be no more than 12 spheres satisfying these conditions simultaneously.

1.4 Outline

In this thesis, three projects, in which clusters are investigated with both mathematical and physical models, will be presented.

In the first project (chapter 7), a special type of metal cluster is investigated. The gold clusters are hollow triangulations of spheres and can therefore be created by wrapping a cut-out from a (111) face-centred cubic sheet of gold around a sphere. Graph-theoretically, they are related to fullerenes as they represent their geometric duals. The structures and energies of the clusters are investigated with quantum mechanical methods and their growth behaviour is examined. Furthermore, photoelectron spectra are simulated and compared to previous experimental results.

The second project (chapter 8) is concerned with the investigation of a relation between two interaction potentials employed in cluster science. The first one is the sticky-hard-sphere (SHS) potential, which is not continuous, thus the stable clusters have to be searched by means of graph theoretical methods through the adjacency relation. The form of this potential represents the mathematical limit of the Lennard-Jones (LJ) potential with respect to the exponents approaching infinity. Starting from the structures obtained by the sticky hard sphere potential geometry optimisations are carried out with LJ potentials with growing exponents and investigated with respect to the convergence of the total number of unique structures towards the SHS limit and their asymptotic exponential growth behaviour.

In the last project (chapter 9), the special case of the Gregory-Newton clusters is revisited. First, the question is posed if very soft (small exponents) LJ potentials allow a 13th sphere to pack with equal distance around a central sphere. The set of SHS clusters is again used as a starting point for the next part. It is searched for Gregory-Newton type clusters, which are then analysed by graph theoretical means. The aim was to understand if the graphs spanned by the 12 surrounding spheres are sub-graphs of the icosahedral graph. The reason for this investigation is linked to the fact that under the conditions of the sticky hard sphere potential icosahedral symmetry cannot be realised. However, this is known to be a very stable structural motif for LJ systems. Therefore, the point at which the symmetry of the PES breaks and the icosahedron is not supported by the PES is investigated. Finally, the set of SHS clusters was analysed for Gregory-Newton clusters where one sphere enters the second coordination shell. Here, the focus was put on finding the

shortest distance this sphere can have to the central sphere.

Part I

Theoretical Background

2 Graph Theory

Graph theory is used intensively in this thesis, therefore a small introduction to this field is provided. Graph theory is a powerful mathematical tool to describe relations between pairs of objects. Its biggest advantage is the broad range of applicability in fields like computer science, biology, social sciences and of course physics and chemistry. In the following sections the focus will be put on introducing graph theory in general and demonstrating its usefulness in the scope of this thesis. If not mentioned otherwise the chapter is mainly based on standard books on graph theory by West[24] and Balakrishnan.[25]

2.1 The Definition of a Graph

The foundations for graph theory were laid out by Euler in his famous solution to the Königsberg Bridge Problem.[26] The problem at hand was concerned with a specific bridge layout that connected the island Kneiphopf with the rest of the mainlands of the city of Königsberg via seven bridges. The

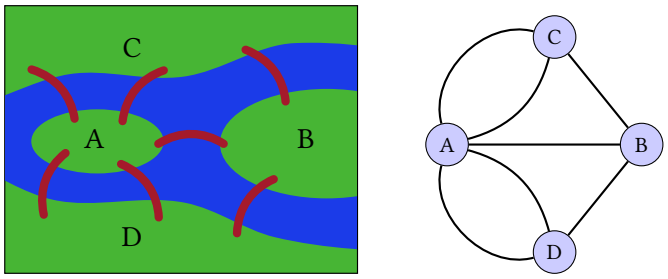

(a) (b)

Figure 2.1 The Königsberg Bridge Problem. (a) Schematic representation of the bridge layout of Königsberg with the river Pregel (blue), landmasses (green) and bridges (red), and (b) respective graph drawing.

bridge layout is depicted schematically in figure 2.1a. Is it possible for a citizen of Königsberg to leave home, cross each bridge exactly once and return? The answer is no and it was proven by Euler using a reduction of the problem as shown in figure 2.1b. Landmasses are reduced to circles and their connections via bridges is shown as lines between them. This simplification makes it easy to realise why the answer to the formerly posed question is no. It is

clear that each landmass would need to be connected by an even number of bridges for the desired traversal to exist.

Mathematically, a *graph* G is a triple that contains a *vertex set* $N(G)$, an *edge set* $E(G)$, and a relation that associates two vertices (not necessarily distinct) with each edge, i.e. it connects pairs of vertices via their endpoints. Edges can form a *loop* by having both endpoints at the same vertex and multiple edges can connect the same vertices. However, *simple graphs* do not contain loops or multiple edges and are more important for most practical applications. A simple graph can now be defined by a set of unordered pairs of vertices by defining each edge as $e = uv$ or $e = vu$ with u and v being the endpoints (or vertices) of the edges. Then, neighbouring or adjacent vertices are those that share an edge.

Graphs are often just represented as a graph drawing such as figure 2.1b, however, sometimes it can be useful to introduce a matrix representation. A simple graph G with vertex set $N(G) = \{v_1, v_2, \ldots, v_n\}$ and edge set $E(G) = \{e_1, e_2, \ldots, e_m\}$ can be defined by writing an *adjacency matrix* $\mathbf{A}$ that encodes the edge-connectivity of the vertex set, i.e. $\mathbf{A}$ is a $n \times n$ matrix where each matrix element A_{ij} represents the number of edges that connect v_i and v_j. For the Königsberg Bridge problem one possible adjacency matrix that corresponds to ordering the vertices alphabetically by their label is:

$$\mathbf{A} = \begin{pmatrix} 0 & 1 & 2 & 2 \\ 1 & 0 & 1 & 1 \\ 2 & 1 & 0 & 0 \\ 2 & 1 & 0 & 0 \end{pmatrix}. \tag{2.1}$$

An adjacency matrix is always symmetric and it can be used to easily determine the *vertex degree*, that is the number of edges connected to a particular vertex, by calculating the sum over all entries in the corresponding row or column.

Alternatively, the *incidence matrix* $\mathbf{M}$ is an $n \times m$ matrix where each matrix element M_{ij} is either 1 or 0 depending on whether v_i is an endpoint of e_j. If the matrix element M_{ij} is 1 the vertex v_i and edge e_j are incident.

The labelling of the vertices in figure 2.1b is arbitrary and so is the ordering of the rows and columns in the adjacency matrix. It is clear that a different ordering still describes the same graph object and should therefore have no influence on the properties of the graph. Permutation of the vertex labelling for a given simple graph G that turns the vertex set $N(G)$ into the vertex set $N(H)$ is called a *bijection*. If such a bijection exists the graphs G and H are *isomorphic* to each other. This property is important for the discussion of a specific type of cluster later on in this thesis (chapter 5.3.1).

If it is possible to order the vertices of a simple graph in such a way that only two consecutively listed vertices are adjacent, the graph can be called a *path*. An extension of this concept is the *cycle*, that requires an equal number

of vertices and edges so that the graph can be drawn as a circle of sequentially listed vertices. Consequently, removing an edge from a cycle always yields a path. In many applications (e.g. road networks) it is not necessary for the whole graph to represent a path or a cycle, but it is only important whether the graph contains a path or a cycle. If the graph G contains the graph H, H is called a sub-graph of G. This requires the vertex set of H to be contained in $N(G)$ ($N(H) \subseteq N(G)$) as well as the edge set $E(H)$ ($E(H) \subseteq E(G)$) as well as the assignment of the endpoints to be the same.

The Königsberg Bridge Problem is not only concerned with the nature of the bridging network, but more so with how to traverse over it. In graph theoretical terms the desired solution is called a closed trail, which is a special case of a walk, where no edge can be repeated (i.e. no bridge can be crossed twice) and the endpoints have to be the same vertex.[a] A walk describes a way to traverse over a graph by defining a list of vertices and edges $v_0, e_1, v_1, \ldots, e_k, v_k$ where the endpoints for each edge e_i have to be v_{i-1} and v_i ($1 \leq i \leq k$). One possible trail (excluding one bridge) is shown in figure 2.2a. For simple graphs

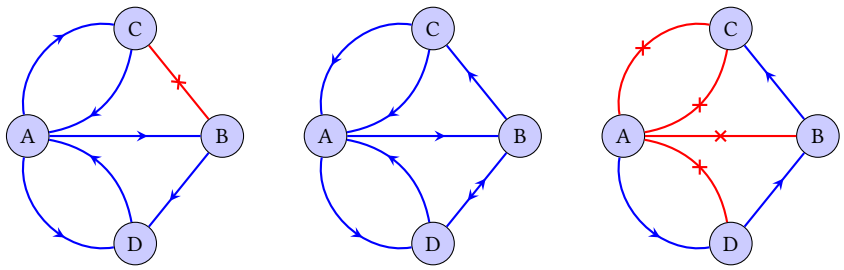

(a) A,D-trail **(b)** C,A-walk **(c)** A,C-path

Figure 2.2 Example of one possible (a) trail, (b) walk and (c) path over the bridges of Königsberg. Traversal is in direction of the arrows. Red edges indicate not-traversed bridges.

walks and trails can be specified by listing only vertices, as there can only be one incoming and one outgoing edge per vertex and no loops. A short hand notation for such a trail or walk can be given by stating its endpoints, e.g. A,D-trail, however there is usually more than one way this trail could be laid out. While trails don't allow for repeated traversal of one edge, paths require all vertex traversals to be distinct.

The definition of a path can also be used to define whether a graph is *connected*. In simple terms a graph is connected if there is a path leading from each vertex to each other one, hence, for all $u, v \in N(G)$ there must be a u, v-path for G to be connected. An example of a disconnected graph is shown in figure 2.3. The maximally connected sub-graphs of a graph are called its

[a] A graph that contains such a closed tail traversing all edges is also called Eulerian in honour of of Euler's significant contribution to solve this long-standing problem.

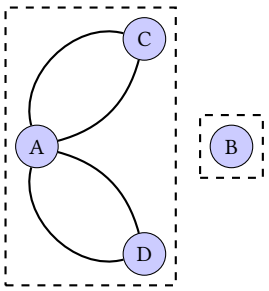

Figure 2.3 Example of a disconnected graph with two components. The vertex B has no path to any of the other vertices, therefore the graph is disconnected. Adding one edge from B to any other vertex would make this graph connected. As a result from being disconnected the graph consists of two components (dashed lines; one contains only the vertex B and the other one contains the other three vertices.

components. In figure 2.3 the vertex B forms one component, while the rest of the vertices form a second one. The vertex B is an *isolated vertex* as it is of degree zero. A graph consisting of only isolated vertices is called a *trivial graph* with each vertex forming its own trivial component.

Adding edges to any graph either reduces the number of components by 1 or 0, and therefore the minimum number of components is at least $n - m$. This can be seen by considering a trivial graph of n vertices and adding m edges such that the number of components k changes by one with each of the m edges. An edge that increases the number of components upon deletion is also called a *cut-edge*.

An important concept utilised in chapter 9 of this thesis is that of induced sub-graphs. If a list of vertices T is removed from a graph G the vertex-induced sub-graph H with the vertex set $N(H) = N(G) - T$ is obtained. All edges incident to the removed vertices need to be removed as well. Removing the edge set S results in the edge-induced sub-graph I with the edge set $E(I) = E(G) - S$, which leaves the vertex set unchanged.

2.2 Planar Graphs

Planar graphs are of particular importance in chemistry and physics, especially when studying clusters and complexes that are related to polyhedral arrangements. A planar graph G is defined as a graph that can be drawn such that none of its edges intercept (except at vertices to which both edges are incident). If a planar graph is drawn in that way it's called a *plane graph*, while any way of drawing that graph in the 2D plane may be referred to as a *planar embedding*.

The importance of planar graphs in cluster sciences stems from the fact that

they are related to convex polyhedra. According to *Steinitz's fundamental theorem on convex types* a graph G is isomorphic to a graph $G(P)$ of a convex polyhedron P if G is planar and 3-connected. A connected graph G is said to be k-vertex-connected (or k-connected) if it has more than k vertices and remains connected whenever fewer than k vertices are removed. A famous special case is a cubic graph with every vertex having degree three. Steinitz's theorem can be illustrated by the following procedure. Take a convex polyhedron like the icosahedron and remove one face (figure 2.4a). Imagine the rest

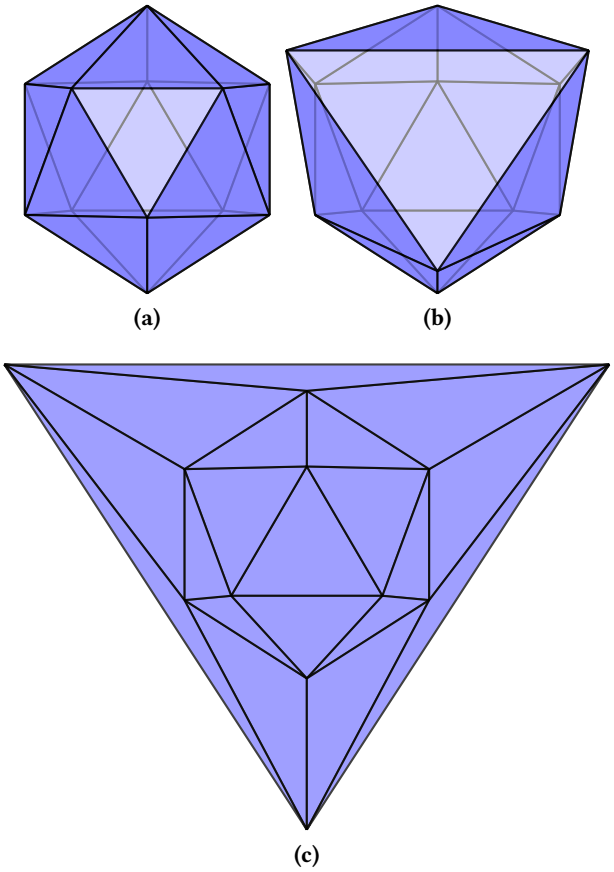

Figure 2.4 Stretching and flattening of a icosahedron surface with one removed face. (a) Icosahedron with on removed face in the centre, (b) stretching of the hole in the surface, (c) fully flattened surface shows a plane graph.

of the polyhedron being made of a rubber material such that it is deformable and stretchable. Take the area of the removed face and stretch it such that the rest of the polyhedron can sit inside the stretched face (figure 2.4b). After flattening the object, what is left is what looks like a planar embedding of a graph.

Notice how no connections were broken in the process, which means the resulting graph accurately represents the connectivity of the original polyhedron.

A plane graph sections the area of the graph into regions (or faces), one of which is exterior while all others are interior. The exterior region is the only one that is not finite. A region is enclosed by a closed walk and its degree is equal to the number of edges contained in the walk.

A relation between the number of vertices $|N|$, regions $|F|$ and edges $|E|$ in a planar graph is given by Euler's polyhedral formula.

$$|N| - |E| + |F| = 2 \tag{2.2}$$

There exist a large amount of proofs for this formula, one of which was published shortly after Euler's death by Cauchy.[27] Take any graph derived from a convex polyhedron like the cubic graph shown in figure 2.5a. As shown in

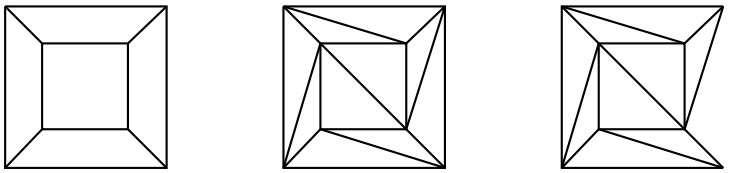

(a) $8 - 12 + 6 = 2$ **(b)** $8 - 17 + 11 = 2$ **(c)** $8 - 16 + 10 = 2$

Figure 2.5 (a) Graph of a cube, (b) triangulation of the internal regions of the same graph, (c) removal of one face and edge.

figure 2.5b, add edges such that every internal region becomes a triangle. This procedure increases both E and F, therefore not affecting the result of equation (2.2). In the final step of the proof, the triangles are removed one by one starting from the outside boundary of the graph. This can either be achieved by removing one edge and a face as shown in figure 2.5c or two edges, one vertex and one face, again leaving equation (2.2) unchanged. In the end, only one internal region will remain: a triangle. This triangle will always result from the procedure described above no matter which planar graph the procedure was started from. Equation (2.2) for this triangle is $3 - 3 + 2 = 2$, therefore proving Euler's relation to be true. The result 2 of Euler's polyhedral formula is true for convex polyhedra and is also called the *Euler characteristic* χ. The formula can be extended to other objects via this value. It is directly related to the genus g of an object via the relation

$$\chi = 2 - 2g. \tag{2.3}$$

Even for disconnected graphs the formula can be modified and expressed in terms of the number of connected components k of the graph.

$$|N| - |E| + |F| = k + 1 \tag{2.4}$$

Euler's polyhedral formula is very simple, but nevertheless very powerful. For example, it shows a symmetry between the number of regions and the number of vertices in a graph, because exchanging N and F does not change its result. This property is known as *duality*. The geometric dual of a graph G' has $|N|$ faces and $|F|$ vertices, while the edge count remains unchanged. It can be constructed by considering the neighbouring regions of an edge e. If e is between region A and B, then the corresponding dual edge e' connects the vertices a and b of the dual graph G'. Repeating this procedure for all edges of G results in a graph that is its geometric dual.

2.3 Graph Matching

In chapter 9 the concepts of isomorphism and sub-graph isomorphism are used to investigate similarities of a certain class of clusters to the icosahedral graph. Such a procedure is required to find a mapping M between the vertices of two graphs, which depends on the external constraints imposed on it. Such a mapping is a bijection and can be expressed by ordered pairs of vertices (a, b).

$$M = \{(a_1, b_1), (a_2, b_2) \dots\} \tag{2.5}$$

Mappings have to be created vertex by vertex, so initially all mappings start as partial mappings that only contain a subset of the vertices of both graphs. This mapping can be found by simply computing all possible partial solutions, that satisfy the desired isomorphism type. However, this becomes increasingly expensive for larger graphs and more efficient methods have been developed. The *VF* algorithm,[28] for example, uses feasibility rules to rule out partial mappings that will definitely not result in a mapping with the desired properties. This can reduce the size of the problem substantially, as dead-end solutions will be removed early in the procedure. The *VF* algorithms memory footprint has been improved in the *VF2* implementation,[29] which is the version included in the *boost graph library*[30] utilised in this thesis.

3 Quantum Chemistry

An accurate description of atoms and molecules is given by the Schrödinger equation and its relativistic extensions. The following chapter introduces the fundamentals of quantum mechanics and their application to chemistry in terms of approximate solutions to the Schrödinger equation. If not noted otherwise the content is based on standard books by Jensen,[31] Szabo and Ostlund[32] and Holthausen and Koch.[33]

3.1 The Schrödinger Equation

The beginning of the 20th century marked a very important stepping stone for modern theoretical sciences. Discoveries like Planck's energy quantisation based on black body radiation[34] or the discovery of the wave particle dualism by de Broglie[35] lead to a complete reformulation of the physical laws governing the smallest of particles. Erwin Schrödinger established a framework based on Hamiltonian mechanics that set the *wave function* $\Psi(\mathbf{x}, t)$ at the centre of attention.[36] It contains all information about the system and its evolution in time. For ground-state calculations it is usually sufficient to look at solutions to the *time-independent Schrödinger equation*.

$$\mathbf{H}\Psi = E\Psi \tag{3.1}$$

In this eigenvalue equation the *Hamilton operator* $\mathbf{H}$ acts on the wave function Ψ resulting in a solution for the total energy E of the system.

The wave function is a function of all spatial $\mathbf{r}$ and spin coordinates ω of all the particles in the system.[a] The combination of these coordinates will be denoted $\mathbf{x}$ on the following pages.

$$\mathbf{x} = \{\mathbf{r}, \omega\} \tag{3.2}$$

The square of the wave function is usually interpreted as a *probability density*, i.e. the probability of finding an electron anywhere in space is set to one (*normalisation condition*). This interpretation is also referred to as *Born's interpretation* of the wave function.[37,38]

$$\int |\Psi(\mathbf{x})|^2 \mathrm{d}\mathbf{x}_1 \mathrm{d}\mathbf{x}_2 \dots \mathrm{d}\mathbf{x}_N = \langle \Psi(\mathbf{x}) | \Psi(\mathbf{x}) \rangle = 1 \tag{3.3}$$

[a] The spin is treated in a more consistent way by the Dirac equation.

The information contained in the wave function can be accessed by an *operator* $\mathbf{O}$ acting on the wave function and forming an eigenvalue equation. In equation (3.1) this operator is the Hamilton operator, but it could be any (self-adjoint) operator connected to a physical observable. Generally, the expectation value of any operator $\langle \mathbf{O} \rangle$ is defined as

$$\langle \mathbf{O} \rangle = \frac{\langle \Psi(\mathbf{x}) | \mathbf{O} | \Psi(\mathbf{x}) \rangle}{\langle \Psi(\mathbf{x}) | \Psi(\mathbf{x}) \rangle}, \tag{3.4}$$

or for normalised wave functions

$$\langle \mathbf{O} \rangle = \langle \Psi(\mathbf{x}) | \mathbf{O} | \Psi(\mathbf{x}) \rangle . \tag{3.5}$$

For a system of N electrons and M nuclei the non-relativistic Hamilton operator in atomic units has the form

$$\begin{aligned} \mathbf{H} =& \mathbf{T}_\mathrm{e} + \mathbf{V}_\mathrm{ee} + \mathbf{T}_\mathrm{n} + \mathbf{V}_\mathrm{nn} + \mathbf{V}_\mathrm{en} \\ =& -\frac{1}{2} \sum_{i=1}^{N} \nabla_i^2 + \sum_{i=1}^{N} \sum_{j>i}^{N} r_{ij}^{-1} - \frac{1}{2} \sum_{A=1}^{M} \frac{\nabla_A^2}{m_A} \\ &+ \sum_{A=1}^{M} \sum_{B>A}^{M} \frac{Z_A Z_B}{r_{AB}} + \sum_{i=1}^{N} \sum_{A=1}^{M} \frac{Z_A}{r_{iA}}. \end{aligned} \tag{3.6}$$

r_{iA} denotes the distance between particles i (electron) and A (nucleus), m_A is the mass of nucleus A and Z_A is its charge. The operator contains the kinetic energy of the electrons $\mathbf{T}_\mathrm{e}$, the electron repulsion $\mathbf{V}_\mathrm{ee}$, the kinetic energy of the nuclei $\mathbf{T}_\mathrm{n}$, the nucleon repulsion $\mathbf{V}_\mathrm{nn}$ and the electron-nucleus attraction $\mathbf{V}_\mathrm{en}$. Additional operators may be added for external field perturbations.

3.2 The Born-Oppenheimer Approximation

For quantum chemical applications the coupling of the movement of the electrons and nuclei is usually neglected. This is possible because the atomic mass m_A is so much greater than the electronic mass m_i, resulting in much smaller velocities for nuclei compared to electrons.[39] Therefore, the electrons can be considered to be moving in a static field of nuclei, meaning the nuclear kinetic term $\mathbf{T}_\mathrm{n}$ can be neglected and the nuclear repulsion term $\mathbf{V}_\mathrm{nn}$ becomes a constant. The resulting electronic Hamilton operator $\mathbf{H}_\mathrm{e}$ describes electrons moving in a field of positive point charges.

$$\mathbf{H}_\mathrm{e} = \mathbf{T}_\mathrm{e} + \mathbf{V}_\mathrm{ee} + \mathbf{V}_\mathrm{en} \tag{3.7}$$

Solving the Schrödinger equation for this operator yields the electronic wave function Ψ_e. It depends explicitly on the electronic coordinates and spin, but

only parametrically on the nuclear coordinates, therefore spanning a potential energy surface upon which the nuclei move. To get the total energy of the system, the constant repulsion between the nuclei has to be added to the electronic operator.

$$\mathbf{H} = \mathbf{H}_\mathrm{e} + V_\mathrm{nn} \tag{3.8}$$

3.3 The Hartree-Fock Approximation

An analytical solution to the Schrödinger equation in the framework of the Born-Oppenheimer approximation for systems containing more than one electron is not attainable. The solution has to be obtained approximately by appropriate methods; one such approximation is given by the Hartree-Fock equations. This set of equations determines the energy variationally from a wave function expressed as a Slater determinant Φ_SD.[40,41]

$$\Phi_{SD} = \frac{1}{\sqrt{N!}} \begin{vmatrix} \phi_1(\mathbf{x}_1) & \phi_2(\mathbf{x}_1) & \cdots & \phi_N(\mathbf{x}_1) \\ \phi_1(\mathbf{x}_2) & \phi_2(\mathbf{x}_2) & \cdots & \phi_N(\mathbf{x}_2) \\ \vdots & \vdots & \ddots & \vdots \\ \phi_1(\mathbf{x}_N) & \phi_2(\mathbf{x}_N) & \cdots & \phi_N(\mathbf{x}_N) \end{vmatrix} \tag{3.9}$$

Here, the ϕ_i denote one-electron spin-orbitals and $\mathbf{x}_i = \{\mathbf{r}_i, \omega_i\}$ are spatial ($\mathbf{r}_i$) and spin (ω_i) coordinates of the electrons. A Slater determinant obeys the Pauli exclusion principle for fermions, which requires the electronic wave function to be anti-symmetric with respect to interchanging the coordinates of any two electrons.

In the Hartree-Fock approximation the energy of a single Slater determinant is used as an approximation for the total energy of the system. As explained previously, the energy of a wave function can be determined by the action of the Hamilton operator on the wave function. The Hamilton operator in the Born-Oppenheimer approximation from equation (3.8) can be rewritten in terms of one-electron operators $\mathbf{h}_i$.

$$\begin{aligned} \mathbf{H} &= \sum_i^N \left(\mathbf{h}_i + \sum_{j>i}^N \frac{1}{|\mathbf{r}_i - \mathbf{r}_j|} \right) + V_\mathrm{nn} \\ \mathbf{h}_i &= -\frac{1}{2}\nabla_i^2 - \sum_A^M \frac{Z_A}{|\mathbf{r}_A - \mathbf{r}_i|} \end{aligned} \tag{3.10}$$

$\mathbf{h}_i$ depends only on the kinetic energy of electron i and its potential energy in the field of all M nuclei. When $\mathbf{h}_i$ acts on a Slater determinant the result is the respective matrix element h_i. Only parts of the Slater determinant without

permutation of electron coordinates can give a non-zero contribution to the eigenvalue.

$$\begin{aligned} h_1 &= \langle \phi_1(\mathbf{x}_1)\phi_2(\mathbf{x}_2)\dots\phi_N(\mathbf{x}_N)|\mathbf{h}_1|\phi_1(\mathbf{x}_1)\phi_2(\mathbf{x}_2)\dots\phi_N(\mathbf{x}_N)\rangle \\ &= \langle \phi_1(\mathbf{x}_1)|\mathbf{h}_1|\phi_1(\mathbf{x}_1)\rangle \langle \phi_2(\mathbf{x}_2)|\phi_2(\mathbf{x}_2)\rangle \dots \langle \phi_N(\mathbf{x}_N)|\phi_N(\mathbf{x}_N)\rangle \\ &= \langle \phi_1(\mathbf{x}_1)|\mathbf{h}_1|\phi_1(\mathbf{x}_1)\rangle \end{aligned} \tag{3.11}$$

The remainder of the Hamilton operator from equation (3.10) depends on two electron coordinates, therefore, it is convenient to define a two-electron operator $\mathbf{g}_{ij}$ with the matrix elements $g_{ij} = r_{ij}^{-1}$. Its action on the part of the Slater determinant with no permutation of electron coordinates results in the Coulomb integral and the corresponding matrix element J_{ij}, which can be interpreted as the classical Coulomb repulsion.

$$\begin{aligned} J_{12} &= \langle \phi_1(\mathbf{x}_1)\phi_2(\mathbf{x}_2)\dots\phi_N(\mathbf{x}_N)|\mathbf{g}_{12}|\phi_1(\mathbf{x}_1)\phi_2(\mathbf{x}_2)\dots\phi_N(\mathbf{x}_N)\rangle \\ &= \langle \phi_1(\mathbf{x}_1)\phi_2(\mathbf{x}_2)|\mathbf{g}_{12}|\phi_1(\mathbf{x}_1)\phi_2(\mathbf{x}_2)\rangle \dots \langle \phi_N(\mathbf{x}_N)|\phi_N(\mathbf{x}_N)\rangle \\ &= \langle \phi_1(\mathbf{x}_1)\phi_2(\mathbf{x}_2)|\mathbf{g}_{12}|\phi_1(\mathbf{x}_1)\phi_2(\mathbf{x}_2)\rangle \end{aligned} \tag{3.12}$$

As $\mathbf{g}_{ij}$ depends on the coordinates of two electrons it also yields non-zero matrix elements for parts of the Slater determinant, where two electron coordinates have been swapped.

$$\begin{aligned} K_{12} &= \langle \phi_1(\mathbf{x}_1)\phi_2(\mathbf{x}_2)\dots\phi_N(\mathbf{x}_N)|\mathbf{g}_{12}|\phi_2(\mathbf{x}_1)\phi_1(\mathbf{x}_2)\dots\phi_N(\mathbf{x}_N)\rangle \\ &= \langle \phi_1(\mathbf{x}_1)\phi_2(\mathbf{x}_2)|\mathbf{g}_{12}|\phi_2(\mathbf{x}_1)\phi_1(\mathbf{x}_2)\rangle \dots \langle \phi_N(\mathbf{x}_N)|\phi_N(\mathbf{x}_N)\rangle \\ &= \langle \phi_1(\mathbf{x}_1)\phi_2(\mathbf{x}_2)|\mathbf{g}_{12}|\phi_2(\mathbf{x}_1)\phi_1(\mathbf{x}_2)\rangle \end{aligned} \tag{3.13}$$

K_{ij} is called the exchange integral and has no classical interpretation. As swapping coordinates in the Slater determinant changes its sign, the result of the exchange integral has a negative sign. The total energy of the system is now given by the sum over all integrals described above.

$$E = \sum_{i=1}^{N} h_i + \frac{1}{2}\sum_{i=1}^{N}\sum_{j=1}^{N}(J_{ij} - K_{ij}) + V_{\mathrm{nn}} \tag{3.14}$$

Defining operators $\mathbf{J}_i$ and $\mathbf{K}_i$ for Coulomb and exchange integral equation (3.14) becomes

$$E = \sum_{i=1}^{N} \langle \phi_i|\mathbf{h}_i|\phi_i\rangle + \frac{1}{2}\sum_{i=1}^{N}\sum_{j=1}^{N}\left(\langle \phi_i|\mathbf{J}_j|\phi_i\rangle - \langle \phi_i|\mathbf{K}_j|\phi_i\rangle\right) + V_{\mathrm{nn}} \tag{3.15}$$

$$\begin{aligned} \mathbf{J}_i\,|\phi_j(\mathbf{x}_j)\rangle &= \langle \phi_i(\mathbf{x}_i)|\mathbf{g}_{ij}|\phi_i(\mathbf{x}_i)\rangle\,|\phi_j(\mathbf{x}_j)\rangle \\ \mathbf{K}_i\,|\phi_j(\mathbf{x}_j)\rangle &= \langle \phi_i(\mathbf{x}_i)|\mathbf{g}_{ij}|\phi_j(\mathbf{x}_i)\rangle\,|\phi_i(\mathbf{x}_j)\rangle\,. \end{aligned} \tag{3.16}$$

For the purpose of quantum chemical calculations the energy of an arbitrary Slater determinant is usually not useful. More interesting, however, is to find

the Slater determinant that minimises the energy under the boundary condition of keeping the orthonormality condition between spin orbitals. In other words, we try to find the derivative of equation (3.15). Minimising the energy under external boundary conditions can be achieved using Lagrange multipliers. With their help it is possible to define the Fock operator $\mathbf{f}_i$, which is an effective one-electron operator.

$$\mathbf{f}_i = \mathbf{h}_i + \sum_j^N (\mathbf{J}_j - \mathbf{K}_j) \tag{3.17}$$

The action of the Fock operator on an element of the Slater determinant yields the Hartree-Fock equations.

$$\mathbf{f}_i \left|\phi_i\right\rangle = \sum_j^N \lambda_{ij} \left|\phi_j\right\rangle \tag{3.18}$$

λ_{ij} are Lagrange multipliers remaining from the constrained minimisation. They can be re-written in matrix form and subsequently diagonalised by a unitary transformation. This yields the canonical Hartree-Fock equations.

$$\mathbf{f}_i \left|\phi'_i\right\rangle = \sum_j^N \varepsilon_i \left|\phi'_j\right\rangle \tag{3.19}$$

ε_i are orbital energies of the electrons. According to Koopman's theorem they can be interpreted as ionisation energies for occupied (and sometimes electron affinities for unoccupied) states. The Fock operator depends on all occupied states, making it a pseudo eigenvalue equation. Hence, solutions have to be found iteratively starting from and arbitrary set of orbitals. After a set of convergence criteria has been met, the effective potential is said to remain unchanged, creating a self-consistent field (SCF) solution.

Solving the canonical Hartree-Fock equations numerically for larger systems will be possible in the future, but is too costly with the algorithms currently available. Instead, they are solved using an analytical basis set expansion to approximate the unknown molecular orbitals. The basis functions are usually chosen to agree with the underlying physics of the system. For example, periodic plane waves are usually used when periodic boundary conditions are required. For calculations in the gas phase the basis functions are usually exponential functions centred at the nuclei. In this case the approximation is called linear combination of atomic orbitals (LCAO). Technically, a basis set expansion is not an approximation, but as one is limited to a finite amount of basis functions P the expansion does not give an exact expression for a

molecular orbital ϕ_i. For a set of P basis functions χ_α the expansion can be expressed as follows.

$$\phi_i = \sum_{\alpha}^{P} c_{\alpha i} \chi_\alpha \tag{3.20}$$

This leads to the Hartree-Fock equations expressed in the basis set approximation.

$$\begin{aligned} \mathbf{f}_i \sum_{\alpha}^{P} c_{\alpha i} \chi_\alpha &= \varepsilon_i \sum_{\alpha}^{P} c_{\alpha i} \chi_\alpha \\ \sum_{\alpha}^{P} c_{\alpha i} \underbrace{\langle \chi_\alpha | \mathbf{f}_i | \chi_\beta \rangle}_{F_{\alpha\beta}} &= \varepsilon_i \sum_{\alpha}^{P} c_{\alpha i} \underbrace{\langle \chi_\alpha | \chi_\beta \rangle}_{S_{\alpha\beta}} \end{aligned} \tag{3.21}$$

These are the Roothaan-Hall equations[42,43] which are usually written in matrix form.

$$\mathbf{FC} = \mathbf{SC}\varepsilon \tag{3.22}$$

$\mathbf{F}$ is the Fock matrix, $\mathbf{S}$ is the overlap matrix and $\mathbf{C}$ contains the orbital coefficients. These equations have to be solved iteratively and to reduce computational cost the first step usually involves calculating a density matrix $\mathbf{D}$.

$$\mathbf{D} = \sum_{i}^{\text{occ. MO}} c_{\mu i} c_{\nu i} \tag{3.23}$$

$\mathbf{D}$ can be used to generate a Fock matrix, which will be diagonalised yielding a new set of orbital coefficients. These will be used to generate a new generation of the density matrix. This procedure will be repeated until the coefficients of the new generation are equal (up to a certain precision) to the ones of the parent generation. This marks the end of the SCF cycle.

3.4 Density Functional Theory

The Hartree-Fock method belongs to the class of mean field approximations, which implies that the electrons do not interact directly with each other, but each electron is moving in a mean field created by all the other electrons. The Hartree-Fock energy E_{HF} is therefore never exact for a multi-electron system even in the infinite basis set limit. The difference to the exact energy E_0 was first named electron correlation energy E_{corr} by Löwdin.[44]

$$E_{\text{corr}} = E_0 - E_{\text{HF}} \tag{3.24}$$

Even though the correlation energy only attributes for about $1\,\%$ of the total electronic energy, it is an important contribution in molecular systems when small changes in energy are involved. A multitude of methods has therefore been developed to treat electron correlation more accurately. They can generally be subdivided into post-Hartree-Fock methods and density functional theory (DFT). While post-Hartree-Fock methods rely on a Hartree-Fock wave function (or its multi-reference analogues) as a starting point, DFT is in principle a wave function free method. It establishes a connection between the energy of the system and the (one-particle) electron density $\rho(\mathbf{r})$ instead of the complex wave function that depends on the coordinates of all particles. The electron density is an observable and a positive real function, which makes DFT easier to grasp than wave function based methods. However, the electron density is related to the wave function via its square.

$$\rho(\mathbf{r}) = N \int \cdots \int |\Psi(\mathbf{x}_1, \mathbf{x}_2, \ldots, \mathbf{x}_N)|^2 \, \mathrm{d}\omega_1 \mathrm{d}\mathbf{x}_2 \ldots \mathrm{d}\mathbf{x}_N \tag{3.25}$$

Equation (3.25) describes the probability density of finding one of the N electrons in the volume $\mathrm{d}\mathbf{r}_1$. As electrons are indistinguishable the probability of finding any of the N electrons in the volume $\mathrm{d}\mathbf{r}_1$ is equal to N times the probability of finding a specific electron in that volume. A justification for using the electron density instead of the wave function was found by Hohenberg and Kohn in 1964.[45]

3.4.1 Hohenberg-Kohn Theorems

The first Hohenberg-Kohn theorem implies that the ground state electron density defines a unique external potential that contains all information about the system (there is a one-to-one mapping between the ground state density and the external potential). If two external potentials are different they cannot lead to the same ground state electron density. From this, the total energy of a system can be expressed as follows.

$$E_0\left[\rho_0(\mathbf{r})\right] = T\left[\rho_0(\mathbf{r})\right] + E_{\mathrm{ee}}\left[\rho_0(\mathbf{r})\right] + E_{\mathrm{Ne}}\left[\rho_0(\mathbf{r})\right] \tag{3.26}$$

The aforementioned external potential corresponds to $E_{\mathrm{Ne}}\left[\rho_0(\mathbf{r})\right]$, which is the only system-dependent term of equation (3.26). The system-independent terms for the kinetic energy $T\left[\rho_0(\mathbf{r})\right]$ and the electron-electron interaction $E_{\mathrm{ee}}\left[\rho_0(\mathbf{r})\right]$ can be combined to the Hohenberg-Kohn functional $F_{\mathrm{HK}}\left[\rho_0(\mathbf{r})\right]$.

$$E_0\left[\rho_0(\mathbf{r})\right] = \int \mathrm{d}\mathbf{r}\rho_0(\mathbf{r})V_{\mathrm{Ne}} + F_{\mathrm{HK}}\left[\rho_0(\mathbf{r})\right] \tag{3.27}$$

If the exact Hohenberg-Kohn functional would be known, equation (3.27) would be an exact solution to the Schrödinger equation. In practice, there are no exact expressions for $T\left[\rho_0(\mathbf{r})\right]$ or $E_{\mathrm{ee}}\left[\rho_0(\mathbf{r})\right]$ known. However, the

latter can be expressed in terms of a classical Coulomb term $J[\rho]$ and a non-classical energy contribution $E_{\text{nc}}[\rho]$.

$$E_{\text{ee}}[\rho] = J[\rho] + E_{\text{nc}}[\rho] = \frac{1}{2}\iint \frac{\rho(\mathbf{r}_1)\rho(\mathbf{r}_2)}{r_{12}}\mathrm{d}\mathbf{r}_1\mathrm{d}\mathbf{r}_2 + E_{\text{nc}}[\rho] \tag{3.28}$$

The second Hohenberg-Kohn theorem warrants that a trial energy density $\widetilde{\rho}$ always yields an energy greater or equal to the exact ground state energy.

$$E_0 \leq E[\widetilde{\rho}] \tag{3.29}$$

It is equivalent to the variational theorem[b] in wave function theory. However, it is only valid for the exact Hohenberg-Kohn functional, which is unknown. A practical solution to this problem was given in 1965 by Kohn and Sham.[46]

3.4.2 Kohn-Sham Theory

One of the biggest problems in orbital free DFT is the poor description of the kinetic energy term. Kohn and Sham realised it would be easier to describe it in terms of a reference system of non-interacting electrons. Their kinetic energy T_S can be expressed in terms of one-electron orbitals ϕ_i, called Kohn-Sham (KS) orbitals.

$$T_S = -\frac{1}{2}\sum_i^N \langle\phi_i|\nabla_i^2|\phi_i\rangle \tag{3.30}$$

The electron density resulting from the KS orbitals $\rho_S(\mathbf{r})$ is required to be equal to the (in principle exact) ground state density of the real system $\rho_0(\mathbf{r})$.

$$\rho_S(\mathbf{r}) = \rho_0(\mathbf{r}) \tag{3.31}$$

For such a system the Coulomb interaction between electrons and nuclei can be calculated exactly. The only terms remaining unknown are the non-classical contribution to the electron-electron interaction E_{nc} and a contribution to the kinetic energy because of electron correlation T_C. These terms can be combined to the exchange-correlation term E_{XC}.

$$E[\rho] = T_S[\rho] + J[\rho] + E_{XC}[\rho] + E_{\text{Ne}}[\rho] \tag{3.32}$$

$$\begin{aligned} &= -\frac{1}{2}\sum_i^N \langle\phi_i|\nabla_i^2|\phi_i\rangle + \frac{1}{2}\sum_i^N\sum_j^N \iint \mathrm{d}\mathbf{r}_1\mathrm{d}\mathbf{r}_2|\phi_i(\mathbf{r}_1)|^2\frac{1}{r_{12}}|\phi_j(\mathbf{r}_2)|^2 \\ &\quad + E_{XC}[\rho] - \sum_i^N \int \mathrm{d}\mathbf{r}_1 \sum_A^M \frac{Z_A}{r_{1A}}|\phi_i(\mathbf{r}_1)|^2 \end{aligned} \tag{3.33}$$

[b] The variational theorem states that no trial wave function can result in a smaller energy than the exact ground state wave function.

Similar to Hartree-Fock theory, the minimal energy can be calculated using Lagrange multipliers. The potential terms from equation (3.33) can be combined to an effective potential V_S, which allows for the definition of a Kohn-Sham operator $\mathbf{f}_{\text{KS}}$ analogous to the Fock operator in Hartree-Fock theory.

$$V_S(\mathbf{r}_1) = \int \mathrm{d}\mathbf{r}_2 \frac{\rho(\mathbf{r}_2)}{r_{12}} + V_{XC}(\mathbf{r}_1) - \sum_A^M \frac{Z_A}{r_{1A}} \tag{3.34}$$

$$\mathbf{f}_{\text{KS}} = -\frac{1}{2}\nabla^2 + V_S(\mathbf{r}_1) \tag{3.35}$$

$$\mathbf{f}_{\text{KS}}\phi_i = \varepsilon_i \phi_i \tag{3.36}$$

These are the Kohn-Sham equations and they have to be solved in an iterative procedure, because of the Kohn-Sham operator depending on the occupied orbitals. The unknown Kohn-Sham orbitals are usually expanded in terms of basis functions such that the equations can be expressed in matrix form, similar to the Roothaan-Hall equations. The Fock matrix is replaced by the Kohn-Sham matrix $\mathbf{F}_{\text{KS}}$.

$$\mathbf{F}_{\text{KS}}\mathbf{C} = \mathbf{S}\mathbf{C}\varepsilon \tag{3.37}$$

3.4.3 Exchange and Correlation Functionals

The key to solving the Kohn-Sham equations is the exchange-correlation energy E_{XC}. Over the years there have been a large number of proposals for its analytical form, the oldest being the local density approximation (LDA). It is based on the uniform electron gas (Thomas-Fermi model) for which analytical functionals for exchange and correlation are known.

$$E_{XC}^{\text{LDA}}[\rho] = \int \rho(\mathbf{r}) \varepsilon_{XC}[\rho(\mathbf{r})]\,\mathrm{d}\mathbf{r} \tag{3.38}$$

The exchange-correlation energy functional $\varepsilon_{XC}[\rho(\mathbf{r})]$ is weighted with the probability of finding an electron at this point in space. After separation of the exchange and correlation parts the exchange energy can be described by a term developed by Slater.

$$\varepsilon_{XC}[\rho(\mathbf{r})] = \varepsilon_X[\rho(\mathbf{r})] + \varepsilon_C[\rho(\mathbf{r})] \tag{3.39}$$

$$E_X^{\text{LDA}}[\rho] = -C_X \int \rho(\mathbf{r})^{\frac{4}{3}} \mathrm{d}\mathbf{r} \tag{3.40}$$

However, no simple formula for the correlation term is known.

LDA describes the inhomogeneous electron density by dividing it up into small homogeneous volumes. An improvement over LDA can be made if the homogeneous electron density is expanded in a Taylor series. Truncating after the first term gives the LDA approximation, including one more term

is called the gradient expansion approximation (GEA). Because GEA does not correctly describe the exchange-correlation hole function it gives worse results than LDA.

A break-through for theoretical chemistry has been achieved with the introduction of the generalised gradient approximation (GGA) by Becke and Perdew. It uses the GEA hole functions and tailors them to physically meaningful boundary conditions.

In this work the PBE functional by Perdew, Burke and Ernzerhof,[47,48] which belongs to the group of GGA functionals, was used for most calculations. They published both correlation and exchange expressions for this functional.

3.4.4 Dispersion Corrections

Long-range dispersive effects are part of the correlation energy and most DFT functionals can only describe these effects to a very limited degree. Grimme et al. developed a method that can be used in conjunction with most density functionals.[49] It relies on the calculation of a dispersive energy contribution E_{disp} (and gradient contribution for optimisations) that can be added to the DFT energy E_{DFT}. The dispersion energy is always of attractive nature and therefore has a negative sign by convention.

$$E = E_{\text{DFT}} + E_{\text{disp}} \tag{3.41}$$

In the third generation dispersion correction (D3), which was used in this work, the calculation of E_{disp} involves solving a two- and three-body term. The two-body term $E^{(2)}$ is more important and is only a function of the distance between two nuclei r_{AB}.

$$E^{(2)} = \sum_{AB} s_6 \frac{C_6^{AB}}{(r_{AB})^6} f_{\text{dmp},6}(r_{AB}) + s_8 \frac{C_8^{AB}}{(r_{AB})^8} f_{\text{dmp},8}(r_{AB}). \tag{3.42}$$

Using only the first term (London dispersion) in equation (3.42) is equal to the second generation dispersion correction D2.[c] s_6 and s_8 are functional specific parameters that need to be adjusted for each different DFT functional. The damping functions $f_{\text{dmp},6}$ and $f_{\text{dmp},8}$ are necessary to cut off the interaction at short distances including the repulsive region, where the density functional without dispersion performs well. The C_6^{AB} dispersion coefficient is calculated by averaging over the dipole polarisabilities α of the hydrides of the elements A and B. The contributions of the hydrogen atoms have to be subtracted. The value of C_6^{AB} can be used to calculate C_8^{AB} and C_9^{AB}, the latter is contained in the three-body (Axilrod-Teller-Muto) term.

[c] The calculation of C_6 parameters is carried out differently for D2.

Usually, a zero damping approach is used for the damping function.

$$f_{\text{dmp},n} = \frac{1}{1 + 6\left(\frac{r_{AB}}{s_{r,n} r_0^{AB}}\right)^{-\alpha_n}} \tag{3.43}$$

The name comes from the limit of the damping function which approaches zero with r_{AB} going to zero. Alternatively, the Becke-Johnson damping function[50] can be used.

3.5 Periodic Boundary Conditions

When dealing with the electronic description of solids and crystals the periodic symmetry needs to be taken into consideration. This is done by describing the solid state system with an infinite three-dimensional grid containing cells which are translation invariant. In the following sections the concept of reciprocal space and its application to problems involving periodic boundary conditions is explained.

3.5.1 Spatial and Electronic Structure

The geometry of a crystal can be described in real and reciprocal space. In real (configuration) space the crystal lattice can be created by the lattice vector $\mathbf{R}$ acting on the atoms contained in the primitive unit cell.

$$\mathbf{R} = n_1\mathbf{a}_1 + n_2\mathbf{a}_2 + n_3\mathbf{a}_3 \tag{3.44}$$

Here, $\mathbf{a}_i$ are basis vectors of the lattice and n_i are integers. As the number of atoms in this system is infinite the total energy is also going to be infinite, and only the energy per unit cell is meaningful. To solve this problem the electronic structure is usually treated in reciprocal space. Instead of solving an infinitely large problem, reciprocal space allows to transform the system into infinitely many sub-systems, with each sub-system having a finite solution.

Real and reciprocal space are connected by a Fourier transformation, which leads to the reciprocal lattice parameters $\mathbf{b}_i$, that relate to the real space lattice vectors via the vector cross product $\cdot \times \cdot$ normalised with respect to the volume of the primitive unit cell V_p.

$$\mathbf{b}_1 = \frac{2\pi}{V_p}(\mathbf{a}_2 \times \mathbf{a}_3),\ \mathbf{b}_2 = \frac{2\pi}{V_p}(\mathbf{a}_3 \times \mathbf{a}_1),\ \mathbf{b}_3 = \frac{2\pi}{V_p}(\mathbf{a}_1 \times \mathbf{a}_2) \tag{3.45}$$

Translation in reciprocal space is therefore defined as:

$$\mathbf{K} = k_1\mathbf{b}_1 + k_2\mathbf{b}_2 + k_3\mathbf{b}_3, \tag{3.46}$$

where k_i are integer values and can be combined into the wave vector $\mathbf{k}$.

The lattice vector in reciprocal space $\mathbf{K}$ is related to $\mathbf{R}$ via $\exp\{i\mathbf{KR}\} = 1$ and the corresponding basis vectors in real and reciprocal space must satisfy the condition $\mathbf{a}_i\mathbf{b}_i = 2\pi\delta_{ij}$.

In reciprocal space the primitive unit cell is also called the Brillouin zone, which can be constructed by applying a Wigner-Seitz construction to the real space primitive unit cell.

3.5.2 Bloch Conditions

As the same structural motif is repeated periodically throughout the infinite system, the same must apply to the inter-atomic potential V.

$$V(\mathbf{r} + \mathbf{R}) \equiv V(\mathbf{r}) \tag{3.47}$$

The periodic wave function for the band n can be expressed using the Bloch theorem.

$$\Psi_n(\mathbf{k}, \mathbf{r}) = \exp\{i\mathbf{kr}\}u_{n\mathbf{k}}(\mathbf{r}) \tag{3.48}$$

The periodic information is encoded in the Bloch factor $u_{n\mathbf{k}}(\mathbf{r})$, which needs to satisfy the condition that it takes on the same value for $\mathbf{r} + \mathbf{R}$ as for $\mathbf{r}$.

The wave function of an electron in the periodic potential of the crystal is then described by the Bloch function $\Psi_{n\mathbf{k}}(\mathbf{r} + \mathbf{R})$.

$$\Psi_{n\mathbf{k}}(\mathbf{r} + \mathbf{R}) = \exp\{i\mathbf{kR}\}u_{n\mathbf{k}}(\mathbf{r}) \tag{3.49}$$

The function $\exp\{i\mathbf{kR}\}$ is also called a plane wave.

3.6 Basis Sets

Both the Hartree-Fock approximation and DFT are usually solved in a basis set expansion of analytical functions. For molecules in the gas phase an atom-centred approach is usually the method of choice as most of the density is located around the nucleus. Depending on the nature of the system it can be beneficial to use a different approach, like plane waves often used in periodic boundary calculations.

3.6.1 Atom-Centred Basis Functions

The most common type of basis functions used in molecular calculations are Gaussian-type orbitals (GTOs) and Slater-type orbitals (STOs) which mainly differ by the computational cost associated with them. STOs are derived from the exact solutions to the hydrogen atom and therefore depend parametrically on the three quantum numbers n, l, m.

$$\chi_{\zeta_S,n,l,m}(r, \theta, \varphi) = NY_{l,m}(\theta, \varphi)r^{n-1}e^{-\zeta_S r} \tag{3.50}$$

The functions are split up into a radial part only depending on the spherical coordinate r and the orbital coefficient ζ_S and an angular part $Y_{l,m}(\theta, \varphi)$ which are spherical harmonics only depending on the angles θ and φ. STOs describe the cusp and the exponential decay in the core region well, but don't have analytical solutions for three- or four-centre two-electron integrals. They are usually only used when very high accuracy is required or in density functional theory codes.

GTOs use the same spherical harmonics to describe the angle dependent part, but contain a Gaussian function to describe the r-dependent term.

$$\begin{aligned} \chi_{\zeta_G,n,l,m}(r,\theta,\varphi) &= NY_{l,m}(\theta,\varphi)r^{2n-2-l}e^{\zeta_G r^2} \\ \chi_{\zeta_G,l_x,l_y,l_z}(x,y,z) &= Nx^{l_x}y^{l_y}z^{l_z}e^{-\zeta r^2} \end{aligned} \tag{3.51}$$

In the core region the function is continuous and its derivative is zero and therefore it gives a worse description of the system. However, it is possible to combine multiple GTOs in a linear combination to approximate the shape of the STO.

$$\chi^{\text{STO}} \approx \sum_i a_i \chi_i^{\text{GTO}} \tag{3.52}$$

In addition to this expansion it is typical to use more than one function per atomic orbital to improve the flexibility of the basis set and therefore the description of the orbital. This is done by choosing different values for the variable ζ and combining them to one orbital. Basis sets with two basis functions per orbital are called "double zeta" basis sets, three basis functions yield a "triple zeta" basis set *etc.*

The inner electrons have the largest contribution to the total energy of a molecule. However, for questions about chemical reactivity or catalytic activity the valence regions are of far greater importance than the core regions. It is therefore beneficial to use split-valence basis sets that use more basis functions to describe the valence region and basis set contractions in the core regions. This usually leads to a smaller computational cost without losing much in accuracy.

3.6.2 Plane Wave Basis Functions

For calculations involving periodic boundary conditions the wave function is usually expanded into a plane wave basis set. Atom-centred basis functions can also be used, but plane waves have the advantage of having intrinsic translational symmetry. Plane waves are not centred around a specific atom but fill the whole unit cell. Crystal orbitals can be constructed in the same

way molecular orbitals are created: by a linear combination of plane waves.

$$\begin{aligned}\Phi_n(\mathbf{k},\mathbf{K}) &= \sum_{\mathbf{K}} C_n(\mathbf{k},\mathbf{K}) \exp\{i(\mathbf{k}+\mathbf{K})\mathbf{r}\} \\ &= \exp\{i\mathbf{k}\mathbf{r}\} \sum_{\mathbf{K}} C_n(\mathbf{k},\mathbf{K}) \exp\{i\mathbf{K}\mathbf{r}\}\end{aligned} \tag{3.53}$$

The oscillation frequency of a plane wave is correlated with its kinetic energy. The size of the basis set is therefore usually defined by setting a maximum kinetic energy cut-off value. A correct description of the core region would require a very large cut-off value, because of the high number of radial nodes in the core orbitals. To avoid this complication, core regions are usually described using pseudo-potentials or the projector-augmented wave (PAW) method described in section 3.7.2.

3.7 Description of Core Electrons

The effect of the innermost electrons, also called core electrons, on chemical bonding and properties is of indirect nature. The interaction between elements happens mainly due to their valence electrons, but the effect of the core electrons on those valence states is still very important to get an accurate description of the system. However, because of the large number of nodal planes in those orbitals it is often necessary to use a lot of basis function to describe them properly. To reduce computational cost, the effect of the inner electrons is often modelled in terms of an effective potential. This also comes with the advantage that scalar relativistic effects can be included as part of the interaction potential. The advantages of these potentials is especially pronounced for heavier elements, because of their sheer amount of core electrons and the increasing importance of relativistic effects.

3.7.1 Effective Core Potentials

An effective core potential (ECP), or sometimes called a pseudo potential, is an approximation that allows to compute accurate properties of atoms at a much lower cost by not treating core electrons explicitly. The quality of such a potential is assessed by the number of valence electrons that make up the ECP. This gives rise to the small- and large-core ECPs that are often used for example for the transition metals. For instance, the large-core ECP for silver has only 11 electrons in the valence shell, while the small-core approximation includes additional *s* and *p* states for a total 19 valence electrons. The small-core potential can improve the quality of energetic and other property calculations significantly.

An ECP has to be based on all-electron calculations that describe the system to the desired accuracy (for example including or excluding scalar relativistic

and/or spin-orbit effects). It also requires the valence functions to be replaced by a set of pseudo-functions that show the correct behaviour in the valence region, but do not contain radial nodes in the core region. The core electrons are not treated explicitly and are replaced by an effective potential, that is parametrised to model the correct interaction potential between the valence and the core region and keeps the valence electrons out of the core. Different potential forms for different angular momenta can be included (semi-local approximation). The parameters for an effective core potential must be fitted to all-electron functions such that the valence pseudo-orbitals match those of the all-electron calculation in the valence region (shape consistency).

As atomic orbitals are usually described by Gaussian functions, it is common practice to use the same type of functions to generate an effective core potential. For example, the Stuttgart pseudo-potentials use Gaussian functions in a semi-local ansatz to describe the core region.[51]

$$\begin{aligned} V_{\mathrm{ECP}}(\mathbf{r}) &= -\frac{Q}{r} + \sum_{lj} V_{lj}(r)\mathscr{P}_{lj} \\ V_{lj}(r) &= \sum_{k} B_{lj,k} \exp\left\{-\beta_{lj,k} r^2\right\} \end{aligned} \tag{3.54}$$

For each combination of orbital l and total angular momentum quantum number $j = l \pm 1/2$ (if spin-orbit is included) a local potential $V_{lj}(r)$ expanded in terms of Gaussian functions is defined. The parameters $B_{lj,k}$ and $\beta_{lj,k}$ have to be adjusted such that they give the correct results for the valence orbitals and/or the valence spectrum (in the latter case these are called energy consistent pseudopotentials) with respect to the all-electron calculation. For large r the semi-local Gaussian expansion approaches zero and the $-\frac{Q}{r}$ term, with the charge of the core Q, becomes dominant.

3.7.2 Projector-Augmented Wave Method

The PAW method was developed by Blöchl[52] and is used in conjunction with a plane wave basis set. The method uses a projection scheme to project the all-electron wave function $|\Psi\rangle$ into a pseudo Hilbert space by utilising pseudo wave functions $|\widetilde{\Psi}\rangle$. Often considered a pseudo potential method, it is technically not part of this group as all electrons are still treated explicitly.

The valence region is described by the plane wave basis set, while the core region is approximated by partial wave functions ϕ_i that can be derived from atomic calculations. The contributions of the partial wave functions to the core electron density are also optimised during the SCF cycle via the wave function coefficients. The all electron wave function can be calculated from the partial wave functions and the so called projector functions $\langle\widetilde{p}_i|$.

$$|\Psi\rangle = |\widetilde{\Psi}\rangle + \sum_i \left(|\phi_i\rangle - |\widetilde{\phi}_i\rangle\right) \langle\widetilde{p}_i|\widetilde{\Psi}\rangle \tag{3.55}$$

The projector functions must be chosen such that

$$\sum_i |\widetilde{\phi}_i\rangle\langle\widetilde{p}_i| = 1, \tag{3.56}$$

which implies that the projector functions must be orthonormal to the pseudo partial wave functions $\widetilde{\phi}_i$.

4 Geometry Optimisation

Whether one uses quantum chemical methods or simple two-body potentials to investigate the properties of molecules and clusters, finding the coordinates of all atoms that minimise the chosen energy function is almost always the starting point of all calculations. Methods for geometry optimisation have been used in all parts of this thesis and will therefore be explained in more detail in the following chapters. If not mentioned otherwise the theory is based on Fletcher's[53] introductory book.

Finding the set of coordinates $\mathbf{x} \in \mathbb{R}^N$ that minimise a given energy function is an optimisation problem. There are a multitude of methods available that are all suited for different types of problems. In the following sections the theory of local minimisation will be discussed in terms of a general objective function f that can be replaced with any continuous energy function.

4.1 General Considerations about Minima

The *objective function* f is said to have a minimum value (or simply *minimum*) at the set of coordinates $\mathbf{x}^*$, which is called a *minimiser* of the objective function f. Usually, optimisation procedures locate local minimisers, while the problem of finding global minimisers is considerably more difficult and requires clever algorithms. General definitions of local minimisers can be formulated in form of *strict local minimisers* ($f(\mathbf{x}) > f(\mathbf{x}^*)$) or *isolated local minimisers* ($\mathbf{x}^*$ is the only local minimiser in its neighbourhood).

The definition becomes simpler when one only considers smooth functions as the minimisers can be characterised in terms of first and second derivatives. A smooth function needs to be continuous and continuously differentiable, therefore, a vector of first partial derivatives $\nabla f(\mathbf{x}) = \mathbf{g}(\mathbf{x})$ must exist for any $\mathbf{x}$.

$$\nabla f(\mathbf{x}) = \begin{pmatrix} \partial f/\partial x_1 \\ \partial f/\partial x_2 \\ \vdots \\ \partial f/\partial x_n \end{pmatrix} \tag{4.1}$$

A twice continuously differentiable function additionally allows for the definition of a matrix of second partial derivatives $\nabla^2 f(\mathbf{x}) = \mathbf{G}(\mathbf{x})$ also called a

Hessian matrix.

$$\nabla^2 f(\mathbf{x}) = \begin{pmatrix} \partial^2 f(\mathbf{x})/\partial {x_1}^2 & \partial^2 f(\mathbf{x})/\partial x_1 \partial x_2 & \dots & \partial^2 f(\mathbf{x})/\partial x_1 \partial x_n \\ \partial^2 f(\mathbf{x})/\partial x_2 \partial x_1 & \partial^2 f(\mathbf{x})/\partial {x_2}^2 & \dots & \partial^2 f(\mathbf{x})/\partial x_2 \partial x_n \\ \vdots & \vdots & \ddots & \vdots \\ \partial^2 f(\mathbf{x})/\partial x_n \partial x_1 & \partial^2 f(\mathbf{x})/\partial x_n \partial x_2 & \dots & \partial^2 f(\mathbf{x})/\partial {x_n}^2 \end{pmatrix} \tag{4.2}$$

Most interatomic potentials have smooth potential energy landscapes, which justifies this simplification.

To derive conditions for a point to be a local minimiser consider any line through the minimiser $\mathbf{x}^*$:

$$\mathbf{x}(\alpha) = \mathbf{x}^* + \alpha \mathbf{s}. \tag{4.3}$$

Using the chain rule the derivative $\frac{\mathrm{d}f}{\mathrm{d}\alpha}$ can be expressed as $\frac{\mathrm{d}f}{\mathrm{d}\alpha} = \mathbf{s}^{\mathrm{T}} \nabla f$.[a] At $\mathbf{x}^*$ ($\alpha = 0$) the objective function f has a slope of zero and a non-negative curvature, which means $\mathbf{s}^{\mathrm{T}} \nabla f(\mathbf{x}^*) = 0$. Following the same argument for the second derivative a second condition $\mathbf{s}^{\mathrm{T}} \nabla^2 f(\mathbf{x}^*) \mathbf{s} \geq 0$ can be derived. As these conditions must be true for all $\mathbf{s}$ we can for example consider the case $\mathbf{s} = \mathbf{e_1}$, with $\mathbf{e_1}$ being a unit vector, to see that

$$\mathbf{g}^* = 0 \tag{4.4}$$

$$\mathbf{s}^{\mathrm{T}} \mathbf{G}^* \mathbf{s} \geq 0. \tag{4.5}$$

Note that $\mathbf{g}^* = \mathbf{g}(\mathbf{x}^*)$ and $\mathbf{G}^* = \mathbf{G}(\mathbf{x}^*)$ are used to simplify the notation. In the following sections this short hand notation will also be extended to the objective function f and general points $\mathbf{x}^{(k)}$, i.e. $f^{(k)}, \mathbf{g}^{(k)}, \mathbf{G}^{(k)}, \dots = f\left(\mathbf{x}^{(k)}\right), \mathbf{g}\left(\mathbf{x}^{(k)}\right), \mathbf{G}\left(\mathbf{x}^{(k)}\right), \dots$.

Equations (4.4) and (4.5) are necessary (but not sufficient) conditions for local minimisers. In fact, as equation (4.4) is derived from first-order variations in f it is considered a first order necessary condition, while equation (4.5) is considered a second-order necessary condition. It can be shown that sufficient conditions for local minimisers are equation (4.4) and $\mathbf{s}^{\mathrm{T}} \mathbf{G}^* \mathbf{s} > 0$.[53] The reason for this minor change for the second-order condition is that equation (4.5) also holds true for points of zero curvature. In other words the sufficient conditions for a local minimiser are the gradient to be zero and the Hessian matrix to be positive definite at $\mathbf{x}^*$.

In practice, minimisation schemes usually locate $\mathbf{x}^*$ that only fulfil the first condition $\mathbf{g}^* = 0$. As those points can either refer to minima, maxima or saddle points they are called stationary points. A located stationary point has to be checked for his character, but it is usually not feasible to check equation (4.5) as it can not be checked numerically. In this work the eigenvalues of $\mathbf{G}^*$ are used to verify local minimisers, which have to be positive.

[a] $\frac{\mathrm{d}}{\mathrm{d}\alpha} = \sum_i \frac{\mathrm{d}}{\mathrm{d}\alpha} x_i(\alpha) \frac{\partial}{\partial x_i} = \sum_i s_i \frac{\partial}{\partial x_i} = \mathbf{s}^{\mathrm{T}} \nabla$

4.2 Properties of Optimisation Algorithms

To have any practical usefulness an iterative optimisation algorithm should obey a few requirements. For instance, the algorithm should move steadily towards the local minimiser $\mathbf{x}^*$ and converge quickly to a user-defined convergence criterion. The rate of convergence, decisive for the performance of the algorithm, can be quantified by defining the error

$$\Delta\mathbf{x}^{(k)} = \mathbf{x}^{(k)} - \mathbf{x}^*. \tag{4.6}$$

Here, $\mathbf{x}^{(k)}$ denotes the kth iterate with $\mathbf{x}^{(1)}$ referring to the starting point of the iterative procedure. The local convergence rate can then be given as the fraction of the Euclidean norm $||\cdot||$ of the errors of consecutive steps.

$$\frac{\left|\left|\Delta\mathbf{x}^{(k+1)}\right|\right|}{\left|\left|\Delta\mathbf{x}^{(k)}\right|\right|^p} \leq a,\ a > 0 \tag{4.7}$$

The rate of convergence a must be positive and p defines the order of convergence, most importantly linear convergence ($p = 1$) and quadratic convergence ($p = 2$). An algorithm is generally desired to convergence quadratically towards $\mathbf{x}^*$, however, linear convergence can be acceptable in case the rate constant is low.

An optimisation algorithm is usually based on a model that approximates the objective function and allows for the prediction of the location of $\mathbf{x}^*$. The methods used in this work belong to the group of quadratic models and use a line search approach to locate the local minimiser. Focus will therefore be put on this kind of approach. The idea of a line search relies on a user-defined starting point $\mathbf{x}^{(1)}$ and is restricted to search for a minimiser along coordinate directions. In a line search procedure the kth iteration requires

1. to determine the search direction $\mathbf{s}^{(k)}$,
2. minimise $f\left(\mathbf{x}^{(k)} + \alpha\mathbf{s}^{(k)}\right)$ with respect to α and
3. to set the new iterate $\mathbf{x}^{(k+1)} = \mathbf{x}^{(k)} + \alpha^{(k)}\mathbf{s}^{(k)}$.

Step 1 depends on the chosen method, while step 2 is independent of the chosen method and corresponds to the line search step. Step 2 is solved by sampling $f(\mathbf{x})$ along the line $\mathbf{s}^{(k)}$ and, in practice, needs to be terminated when a convergence criterion is met. This is because an exact line-search, which corresponds to sampling $f\left(\mathbf{x}^{(k)} + \alpha\mathbf{s}^{(k)}\right)$ until the true minimum has been found, is not possible to be implemented with a finite amount of steps. Especially for points far from $\mathbf{x}^*$ it is sensible to choose loose convergence criteria and tighten them around $\mathbf{x}^*$.

The line-search convergence criterion is usually not a user-defined value, however, the termination criterion ε of the optimisation procedure needs to

be supplied by the user. There are several possibilities of choosing a convergence test with the most obvious approach being to test for convergence in the minimum value $f^{(k)} - f^* \leq \varepsilon$ or the minimiser itself $\left|x_i^{(k)} - x_i^*\right| \leq \varepsilon_i$. However, these criteria require knowledge of exact minimiser or minimum value of the objective function and it is easy to see, that this is paradoxical. A more useful criterion can be based on the Euclidean norm of the gradient at the kth iterate

$$\left|\left|\mathbf{g}^{(k)}\right|\right| \leq \varepsilon. \tag{4.8}$$

4.3 Quadratic Models

An optimisation method is said to be derived from a quadratic model if the method approximates the objective function by a quadratic function around the minimiser. A quadratic model has to be applied iteratively to a general function to lead to convergence. Applied to a quadratic function it can be shown that it should locate the minimiser in a finite amount of steps. The use of a quadratic model has several advantages and most successful methods are based on it. The most obvious way to derive a quadratic model is probably by using information from both the gradient and the second derivatives, which gives rise to the Newton-Raphson method (or quasi-Newton-Raphson if second derivatives are estimated). However, it is possible to build a quadratic method without using second derivatives and one such example is the conjugate gradient method.

4.3.1 Newton-like Methods

As mentioned above, a quadratic model can be derived by including information from the second derivatives, which in the case of Newton-like methods is achieved by truncating a Taylor expansion of the objective function around the iterate minimiser $\mathbf{x}^{(k)}$.

$$f\left(\mathbf{x}^{(k)} + \boldsymbol{\delta}\right) \approx q^{(k)}(\boldsymbol{\delta}) = f^{(k)} + \mathbf{g}^{(k)^{\mathbf{T}}}\boldsymbol{\delta} + \frac{1}{2}\boldsymbol{\delta}^{\boldsymbol{T}}\mathbf{G}^{(k)}\boldsymbol{\delta} \tag{4.9}$$

Here, $\boldsymbol{\delta} = \mathbf{x} - \mathbf{x}^{(k)}$ and $q^{(k)}(\boldsymbol{\delta})$ is the quadratic approximation of the objective function around $\mathbf{x}^*$. The next step in the optimisation $\mathbf{x}^{(k+1)}$ is then chosen based on $\boldsymbol{\delta} = \boldsymbol{\delta}^{(k)}$ which minimises $q^{(k)}(\boldsymbol{\delta})$. It can be shown, that the derivative $\nabla q^{(k)}(\boldsymbol{\delta})$ can be expressed as

$$\nabla q^{(k)}(\boldsymbol{\delta}) = \mathbf{G}^{(k)}\boldsymbol{\delta} + \mathbf{g}^{(k)}, \tag{4.10}$$

and it is said to be 0 at $\boldsymbol{\delta} = \boldsymbol{\delta}^{(k)}$. The last condition results in $n \times n$ linear equations that can be solved programmatically, and the result can be used to construct the next iterate $\mathbf{x}^{(k+1)} = \mathbf{x}^{(k)} + \boldsymbol{\delta}^{(k)}$.

In practice Newton's method is usually implemented in combination with a line-search algorithm. Because it is not guaranteed that the iterates $\left\{f^{(k)}\right\}$ decrease towards the minimum value, it can be useful to define the direction of search as

$$\mathbf{s}^{(k)} = -{\mathbf{G}^{(k)}}^{-1}\mathbf{g}^{(k)}. \tag{4.11}$$

If $\mathbf{G}$ is positive definite so is $\mathbf{G}^{-1}$ and $\mathbf{s}$ is a descent direction.

Problems arise if $\mathbf{G}$ is not positive definite, which can happen if the current iterator is far from the local minimiser. In that case it is still possible to calculate a search direction and search along positive and negative direction to find a lower $f^{(k)}$. This means, however, that the approximating quadratic function does not necessarily possess the same minimum as the objective function. One possible solution proposed by Goldstein and Price[54] is to iterate in a steepest descent direction $\mathbf{s}^{(k)} = -\mathbf{g}^{(k)}$ in case the Hessian matrix is not positive definite. Nonetheless, this method is prone to oscillatory behaviour that would be introduced into the optimisation iteration.

If the Hessian matrix is almost positive definite a feasible approach might be to modify $\mathbf{G}^{(k)}$ to make it positive definite. A better search direction can be defined by adding a small multiple ν of a unit matrix $\mathbf{I}$.[55–57]

$$\mathbf{s}^{(k)} = -\left(\mathbf{G}^{(k)} + \nu\mathbf{I}\right)^{-1}\mathbf{g}^{(k)} \tag{4.12}$$

In this approach the quadratic information is still used, but no oscillatory behaviour is being introduced. Instead of modifying the Hessian matrix with multiples of the unit matrix it can also be modified more generally with a diagonal matrix $\mathbf{D}$, which is advantageous in case the Hessian matrix is indefinite.[58,59]

Finally, the problem can be solved by computing a negative curvature descent direction by solving

$${\mathbf{s}^{(k)}}^{\mathbf{T}}\mathbf{G}^{(k)}\mathbf{s}^{(k)} < 0 \tag{4.13}$$

$${\mathbf{s}^{(k)}}^{\mathbf{T}}\mathbf{g}^{(k)} \leq 0 \tag{4.14}$$

for $\mathbf{s}^{(k)}$.[60]

4.3.2 Quasi-Newton Methods

Especially for quantum chemical potentials like Hartree-Fock or density functional theory potentials the evaluation of a full Hessian matrix can be very computationally expensive. It can therefore be useful to just use an approximation for the Hessian matrix. In the most simple case this results in a finite

difference Newton method where $\mathbf{G}^{(k)}$ is approximated in terms of differences of the gradient vector with respect to each coordinate direction $\mathbf{e_i}$.

$$\mathbf{\Delta g_i^{(k)}} = \frac{1}{h_i}\left[\mathbf{g}\left(\mathbf{x}^{(k)} + h_i\mathbf{e_i}\right) - \mathbf{g}^{(k)}\right] \tag{4.15}$$

$$\mathbf{G}^{(k)} \approx \overline{\mathbf{G}} = \begin{pmatrix}\mathbf{\Delta g_1^{(k)}} & \mathbf{\Delta g_2^{(k)}} & \cdots & \mathbf{\Delta g_n^{(k)}}\end{pmatrix} \tag{4.16}$$

The approximated matrix needs to be symmetrised by calculating $\frac{1}{2}\left(\overline{\mathbf{G}} + \overline{\mathbf{G}}^{\mathbf{T}}\right)$. However, this approach has some disadvantages, e.g. the symmetrised matrix is not guaranteed to be positive definite and for the calculation of $\overline{\mathbf{G}}$ the gradient has to be evaluated n times making this approximation potentially as expensive as the exact Hessian calculation.

The class of quasi-Newton methods tries to avoid these problems by approximating ${\mathbf{G}^{(k)}}^{-1}$ with a symmetric positive definite matrix $\mathbf{H}^{(k)}$, which can then be updated in each iteration. The kth iteration of a quasi-Newton optimisation requires to

1. determine the search direction $\mathbf{s}^{(k)} = -\mathbf{H}^{(k)}\mathbf{g}^{(k)}$,
2. minimise $f\left(\mathbf{x}^{(k)} + \alpha\mathbf{s}^{(k)}\right)$ in a line-search procedure,
3. set the new iterate $\mathbf{x}^{(k+1)} = \mathbf{x}^{(k)} + \alpha^{(k)}\mathbf{s}^{(k)}$ and
4. update $\mathbf{H}^{(k)}$.

The initial choice of $\mathbf{H}^{(1)}$ is not important as long as the matrix is symmetric and positive definite. Simply choosing a unit matrix is sufficient, which turns the first step of the optimisation into a steepest descent step as $\mathbf{s}^{(k)} = -\mathbf{g}^{(k)}$.

The method is practically identical with a line-search Newton-like method, with the difference being the representation of the matrix of second derivatives. The step in the procedure that defines and updates $\mathbf{H}^{(k)}$ is therefore very important for quasi-Newton methods. The goal is that updating $\mathbf{H}^{(k)}$ in each iteration to $\mathbf{H}^{(k+1)}$ results in a good approximation for ${\mathbf{G}^{(k)}}^{-1}$. Using equation (4.10) and choosing $\mathbf{x} = \mathbf{x}^{(k+1)}$ such that $\boldsymbol{\delta}^{(k)} = \mathbf{x}^{(k+1)} - \mathbf{x}^{(k)}$ it is easy to see that in the quadratic approximation the difference between the gradient vectors $\boldsymbol{\gamma}^{(k)} = \mathbf{g}^{(k+1)} - \mathbf{g}^{(k)}$ is mapped to the distance vector between the points by the Hessian matrix.

$$\boldsymbol{\gamma}^{(k)} = \mathbf{G}^{(k)}\boldsymbol{\delta}^{(k)} \tag{4.17}$$

However, $\mathbf{x}^{(k)}$ is only known after the line-search completed, which means that $\mathbf{H}^{(k)}$ (the inverse of $\mathbf{G}^{(k)}$) does not map them properly. Yet, this relation can be used to improve the approximated inverse Hessian matrix for the next step $\mathbf{H}^{(k+1)}$.

$$\mathbf{H}^{(k+1)}\boldsymbol{\gamma}^{(k)} = \boldsymbol{\delta}^{(k)} \tag{4.18}$$

This is the so-called quasi-Newton condition and the differences in different quasi-Newton methods lie within the way this condition is fulfilled computationally.

One way to generate $\mathbf{H}^{(k+1)}$ is to update $\mathbf{H}^{(k)}$ by adding a symmetric rank one matrix $\mathbf{E}^{(k)} = a\mathbf{u}\mathbf{u}^\mathbf{T}$.

$$\mathbf{H}^{(k+1)} = \mathbf{H}^{(k)} + a\mathbf{u}\mathbf{u}^\mathbf{T} \tag{4.19}$$

Using equation (4.18) it can be seen that $\mathbf{u}$ is proportional to $\boldsymbol{\delta}^{(k)} - \mathbf{H}^{(k)}\boldsymbol{\gamma}^{(k)}$ with a proportionality constant of $a\mathbf{u}^\mathbf{T}\boldsymbol{\gamma}^{(k)}$. Since the proportionality can just be chosen to be one by changing a, it follows that $\mathbf{u} = \boldsymbol{\delta}^{(k)} - \mathbf{H}^{(k)}\boldsymbol{\gamma}^{(k)}$ and hence the formula for updating $\mathbf{H}^{(k)}$ can be expressed as

$$\mathbf{H}^{(k+1)} = \mathbf{H} + \frac{(\boldsymbol{\delta} - \mathbf{H}\boldsymbol{\gamma})(\boldsymbol{\delta} - \mathbf{H}\boldsymbol{\gamma})^\mathbf{T}}{(\boldsymbol{\delta} - \mathbf{H}\boldsymbol{\gamma})^\mathbf{T}\boldsymbol{\gamma}}. \tag{4.20}$$

The superscript (k) has been omitted on the right sight to improve readability and this notation will be adopted for following update formulae as well. Originally, this formula was proposed by multiple people independently.[60–62] It is natural to assume that this formula could be improved by introducing a second independent change to $\mathbf{H}^{(k)}$.

$$\mathbf{H}^{(k+1)} = \mathbf{H}^{(k)} + a\mathbf{u}\mathbf{u}^\mathbf{T} + b\mathbf{v}\mathbf{v}^\mathbf{T} \tag{4.21}$$

Unfortunately, the expressions for $\mathbf{u}$ and $\mathbf{v}$ can not be established as easily as before. However, $\mathbf{u} = \boldsymbol{\delta}^{(k)}$ and $\mathbf{v} = \mathbf{H}^{(k)}\boldsymbol{\gamma}^{(k)}$ have shown to be sensible choices and give rise to the Davidon-Fletcher-Powell (DFP) formula.[63,64]

$$\mathbf{H}^{(k+1)}_{\mathbf{DFP}} = \mathbf{H} + \frac{\boldsymbol{\delta}\boldsymbol{\delta}^\mathbf{T}}{\boldsymbol{\delta}^\mathbf{T}\boldsymbol{\gamma}} - \frac{\mathbf{H}\boldsymbol{\gamma}\boldsymbol{\gamma}^\mathbf{T}\mathbf{H}}{\boldsymbol{\gamma}^\mathbf{T}\mathbf{H}\boldsymbol{\gamma}} \tag{4.22}$$

The probably most successful quasi-Newton method is based on the Broyden-Fletcher-Goldfarb-Shanno (BFGS) formula,[65–69] which is closely related to the DFP formula.

$$\mathbf{H}^{(k+1)}_{\mathbf{BFGS}} = \mathbf{H} + \left(1 + \frac{\boldsymbol{\gamma}^\mathbf{T}\mathbf{H}\boldsymbol{\gamma}}{\boldsymbol{\delta}^\mathbf{T}\boldsymbol{\gamma}}\right)\frac{\boldsymbol{\delta}\boldsymbol{\delta}^\mathbf{T}}{\boldsymbol{\delta}^\mathbf{T}\boldsymbol{\gamma}} - \left(\frac{\boldsymbol{\delta}\boldsymbol{\gamma}^\mathbf{T}\mathbf{H} + \mathbf{H}\boldsymbol{\gamma}\boldsymbol{\delta}^\mathbf{T}}{\boldsymbol{\delta}^\mathbf{T}\boldsymbol{\gamma}}\right) \tag{4.23}$$

The relation can be illustrated by denoting $\mathbf{H}^{-1}$ as $\mathbf{B}$ and substitute in equation (4.23).

$$\mathbf{B}^{(k+1)}_{\mathbf{BFGS}} = \mathbf{B} + \frac{\boldsymbol{\gamma}\boldsymbol{\gamma}^\mathbf{T}}{\boldsymbol{\gamma}^\mathbf{T}\boldsymbol{\delta}} - \frac{\mathbf{B}\boldsymbol{\delta}\boldsymbol{\delta}^\mathbf{T}\mathbf{B}}{\boldsymbol{\delta}^\mathbf{T}\mathbf{H}\boldsymbol{\delta}} \tag{4.24}$$

The similarity to equation (4.22) is obvious. Because both formulae are related by exchanging $\boldsymbol{\gamma} \leftrightarrow \boldsymbol{\delta}$ and $\mathbf{B} \leftrightarrow \mathbf{H}$, they are called dual or complementary.

In quantum chemistry an improvement of the BFGS method (or any optimisation method) can be achieved by defining internal redundant coordinates $\mathbf{q}$ based on bond lengths, angles and dihedral angles.[70–72] The transformation from the cartesian to the internal redundant coordinate space can be carried out using the Wilson $\mathbf{W}$ matrix, which is defined in terms of the displacements in internal redundant $\Delta\mathbf{q}$ and cartesian coordinates $\Delta\mathbf{x}$.

$$\Delta\mathbf{q} = \mathbf{W}\Delta\mathbf{x} \tag{4.25}$$

This can be used to transform the gradient vector and Hessian matrix into internal redundant coordinates.

$$\mathbf{W}^\mathbf{T}\mathbf{g}_q = \mathbf{g}_x \tag{4.26}$$

$$\mathbf{W}^\mathbf{T}\mathbf{H}_q\mathbf{W} + \mathbf{W}'^\mathbf{T}\mathbf{g}_q = \mathbf{H}_x \tag{4.27}$$

The first derivative of the Wilson matrix $\mathbf{W}'$ is calculated analytically. It was shown that this approach can reduce the number of steps needed to optimise various organic molecules significantly.[73]

4.3.3 Conjugate Gradient Methods

The origin of the Newton-like and quasi-Newton methods being the quadratic model is conceptually obvious. There are however methods that belong to this group, but don't rely on calculating or approximating a matrix of second derivatives. One of those methods is the conjugate gradient method. As the name suggests, they take advantage of the concept of conjugacy of the search vectors $\mathbf{s}^{(1)}, \mathbf{s}^{(2)}, \ldots, \mathbf{s}^{(n)}$ and the Hessian matrix $\mathbf{G}$, i.e.

$$\mathbf{s}^{(i)^\mathbf{T}}\mathbf{G}\mathbf{s}^{(j)} = 0,\ \forall i \neq j. \tag{4.28}$$

It should be noted that quadratic termination is only guaranteed for exact line searches. The conjugate gradient method tries to combine the conjugacy property with the steepest descent method, therefore the first step is equal to

$$\mathbf{s}^{(1)} = -\mathbf{g}^{(k)} \tag{4.29}$$

and for successive iterations

$$\mathbf{s}^{(k+1)} = \text{component of } -\mathbf{g}^{(k+1)} \text{conjugate to } \mathbf{s}^{(1)}, \mathbf{s}^{(2)}, \ldots, \mathbf{s}^{(n)}. \tag{4.30}$$

From the conjugacy condition (4.28) it follows that $\mathbf{s}^{(k+1)}$ can be calculated from a Gram-Schmidt orthonormalisation.

$$\mathbf{s}^{(k+1)} = -\mathbf{g}^{(k+1)} + \beta^{(k)}\mathbf{s}^{(k)} \tag{4.31}$$

$$\beta^{(k)} = \frac{\mathbf{g}^{(k+1)^\mathbf{T}}\mathbf{g}^{(k+1)}}{\mathbf{g}^{(k)^\mathbf{T}}\mathbf{g}^{(k)}} \tag{4.32}$$

This is also known as the Fletcher-Reeves (FR) method.[74] One advantage of the FR method over the quasi-Newton methods is that it does not need any matrix calculation, which can be seen in equation (4.32). However, the procedure is not guaranteed to terminate for non-quadratic functions. There are several ways that try to resolve this disadvantage, one of which is a simple reset of the search direction to the steepest descent direction. If the iterates converge towards a region that is approximated well by a quadratic function, then a reset of the search direction may improve the overall convergence of the method.

Another solution to the aforementioned problem is to use a different expression for $\beta^{(k)}$. One possible modification is

$$\beta^{(k)} = -\frac{\mathbf{g}^{(k+1)^{\mathbf{T}}}\mathbf{g}^{(k+1)}}{\mathbf{g}^{(k)^{\mathbf{T}}}\mathbf{s}^{(k)}}, \tag{4.33}$$

which results in a stronger descent property $\mathbf{s}^{(k)^{\mathbf{T}}}\mathbf{g}^{(k)} < 0$. Another notable mention is the formula by Polak and Ribiere[75] shown in equation (4.34).

$$\beta^{(k)} = \frac{\left(\mathbf{g}^{(k+1)} - \mathbf{g}^{(k)}\right)^{\mathbf{T}}\mathbf{g}^{(k+1)}}{\mathbf{g}^{(k)^{\mathbf{T}}}\mathbf{g}^{(k)}} \tag{4.34}$$

4.4 Implementation for Two-Body Interaction Potentials

In the special case of optimising the geometry of a collection of objects in three-dimensional space that interact via a given potential some modifications have to be made to use the previously described methods. In the following paragraphs the mathematical background for the implementation of potentials that only depend on the distance between two objects like Lennard-Jones (LJ) and extended Lennard-Jones (eLJ) for the program Spheres (chapter 6) is explained. The physical objects in this case are called spheres and the optimisation procedure tries to locate the minimiser corresponding to the lowest total energy of the system.

Let $\mathbf{x}_i$ be the Cartesian coordinates of sphere i and the collection of all the coordinates of all N spheres in the system shall be denoted $\mathbf{X}$.

$$\begin{aligned} \mathbf{X} = \begin{pmatrix} \mathbf{x}_1 & \mathbf{x}_2 & \cdots & \mathbf{x}_N \end{pmatrix} &= \begin{pmatrix} x_1 & x_4 & \cdots & x_{3N-2} \\ x_2 & x_5 & \cdots & x_{3N-1} \\ x_3 & x_6 & \cdots & x_{3N} \end{pmatrix} \\ \mathbf{x}_i &= \begin{pmatrix} x_{3i-2} \\ x_{3i-1} \\ x_{3i} \end{pmatrix} \end{aligned} \tag{4.35}$$

The distance between two spheres i and j is now given by the norm r_{ij} of the distance vector $\mathbf{r}_{ij}$.

$$\mathbf{r}_{ij} = \mathbf{x}_i - \mathbf{x}_j = \begin{pmatrix} x_{3i-2} - x_{3j-2} \\ x_{3i-1} - x_{3j-1} \\ x_{3i} - x_{3j} \end{pmatrix} \tag{4.36}$$

$$|\mathbf{r}_{ij}| = r_{ij} = \sqrt{(x_{3i-2} - x_{3j-2})^2 + (x_{3i-1} - x_{3j-1})^2 + (x_{3i} - x_{3j})^2} \tag{4.37}$$

The energy of the system is a function of all sphere coordinates $\mathbf{X}$, but it can be rewritten in terms of an energy function $\varepsilon(r_{ij})$ that only depends on the distance between two spheres.

$$E(\mathbf{X}) = \sum_{i}^{N} \sum_{j>i}^{N} \varepsilon(r_{ij}) \tag{4.38}$$

The gradient of the system is a vector of $3N$ scalars, where each component refers to the gradient with respect to each coordinate x. The derivative with respect to the mth coordinate x_m can be expressed as in equation (4.39) by using the chain rule for derivatives.

$$\frac{\partial E(\mathbf{X})}{\partial x_m} = \sum_{i}^{N} \sum_{j>i}^{N} \frac{\partial \varepsilon(r_{ij})}{\partial r_{ij}} \frac{\partial r_{ij}}{\partial \mathbf{r}_{ij}} \frac{\partial \mathbf{r}_{ij}}{\partial x_m} \tag{4.39}$$

It is clear, that the terms that contain vectors are separated from the energy function. This means that the energy term can be exchanged easily without having to change all parts of the routine. The first term represents the derivative of the energy function with respect to the distance between two spheres. The second term can be rewritten in terms of the normalised form of the distance vector $\mathbf{r}_{ij}$, which follows directly from equations (4.36) and (4.37).

$$\frac{\partial r_{ij}}{\partial \mathbf{r}_{ij}} = \frac{\mathbf{r}_{ij}}{r_{ij}} \tag{4.40}$$

The last term is responsible for the right sign of the gradient component and is best explained by giving an example. Firstly, if x_m is neither in sphere i nor in j its result is a zero vector making the whole expression vanishes. Let's assume $m = 3i + 1$, then the last expression becomes:

$$\frac{\partial \mathbf{r}_{ij}}{\partial x_{3i-1}} = \begin{pmatrix} 0 \\ 1 \\ 0 \end{pmatrix}. \tag{4.41}$$

For this example the inner product of this vector with the normalised distance vector $\mathbf{r}_{ij}$ is $\frac{1}{r_{ij}}(x_{3i-1} - x_{3j-1})$. Therefore, the last term ensures that the mth component of the gradient vector only collects contributions from interactions between spheres that contain the coordinate x_m. If x_m was a coordinate present in sphere j the last term swaps the sign of the gradient. This is a result of the fact, that the gradient at sphere j should be opposite of the gradient at sphere i. The final gradient is given by calculating all partial derivatives with respect to x_m.

$$\nabla E(\mathbf{X}) = \begin{pmatrix} \partial E(\mathbf{X})/\partial x_1 \\ \partial E(\mathbf{X})/\partial x_2 \\ \vdots \\ \partial E(\mathbf{X})/\partial x_{3N} \end{pmatrix} \tag{4.42}$$

The separation of the vector and scalar components allows for easy exchange of the energy functions as the calculations that take care of the direction of the gradient can be completely separated out.

The same procedure can be applied to the second derivative to calculate a Hessian matrix. Again, the important part is to separate the scalar energy function from vector parts. This leads to the following equations.

$$\frac{\partial^2 E(\mathbf{X})}{\partial x_m \partial x_n} = \sum_i^N \sum_{j>i}^N \left[\begin{array}{l} \frac{\partial^2 \varepsilon(r_{ij})}{\partial {r_{ij}}^2} \frac{\partial r_{ij}}{\partial \mathbf{r}_{ij}} \frac{\partial \mathbf{r}_{ij}}{\partial x_m} \frac{\partial r_{ij}}{\partial \mathbf{r}_{ij}} \frac{\partial \mathbf{r}_{ij}}{\partial x_n} \\ + \frac{\partial \varepsilon(r_{ij})}{\partial r_{ij}} \frac{\partial^2 r_{ij}}{\partial {\mathbf{r}_{ij}}^2} \frac{\partial \mathbf{r}_{ij}}{\partial x_m} \frac{\partial \mathbf{r}_{ij}}{\partial x_n} \end{array} \right] \tag{4.43}$$

$$\nabla^2 E(\mathbf{X}) =$$

$$\begin{pmatrix} \partial^2 E(\mathbf{X})/\partial {x_1}^2 & \partial^2 E(\mathbf{X})/\partial x_1 \partial x_2 & \dots & \partial^2 E(\mathbf{X})/\partial x_1 \partial x_{3N} \\ \partial^2 E(\mathbf{X})/\partial x_2 \partial x_1 & \partial^2 E(\mathbf{X})/\partial {x_2}^2 & \dots & \partial^2 E(\mathbf{X})/\partial x_2 \partial x_{3N} \\ \vdots & \vdots & \ddots & \vdots \\ \partial^2 E(\mathbf{X})/\partial x_{3N} \partial x_1 & \partial^2 E(\mathbf{X})/\partial x_{3N} \partial x_2 & \dots & \partial^2 E(\mathbf{X})/\partial {x_{3N}}^2 \end{pmatrix} \tag{4.44}$$

4.5 Global Optimisation

In the most simple case, the objective function possesses only one (global) minimum. However, in a real scenario, like in a cluster or molecule bound by a physical interaction potential, there can be many local minima connected by first order stationary points. Knowledge about the nature and location of first- and higher-order stationary points is crucial for a thorough understanding of the topology of the underlying system. The global minimum is an important information as it represents the most likely configuration of the system and efforts are usually focussed on locating this particular arrangement. As this requires the whole configuration space to be scanned, local minima will also be located with global optimisation methods as a side effect. Such global

optimisation problems belong to the complexity class of "NP-complete" problems, meaning no algorithm is currently known that is guaranteed to find a solution within a time scaling as a power of the system size. However, a multitude of heuristic global optimisation algorithms have been proposed and a few selected ones will be discussed briefly in the following sections.

4.5.1 Algorithms

If the potential hypersurface of a system is completely unknown, the *eigenvector following* method can be used to gain valuable insights into its nature. It was first developed as a transition state location method,[76] but can be applied to global optimisation problems by repeating the process and following all eigenmodes of the system. It makes use of a modified Newton-Raphson step,[b] which requires the matrix of second derivatives $\mathbf{G}$ to be calculated.

$$\Delta\mathbf{s} = (\lambda\mathbf{1} - \mathbf{G})^{-1} \cdot \mathbf{g} \tag{4.45}$$

$$\Delta^2 = \Delta\mathbf{s} \cdot \Delta\mathbf{s} = \mathbf{g} \cdot (\lambda\mathbf{1} - \mathbf{G})^{-1} \cdot \mathbf{g} \tag{4.46}$$

Here, $\mathbf{1}$ and $\mathbf{g}$ are the identity matrix and the gradient vector, respectively. The Lagrange multiplier λ was introduced to minimise the objective function under the constraint of a medium sized step size Δ^2 and needs to be determined according to equation (4.46). After λ is calculated it can be used to calculate the actual step $\Delta\mathbf{s}$ via equation (4.45). This step will then move upwards in energy instead of downwards, effectively moving away from a local minimum towards a saddle point. This will make the lowest eigenvalue of the Hessian matrix negative, and the corresponding eigenvector represents the reaction coordinate of this deformation. Close to the saddle point the standard Newton-Raphson step is the most efficient choice for convergence towards the stationary point and it can be easily seen that this follows from equation (4.45) for $\lambda = 0$. This procedure can be implemented to scan a hypersurface.[77] Starting from any distribution of coordinates a standard geometry optimisation can be carried out to find a minimum of the hypersurface. From there, the modified Newton-Raphson method can be used to find the closest saddle point. Calculating and diagonalising the Hessian matrix at this point should lead to one negative eigenvalue and the eigenvector corresponding to this eigenvalue should lead to at least one unknown structure. From there on the procedure can start from the beginning, moving to larger eigenvalues.

One of the first global optimisation algorithms was the *simulated annealing* algorithm.[78] The name is related to the fact that the method is strongly connected to statistical thermodynamics by introducing an effective

[b] The normal Newton-Raphson step is shown in equation (4.11).

temperature parameter that allows for the simulation of a slow cooling procedure. The effective temperature is simply a control parameter in the units of the objective function and should not be equated to a real temperature. In the procedure the particles are moved by a small random displacement and the energy of the result is calculated. Whether this step is accepted is decided by the Metropolis criterion.[79] If the difference in the value of the objective function Δf of the new configuration to the previous one is negative, it is accepted as the next step. If the difference is positive it is accepted with a probability P of

$$P = \exp\left\{-\frac{\Delta f}{kT}\right\}. \tag{4.47}$$

Repetition of this step is equivalent to simulating a system of particles in a heat bath at the effective temperature T and leads to the system to be represented by a Boltzmann distribution. This procedure is first carried out at a high temperature, effectively simulating a "melted" state of the system. Subsequently, the temperature is reduced in small steps until the system "freezes", meaning a steady state is reached. In comparison to a purely iterative method, simulated annealing has the advantage of not getting stuck in local minima as it is always possible to transition out of a local minimum at non-zero temperature. To locate the global minimum with a simulated annealing method the temperature needs to decrease logarithmically with time, which makes this method computationally rather expensive. The rate at which the temperature decreases is called an annealing schedule and is usually chosen empirically.

Basin-hopping is a hypersurface transformation method and has been applied successfully to global optimisation problems.[80–82] It was first used to solve multiple-minima problems in protein folding.[83] The transformation of the hypersurface upon which the particles move is carried out by applying a geometry optimisation to some point in configuration space as outlined in the sections above. This effectively maps the chosen point in configuration space to a (local) minimum.

$$\widetilde{f} : (\mathbf{X}) \mapsto \min\{f : (\mathbf{X})\} \tag{4.48}$$

The result is a hypersurface that is divided into basins of attraction, while preserving the information about the energies of the minima. An illustration of this process is depicted in figure 4.1. The mapping procedure is usually combined with a Monte-Carlo-type sampling procedure.[80] A new sample is created by introducing a small random displacement, analogous to the simulated annealing approach, followed by a geometry optimisation. The acceptance of the result is, again, determined by the Metropolis criterion. The effect of the transformation is that transition states are removed from

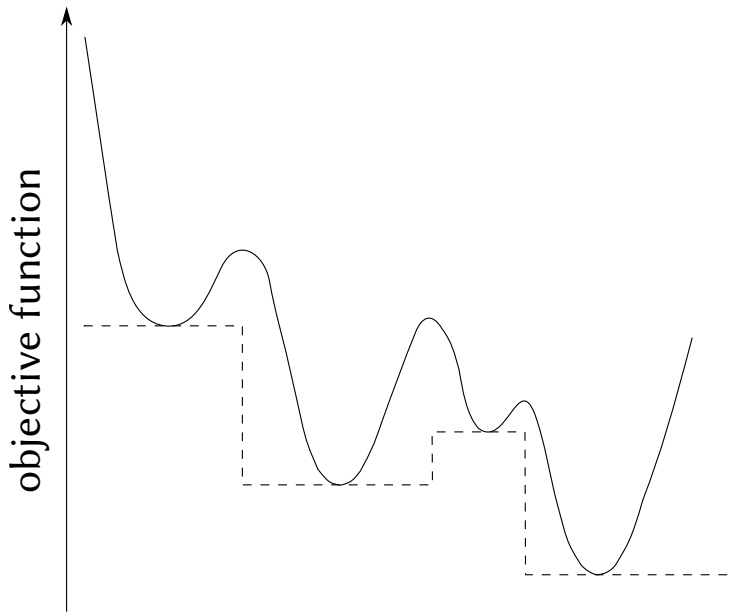

Figure 4.1 Hypersurface transformation in the basin-hopping method. The original hypersurface (solid line) is mapped onto the transformed surface (dashed line) by a geometry optimisation.

the hypersurface and dynamics are accelerated as local minima can be left easily by fixing the acceptance ratio to the desired value via the effective temperature in the Metropolis step. Contrary to the simulated annealing method, the basin-hopping approach is capable of finding the global minimum even on hypersurfaces with multiple almost degenerate low-lying minima.

In the *genetic algorithm* approach[84] the hypersurface is explored by utilising ideas from evolution theory, in particular natural selection. A "gene" is represented by the coordinates of the particles, forming a "chromosome". The "fitness" of a structure is determined by the potential energy with respect to the objective function. The structural information is often encoded in a binary bit string, but it is also possible to just use coordinates directly. In the first step of the algorithm an initial population is generated randomly and their fitness is calculated. A pair of "parents" is chosen, one of which is picked randomly while the other is selected based on its fitness. The structures of the parents are combined to create two "children" with a fixed probability of a single bit to cross-over. Additionally, a low probability for random mutations is incorporated into the algorithm as well. After the next generation is created the parent generation is discarded to leave the population size constant. The algorithm is inherently

parallel as multiple pairs of parents can be treated simultaneously. In its first application to clusters it was shown that a genetic algorithm can lead to convergence towards the global minimum in far fewer steps than for example the simulated annealing method.[85]

The algorithms mentioned in this section represent only a subset of all available global optimisation methods for the search of stationary points on a potential energy surface (PES). Other algorithms that can be used to solve the problem at hand are, for example, the particle swarm algorithm or the ant colony optimisation method.

5 Interaction Potentials

Systems of large numbers of atoms or complete scans of potential hypersurfaces are usually not treatable by accurate quantum chemical methods as introduced in chapter 3. In those cases more simple interaction potentials have to be employed, without loosing crucial information about the system. In the following sections two potentials used in this thesis will be introduced. If not noted otherwise the following sections are based on a book by Hirschfelder et al.[86]

5.1 Thermodynamic Considerations

The need to find intermolecular interaction potentials arose from the desire to have a good description for the equation of state of a gas. A purely empirical relation was first found by Kamerlingh Onnes.[87]

$$pv = A' + \frac{B'}{v} + \frac{C'}{v^2} + \frac{D'}{v^4} + \frac{E'}{v^6} + \frac{F'}{v^8} \tag{5.1}$$

Here, p represents the pressure of the gas, v the molar volume of the container and the parameters A' to F' are the *virial coefficients*. The latter are functions of temperature T and can be adjusted to fit the polynomial to experimental data obtained from various gases. It is often sufficient to focus on the first three virial coefficients to obtain a useful equation of state.

This formulation can be generalised in terms of Taylor expansion

$$\frac{pv}{RT} = 1 + \frac{B}{v} + \frac{C}{v^2} + \frac{D}{v^3} + \dots, \tag{5.2}$$

which allows the virial coefficients[a] to be expressed as functions of intermolecular potentials. If all virial coefficients are 0, equation (5.2) is equal to the ideal gas equation, which means that the virial coefficients are connected to the interactions between gas molecules not included in the ideal gas law. Analytic expressions for the virial coefficients can be derived as explained in the following section. It is clear that this expansion converges if the virial coefficients are small compared to the volume v.

[a] Note that the prime notation was dropped to emphasise that the virial coefficients in this equation are different to the ones originally proposed in equation (5.1).

5.1.1 Equation of State from the Partition Function

The partition function Z_N can be used to derive various thermodynamic quantities, for instance the pressure p.

$$p = kT \left(\frac{\partial \ln Z_N}{\partial V} \right)_T \tag{5.3}$$

In this equation, k is the Boltzmann constant, T the temperature and V the volume of the vessel. Using the expression for the classical partition function of a system of N identical particles[b] the partition function can be reformulated in terms of Boltzmann factors $W_N\left(\mathbf{r}^N\right) = e^{-\beta\Phi\left(\mathbf{r}^N\right)}$ and a configurational integral Q_N.

$$Q_N = \frac{1}{N!} \int W_N\left(\mathbf{r}^N\right) \mathrm{d}\mathbf{r}^N \tag{5.4}$$

$$Z_N = \frac{Q_N}{\lambda^{3N}} \text{ with } \lambda^2 = \frac{h^2}{2\pi m k T} \tag{5.5}$$

Here, $\mathbf{r}^N$ refers to the set of coordinates defined by the set of N molecules, h is Planck's constant, m the particle mass and $\beta = 1/kT$. The potential function $\Phi\left(\mathbf{r}^N\right)$ depends on all particle coordinates and is not yet defined explicitly. However, expressions for the virial coefficients can be found without defining the interaction potential by using a method introduced by Ursell.[88] This method requires the definition of "U-functions" $U_l\left(\mathbf{r}^\lambda\right)$ that are expressed as combinations of Boltzmann factors. The subscript l refers to how many molecules the U-function includes and λ denotes which molecules. For example, the first two U-functions are defined as:

$$U_1\left(\mathbf{r}_i\right) = W_1\left(\mathbf{r}_i\right) \tag{5.6}$$

$$U_2\left(\mathbf{r}_i, \mathbf{r}_j\right) = W_2\left(\mathbf{r}_i, \mathbf{r}_j\right) - W_1\left(\mathbf{r}_i\right) W_1\left(\mathbf{r}_j\right). \tag{5.7}$$

The advantage of using these expression can be demonstrated by considering the condition under which $U_l\left(\mathbf{r}^\lambda\right)$ vanishes. For example, for the second U-function to be equal to zero, both terms containing Boltzmann factors must be equal.

$$W_2\left(\mathbf{r}_i, \mathbf{r}_j\right) = W_1\left(\mathbf{r}_i\right) W_1\left(\mathbf{r}_j\right) \tag{5.8}$$

$$\Phi\left(\mathbf{r}_i, \mathbf{r}_j\right) = \Phi\left(\mathbf{r}_i\right) + \Phi\left(\mathbf{r}_j\right) \tag{5.9}$$

The latter is true if the molecules i and j are sufficiently far apart for their interaction to be negligible. For the higher order U-functions this concept can be extended to two or more groups of molecules being far enough apart for

[b] See page 106 in reference [86].

their interaction to become 0. By reversing the definition of the U-functions, the Boltzmann factors can be expressed in terms of U-functions.

$$W_N\left(\mathbf{r}^N\right) = \sum_{\sum lm_l = N} \prod U_l\left(\mathbf{r}^\lambda\right) \tag{5.10}$$

The summation has to be carried out over all divisions of N molecules into m_l groups of l molecules. With this expression equation (5.4) can now be solved.

$$Q_N = \sum_{\sum lm_l = N} \prod_{l=1}^{N} \frac{(Vb_l)^{m_l}}{m_l!} \tag{5.11}$$

The U-functions are now included in the *cluster integrals* b_l which are defined in the following way.

$$b_l = (Vl!)^{-1} \int U_l(\mathbf{r}_1, \mathbf{r}_2, \ldots, \mathbf{r}_l)\, \mathrm{d}\mathbf{r}_1\, \mathrm{d}\mathbf{r}_2 \ldots \mathrm{d}\mathbf{r}_l \tag{5.12}$$

Equation (5.5) can now be expressed in terms of the cluster integrals and the equation of state in virial form can be derived from equation (5.3).

$$\ln Z_N = -N \ln z\lambda^3 + \sum_{l=1}^{\infty} Vb_l z^l \tag{5.13}$$

$$pV = kTV \left(\frac{\partial \ln Z_N}{\partial V}\right)_T = kT \sum_l Vb_l z^l \tag{5.14}$$

$$z = \frac{N}{V} \exp\left(-\sum_{i=1}^{\infty} \gamma_i \left(\frac{N}{V}\right)^i\right) \tag{5.15}$$

Here, z has the dimension of a concentration and is called the *active number density*. γ_i are combinations of cluster integrals and the first two are

$$\gamma_1 = 2b_2 \tag{5.16}$$

$$\gamma_2 = 3b_3 - 6b_2^2. \tag{5.17}$$

Combining the equations above leads to an equation similar to equation (5.2).

$$\frac{pv}{RT} = 1 - \sum_{i=1}^{\infty} \frac{i\gamma_i}{i+1} \left(\frac{N}{V}\right)^i \tag{5.18}$$

Comparing equations (5.2) and (5.18) it is clear that the virial coefficients can be expressed in terms of cluster integrals.

$$B(T) = -\frac{1}{2} N_A \gamma_1 \tag{5.19}$$

$$C(T) = -\frac{2}{3} N_A^2 \gamma_2 \tag{5.20}$$

As stated before, the virial coefficients arise from the molecular interactions as they are functions of the cluster integrals that in turn consist of many-body interactions. Additionally, it can be seen, that the second virial coefficient B depends only on two-body interactions, the third virial coefficient C on two- and three-body interactions and so on.

Further simplification can be achieved by the assumption of additivity, which allows the total potential energy of the system to be expressed in terms of pairwise interactions φ_{ij}.

$$\Phi\left(\mathbf{r}^N\right) = \frac{1}{2}\sum_i \sum_j \varphi_{ij} \tag{5.21}$$

The magnitude of the error introduced by this treatment has been calculated by Axilrod et al.[89] to scale with r^{-9}. The U-functions can now be expressed in terms of modified Boltzmann factors $f_{ij}(r_{ij})$, which are defined such that they only differ from zero if the interaction energy is significant.

$$f_{ij}(r_{ij}) = e^{-\beta\varphi_{ij}} - 1 \tag{5.22}$$

For the U-functions this results in the following expressions.

$$\begin{aligned} U_1(\mathbf{r}_1) &= 1 \\ U_2(\mathbf{r}_1, \mathbf{r}_2) &= f_{12} \\ U_3(\mathbf{r}_1, \mathbf{r}_2, \mathbf{r}_3) &= f_{12}f_{23}f_{13} + f_{12}f_{23} + f_{23}f_{13} + f_{12}f_{23} \end{aligned} \tag{5.23}$$

From these definitions, expressions depending on two-body interactions for the virial coefficients can be derived.

$$B(T) = -\frac{2\pi N}{3kT}\int_0^\infty r^3 \frac{\mathrm{d}\varphi}{\mathrm{d}r} e^{-\beta\varphi(r)}\,\mathrm{d}r \tag{5.24}$$

In diluted gases, where interactions of more than two particles are rare, an equation of state only containing the second virial coefficient describes the system well enough.

$$\frac{pv}{RT} = 1 + \frac{B}{v} \tag{5.25}$$

5.2 Lennard-Jones Potential

One of the most widely used interaction potentials today is the Lennard-Jones (LJ) potential. It was first introduced by Jones (later Lennard-Jones) on April 22, 1924,[90] however, the same potential was submitted for publication by

Simon et al. only a few days later.[91] The potential introduced by Lennard-Jones depending on the distance r between two objects was of the form

$$V_{m,n}^{\mathrm{LJ}}(r) = \frac{\lambda_n}{r^n} - \frac{\lambda_m}{r^m},\ m < n, \tag{5.26}$$

with m and n not being set at that time. However, even though this general potential form is nowadays known as the Lennard-Jones potential, there had been other attempts at defining similar interaction potentials earlier. In 1920, Kratzer[92] already published a less general potential of the same form with the exponents m and n set to 1 and 2, respectively. The general idea behind these two potential forms was already discussed earlier in the beginning of the 20th century by Mie.[93] In all those potentials attractive and repulsive distance dependent terms are combined such that the resulting potential energy function has a minimum value at some equilibrium distance. For distances larger than the equilibrium distance the potentials approach zero asymptotically from below, while they diverge towards $+\infty$ for distances close to zero.

Lennard-Jones used this potential form to solve the integral expression in the second virial coefficient B. Analytical expressions can also be found for purely repulsive potentials and the attractive Sutherland potential. Lennard-Jones, however, introduced the potential in equation (5.26) and solved the equation of state analytically to derive parameters for λ_n and λ_m based on experimental results for noble gases[90] and later on for the solid state.[94]

Equation (5.26) can be redefined in terms of parameters for the depth of the potential energy well ε and equilibrium distance r_e. Under the constraint of $V_{m,n}(r_e) = -\varepsilon$ and $\frac{\mathrm{d}V_{m,n}(r_e)}{\mathrm{d}r} = 0$ a more common notation of the LJ potential can be derived.

$$V_{m,n}^{\mathrm{LJ}}(r) = \frac{\varepsilon}{n-m}\left[m\left(\frac{r_e}{r}\right)^n - n\left(\frac{r_e}{r}\right)^m\right] \tag{5.27}$$

Both parameters ε and r_e can be determined by the size of the interacting atoms and the interaction strength. The evaluation of the exponents m and n, however, is more complicated. The exponent m is mainly important for the correct long range behaviour, while n dominates for distances smaller than r_e. First attempts at deriving the correct long range behaviour have been made by considering two hydrogen atoms.[95] The attractive force was shown to scale with r^{-7}, which is in agreement with other investigations, showing the *potential* of the attractive field[c] to be on the order of r^{-6}.[96–99] First attempts were made to relate the long-range behaviour to the polarisability of the atoms,[99,100] a correlation that is used to treat van-der-Waals interactions parametrically, today (see section 3.4.4). Lennard-Jones calculated force constants for various gases showing the same long-range behaviour from studying their equation of state.[90,101–104]

[c] Note that the force is the first derivative of the potential.

The repulsive part is more complicated, as it can not be derived directly from the equation of state. Lennard-Jones used lattice parameters and heats of sublimation from experiments to fit his potential. He found $n = 12$ and $m = 6$ to fit the data well, giving rise to the most commonly used form of the LJ potential: $V_{6,12}(r)$.[105] Some examples for potential curves with exponents $n = 12$ and $m = 6$ can be found in figure 5.1.

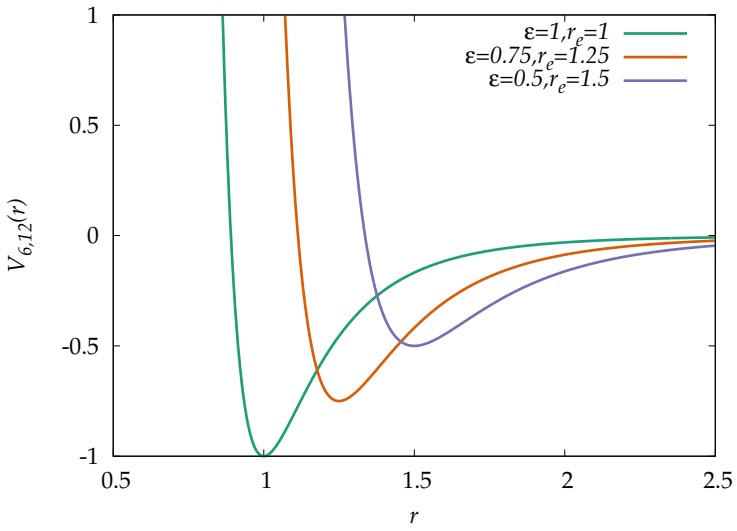

Figure 5.1 Examples of Lennard-Jones potential curves for the (6,12)-LJ potential with different values for ε and r_e.

5.2.1 Extended Lennard-Jones Potential

A more sophisticated solution to describing intermolecular interactions can be achieved with the extended Lennard-Jones (eLJ) potential. The choice of the exponents m and n in the LJ potential is arbitrary and lacks flexibility. Any effect that scales differently from r^{-12} or r^{-6} can not be described accurately. Therefore, it seems almost natural to extend the LJ potential by a sum over different r^{-i} terms weighted by coefficients c_i.

$$V_{\mathrm{eLJ}}(r) = \sum_{i=n_{\min}}^{n_{\max}} c_i r^{-i} \tag{5.28}$$

The number and type of the exponents $n_{\min}$ to $n_{\max}$ needs to be determined based on the investigated system. For example, in the original publication only even exponents from 6 to 16 were included.[106] A later study investigated the Xenon dimer and it was decided to include exponents up to $i = 18$ and also some odd numbered ones.[107] In both cases the coefficients c_i are determined by a fitting procedure to very accurate dissociation curves of the

respective dimer molecules calculated by coupled-cluster theory. For such a potential the cohesive energy of the solid state can be expressed analytically in terms of lattice sums.[106]

5.2.2 Lennard-Jones Clusters

The LJ potential has been used extensively to study nucleation of clusters and as a benchmark for global optimisation methods (section 4.5). From the derivation of the LJ potential as an interaction potential to obtain analytical solutions for the second virial coefficient, it should be clear that it is a rather crude approximation for the forces between atoms in a cluster of the size of a few atoms. Nevertheless, the LJ potential is capable of making verifiable predictions especially in the case of the rare gas clusters.[12] For example, the most stable arrangement is often predicted to be a Mackay icosahedron in agreement with experimental results.[108] The reason for this agreement lies within the nature of the interaction between rare gas atoms due to dispersive forces, which are approximated well by the LJ potential.

The hypersurface upon which the particles move, also called a potential energy surface (PES) or energy landscape, has been explored extensively for the LJ potential.[20,109,110] Doye et al.[110] employed the eigenvector following method (section 4.5.1) to find an initial set of minima and transition states with Hessian index 1.[d] From this set higher order Hessian index saddle point can be found by randomly perturbing the found minima and transition states and following the eigenvector to a new stationary point. Additionally, stationary points were searched for in reverse order, meaning the search was started from a high order index saddle point and structures with lower Hessian index were located by perturbing the initial structure randomly.

Absolute numbers of local minima of LJ clusters can be found in the results part (table 8.1, page 100).

5.3 Sticky-Hard-Sphere Potential

A variation of the sticky-hard-sphere (SHS) potential was originally introduced by Baxter[111] and can be regarded as a rigid sphere interaction with surface adhesion. In the simpler rigid sphere model the interaction potential is 0 for distances larger than the equilibrium distance r_s and goes to infinity when the particles "touch". The rigid sphere model with surface adhesion builds upon this by introducing a region of attraction of width $R(r_s - 1)$ in

[d] The Hessian index gives the number of negative eigenvalues of the Hessian matrix.

which the potential is defined to be $-\varepsilon$. The potential can be expressed as

$$V^{\mathrm{SW}}(r) = \begin{cases} \infty & 0 < r < r_s. \\ -\varepsilon & r_s < r < Rr_s. \\ 0 & r > Rr_s. \end{cases} \tag{5.29}$$

For this potential the second and third virial coefficients have been evaluated analytically. For clarity only the more important second virial coefficient $B(T)$ is shown.

$$B(T) = \frac{2}{3}\pi N_A {r_s}^3 \left[1 - (R^3 - 1)\left(\exp\left\{\frac{\varepsilon}{kT}\right\} - 1\right)\right] \tag{5.30}$$

Interestingly, this potential shows a relationship to the (6,12)-LJ potential. For values of $R = 1.8$ and $\varepsilon = 0.56$ the second virial coefficient becomes

$$B(T) = \frac{2}{3}\pi N_A {r_s}^3 \left(1 - 4.832\left(\exp\left\{\frac{\varepsilon}{kT}\right\} - 1\right)\right), \tag{5.31}$$

which approximates the second virial coefficient of the (6,12)-LJ potential quite well.[86]

More important for the scope of this thesis is, however, the relation to the LJ potential for when the width of the potential well goes to 0. In this case the potential can be written as

$$V^{\mathrm{SHS}}(r) = \begin{cases} \infty & 0 < r < r_s, \\ -\varepsilon & r = r_s, \\ 0 & r > r_s, \end{cases} \tag{5.32}$$

which is then often called the SHS potential. If the LJ potential is expressed in terms of equation (5.27), equation (5.32) represents the limit with respect to the exponents (n, m) approaching infinity.[e]

$$\lim_{m,n\to\infty} V^{\mathrm{LJ}}_{m,n} = V^{\mathrm{SHS}} \tag{5.33}$$

This can easily be shown by applying l'Hôpital's rule to equation (5.27) and deriving the limits for the cases presented in equation (5.32).

5.3.1 Sticky Hard Sphere Clusters

Similar to the LJ clusters, the SHS clusters can be found by investigating combinations of spheres that minimise the potential in equation (5.32). As the SHS potential is not a continuous function, common optimisation algorithms can not be used to investigate the potential energy landscape. However, the nature of the SHS potential results in a neat property that allows the clusters to

[e] An illustration of this property is shown in figure 8.1.

be defined in terms of graph theory. Only pairs of spheres that have the right distance of $r = r_s$ contribute to the overall energy, allowing the energy to be expressed in terms of the contact number N_c.

$$E = -\varepsilon N_c = -\varepsilon \sum_{i>j} A_{ij} \tag{5.34}$$

This allows the clusters to be represented by adjacency matrices $\mathbf{A}$, where a contact state is represented by a matrix element of $A_{ij} = 1$ and every other position by $A_{ij} = 0$.[112] The problem of minimising the energy now becomes a problem of maximising the contact number N_c, or the number of 1 entries in the adjacency matrix. The adjacency matrix of a cluster will be symmetric, which means there are $2^{N(N-1)/2}$ different combinations that could all potentially represent a cluster structure. To find all possible packings, all adjacency matrices have to be analysed with respect to their suitability for a stable cluster structure, a method called *exact enumeration*. A large number of possible adjacency matrices can be rejected immediately, because they represent an already found structure with a different particle labelling. This particle labelling degeneracy is due to the fact that the spheres are all equal and therefore swapping two rows or columns in the adjacency matrix will not change the underlying cluster structure. If two adjacency matrices correspond to the same structure they are said to be *isomorphic* (see chapter 2.1).

Besides the obvious rejection of adjacency matrices that are isomorphic, other restrictions can be imposed to reduce the numbers of adjacency matrices further. Most importantly, the resulting structures should be rigid, meaning not continuously deformable. Thus, each sphere needs to be in contact with at least three other spheres, which is true if each row or column of the adjacency matrix contains at least three matrix elements of 1. Another restriction that has often been imposed on the adjacency matrices is the Maxwell criterion, which states that the contact number needs to fulfil $N_c \geq 3N - 6$ for a structure to be rigid.[113] However, recent investigations revealed the existence of rigid structures with $N_c < 3N - 6$.[114] Up to a size of $N = 4$ all inter-particle distances are completely defined by the adjacency matrix. Starting from $N = 5$ there will be at least one unknown inter-particle distance, which needs to be determined algebraically. For this, the distance matrix $\mathbf{D}$ needs to be constructed from the adjacency matrix. This can be achieved by defining $3N - 6$ equations (and $N(N-1)/2 - (3N-6)$ inequalities) from the adjacency information.

$$A_{ij} = 1 \rightarrow r_{ij} = 2r \tag{5.35}$$

$$A_{ij} = 0 \rightarrow r_{ij} > 2r \tag{5.36}$$

The system has $3N$ variable coordinates, but by fixing one sphere at the origin of the coordinate system and a second one along one of the coordinate axis,

the number can be reduced to $3N - 6$, and the system is completely defined by the equations above. In case the structure has more contacts than $3N - 6$ the system is overdefined, but still solvable. Deriving an efficient method for mapping the adjacency matrix into the distance matrix is the crucial step to examine clusters bound by the SHS potential.

A set of geometric elimination rules and distance rules have been derived by Arkus et al.[112] An elimination rule sorts out unphysical adjacency matrices, while a distance rule solves for the mapping $A_{ij} \rightarrow D_{ij}$. These rules can be derived from geometric considerations about the neighbourhood of a sphere. If another sphere touches a sphere of radius r, it must lie on the surface of a sphere with radius $R = 2r$. For two spheres in contact, their surrounding spheres intersect and form an *intersection circle* with radius $\frac{\sqrt{3}}{2}R$. Therefore, each matrix element A_{ij} can be related to an intersection circle between spheres i and j. Several rules can be derived from considering the intersection circles of the particles, for instance, the fact that more than one intersection circle can only intersect in 0, 1 or 2 points (and never more) implies that three connected spheres can never be touched by more than two spheres simultaneously. The article by Arkus et al. referenced above contains many more such rules that can be used to construct SHS clusters.

Results for complete exact enumeration of up to 14 spheres[112,114–116] have been published. The results by Holmes-Cerfon[114] also showed evidence of so called hypostatic clusters with less than $3N-6$ contacts. This is due to the fact that in this study a modification of the exact enumeration method was used, which follows one-dimensional transition paths created from breaking a random contact in an already found cluster. Another interesting find in this publication was the existence of clusters that share the same adjacency matrix representation. This means that the mapping from adjacency matrix to cluster embedding is not a bijection, but only surjective. An overview of these results can be found in table 8.1 (page 100).

Part II

Methods

6 Program Package SPHERES

For the projects outlined in chapters 8 and 9 a program to optimise 3-dimensional coordinates of cluster structures with respect to a two-body potential was required to be created. The optimisation routine needed to be flexible in the way that it would be easy to implement different two-body potentials like Lennard-Jones (LJ) or extended Lennard-Jones (eLJ). Furthermore, the program needed to be able to analyse the results regarding structure, energy and the matrix of second derivatives. The resulting program was written in C++ with standard library version 11 and was tested to compile in a Linux environment with the `clang++` compiler version 6.0. In the following sections, main features are explained and more important functionalities are outlined in more detail.

6.1 Structural Optimisation and Analysis

The main functionality of the program is implemented in three different executables. Each carries out a different task, i.e. optimising given input structures and output the results, removing duplicate structures from a set of input structures and finding differences of two sets of input structures. The programs are set up in such a way that their outputs can be used as input files for the other program parts. This allows the programs to be used sequentially while retaining the flexibility of using each executable separately. This chain-like execution scheme is depicted in figure 6.1. A set of input structures (Input 1) is provided to the first executable program `optimize`, which optimises the structures and generates Output 1, which is a list of optimised coordinates in the same format as the input. This can be used as input for the second executable program `analyze`, which uses the distance matrix to identify duplicate structures and outputs a list of optimised structures with no duplicates (Output 2). In combination with a secondary set of structures (Input 2) the third executable program `match` can be used to compare both sets of structures and output coordinates of structures that are missing from either set 1 or 2 (Output 3).

6.1.1 Optimisation of Input Structures

The optimisation of input structures with a chosen potential can be carried out with the program `optimize`. The coordinates of the input structures have

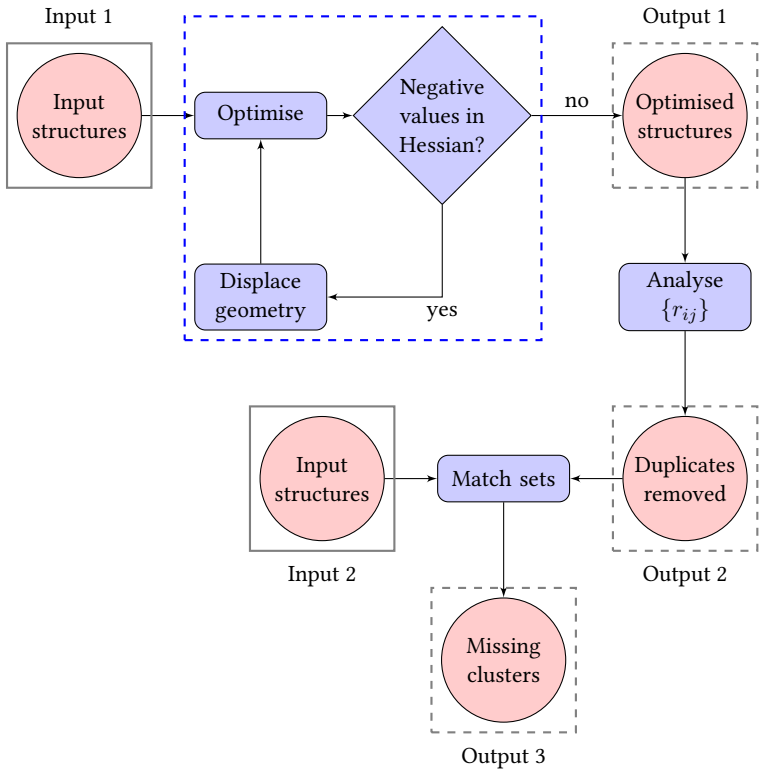

Figure 6.1 Schematic representation of the optimisation, analysis and matching procedure. Red circles: program input or output, blue ellipses: program executions.

to be provided in a single file where each line contains three numbers representing the position of one sphere. Multiple structures can be included by separating the list of coordinates by single blank lines. The program automatically moves the input structures to their respective centres of mass, and rotates them onto the principal axis system. To speed up the optimisation the environment variable `OMP_NUM_THREADS` can be set to a value greater than one to enable Open Multi-Processing (OMP) parallelisation. Each optimisation is carried out in a separate thread, while the number of simultaneously running threads is equal to `OMP_NUM_THREADS`.

Various parameters of the program run can be controlled using a `settings` file in the working directory, which is parsed with help of the library *libconfig*.[117] For example, the optimisation can be controlled using the `opt` group. In this group, the optimisation model can be chosen with the `name` setting, which currently can be set to either `BFGS` for the Broyden-Fletcher-Goldfarb-Shanno (BFGS) algorithm or `CG` for the conjugate gradient method. The optimiser uses the machine learning library dlib[118] as a back-end, which allows

for the implementation of additional optimisation models with relative ease. The energy termination criterion is defined using the `dforce` setting and the maximum number of steps can be set with the `nsteps` setting. An example is given in the box below.

settings file - opt tag

```
opt: {
    name = "BFGS";
    dforce = 1e-10;
    nsteps = 100;
};
```

A potential model has to be chosen for the optimisation procedure. Custom models can be added easily, which will be explained later. The current implementation allows the selection of three pair potentials, LJ, eLJ and a LJ potential with a cut-off range. For the LJ potential four parameters have to be given to the `potential` group as shown in the box below.

settings file - potential tag

```
potential: {
    name = "LJ";
    epsilon = 1.0;
    rm =  1.0;
    exp1 = 12.0;
    exp2 = 6.0;
};
```

The `name` setting enables the LJ potential and the four parameters `epsilon`, `rm`, `exp1` and `exp2` define the potential. The values shown in the example are the default values, which the program will fall back to if no values are provided by the user. The eLJ potential can be chosen by setting the `name` setting to `ELJ` and a range cut-off value can be chosen with the `RangeLJ` potential. For the eLJ potential the c_n coefficients have to be provided in a separate file located in the working directory and named `ext`, where each line contains two numbers. The first integer represents n and the second floating point number defines the corresponding coefficient.

After each structural optimisation the program checks if the result is a true minimum by calculating the Hessian matrix eigenvalues. If this check fails the eigenvectors of the Hessian matrix are calculated and the non-minimum structure is displaced in both possible directions according to the eigenvector belonging to the first negative eigenvalue in the Hessian matrix. The algorithm tries to re-optimise until there are no negative eigenvalues in the Hessian matrix or until a maximum number of five re-optimisations is reached.

The resulting structures are printed in the file `coord` in the same format as the input. To analyse the optimisation procedure the additional files `opt` and

`reopt` are created, which contain the intermediate coordinates of the optimisation and re-optimisation procedures for each individual input structure.

6.1.2 Removing Duplicate Structures

Duplicated geometries in a set of input structures can be identified using the second program `analyze`. The input has to be provided in the same format as for the `optimize` program. The read-in procedure is equivalent to the `optimize` program. The program uses two methods to identify unique structures, one of which uses the energy of the cluster as a criterion, therefore the `potential` group has to be set in the `settings` file.

The first method uses four values to uniquely identify a structure. Those are the values for energy and the three eigenvalues of the moment of inertia tensor. This sorting procedure uses a `map` container from the C++ standard library, which is an implementation of a binary search tree. The `map` stores key-value pairs, which are guaranteed to be stored in order with respect to the key.[119] In this specific case, the ordering is implemented as a custom comparator function that sorts by energy first, then smallest moment of inertia tensor eigenvalue followed by the two larger moment of inertia tensor eigenvalues. The comparator function returns `true` if the first argument is considered smaller than the second argument. This procedure is shown as pseudocode in algorithm 1. The key is mapped to a value, which is simply

Algorithm 1 Comparator function for sorting by energy E and moment of inertia eigenvalues $I_1 \leq I_2 \leq I_3$.

```
1:  procedure COMPARE(structure a, structure b)
2:      if E^a < E^b then
3:          return true
4:      else if E^a = E^b and I_1^a < I_1^b then
5:          return true
6:      else if E^a = E^b and I_1^a = I_1^b and I_2^a < I_2^b then
7:          return true
8:      else if E^a = E^b and I_1^a = I_1^b and I_2^a = I_2^b and I_3^a < I_3^b then
9:          return true
10:     else
11:         return false
12:     end if
13: end procedure
```

the number of structures. The advantage of this method is its great scalability with respect to the number of input structures as values can be retrieved quickly based on the key.

The second method uses the Euclidean distance matrix (EDM) as the differ-

entiation criterion. The EDM is the matrix of all inter-particle distances d_{ij} where each entry is defined as the Euclidean norm $||\cdot||$ between two spheres.

$$d_{ij} = ||\mathbf{x}_i - \mathbf{x}_j||^2 \tag{6.1}$$

Each unique embedding of the cluster in space can be represented by an EDM, however information about the absolute position, orientation and chirality is not contained in this representation. That means rigid transformations of clusters (translations, rotations, reflections) don't affect the EDM as they don't change fixed distances between points in space.[120] If at least one inter-particle distance is different, the structures are said to be not equal. The algorithm is implemented in such a way that a structure's distance matrix is compared to the distance matrix of all other already sorted structures and is added to the matching group if they are equal up to a set threshold. If not, the structure is added to the array as a new group. If the optimisation results in many unique structures, this method of sorting becomes slow, as each trial structure has to be compared to all other already sorted structure groups.

6.1.3 Matching Structures

To compare the results from the optimisations procedures to previously published sets of clusters the program `match` can be used. It takes two files as input that each contain a set of structures of equal or different size and compares them based on the EDM. The number of atoms in each set must be equal, otherwise the program will be terminated. If both sets are found to be identical no output files are created. In case there are unmatched structures they will be printed in `xyz` format in the `output` directory for further analysis.

6.2 Graph-Theoretical Analysis

Graph theoretical analysis of cluster structures can be done with `ico-subgraph`, which is a very specialised program designed to compare contact graphs of Gregory-Newton (GN) clusters to the icosahedral graph. The input format for the structures remains unchanged.[a]

All graph objects are handled by the *Boost Graph Library*[30] and are implemented as undirected graphs as the direction of the connectivity in clusters is not meaningful. The graphs are automatically generated from three-dimensional coordinate input given by an object of type `structure`. Two types of graphs can be generated from these: (1) the graph of the complete structure and (2) the contact graph containing all spheres but the central one (if it exists). The latter is the more important one as it was used to carry out

[a] This part of the program was used in chapter 9. For a definition of contact graphs and GN clusters refer to the introduction in that part of the thesis.

the analyses in chapter 9. The decision whether two spheres are connected is based on two parameters: the equilibrium distance r_e and a threshold value ϵ. The default values for these are $r_e = 1$ and $\epsilon = 10^{-10}$, respectively.

$$d_{ij} - r_e < \epsilon \tag{6.2}$$

The icosahedral graph is compared to the input structures via their graphs and the *VF2* graph matching algorithm.[29,121] The algorithm finds all mappings of the vertices of the icosahedral graph to the graph of the input structure. As the icosahedron represents the complete planar graph for 12 vertices, every graph that is a subgraph of the icosahedral graph can be represented by the number and type of edges removed from the icosahedral graph. For this application the mapping was chosen based on the root mean square (RMS) value of the distances between the spheres corresponding to removed edges. From all the possible mappings of the investigated graphs to the icosahedral graph the one with the lowest RMS value was chosen.

The graphs of the input structures are analysed with respect to their vertex and face degrees. Vertex degrees are calculated directly by the library and can be accessed with the `degree` function. For face degrees the `planar_face_traversal` function has to be invoked. This algorithm iterates over all faces in the planar embedding counting the number of vertices constructing each face. The graphs of the input structures are then sorted based on the calculated degree values, starting with the vertex degree in descending order and followed by the face degree in ascending order. If two or more graphs have the same amount of face and vertex degrees they are grouped together. The sorted graphs are printed to the standard output in the same form as table A.2 (page 144). Additionally, the investigated graphs are printed in terms of removed edges from the icosahedral graph as shown in table A.1 (page 129).

6.3 Additional Functionalities

Besides the main parts of the program, which have been described on the previous pages, a few script-like executable programs are provided. These were used to calculate various different properties of the investigated clusters.

Analyse Bond Lengths The bond variance in optimised structures can be calculated with `app-bondvariance`. The bond variance is simply defined as the difference between the shortest and longest bond of a cluster structure. In clusters optimised by soft potentials a bond is not as well defined as for sticky-hard-sphere (SHS) clusters. Therefore, it has to be determined with respect to a threshold value and the variance of the bond lengths can not be larger

than this threshold. This application has been used in chapter 8.4 to calculate the bond variance of the optimised $(6, 12)$-LJ structures. A more specialised version called `app-shortestbond` is also provided that can be used to find the cluster with the shortest bond distance.

Sort Structures by N_c Analysing the total contact numbers N_c or specific kissing numbers can be done with the programs `app-Nc` and `app-GN`. The latter looks for clusters with a central atom that has exactly 12 spheres arranged around it, so called Gregory-Newton clusters.

6.4 Implementations in Detail

In the following sections the basic implementation of cluster structures and two-body potentials will be explained in more detail.

6.4.1 Treating Cluster Structures

The main purpose of program SPHERES was to optimise an input set of structures with given Cartesian coordinates and analyse the results of the optimisation based on properties of the resulting structures. The handling of those structures and respective properties was therefore crucial to the functioning of the program.

The Cartesian coordinates are read from a file with blank lines separating different starting geometries. For each of these individual sets of coordinates a `structure` object is created. The `structure` class, however, has much more functionality than storing 3D coordinates. In fact, it serves as a complex data type storing properties besides coordinates as well as member functions to calculate those properties. They are stored in data members defined in private fields, such that they can only be manipulated by functions owned by the `structure` class. The `structure` class is designed to store values for:

- Cartesian coordinates
- energy (depending on the chosen potential),
- an integer number for labelling,
- moment of inertia,
- the EDM and adjacency matrix representations and
- an `undirectedGraph` that contains the connectivity information.

The Cartesian coordinates of each individual sphere are stored in an object of type `coord3d`, which is a modified version of the `coord3d` implementation used in program FULLERENE.[122]

The moment of inertia tensor determines the torque needed to accelerate a rigid body to spin around a rotational axis through the origin of the coordinate system. It is therefore analogous to mass in case of linear, translational acceleration. For cluster structures the tensor is equal to the sum over the moments of inertia of all constituent particles. As the clusters investigated in this thesis are only made up of one type of particle the mass term was set to unity. The inertia tensor $\mathbf{I}$ can then be calculated via the equations below.

$$\begin{gathered}\mathbf{I} = \begin{pmatrix} I_{xx} & I_{xy} & I_{xz} \\ I_{yx} & I_{yy} & I_{yz} \\ I_{zx} & I_{zy} & I_{zz} \end{pmatrix} \\ I_{xx} = \sum_i (y_i^2 + z_i^2) \quad I_{yy} = \sum_i (x_i^2 + z_i^2) \quad I_{xx} = \sum_i (y_i^2 + x_i^2) \\ I_{xy} = I_{yx} = -\sum_i x_i y_i \quad I_{xz} = I_{zx} = -\sum_i x_i z_i \quad I_{yz} = I_{zy} = -\sum_i y_i z_i \end{gathered} \tag{6.3}$$

Here, x_i, y_i and z_i denote the respective coordinate of sphere i. Diagonalising the inertia tensor yields a set of eigenvalues and eigenvectors, with the latter representing the principal axis system. Upon creation of a `structure` object the coordinates are transformed, such that the coordinate origin lies at the centre of mass and the structures principal axis are aligned with the basis vectors of the Cartesian coordinate system.

The class is designed to ensure that when any of the particle coordinates change, all properties are recalculated such that there is never a mismatch between the properties and the coordinates they refer to.

6.4.2 Treating Two-Body Potentials

For the geometry optimisation of the cluster structures, methods to calculate the energy and gradient need to be provided to the optimisation library. As shown in section 4.4 the gradient can be expressed as in equation (6.4).

$$\frac{\partial E(\mathbf{X})}{\partial x_m} = \sum_{j>i}^{N} \frac{\partial \varepsilon(r_{ij})}{\partial r_{ij}} \frac{\partial r_{ij}}{\partial \mathbf{r}_{ij}} \frac{\partial \mathbf{r}_{ij}}{\partial x_m} \tag{6.4}$$

The last two terms of the sum will be the same independent of the choice for the potential function $\varepsilon(r_{ij})$. The implementation therefore focused on reducing redundancies by making use of class inheritance features. As explained in the following paragraphs, this makes exchanging the type of two-body potential trivial.

For this, a base class called `pairPotential` was defined. It is an abstract class and therefore cannot be instantiated. Its private fields hold declarations of virtual methods for calculating energy $E(r)$, first derivative $\mathrm{d}E/\mathrm{d}r$ and

second derivative $\mathrm{d}^2E/\mathrm{d}r^2$ based on particle distance r. They are declared virtual, because they will be overwritten with the respective functions in the derived classes of the actual potentials. In the bare `pairPotential` class those functions are only declared but never defined and cannot be used for calculations. The public members of the class are the constructor and the user-accessible functions for calculating energy, gradient vector and Hessian matrix as well as the optimiser.

As an example, the C++ implementation for the member function that calculates the energy of the system is shown in listing 6.1. The method takes a

Listing 6.1 Implementation of the redundant part of the energy calculation.

```
double pairPotential::calcEnergy (structure &S) {
  double f(0);
  for (int i = 0; i < S.nAtoms(); i++) {
    for (int j = i + 1; j < S.nAtoms(); j++) {
      f += this->E (coord3d::dist (S[i],S[j]));
    }
  }
return f;
}
```

`structure` object as input and uses the virtual energy function to calculate the energy contributions of all unique pairs of spheres. The method `nAtoms()` returns the number of spheres in the `structure` and `dist` calculates the Euclidean distance between two spheres `i` and `j`.

Listing 6.2 Implementation of the distance dependant energy for the Lennard-Jones potential.

```
class LJ : public pairPotential {
  private:
    double E (double distance) {
      return (_epsilon / (_exp1/_exp2 - 1))
             * ( (pow (_rm / distance, _exp1)) - (_exp1/_exp2)
             * (pow (_rm / distance, _exp2)) );
    }
    //methods for first and second derivatives go here
};
```

To define a potential, a derived class that overwrites the virtual function declarations is required. The virtual member functions of the base class are overwritten in the private field of the derived class by providing properly de-

fined methods. Additionally, any parameters, that the potential form depends on, are declared in the private fields. In the public fields, constructors for the respective potential as well as a function that reads the potential parameters from a user provided file need to be declared. The last function is important as it also creates a pointer to the potential object on heap memory, which is necessary, because the exact nature of the potential is not known at compile time. For the LJ potential the energy function can be defined as shown in listing 6.2. The variables starting with an underscore are data members defined on object creation and refer to the two exponents `_exp1` and `_exp2` the equilibrium distance `_rm` and the depth of the potential energy well `_epsilon`. A different potential can be implemented in the same way. A new derived class has to be defined, containing the methods to calculate energy, first and second derivative. Additionally, a function that reads parameters that define the respective potential form has to be provided. By design, the function needs to return a pointer to an instance of the class on heap memory. In case of the LJ potential this can be achieved as shown in listing 6.3. Because memory on

Listing 6.3 Minimal example for the method `readPotential()`.

```
LJ *LJ::readPotential () {
  //instructions to read parameters from file go here

  LJ *potential = new LJ(epsilon, rm, exp1, exp2);
  return potential;
}
```

heap has to be managed by the user, the pointer should be used in conjunction with `unique_ptr` to ensure destruction of the object upon exiting the scope. An example for this is given below.

```
//read potentialName from settings file

std::unique_ptr< pairPotential > potential;
if (potentialName = "LJ") {
  potential.reset( LJ::readPotential() );
}
```

Part III

Results

7 Golden Dual Fullerenes[a]

7.1 Introduction

With the discovery of the catalytic activity of gold nano-clusters,[124–127] research interest in this field has resurged over the recent years.[128–134] Gold compounds can show rather interesting topologies, like barrel shaped structures[135] and planar sheets,[136–138] mainly because of strong relativistic effects compared to its lighter congeners copper and silver.[139–145] These effects are also responsible for an unusually high electronegativity, allowing gold to act as an electron acceptor in mixed-metal complexes.[140] This property could be used for electronic fine-tuning of physical and chemical properties in gold containing nano-materials of a certain size.[128] The growth behaviour of such clusters is, however, still debated heavily[146–148] and even the exact nature of the transition from planar structures to three-dimensional compact geometries in small gold clusters is not entirely resolved.[149–156]

In 2004 the first hollow gold cluster Au_{32} was proposed by Johansson et al.[157] adopting an I_h symmetric structure that can be created via a dual transformation of I_h-C_{60}, effectively replacing every face in the carbon fullerene with a gold atom, resulting in a triangulated surface. Karttunen et al.[158] have predicted another cage-like gold cluster I-Au_{72}, which they expect to be spherically aromatic. For clusters of copper or silver such hollow structures are not very stable.[157,159] The discovery of these types of structures has sparked interest in this field and many more hollow cages[148,150,158,160–167] and clusters enclosing a central metal atom[168–176] have been found. Most importantly, I_h-Au_{32}^-, T_d-Au_{16}^-, C_{2v}-Au_{17}^- and C_{2v}-Au_{18}^- were found to sufficiently explain gas phase photoelectron spectra of small gold clusters.[177,178]

On the following pages the relationship between carbon and gold fullerene cages in terms of their topology is investigated. The similarities arise from the fact, that topological features known for carbon fullerenes,[179–181] like the Goldberg-Coxeter transformation,[182,183] can also be applied to golden dual fullerenes to construct larger structures. A new class of gold clusters emerges naturally from a one-to-one mapping of the isomer space of fullerenes to hollow gold clusters. In the following sections, the stability of such clusters as

[a] This chapter is composed of sections previously published in the article "Hollow Gold Cages and Their Topological Relationship to Dual Fullerenes"[123] and is reprinted by permission from the publisher ©2016 John Wiley and Sons. Some sections have been modified to fit the style of this thesis.

well as their photoelectron spectra are investigated.

7.2 Topological Aspects

The construction of carbon fullerenes can be explained by starting from a graphene sheet and wrapping it around a sphere[b], which requires 12 of the hexagonal faces to be replaced by pentagons. This is a requirement imposed by Euler's polyhedral formula.

$$|N| - |E| + |F| = \chi \tag{7.1}$$

Here, $|N|$ is the number of vertices (or atoms), $|E|$ the number of edges (or bonds), $|F|$ the number of faces and $\chi = 2 - 2g$ the Euler characteristic, which is 2 for genus $g = 0$ surfaces as in convex polyhedra. As shown in section 2.2 the number of faces and vertices can be exchanged without changing the result of Euler's formula. This is also called a dual transformation, and in the case of the graphene sheet this transformation results in a (111) face-centered cubic (fcc) sheet of, for example, gold bulk. Because the symmetry is preserved by this transformation both objects belong to the hexagonal 2D lattice group *p3m1*. To distinguish the two sheets, the graphene sheet will be denoted *p3m1*-G and the gold sheet *p3m1*-T (figure 7.1).

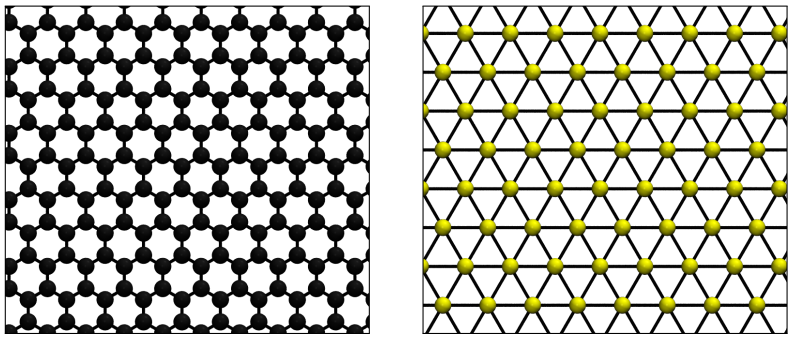

(a) **(b)**

Figure 7.1 (a) *p3m1*-G graphene and (b) its dual sheet *p3m1*-T adopted in the (111) surface of fcc gold.

Small cut-outs of the *p3m1*-T sheet can be found as global minima for smaller gold clusters, indicating that this represents a very stable structural motif for gold compounds.[151]

This concept can be extended to non-spherical structures like carbon nanotubes to construct gold nanowires, and there has been experimental evidence

[b] Or any surface with genus 0.

supporting the existence of such structures.[184] Because they are the duals of the carbon nano-tubes they can be constructed in the same way.[185] Two examples of cylindrically shaped carbon and gold structures are shown in figure 7.2.

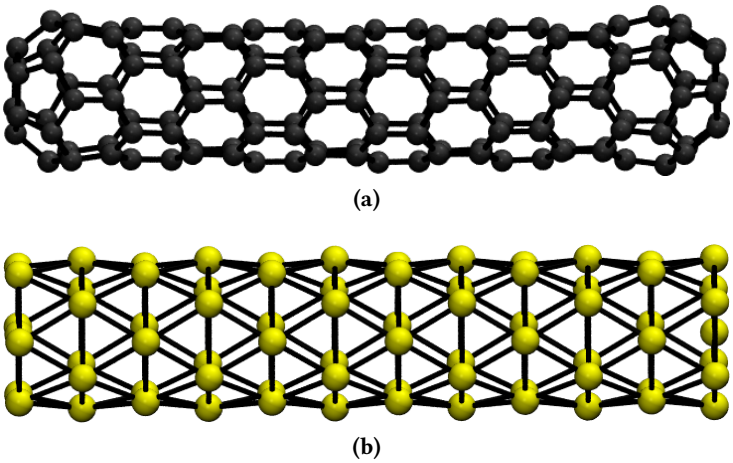

Figure 7.2 (a) $D_{6\mathrm{d}}-\mathrm{C}_{144}$ zig-zag fullerene nanotube and (b) its dual $D_{6\mathrm{d}}-\mathrm{Au}_{74}$.

As fullerenes need to have exactly 12 pentagons, a dual fullerene will have 12 vertices of degree five instead. All other vertices will have degree six and there are exactly as many as there are hexagons in the corresponding carbon fullerene. The smallest carbon fullerene C_{20} has $|F_h| = 0$ hexagons, and all larger ones at least $|F_h| > 1$. The fullerene C_{22}, which would contain exactly one hexagon, is non-existent,[186] thus, the hypothetical golden dual fullerene (GDF) Au_{13}[c] also cannot exist. Fullerenes often have much more than one stable isomer (non-isomorphic graphs)[181] and because of the dual relationship there should be as many isomers for the GDFs. Additionally, the growth of this isomer space for fullerenes should scale the same with respect to the number of vertices, which was found to be $\mathcal{O}\left(|N|^9\right)$.[187]

Both C_{60} and its dual Au_{32}, as well as their graph representations are depicted in figure 7.3. This relationship was first noticed in conjunction with the prediction of Au_{32},[157] and it allows the usage of the same algorithms used to construct fullerenes to create GDFs. For example, using the generalised face-spiral algorithm[122,180,181,188] followed up by an embedding of the graph on a genus 0 surface and a dual transformation.

A recent investigation of photoelectron spectra of gold clusters considered the existence of a T_{d}-Au_{16}^{-} cluster to explain the experimental findings.[178]

[c] The relation between the number of vertices in a fullerene $|N_f|$ and the number of vertices in the corresponding dual fullerene $|N_d|$ is $|N_d| = |F_f| = |N_f|/2 + 2$.[180]

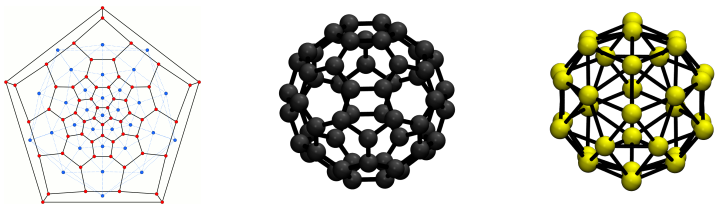

Figure 7.3 (a) Schlegel diagram of C_{60} (red vertices) and its dual (blue vertices and dashed edges), (b) the C_{60} structure, and (c) its dual Au_{32} structure.

This cluster would be dual to C_{28} and has exactly two isomers: T_d-Au_{16} and D_2-Au_{16}. In the above study, the D_2-symmetric isomer has not been considered to explain the observed spectra, which naturally raises the question whether this isomer's photoelectron spectra is similar or even capable of explaining the observations better.

The question of which structure is dominating the experimental spectrum is closely related to the question of which structure is thermodynamically more stable. For regular carbon fullerenes there exists an "isolated pentagon rule", that states that a carbon fullerene is more stable when none of the pentagons are in direct contact with each other.[189] It is hitherto unknown if there is an equivalent "isolated vertex of degree five rule" for dual fullerene structures.

As mentioned before, methods like the Goldberg-Coxeter transformation can be used to construct larger dual fullerenes from smaller ones.[182,183,190] The original Goldberg-Coxeter transformation was carried out on the dodecahedron (C_{20} fullerene),[182,183] but it can be shown that it can be applied to any fullerene graph.[180] The transformation $GC_{k,l}$ can be controlled by two integer parameters k, l describing the scaling and rotation of the mesh on which the transformation is carried out. The symmetry of the original fullerene is preserved if $k = l$ (leapfrog transformation) or $l = 0$ (halma transformation). Some important transformations are for example $GC_{1,1}[I_h{-}C_{20}]{=}I_h{-}C_{60}$[181] and $GC_{2,0}[I_h{-}C_{20}]{=}I_h{-}C_{80}$, both preserving the initial point group symmetry. In case of the gold clusters the same transformations results in the respective dual representations, i.e. $GC_{1,1}[I_h{-}Au_{12}]{=}I_h{-}Au_{32}$ and $GC_{2,0}[I_h{-}Au_{12}]{=}\ I_h{-}Au_{42}$. Both of these structures have been proposed previously to be stable hollow cages.[157] The new vertex count of $GC_{k,l}[Au_{|N_d|}]$ is

$$|N'_d| = (k^2 + kl + l^2)(|N_d| - 2) + 2. \tag{7.2}$$

An often encountered structural motif in gold clusters is the Mackay icosahedron.[153,191] Although this is not a hollow structure, it is related to dual

fullerenes as it is made up of multiple icosahedral shells. Each individual shell m consists of

$$|N_{\text{shell}}| = 10m^2 + 2 \tag{7.3}$$

atoms, resulting, when summing up, in the magical cluster numbers 13, 55, 147, 309, and so on.[192,193] Figure 7.4 shows one such icosahedral structure with $m = 7$ shells and 1415 atoms. The number of shells can be deduced from

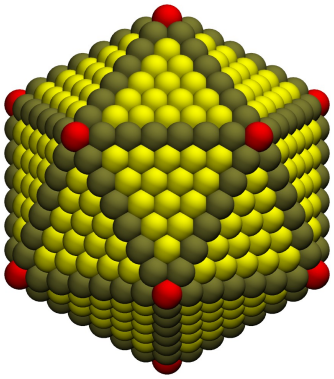

Figure 7.4 Mackay icosahedron with 7 shells and 1415 atoms. The outer icosahedral shell is the dual of the halma transform $GC_{7,0}[I_{\text{h}}{-}\text{C}_{20}]{=}I_{\text{h}}{-}\text{C}_{980}$.

the number of spheres on one edge of the icosahedron, including the spheres marked in red. There is exactly one sphere more on the edges than there are shells, thus $m = |N_{\text{edge}}| - 1$. The halma pattern of a $GC_{k,0}$ transformation is clearly visible on the faces of the icosahedron, and it turns out the icosahedral shells are in fact related to the smallest fullerene C_{20} by such a transformation and a subsequent dualisation. For this process equation (7.2) becomes

$$|N'_{\text{d}}| = k^2(|N_{\text{d}}| - 2) + 2, \tag{7.4}$$

and with $|N_{\text{d}}| = 12$ (as Au_{12} is the dual of C_{20}) this is equal to equation (7.3). The parameter k of the transformation $GC_{k,0}[\text{C}_{20}]$ therefore defines which shell of the icosahedron is created by the Goldberg-Coxeter transformation with subsequent dualisation.

The relationship between carbon fullerenes and hollow gold clusters can be used to name the latter in the same way as the carbon fullerenes. For example, this can be achieved by using the canonical face spiral pentagon indices (FSPI) in combination with the numbering scheme introduced by Manolopoulos.[181] A complete and unique method for naming polyhedra extending the original algorithm by Manolopoulos has been developed recently.[194] In the following sections the golden dual fullerenes from Au_{12} to Au_{20} (excluding Au_{13}) will be investigated by means of density functional theory (DFT) calculations.

7.3 Computational Details

Program FULLERENE[122] has been used to construct initial structures of all isomers of the golden dual fullerenes from Au_{12} to Au_{20} using a recently developed force-field for fullerenes[195] (excluding the non-existing golden dual fullerene Au_{13}). The following isomers need to be considered according to the isomer list for the fullerenes (number in parenthesis gives the number of different isomers of same symmetry):[122,196] I_h−Au_{12}, D_{6d}−Au_{14}, D_{3h}−Au_{15}, D_2−Au_{16}, T_d−Au_{16}, D_{5h}−Au_{17}, C_{2v}−Au_{17}(2), D_{3h}−Au_{18}, D_{3d}−Au_{18}, D_3−Au_{18}, D_2−Au_{18}, C_3−Au_{18}(2), C_{3v}−Au_{19}, C_2−Au_{19}(3), C_s−Au_{19}(2), D_{6h}−Au_{20}, D_{3h}−Au_{20}, D_{2d}−Au_{20}(2), C_{2v}−Au_{20}, D_2−Au_{20}(2), C_2−Au_{20}(3), C_2−Au_{20}(2), C_1−Au_{20}(2) and I_h−Au_{32}. The initial force-field optimised structures scaled to an approximate internuclear distance were then refined by using the Predew-Burke-Ernzerhof generalised gradient approximation (GGA) functional[47,48] corrected for dispersion interactions using Grimme's method (PBE-D3)[49,50] together with a Los-Alamos scalar relativistic effective core potential for gold and the accompanying double-zeta basis sets.[197] Note that the PBE functional was recently considered to perform well for gold clusters.[198] For several selected clusters the geometries obtained were checked for accuracy by carrying out calculations using a small core scalar relativistic Stuttgart pseudopotential[51] together with an augmented valence double-zeta basis set by Peterson and Puzzarini.[199] For comparison, the compact global minimum cluster structures recently published for the neutral compounds[151] and for the negatively charged species[200,201] were calculated.

The simulation of the photoelectron spectra has been carried out by artificial broadening the spectrum of orbital energies with Gaussian functions. The standard deviation σ for these functions was chosen to be 0.035 eV in qualitative agreement with the experimental spectra. The orbital energies were calculated using the PBE density functional with the def2-SVP[202] double-zeta basis implemented in TURBOMOLE 7.0.[203] The core region was described using an effective core potential including scalar relativistic effects. The calculated electron affinities were used as the onset value for simulating the photoelectron spectra.

For the calculation of the (111) fcc sheet and the fcc bulk structure of gold the program package VASP5[204] was used, utilizing a plane-wave basis set (cut-off energy $E_c = 350$ eV) and the standard projector-augmented wave (PAW) datasets for the elements to model the electron-ion interaction.[52,205] The electron-electron interaction was modelled within the GGA to the exchange-correlation energy functional as described above and dispersive effects were taken into account by employing Grimme's D3 dispersion correction with Becke-Johnson damping.[49,50] Brillouin zone

integrations were carried out on Γ-centred Monkhorst-Pack grids of k-points with a distance of 0.2 $Å^{-1}$. The cohesive energy is defined as the atomisation energy per atom keeping in mind that one gold atom is negatively charged for the anionic clusters.

In order to discuss how much the gold cages deviate from sphericity compared to the dual fullerene structure, the previously introduced definition of a minimum distance sphere (MDS) was used,[122]

$$\min_{c_{\mathrm{MDS}} \in \mathrm{CH}(S)} \frac{1}{N} \sum_i |R_{\mathrm{MDS}} - \|\mathbf{p}_i - \mathbf{c}_{\mathrm{MDS}}\||| \tag{7.5}$$

with the MDS radius defined as

$$R_{\mathrm{MDS}} = \frac{1}{N} \sum_i \|\mathbf{p}_i - \mathbf{c}_{\mathrm{MDS}}\|. \tag{7.6}$$

Here S is the set of n points $\mathbf{p}_i$ ($i = 1, \ldots, n$) in 3-dimensional space, $\mathrm{CH}(S)$ its convex hull, $\|\cdot\|$ the Euclidean norm, and $\mathbf{c}_{\mathrm{MDS}}$ is the barycentre of the MDS with radius R_{MDS}. In other words, the procedure tries to locate a sphere that approximates the position of the vertices well. A measure for distortion from spherical symmetry through the MDS is defined as[122]

$$D_{\mathrm{MDS}} = \frac{100}{N R_{\min}} \sum_{i=1}^{N} |R_{\mathrm{MDS}} - \|\mathbf{p}_i - \mathbf{c}_{\mathrm{MDS}}\||\,, \tag{7.7}$$

where $R_{\min}$ is the smallest bond distance found in the cluster. The pentagon index N_p is defined as

$$N_p = \frac{1}{2} \sum_{k=1}^{5} k p_k \quad \text{with} \quad \sum_{k=0}^{5} p_k = 12 \tag{7.8}$$

where the pentagon indices $(p_i | i = 0, \ldots, 5)$ define the number of pentagons attached to another pentagon.[181]

7.4 Structure and Stability

The results for the neutral and negatively charged gold clusters are collected in tables 7.1 and 7.2 respectively. The dual fullerene structures are compared to the known global minimum structures in these tables, and the different isomers are numbered according to their canonical degree 5 vertex spiral, identical to the canonical face spiral pentagon indices for fullerenes.[181] Calculations for the most stable neutral and anionic compact Au_n clusters for comparison are also included and are listed in table 7.3. The investigated structures for the negatively charged gold clusters are depicted in figures 7.5

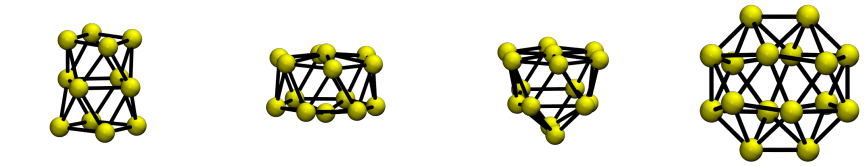

(a) 12:1 **(b)** 14:1 **(c)** 15:1 **(d)** 16:1

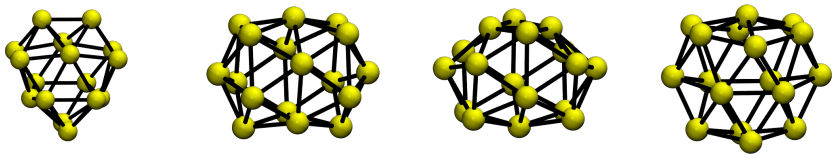

(e) 16:2 **(f)** 17:1 **(g)** 17:2 **(h)** 17:3

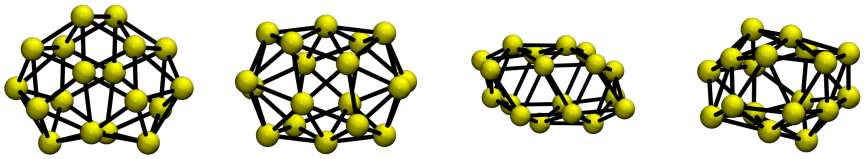

(i) 18:1 **(j)** 18:2 **(k)** 18:3 **(l)** 18:4

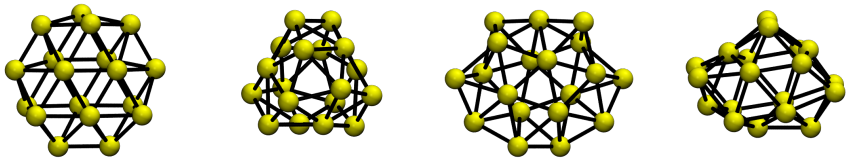

(m) 18:5 **(n)** 18:6 **(o)** 19:1 **(p)** 19:2

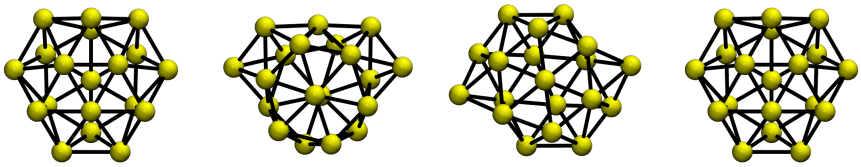

(q) 19:3 **(r)** 19:4 **(s)** 19:5 **(t)** 19:6

Figure 7.5 Structures of anionic gold clusters (Au_{12}^- to Au_{19}^-).

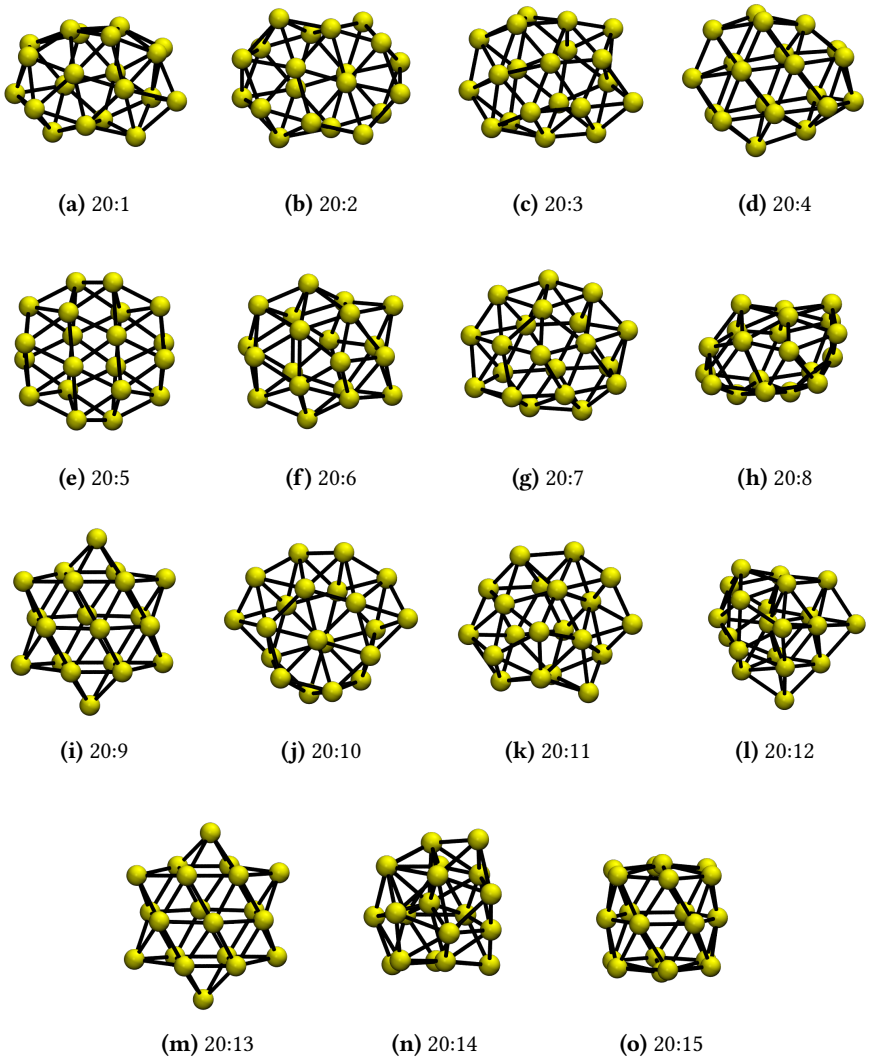

(a) 20:1 **(b)** 20:2 **(c)** 20:3 **(d)** 20:4

(e) 20:5 **(f)** 20:6 **(g)** 20:7 **(h)** 20:8

(i) 20:9 **(j)** 20:10 **(k)** 20:11 **(l)** 20:12

(m) 20:13 **(n)** 20:14 **(o)** 20:15

Figure 7.6 Structures of anionic gold clusters (Au_{20}^{-}).

and 7.6, and the energy differences compared to the global minimum structures are shown in figure 7.8.

The optimised gold clusters can be sorted according to whether they can be derived from a dual fullerene structure, or more generally from a cubic polyhedral graph, or not. In this case Euler's polyhedral formula can be simplified, which upon dualisation gives a triangulation of a sphere obeying the formula

$$\Gamma = \sum_{n=3} (6-n)|N_n| = 12, \tag{7.9}$$

where $|N_n|$ denotes the number of n-valent vertices. Any deviation from $\Gamma = 12$ implies that the polyhedron is not a triangulation of a sphere. As mentioned before, for dual fullerenes only values of $N_5 = 12$ and $N_6 = \{0, 2, 3, 4, 5, \dots\}$ are allowed. Hence, a true dual fullerene structure is obtained in case of a complete triangulation and 12 vertices of degree five.

Tables 7.1 and 7.2 show vertex counts as well as results from equation (7.9) for the neutral and anionic clusters, respectively. Considering only the topological parameter Γ it is clear that most of the optimised structures can be derived from a dual planar cubic graph and therefore only consist of triangles. The few notable exceptions are the isomers 12:1 and 20:12 for both the anionic and neutral structure. The ideal icosahedral structure for the Au_{12} cluster is not stable under the present level of theory, and the optimised structure does not correspond to a triangulation of a sphere. However, it has already been shown that this cage can be stabilised by inserting a transition metal (e.g. tungsten) atom into the central position of the icosahedron such that the 18 valence electron rule is fulfilled.[168,206] Additional stabilisation of such an endohedral gold cluster can be achieved by attaching ligands to the surface of the cluster.[207] Structure 20:12 converges towards a more compact cluster with an 8-fold coordinated gold atom in the centre for both the anionic and the neutral cluster.

Figure 7.7 gives an overview over all optimised structures. A green field marks a dual fullerene structure with exactly 12 vertices of degree five and the remaining vertices being of degree six. These are also the structures used in figure 7.9b and they are more abundant for clusters of size 14 to 19 atoms. Structures with an orange mark do not fulfil the requirement of being a dual fullerene as they contain vertices of degree 4. However, they are still hollow gold cages and, as mentioned before, show a value of $\Gamma = 12$. These structures can be rather similar to the initial dual fullerene structures obtained from a force-field optimization of the corresponding carbon cage, and are usually a result of a flattening towards a more oblate geometry. Most of the clusters shown here preserve their hollow cage structure with only few clusters optimising into more stable compact structures. These are marked as red in figure 7.7.

As illustrated by the distortion parameter D(F) in tables 7.1 and 7.2, carbon

Table 7.1 Topological parameters for the neutral gold clusters. Number of gold atoms and isomer numbers of the corresponding fullerene in canonical order of the pentagon spiral indices,[181] ideal and actual point group symmetry, energy differences ΔE_g to the most stable neutral cluster of same size and binding energy per atom $\Delta E_n = [E(\mathrm{Au}_n) - nE(\mathrm{Au})]/n$ (in eV), shortest and largest bond distance (in Å), pentagon index (PI) N_p, and distortion parameter D (in %) for the initial force-field optimised fullerene structure (F) and the GDF.

	symmetry		stability		vertices					bondlengths		PI	D	
isomer	ideal	actual	ΔE_n	ΔE_g	$\lvert N_4\rvert$	$\lvert N_5\rvert$	$\lvert N_6\rvert$	$\lvert N_7\rvert$	Γ	shortest	largest	N_p	F	GDF
12:1	I_h	$D_{4\mathrm{h}}$	−2.058	0.485	8	0	4	0	16	2.798	2.895	30	0	21.1
14:1	$D_{6\mathrm{d}}$	$D_{2\mathrm{d}}$	−2.134	1.173	0	12	2	0	12	2.739	3.048	24	6.1	23.4
15:1	$D_{3\mathrm{h}}$	$C_{2\mathrm{v}}$	−2.192	−0.083	0	12	3	0	12	2.786	2.901	21	5.1	29.2
16:1	D_2	D_2	−2.247	0.223	0	12	4	0	12	2.770	2.917	20	7.9	24.3
16:2	T_d	$D_{2\mathrm{d}}$	−2.233	0.440	0	12	4	0	12	2.716	2.996	18	1.3	28.5
17:1	$D_{5\mathrm{h}}$	C_s	−2.259	0.177	2	8	3	3	12	2.747	3.026	20	11.5	17.3
17:2	$C_{2\mathrm{v}}$	$C_{2\mathrm{v}}$	−2.272	−0.038	0	12	5	0	12	2.769	2.931	18	7.6	19.1
17:3	$C_{2\mathrm{v}}$	$C_{2\mathrm{v}}$	−2.277	−0.128	0	12	5	0	12	2.762	3.139	17	5.5	20.8
18:1	C_2	C_2	−2.307	0.321	0	12	6	0	12	2.736	2.934	17	9.2	16.9
18:2	D_2	D_2	−2.290	0.627	0	12	6	0	12	2.733	2.935	18	11.6	17.2
18:3	$D_{3\mathrm{d}}$	$D_{3\mathrm{d}}$	−2.275	0.896	0	12	6	0	12	2.714	2.894	18	12.1	18.2
18:4	C_2	C_2	−2.321	0.073	0	12	6	0	12	2.749	2.931	16	7.2	18.7
18:5	$D_{3\mathrm{h}}$	$D_{3\mathrm{h}}$	−2.303	0.386	0	12	6	0	12	2.763	3.159	8	15.1	27.3
18:6	D_3	D_3	−2.310	0.270	0	12	6	0	12	2.742	2.945	15	5.8	15.2
19:1	C_2	C_2	−2.298	1.196	0	12	7	0	12	2.745	3.006	17	14.9	26.0
19:2	C_s	C_s	−2.307	1.014	0	12	7	0	12	2.747	2.972	15	7.5	20.0
19:3	C_s	C_s	−2.304	1.077	0	12	7	0	12	2.737	2.957	15	11.9	28.3
19:4	C_2	C_2	−2.311	0.935	0	12	7	0	12	2.745	2.905	15	7.0	17.7
19:5	C_2	C_2	−2.313	0.911	0	12	7	0	12	2.734	2.947	14	6.6	18.7
19:6	$C_{3\mathrm{v}}$	$C_{3\mathrm{v}}$	−2.316	0.854	0	12	7	0	12	2.765	2.890	15	12.7	30.6
20:1	C_2	C_1	−2.324	1.684	2	8	10	0	12	2.711	2.984	16	15.3	36.7
20:2	D_2	D_2	−2.295	2.271	0	12	8	0	12	2.699	3.023	18	20.4	22.0
20:3	C_1	C_1	−2.339	1.395	2	8	10	0	12	2.724	2.954	15	13.1	129.1
20:4	C_s	C_s	−2.324	1.695	0	12	8	0	12	2.709	3.023	16	13.7	25.5
20:5	D_2	D_2	−2.332	1.541	0	12	8	0	12	2.749	3.080	16	18.5	17.3
20:6	$D_{2\mathrm{d}}$	$C_{2\mathrm{v}}$	−2.337	1.440	2	8	10	0	12	2.752	2.977	14	9.8	26.6
20:7	C_1	C_1	−2.325	1.663	2	9	8	1	12	2.712	3.019	14	10.9	25.8
20:8	C_s	C_s	−2.346	1.256	2	8	10	0	12	2.748	3.057	14	8.4	40.7
20:9	$C_{2\mathrm{v}}$	$D_{6\mathrm{h}}$	−2.362	0.938	6	0	14	0	12	2.744	2.971	13	3.8	23.2
20:10	C_2	C_2	−2.344	1.299	2	8	10	0	12	2.726	3.004	14	12.6	23.9
20:11	C_2	C_s	−2.346	1.256	2	8	10	0	12	2.747	3.056	13	8.1	35.8
20:12	C_2	C_1	−2.366	0.861	3	5	4	7	4	2.719	3.048	13	5.4	21.1
20:13	$D_{3\mathrm{h}}$	$D_{6\mathrm{h}}$	−2.362	0.938	6	0	14	0	12	2.744	2.970	15	6.5	27.9
20:14	$D_{2\mathrm{d}}$	$D_{2\mathrm{d}}$	−2.311	1.948	0	12	8	0	12	2.779	2.929	12	3.7	22.0
20:15	$D_{6\mathrm{h}}$	$D_{6\mathrm{h}}$	−2.362	0.936	6	0	14	0	12	2.744	2.972	12	4.5	25.6
32:1082	I_h	I_h	−2.494	1.537	0	12	20	0	12	2.793	2.835	0	0	7.5
(111)	2D	sheet	−2.994	–	0	0	∞	0	–	2.722	2.722	0	0	0
fcc	3D	bulk	−3.677	–	–	–	–	–	–	2.897	2.897	–	–	–

Table 7.2 Topological parameters for the anionic gold clusters. Number of gold atoms and isomer numbers of the fullerene in canonical order of the pentagon spiral indices,[181] ideal and actual point group symmetry, energy differences ΔE_g to the most stable anionic cluster of same size and binding energy per atom $\Delta E_n = [E(\mathrm{Au}_n) - (n-1)E(\mathrm{Au}) - E(\mathrm{Au}^-)]/n$ (in eV), shortest and largest bond distance (in Å), and distortion parameter D (in %) for the GDF.

	symmetry		stability		vertices					bondlengths		D
isomer	ideal	actual	ΔE_n	ΔE_g	$\lvert N_4\rvert$	$\lvert N_5\rvert$	$\lvert N_6\rvert$	$\lvert N_7\rvert$	Γ	shortest	largest	GDF
12:1	I_h	D_2d	−2.137	0.665	8	0	4	0	16	2.780	2.869	23.0
14:1	D_6d	D_2d	−2.242	−0.089	0	12	2	0	12	2.758	2.989	20.3
15:1	D_3h	C_2v	−2.281	0.473	0	12	3	0	12	2.741	3.029	21.2
16:1	D_2	D_2	−2.328	0.020	0	12	4	0	12	2.764	2.905	17.7
16:2	T_d	D_2d	−2.330	0.000	0	12	4	0	12	2.738	2.907	16.2
17:1	D_5h	D_5h	−2.353	0.469	0	12	5	0	12	2.757	3.017	13.2
17:2	C_2v	C_2v	−2.368	0.215	0	12	5	0	12	2.742	2.994	14.4
17:3	C_2v	C_2v	−2.376	0.087	0	12	5	0	12	2.731	3.019	14.2
18:1	C_2	C_2	−2.360	0.589	0	12	6	0	12	2.734	2.968	16.8
18:2	D_2	C_2	−2.346	0.848	0	12	6	0	12	2.733	3.059	16.8
18:3	D_3d	C_2	−2.348	0.817	4	4	10	0	12	2.701	3.038	24.3
18:4	C_2	C_1	−2.364	0.529	0	12	6	0	12	2.740	3.048	19.0
18:5	D_3h	D_3h	−2.364	0.516	0	12	6	0	12	2.710	3.023	27.5
18:6	D_3	D_3	−2.357	0.642	0	12	6	0	12	2.734	2.912	14.7
19:1	C_2	C_2	−2.384	0.967	4	4	11	0	12	2.732	2.985	28.5
19:2	C_s	C_s	−2.368	1.268	2	9	7	1	12	2.727	2.989	16.9
19:3	C_s	C_3v	−2.381	1.022	0	12	7	0	12	2.755	3.046	32.6
19:4	C_2	C_2	−2.390	0.853	2	8	9	0	12	2.744	3.003	22.1
19:5	C_2	C_2	−2.398	0.698	2	8	9	0	12	2.743	2.963	31.3
19:6	C_3v	C_3v	−2.381	1.023	0	12	7	0	12	2.756	3.044	32.4
20:1	C_2	C_1	−2.386	0.927	2	8	10	0	12	2.748	3.032	25.0
20:2	D_2	D_2	−2.365	1.348	0	12	8	0	12	2.731	2.971	43.8
20:3	C_1	C_1	−2.396	0.716	2	8	10	0	12	2.745	2.926	23.4
20:4	C_s	C_s	−2.385	0.950	0	12	8	0	12	2.740	2.939	24.4
20:5	D_2	D_2	−2.390	0.850	0	12	8	0	12	2.775	2.907	37.4
20:6	D_2d	C_s	−2.382	1.001	2	8	10	0	12	2.770	2.948	20.5
20:7	C_1	C_1	−2.384	0.974	0	12	8	0	12	2.739	3.079	25.3
20:8	C_s	C_s	−2.388	0.888	2	8	10	0	12	2.761	2.977	22.0
20:9	C_2v	D_6h	−2.402	0.610	6	0	14	0	12	2.731	2.971	27.1
20:10	C_2	C_2	−2.404	0.568	2	8	10	0	12	2.743	2.984	37.1
20:11	C_2	C_1	−2.378	1.093	3	8	7	2	12	2.732	3.018	26.5
20:12	C_2	C_s	−2.412	0.407	2	8	3	6	6	1.755	2.996	192.0
20:13	D_3h	D_6h	−2.402	0.610	6	0	14	0	12	2.731	2.972	27.0
20:14	D_2d	C_1	−2.405	0.544	2	8	1	8	12	2.710	3.010	199.2
20:15	D_6h	D_6h	−2.361	1.430	0	12	8	0	12	2.792	2.933	15.2
32:1082	I_h	D_2h	−2.524	2.201	0	12	20	0	12	2.766	3.004	10.4

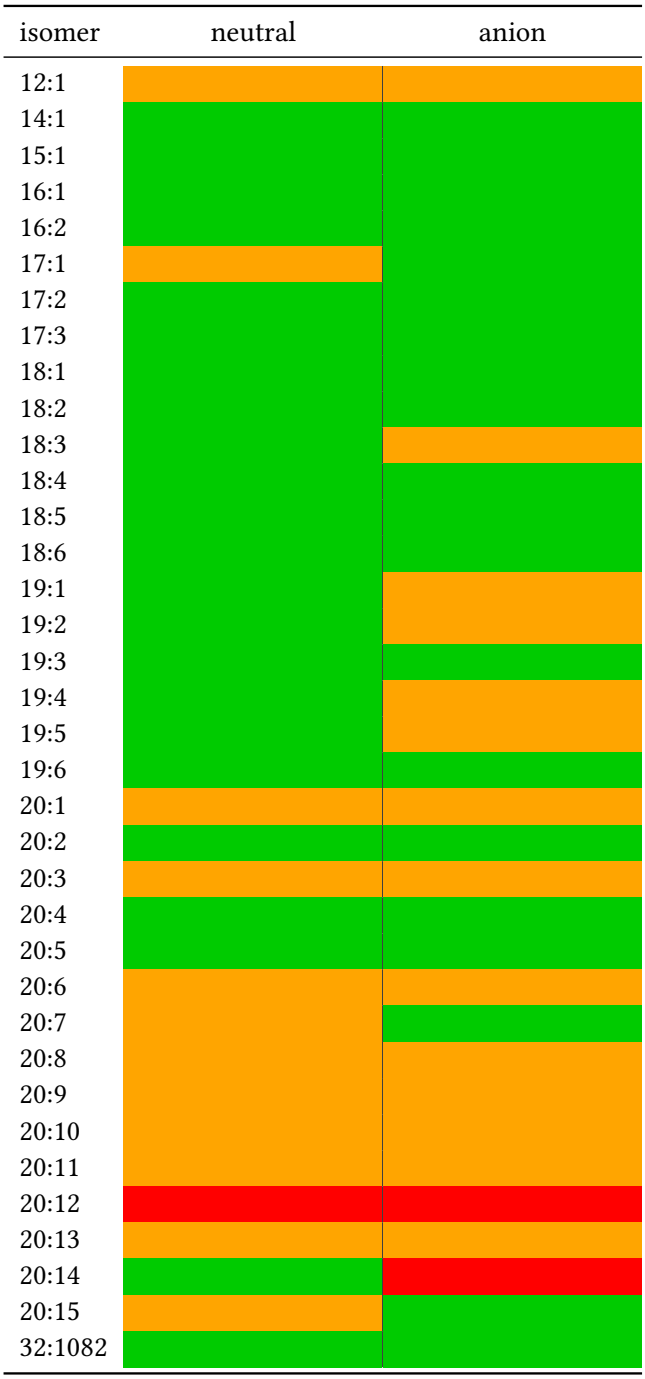

Figure 7.7 Overview of PBE-D3 optimisation results for the dual fullerene structures. Green: dual fullerene structure, orange: hollow structure, red: non-hollow structure.

fullerenes try to adopt "spherical" shapes if permitted by the distribution of pentagons. This is especially the case for I_h-C_{20} and I_h-C_{60} with a distortion parameter of exactly zero (i.e. all atoms lie on a sphere). In contrast, the golden dual fullerene structures have much larger distortion parameters D(GDF) than their carbon equivalent and are therefore less spheroidal. The golden dual fullerenes usually distort into less symmetric structures, for example into oblate structures as mentioned above.

Figure 7.8 shows the relative energies ΔE_g per atom compared to the most stable compact arrangement for all optimised hollow gold clusters. It is imme-

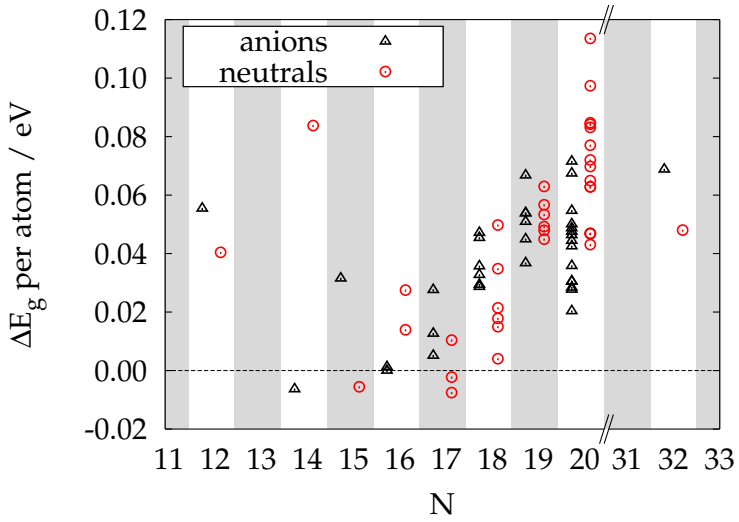

Figure 7.8 Relative energies for the investigated dual fullerene clusters. Energy differences compared to the most stable compact cluster (per atom) are given in eV.

diately apparent, that the most stable dual fullerene structures can be found in the region of 14 to 18 atoms. Some clusters in this region even exceed the stability of formerly proposed global minimum structures. For example, for Au_{16}^- the global minimum has been proposed previously to be the tetrahedral hollow cluster,[200,201] which is the dual of the tetrahedral C_{28} isomer as observed experimentally in photoelectron spectra.[178] It should be noted, that Chen et al. have found the tetrahedral structure to lie 0.22 eV above a sheet-like structure.[164] However, our results contradict these findings as the planar structure is predicted to be 0.939 eV higher in energy. Another interesting result from the investigation of the cohesive energies is that the D_2 symmetric isomer 16:1 lies only 0.02 eV above the tetrahedral structure. Therefore, it should also be possible to observe this isomer by experimental methods.

Possible Au_{32} structures have been investigated intensively by Jalbout et al.[208] Table 7.3 shows their results in comparison with results from this work.

For both neutral and anionic clusters, isomer 10 in their work turns out to

Table 7.3 Binding energy per atom (in eV) for investigated neutral and anionic compact cluster compounds. For the definition of the binding energy see tables 7.1 and 7.2, and for the definition of the isomers 1 and 10 for Au_{32} see Jalbout et al.[208]

N	sym.	ΔE_n(neutral)	N	sym.	ΔE_n(neutral)	N	sym.	ΔE_n(anion)
2	$D_{\infty h}$	-1.105	13	C_{2v}	-2.087	12	D_{3h}	-2.192
3	C_{2v}	-1.152	14	C_{2v}	-2.218	14	D_{2h}	-2.236
4	D_{2h}	-1.486	15	C_s	-2.186	15	C_1	-2.313
5	C_{2v}	-1.631	16	C_s	-2.261	16	D_{2d}	-2.330
6	D_{3h}	-1.875	17	C_s	-2.270	17	C_{2v}	-2.381
7	C_s	-1.833	18	C_s	-2.325	18	C_{2v}	-2.393
8	D_{4h}	-1.959	19	C_{3v}	-2.361	19	C_{3v}	-2.435
9	C_{2v}	-1.944	20	T_d	-2.409	20	T_d	-2.432
10	D_{2h}	-2.028	32	C_{3v}	-2.491	32	C_{3v}	-2.548
11	D_{3h}	-2.063	32	Isomer 1	-2.536	32	Isomer 1	-2.590
12	D_{3h}	-2.098	32	Isomer 10	-2.542	32	Isomer 10	-2.593

be the most stable compact geometry and the icosahedral hollow structure 32:1082 is less stable in both the neutral and the anionic cases. The C_{3v}-symmetric compact structure not investigated before is also included in table 7.3. It is derived from the ideal Au_{35} tetrahedron by removing three of the corner atoms of the tetrahedron and can be viewed as a cut-out of the fcc bulk structure. This cluster is also very stable compared to the other structures proposed by Jalbout et al. As reflected by the distortion parameter D of the Au_{32} hollow cage ($D(Au_{32}) = 10.4$) it deviates slightly from an ideal icosahedral symmetry and can be seen as pseudo-spherical.

7.5 Convergence Towards the Infinite Structure

The neutral gold clusters and their property convergence towards the bulk has already been discussed in previous papers.[151] Increasing the size of non-hollow compact clusters lowers the cohesive energy until the clusters are large enough to be a valid representation of the bulk gold structure. This can be seen in figure 7.9a, where a clear linear correlation between $N^{-1/3}$ and the cohesive energy is depicted. Hollow gold clusters can be created by wrapping a cut-out from a (111) gold 2D sheet around a sphere while introducing 12 vertices of degree 5 to satisfy Euler's theorem. Therefore, an infinitely large 2D gold sheet represents a golden dual fullerene cage with an infinite sphere radius. As the cohesive energy of the compact structures converges towards the bulk cohesive energy, the cohesive energy of the 2D triangulated gold sheet should represent the infinite limit for the dual golden fullerene structures. This is indeed the case and is depicted in figure 7.9b using a N^{-1}

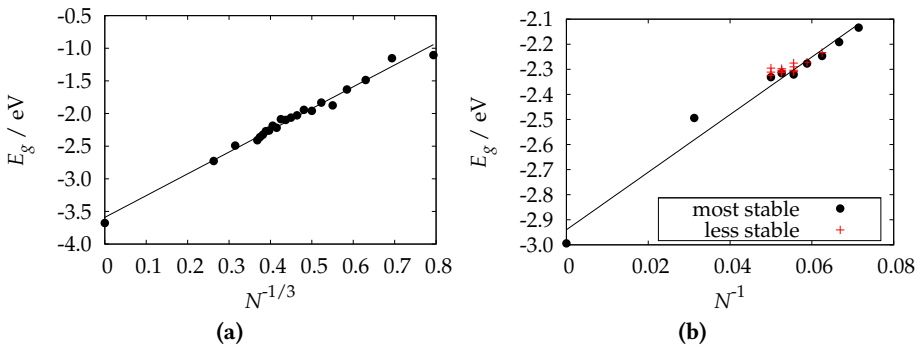

Figure 7.9 Cohesive energies for (a) the compact gold clusters with cluster size N and convergence toward the bulk fcc structure and (b) for the hollow gold clusters with cluster size N and convergence toward the (111) gold sheet.

scaling law analogous to the one used for fullerenes.[195]

An interesting result was the difference between the cohesive energy of the bulk fcc structure compared to the (111) 2D sheet. Creating the bulk structure from stacking (111) sheets only accounts for ∼0.68 eV of the total cohesive energy of the bulk which is 3.81 eV.[209] This implies that most of the cohesive energy of bulk gold originates from the (111) sheet, which is therefore exceptionally stable and can be seen as a reason for the preferred planar arrangement of many small gold clusters. As pointed out by Takeuchi et al, relativistic effects increase the cohesive energy of bulk gold by 1.5 eV.[209] A similar large relativistic effect is expected for the (111) sheet of gold.

7.6 Simulation of Photoelectron Spectra

Photoelectron spectra of several GDFs have been determined experimentally and simulated with theoretical methods by Bulusu et al.[178] Before the discussion of results produced in this work can commence, the spin-orbit effects from substantial 5d-mixing into the 6s orbitals in gold need to be considered. Figure 7.10 shows a comparison of simulated photoelectron spectra of the three golden dual fullerene isomers of Au_{17}^-. The results clearly indicate that spin-orbit effects can be safely neglected in this energy range.

Bulusu et al. considered only the T_d-Au_{16} structure. From the simulations carried out in this section there is reason to believe that the other possible isomer 16:1 is also present in the measured spectrum. Figure 7.11a shows these simulation results for the isomers 16:1 and 16:2 and a simulation for a mixture of both compounds with a ratio of 1:1 as the energy of both isomers is comparable. Looking at the experimental data, a shoulder can be identified in the first peak. This feature can be reproduced by shifting the spectra for

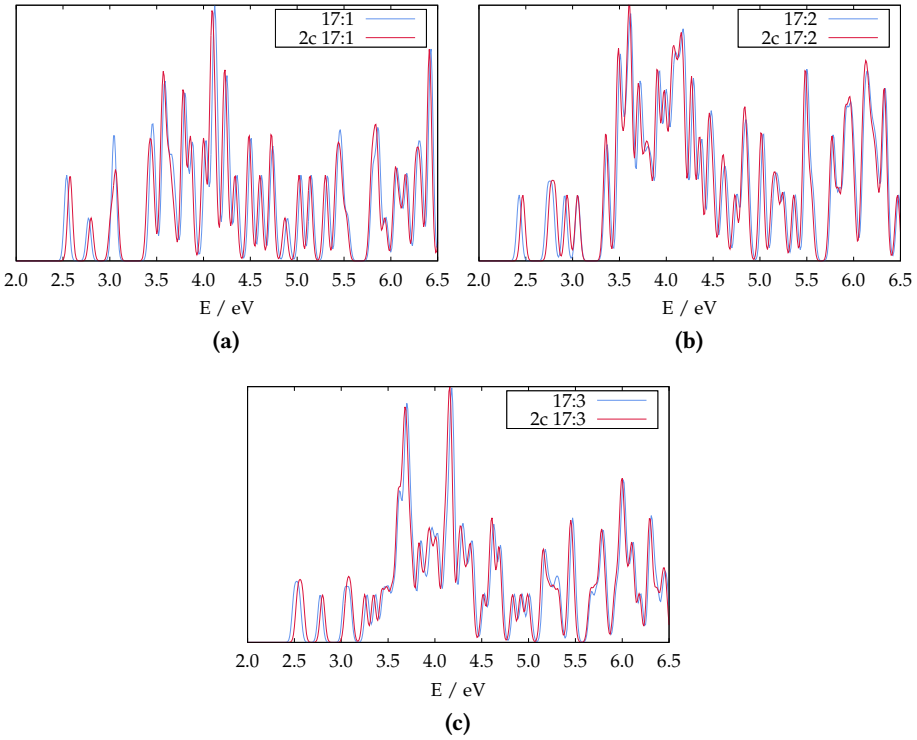

Figure 7.10 Comparison of simulated photoelectron spectra of the three dual fullerene isomers of Au_{17}^- with (2c) and without spin-orbit coupling.

16:1 and 16:2 according to the corresponding vertical ionisation potential, superimposing both spectra and shifting the result by 0.18 eV to better fit the experimental data as pictured in figure 7.11a. This indicates that the second hollow cage isomer has also been produced. Further evidence for this could be the experimental peak at 5.51 eV. The simulated spectrum for the tetrahedral cluster shows a dip at this energy, while the D_2 structure has a clear intensity maximum.

Figure 7.11b shows the simulated spectra for the three possible dual fullerene isomers for Au_{17}^-. The spectra have been shifted according to the vertical ionisation potential of the negatively charged clusters. The most stable structures are 17:2 (red) and 17:3 (green) of which 17:2 fits reasonably well for the first 4 peaks. The peak at 4.73 eV could be accounted to the 17:3 isomer identical to Bulusu et al.'s C_{2v} symmetric structure.

From the relative energies in figure 7.8 it is clear that anionic dual fullerene structures start to become rather unstable for $N = 18$. Therefore, compact clusters might dominate the experimental spectrum. Figure 7.11c shows our calculated spectra in comparison with the experimental data. The calculated spectra have been shifted to the corresponding vertical ionisation potential

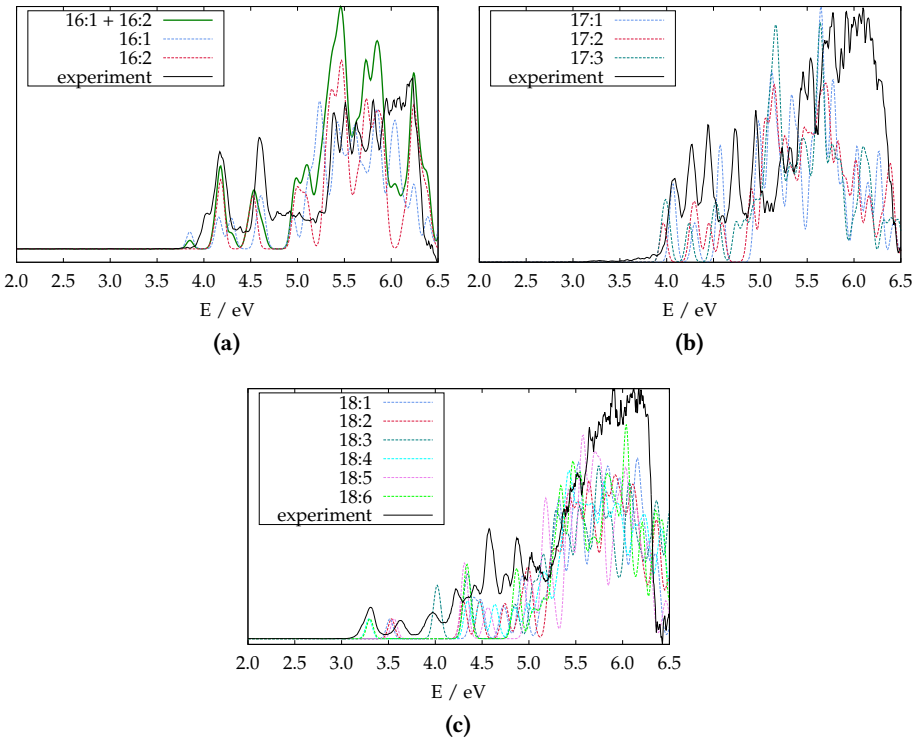

Figure 7.11 Simulated photoelectron spectra for the negatively charged hollow gold clusters (shifted to the experimental threshold energy). (a) The two possible dual fullerene isomers of Au_{16}^-. The green curve shows a combination of the D_2 and T_d spectra with a ratio of 1:1.; (b) The three possible dual fullerene isomers of Au_{17}^-; (c) The six possible dual fullerene isomers of Au_{18}^- (shifted to the experimental threshold energy).

first and subsequently shifted by 0.25 eV to better fit the experimental data. The most stable dual fullerene clusters are 18:1, 18:4 and 18:5. 18:1 and 18:5 could be responsible for the second peak in the experimental data at 3.63 eV, while 18:4 agrees with the first peak. The signal at 3.97 eV could be an indication that isomer 18:3 was produced as it is the only structure that shows a peak in that area, however, it is the least stable of the hollow structures.

Finally, for future experiments a simulated photoelectron spectrum for Au_{32}^- is shown in figure 7.12.

7.7 Conclusion

An interesting topological relationship between fullerenes and the cage-like gold clusters resulting in a triangulation of a sphere with vertices of degrees

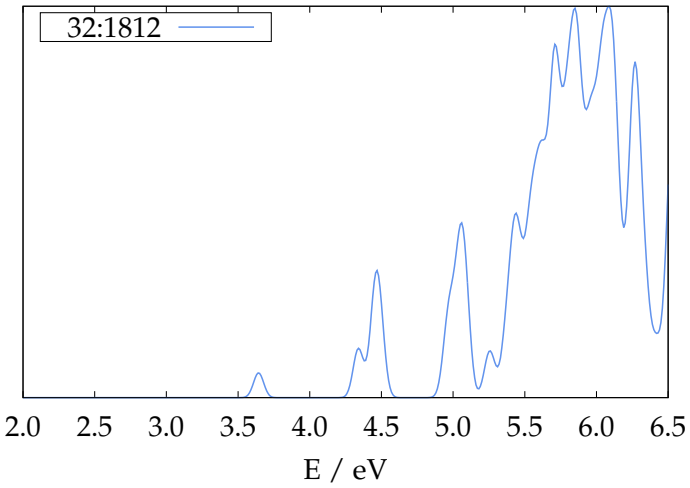

Figure 7.12 Simulated photoelectron spectra for isomer 32:1812 of Au_{32}^-.

5 and 6 fulfilling Euler's polyhedral formula was found. Because of this isomorphism between the two types of structures by dualisation, there are as many golden fullerene isomers as there are fullerene isomers. Gold nanotubes and carbon nano-tubes and halma transforms of C_{20} to the shells of a Mackay icosahedron are related in the same way. The stability of these golden fullerenes was investigated. While they perhaps may not compete in energy with the more compact gold clusters at larger cluster size, the smaller cage structures are stable as observed by photoelectron spectroscopy. The simulated photoelectron spectra suggest that more than one golden fullerene isomer was observed.

A natural step in the next direction would be to stabilise such hollow gold clusters by either endohedral enclosure of gold or other metal atoms, by attaching appropriate ligands to the outside of the cage, or both. Results have already shown that enclosing a transition metal with the right amount of valence electrons can stabilise otherwise instable hollow structures, like the icosahedral Au_{12}, drastically.[206]

8 From Sticky-Hard-Sphere to Lennard-Jones-Type clusters[a]

8.1 Introduction

Nucleation is a phenomenon that is a part of many natural processes and is present in many everyday phenomena. Naturally, there is a large research interest in this field, especially with respect to the nucleation of atoms and molecules to clusters, eventually leading to the solid state.[21,211–217] In an early Faraday Discussion taking place in Bristol in 1949 Rowland concluded the meeting with the assessment "that the gap between the theoretical and experimental approaches has been too wide".[218] Here, he was referring to the subject of nucleation. In a Faraday discussion about half a century later Vlieg et al. stated that "the gap between the quite detailed experimental information [...] and theoretical models, though getting smaller, is still large".[213]

One reason for this slow progress in the theoretical description of nucleation processes is that it is related to global optimisation problems. Exploring the multi-dimensional potential energy surface belongs to the computational complexity class "NP-complete", as already mentioned in chapter 4.5. The number of local minima is expected to grow exponentially,[18,21,219–223] which is problematic, because interesting phase transitions usually occur for larger cluster sizes N that can not be treated by accurate quantum mechanical methods as introduced in chapter 3. One such phase transition is the transformation of argon clusters from icosahedral clusters into anti-Mackay clusters for sizes of $N > 2000$ and finally into face-centered cubic (fcc) or hexagonal-closed packed (hcp) solid state structures for $N > 10^5$.[224] Similar results are predicted by the Lennard-Jones (LJ) potential.[106,211,225]

Because of the exponentially growing potential energy landscapes and the large cluster sizes required to model phase transitions, investigations of this type often have to rely on approximate interaction potentials. In this part of the thesis two interaction potentials introduced in chapter 5 are used. The first and maybe simpler one is the sticky-hard-sphere (SHS) potential V_{SHS},

[a] This chapter is composed of sections previously published in the article "From Sticky-Hard-Sphere to Lennard-Jones-Type Clusters"[210] and is reprinted with permission from the publisher ©2018 American Physical Society. Some sections have been modified to fit the style of this thesis.

originally introduced by Baxter.[111]

$$V_{\mathrm{SHS}}(r) = \begin{cases} \infty, & r < r_s \\ -\varepsilon, & r = r_s \\ 0, & r > r_s \end{cases} \tag{8.1}$$

ε and the equilibrium distance r_s can be set to unity without changing the qualitative information contained in the potential energy surface (PES).

One of the defining properties for clusters bound by the SHS potential is the contact number N_c, which is directly related to the energy of the cluster $E = -N_c\varepsilon$. How the number of contact points a cluster possesses grows with its size N is still researched actively. From the Gregory-Newton argument,[b] which was proven in 1953, it follows that each sphere can not be surrounded by more than 12 other spheres of the same size. For small clusters, the maximum number is governed by the total number of (unique) entries in the adjacency matrix, i.e. max $\leq N(N-1)/2$. Combining these two facts leads to a loose upper bound

$$N_c^{\max}(N) \leq \min\{N(N-1)/2, f(N)\}. \tag{8.2}$$

Using the Gregory-Newton argument results in $f(N) = 6N$, however, a tighter upper bound has been published more recently by Bezdek et al.[226]

$$f(N) = 6N - 3(18)^{1/3}\pi^{-2/3}N^{2/3}. \tag{8.3}$$

Theoretical investigations of the cluster landscape by means of the exact enumeration method revealed that the contact numbers for clusters of size $4 \leq N \leq 19$ are[114,116]

$$N_c^{\max}(N) = \{6, 9, 12, 15, 18, 21, 25, 29, 33, 36, 40, 44, 48, 52, 56, 60\}. \tag{8.4}$$

The exact solution for $N_c^{\max}(N)$ for arbitrary N is called the Erdős unit distance problem, which remains unsolved.[227]

The number of non-isomorphic cluster structures $|\mathcal{M}(N)|$[c] is expected to grow exponentially.[22,219,228] The exact numbers for $|\mathcal{M}(N)|$ have been determined via exact enumeration studies for clusters of size $N \leq 14$.[114,116] Studies of this type are difficult to carry out, because they are computationally expensive.[229]

Another interaction potential often used in cluster science is the Lennard-Jones (LJ) potential, as introduced in section 5.2. It is most commonly used in

[b] For a more thorough discussion of this argument please refer to chapter 9.

[c] $\mathcal{M}(N)$ refers to the set of all non-isomorphic cluster structures, while the size of the set is denoted $|\mathcal{M}(N)|$.

the $(6, 12)$ form, but in this section it will be employed with arbitrary integer exponents (m, n).

$$V_{m,n}^{\mathrm{LJ}}(r) = \frac{\varepsilon}{n-m}\left[m\left(\frac{r_e}{r}\right)^n - n\left(\frac{r_e}{r}\right)^m\right] \qquad (\text{with } n > m) \qquad (8.5)$$

The two parameters ε and r_e are the depth of the potential energy well and the equilibrium distance, respectively. The values for ε and r_e will be set to unity in the following for the same reasons as for the SHS potential. As already mentioned in chapter 5, the SHS potential emerges from the LJ potential as the limit for large exponents (m, n) (figure 8.1).

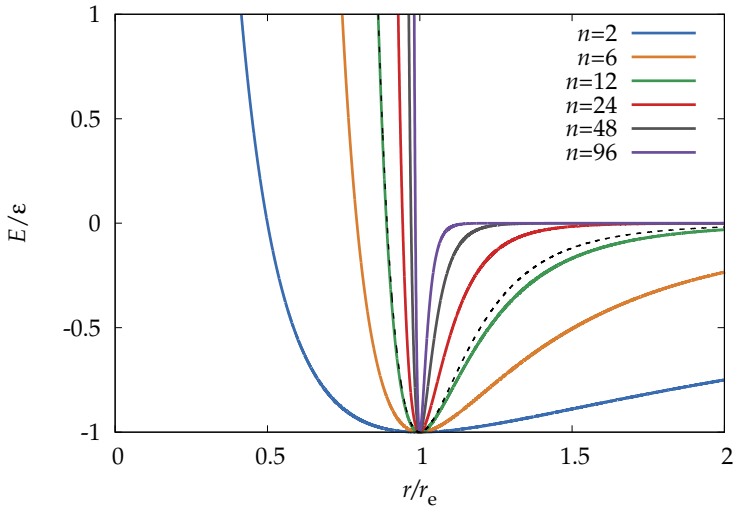

Figure 8.1 Lennard-Jones potentials for different exponents (m, n) with fixed $n = 2m$. As the exponents grow larger, the well of attraction becomes narrower and its shape approaches the SHS potential. The dashed line shows the extended Lennard-Jones potential for the xenon dimer.[107]

At first, it seems surprising that the absolute number of structures for a certain size N differs substantially between the two potentials. For $N = 13$ there are $|\mathcal{M}_{\mathrm{SHS}}| = 97,221$ non-isomorphic SHS clusters,[114,116] but only $|\mathcal{M}_{\mathrm{LJ}}| = 1,510$ $(6, 12)$-LJ clusters.[230] However, this is a known behaviour of energy landscapes of long-range (LJ) and short-range (SHS) potentials, with the latter generally supporting many more local minima compared to the former.[231,232] Decreasing the exponents (m, n) increases the range of the potential, which leads to increased second-nearest-neighbour interactions. Furthermore, fold catastrophes[12,232] lead to the collapse of several stable SHS structure into a single LJ minimum, leading to a decrease in the overall size of $|\mathcal{M}(N)|$.

In the following sections, the evolution of LJ clusters towards SHS clusters by gradually decreasing the range of the LJ potential is explored. Additionally,

the results from optimising with a LJ potential starting from the SHS cluster is compared to the traditional approach of global optimisation.

8.2 Computational Details

The *pele* program[233] was used to generate putatively complete sets of local minima for (m, n)-Lennard-Jones potentials $V_{mn}^{\mathrm{LJ}}(r)$ as defined in equation (8.5). This program applies a basin-hopping algorithm that divides the potential energy surface into basins of attraction, effectively mapping each point in configuration space to a local minimum structure.[80,83,234] The results confirmed the number of local minima reported in previous work.[110] Finite computer time limited the search to clusters of size $N \leq 13$.

Starting from the sticky hard sphere packings up to $N = 14$, with Cartesian coordinates given by the exact enumeration algorithm[115] including rigid hypostatic clusters ($N_c < 3N - 6$),[114] geometry optimisations with (m, n)-Lennard-Jones potentials using the multidimensional function minimiser from the C++ library *dlib*[118] were carried out with the previously described program package SPHERES (Chapter 6). The optimisation scheme was either the Broyden-Fletcher-Goldfarb-Shanno (BFGS) or the conjugate gradient algorithm. The optimisations were terminated when the change in energy (in reduced units) over the course of one optimisation cycle was smaller than 10^{-15}.

Subsequently, the eigenvalues of the Hessian were checked for all stationary points. If negative eigenvalues were found, the affected structures were re-optimised following displacements in both directions along the corresponding eigenvectors to locate true local minima. This procedure assures that the floppy SHS packings are successfully mapped into LJ minima.

As the optimisations often result in many duplicates, especially for small values of n and m where $|\mathcal{M}_{(m,n)-\mathrm{LJ}}| \ll |\mathcal{M}_{\mathrm{SHS}}|$, the final structures were further analysed and sorted. Non-isomorphic SHS clusters can be distinguished (apart from permutation of the particles) by their different adjacency matrices for $N \leq 13$.[114] This is not the case for soft potentials like the LJ potential since drawing edges (bonds) between the vertices (atoms) becomes a matter of defining the distance cut-off criterion for a bond to be drawn. Therefore, the clusters were compared based on the Euclidean distance matrix (EDM) (the matrix of inter-particle distances $\{r_{ij}\}$) as described previously: two clusters are isomorphic (structurally identical) if they have the same ordered set of inter-particle distances $\{r_{ij}\}$. While enantiomers cannot be separated using this methodology, permutation-inversion isomers are usually lumped together, since the number of distinct minima is analytically related to the order of the corresponding point group.[12] To verify the number

of distinct structures a second ordering scheme using the energy and moment of inertia tensor eigenvalues was introduced.

Two sets of structures are obtained from the optimisation procedure: the first set contains all possible LJ minima $\mathcal{M}_{\mathrm{LJ}}$ from the basin-hopping algorithm, while the second set $\mathcal{M}_{\mathrm{SHS}\to\mathrm{LJ}}$ contains the LJ minima obtained using only the $\mathcal{M}_{\mathrm{SHS}}$ sticky-hard-sphere cluster structures as starting points for the geometry optimisation. To compare and identify corresponding structures between the two sets, the $N(N-1)/2$ inter-particle distances $\{r_{ij}\}$ were again used as an identifying fingerprint.

Two-body extended Lennard-Jones (eLJ) potentials that accurately model two-body interactions in rare-gas clusters can be written as expansions of inverse-power-law terms:[106]

$$V_{\mathrm{E}LJ}(r) = \sum_n c_n r^{-n}, \tag{8.6}$$

where in reduced units the condition $\sum_n c_n = -1$ holds. For comparison to the simple (6,12)-LJ potential, the eLJ potential derived from relativistic coupled-cluster theory applied to the xenon dimer was used with the following coefficients (in reduced units): $c_6 = -1.0760222355$; $c_8 = -1.4078314494$; $c_9 = -185.6149933139$; $c_{10} = +1951.8264493941$; $c_{11} = -8734.2286559729$; $c_{12} = +22273.3203327203$; $c_{13} = -35826.8689874832$; $c_{14} = +37676.9744744424$; $c_{15} = -25859.2842295062$; $c_{16} = +11157.4331408911$; $c_{17} = -2745.9740079192$; $c_{18} = +293.9003309498$.[107] The eLJ potential for xenon is shown in figure 8.1 (dashed line).

8.3 Exploring the Limits of Lennard-Jones

To study the convergence behaviour of the number of distinct (non-isomorphic) LJ minima in the SHS limit, geometry optimisations were carried out, starting from all non-isomorphic SHS structures. It will be shown later that the number of unique minima obtained in this procedure $|\mathcal{M}_{\mathrm{SHS}\to\mathrm{LJ}}|$ only misses out on a small portion of minima obtained from the more exhaustive basin-hopping approach, i.e. $|\mathcal{M}_{\mathrm{SHS}\to\mathrm{LJ}}| \approx |\mathcal{M}_{\mathrm{LJ}}|$. The results for a constant chosen ratio of LJ exponents $n/m = 2$ are shown in figure 8.2 (top). $|\mathcal{M}_{\mathrm{SHS}\to\mathrm{LJ}}|$ smoothly converges towards the SHS limit (dashed line, values in table 8.1) from below, thus demonstrating that for LJ systems the number of distinct minima does not grow faster than exponentially. The (48,96)-LJ potential has $\Delta\mathcal{M} \equiv |\mathcal{M}_{\mathrm{LJ}}| - |\mathcal{M}_{\mathrm{SHS}\to\mathrm{LJ}}| = \{1, 1, 7, 91, 1019, 14890, 209938\}$ fewer stable minima than the SHS potential. The fractions of missing minima $\Delta\mathcal{M}/|\mathcal{M}_{\mathrm{SHS}}|$ for this potential grow with increasing N and are, respectively, $\{7.69, 1.92, 2.67, 5.46, 8.62, 15.32, 23.44\}\%$. Note that for

Table 8.1 Number of distinct local minima $|\mathcal{M}_{\mathrm{SHS}}|$ for cluster size N (from references [114–116]) and contact number N_c from the exact enumeration, compared to the number of different structures obtained from a geometry optimisation starting from the set $\mathcal{M}_{\mathrm{SHS}}(N, N_c)$ for a (6,12)-LJ potential. The overall number of unique minima $|\mathcal{M}_{\mathrm{SHS}\to\mathrm{LJ}}| = \sum_{N_c} |\mathcal{M}_{\mathrm{SHS}\to\mathrm{LJ}}(N_c)| -$ (# of duplicate structures) is shown in the following column. This result can be compared to the number of unique minima found using the basin-hopping method ($|\mathcal{M}_{\mathrm{LJ}}|$). The difference $\Delta\mathcal{M} = |\mathcal{M}_{\mathrm{LJ}}| - |\mathcal{M}_{\mathrm{SHS}\to\mathrm{LJ}}|$ is also listed.

N	N_c	$\lvert\mathcal{M}_{\mathrm{SHS}}(N_c)\rvert$	$\lvert\mathcal{M}_{\mathrm{SHS}\to\mathrm{LJ}}(N_c)\rvert$	$\lvert\mathcal{M}_{\mathrm{SHS}\to\mathrm{LJ}}\rvert$	$\lvert\mathcal{M}_{\mathrm{LJ}}\rvert$	$\Delta\mathcal{M}$
8	18	13	8	8	8	0
9	21	52	20	20	21	1
10	23	1	1			
	24	259	60	62	64	2
	25	3	3			
11	25	2	2			
	26	18	6			
	27	1620[a]	158	165	170	5
	28	20	12			
	29	1	1			
12	28	11	6			
	29	148	24			
	30	11638	483	504	515	11
	31	174	69			
	32	8	6			
	33	1	1			
13	31	87	23			
	32	1221	100			
	33	95810[a]	1418	1476	1510	34
	34	1318[a]	293			
	35	96	49			
	36	8	6			
14	33	1	1			
	34	707	101			
	35	10537	410			
	36	872992	3939	4093	(4187)[b]	(94)[b]
	37	10280	1002			
	38	878	237			
	39	79	42			
	40	4	3			

[a] Largest value for $|\mathcal{M}_{\mathrm{SHS}}|$ taken from references [114–116]. [b] Estimated.

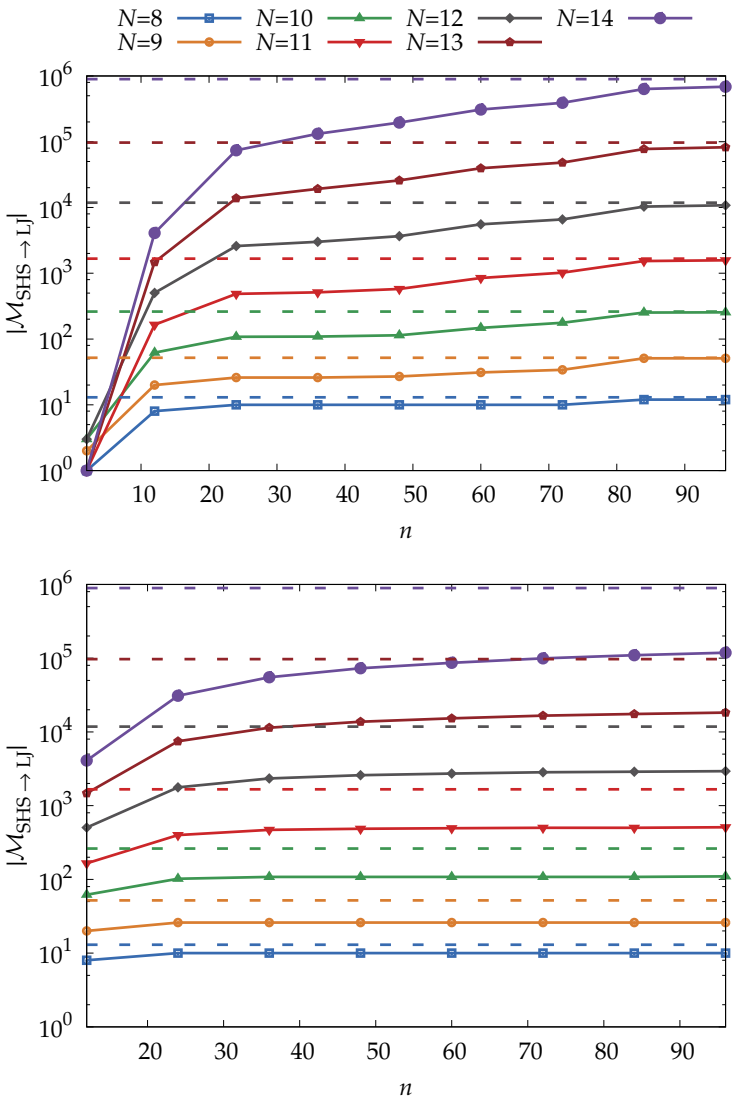

Figure 8.2 Convergence of the number of distinct LJ local minima $|\mathcal{M}_{\mathrm{SHS}\to\mathrm{LJ}}|$ obtained through geometry optimisations starting from the non-isomorphic SHS structures with increasing LJ exponent n. Permutation-inversion isomers and enantiomers are not distinguished. The dashed line gives the exact SHS limit $|\mathcal{M}_{\mathrm{SHS}}|$. Top panel: $m = n/2$. Bottom panel: fixed $m = 6$.

$N \geq 10$ most of these missing minima correspond to high energy ($N_c < N_c^{\max}$) structures.

If the exponent n for the repulsive part of the LJ potential is increased with m kept constant, the LJ potential becomes equivalent to the SHS potential in the repulsive range but remains attractive at long range. This limit is also called the Sutherland potential. Figure 8.2 (bottom) shows the convergence of the number of unique structures with respect to n at set $m = 6$ towards the SHS limit. Here, the number of distinct minima converges towards a number that is much smaller than the total number of SHS packings demonstrating that (as expected) the attractive part of the potential contributes significantly to the decrease of the number of local minima compared to the rigid SHS model.

To see if the asymptotic increase in the number of distinct minima $|\mathcal{M}(N)| \sim e^{\alpha N}$ is indeed exponential, an expression for the asymptotic exponential rise rate parameter developed by Stillinger was used:[22]

$$\alpha = \lim_{N\to\infty} \left(N^{-1}\ln|\mathcal{M}(N)|\right). \tag{8.7}$$

Figure 8.3 shows the number of distinct minima for SHS clusters obtained from the data shown in table 8.1. The $N \geq 12$ SHS data gives $\alpha_{\mathrm{SHS}} \approx$

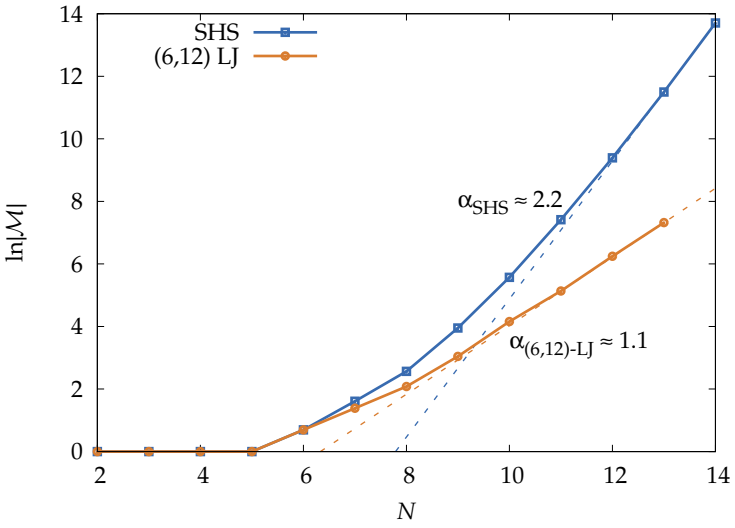

Figure 8.3 Growth behaviour of $|\mathcal{M}(N)|$ of SHS and (6,12)-LJ clusters and corresponding asymptotic exponential rise rate parameter α for $N \geq 12$ as defined in equation (8.7). The intercepts $\ln|\mathcal{M}(N = 0)|$ are -17.19 and -6.94 for the SHS and (6,12)-LJ cases, respectively.

2.21. Figure 8.3 also shows the (6,12)-LJ results obtained using basin-hopping; these yield $\alpha_{\mathrm{LJ}} \approx 1.10$, which is close to the $\alpha = 0.8$ value estimated by Wallace[235] or to the recently given value of $\alpha = 1.04$ by Forman and

Cameron.[228] Note that the rapid increase of $|\mathcal{M}_{\mathrm{SHS}}|/|\mathcal{M}_{\mathrm{LJ}}|$ with N is explained by the much larger values of α for the SHS compared to the LJ clusters.

Using the results for $N \geq 13$ depicted in figure 8.2, the dependence of α on the LJ range parameter n can be calculated. As shown in figure 8.4, a general function of the form

$$\alpha(n) = \alpha_{\mathrm{max}} + \frac{a}{(n - n_0)^p} \tag{8.8}$$

fits the results nicely, allowing the prediction of growth behaviour for different LJ potentials. For $|\mathcal{M}_{(n/2,n)-\mathrm{LJ}}|$, α_{max} is equivalent to $\alpha_{\mathrm{SHS}} = 2.207$. The

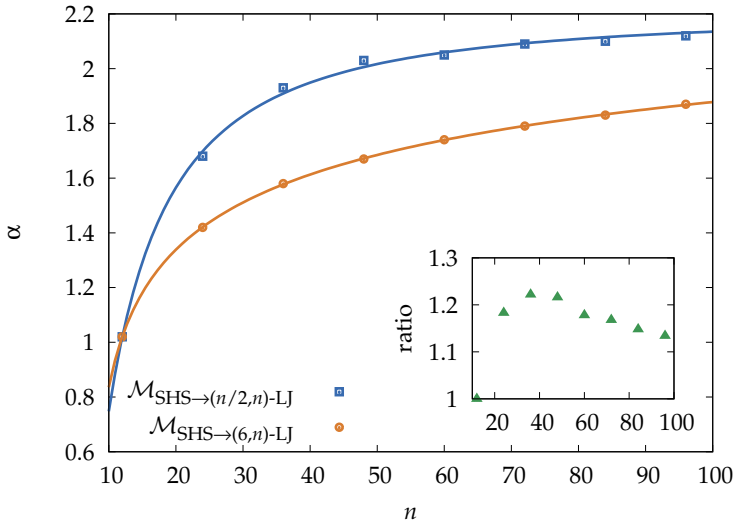

Figure 8.4 Convergence behaviour of the asymptotic exponential rise rate parameter α (equation (8.7)) towards the SHS limit with respect to the LJ exponent n. The inlet shows the ratio of the two quantities $\alpha(|\mathcal{M}_{\mathrm{SHS}\to(n/2,n)-\mathrm{LJ}}(N)|)/\alpha(|\mathcal{M}_{\mathrm{SHS}\to(6,n)-\mathrm{LJ}}(N)|)$.

other adjusted parameters are $a = -66.588$, $n_0 = -3.386$ and $p = 1.473$ (figure 8.4). We also show the ratio $\alpha(|\mathcal{M}_{\mathrm{SHS}\to(n/2,n)-\mathrm{LJ}}|)/\alpha(|\mathcal{M}_{\mathrm{SHS}\to(6,n)-\mathrm{LJ}}|)$ between the two different LJ asymptotic exponential rise rate parameters, which shows that larger cluster sizes need to be studied to correctly describe the asymptotic limit.

The distribution of minima as a function of (free) energy was suggested to be Gaussian.[236] Figure 8.5 shows the energy distribution of minima for different $(n/2, n)$-LJ potentials derived from SHS initial structures. A Gaussian type distribution was not observed; this result does not change if the free energy at finite temperatures is used instead. The results indicate a "phase transition" in the potential energy landscape away from low energy to high energy minima as n increases. The transition occurs at fairly small n. Results for the $(9, 18)$-LJ potential indicate two SHS-like maxima that are not

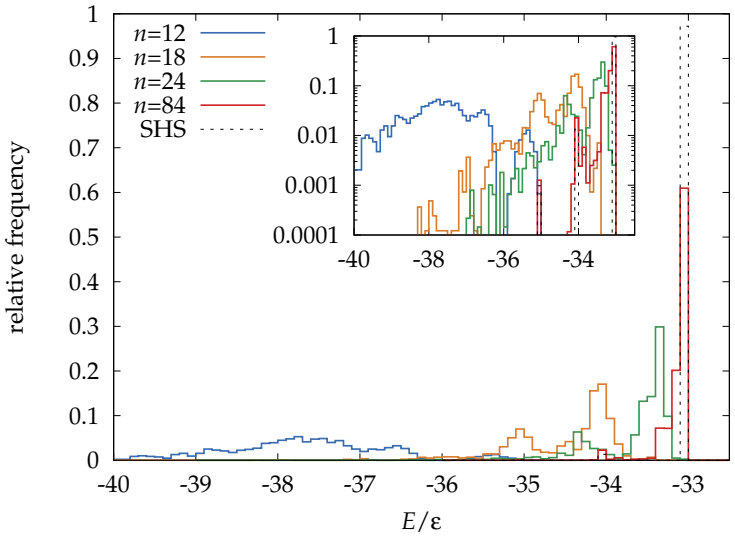

Figure 8.5 Histogram of the energies (bin size $\Delta E = 0.1$) of minima $\mathcal{M}_{\mathrm{SHS}\to(n/2,n)-\mathrm{LJ}}(N)$ for $N = 13$ and different exponents n up to the SHS limit. For better visibility, the height of the bars are set to $\Delta|\mathcal{M}|/|\mathcal{M}|$ in the interval $\Delta(E/\epsilon)$. The inlet shows the same data in logarithmic scale.

present for the $(6, 12)$-LJ potential; these are associated with the $N_c = 34$ and $N_c = 35$ SHS clusters, respectively. It is also clear that (as expected) the distributions narrow with increasing n.

It is well known that the global minimum for rare gas clusters with 13 atoms is the ideal Mackay icosahedron.[237–239] Simple geometric considerations imply that such a symmetric cluster is not possible for sticky hard spheres; all vertices of a regular icosahedron with unit edge length lie on a circumscribing sphere with radius $r_c \approx 0.951$, making it impossible to insert a sphere of the same radius into the centre of the polyhedron. Therefore, there must be well-defined LJ exponents (m, n) at which the icosahedral $N = 13$ LJ cluster breaks symmetry to form a rigid cluster. For the $n = 2m$ case considered above, this symmetry-breaking occurs at $m \simeq 15$.

We also explored a more realistic eLJ potential (equation (8.6); figure 8.1) for one of the rare gas dimers (xenon) in comparison with other LJ potentials. It can be seen that the repulsive part agrees nicely with the conventional (6,12)-LJ potential, while for $r > 1$ the extended LJ potential is slightly less attractive. This change should lead to an increase in the number of local minima compared to the conventional (6,12)-LJ potential. This prediction could be confirmed, i.e. $|\mathcal{M}_{\mathrm{SHS}\to\mathrm{ELJ}}| = \{8, 21, 74, 205, 685, 2179, 6863\}$ for $N = \{8, 9, 10, 11, 12, 13, 14\}$. For $N = 13$ the number of distinct minima is 44% larger than for the simple (6,12)-LJ potential, which shows that $|\mathcal{M}(N)|$ is rather sensitive to the potential chosen. Hence, to correctly describe the

topology of real systems, one has to take care of the correct form of the 2-body contribution (as well as higher n-body contributions).[240]

8.4 (6,12)-Lennard-Jones Clusters from Basin-Hopping

Table 8.1 shows the number of distinct minima found by the cluster geometry optimisation procedure employed in this work using the (6,12)-LJ potential compared to results from exact enumeration for SHSs and from basin-hopping for the (6,12)-LJ potential. As the SHS clusters for a specific N value can be grouped by their contact number N_c, the geometry optimisations were carried out separately for each group of $\mathcal{M}_{\mathrm{SHS}}(N_c)$. Hoy et al.[115,116] and Holmes-Cerfon[114] reported slightly different results for $N = 11$ and $N = 13$; however, upon geometry optimisation, their datasets yield the same final clusters $|\mathcal{M}_{\mathrm{SHS}\to\mathrm{LJ}}(N_c)|$. As identical LJ clusters appear in multiple groups with different contact numbers, the duplicates were removed to create the set $\mathcal{M}_{\mathrm{SHS}\to\mathrm{LJ}}$ of distinct minima, which can be directly compared to the set of LJ minima $\mathcal{M}_{\mathrm{LJ}}$ obtained from the basin-hopping method. It should be noted that including the hypostatic clusters and the different $|\mathcal{M}_{\mathrm{SHS}}|$ for $N = 11$ and $N = 13$ from Holmes-Cerfon[114] did not change our results, implying that hypostatic clusters are not an important feature for the LJ energy landscape.

Interestingly, the gradient-based minimisation procedure employed here does not in general lead to a complete set of LJ minima; the mapping from SHS minima to LJ minima is non-injective and non-surjective. Clearly, some structural motifs found in LJ clusters are not found in SHS clusters and vice versa, and the topology of the hypersurface changes in a non-trivial fashion from SHS to LJ. However, it is surprising that the fraction of structures that are missed by this optimisation procedure is so small (see table 8.2). To gain further insights, the energetics and structures of the unmatched clusters were investigated in more detail.

Figure 8.6 shows an analysis of the difference between the longest to the shortest bond lengths $d_\Delta = d_{max} - d_{min}$ obtained for the largest clusters in $\mathcal{M}_{\mathrm{LJ}}$ with $N = \{11, 12, 13\}$.[d] The histograms show that the clusters most commonly have a d_Δ of about 0.03. In contrast, as shown by the orange bars, the unmatched structures have significantly larger d_Δ values of at least 0.05, with most of them having $d_\Delta \simeq 0.06$. This is a first indication of why these structures are not found by starting from SHS packings. The latter only form bonds of length one, and a large variation in bond length could imply that a SHS packing similar to the LJ structure does not exist as the SHS boundary conditions are not satisfied. The data in table 8.3 shows that the unmatched

[d] We define spheres that have a equilibrium distance between $0.9 - 1.1$ to be bound.

Table 8.2 Number of missing structures after optimisation belonging to the same "seed" (figure 8.7). $N = 8$ is excluded because all LJ minima were found starting from the SHS model.

seed	$N = 9$	$N = 10$	$N = 11$	$N = 12$	$N = 13$
a	1	1	-	3	8
b	-	1	3	4	12[a]
c	-	-	1	1[a]	-
d	-	-	1	1	5
e	-	-	-	1	6
f	-	-	-	1	1
remaining	-	-	-	-	2
total	1	2	5	11	34
%	4.76	3.13	2.94	2.14	2.25

[a] Some structures do not resemble a perfect capped cluster, but undergo a slight rearrangement. Specifically, two structures belonging to seed (b) and one structure belonging to seed (c) were found to deviate slightly from the perfect arrangement, but minor rearrangements of these structures lead to the desired geometry and they can be reasonably associated with these seeds.

(UM) structures for a specific N value have much higher energies compared to the one of the global minimum (which is set to zero, i.e. $E_0 = 0$). They are always positioned in the upper half of the energy spectrum, making them energetically unfavourable. However, no correlation between d_Δ and the energetic position of the LJ clusters was found.

Table 8.3 Range $[E_0 = 0, E_{\text{max}}]$ of the energy spectrum of all LJ minima, position of the second lowest minimum structure E_1 and position of the first unmatched (UM) structure E_0^{UM} relative to the respective global minimum (in reduced units).

N	E_{max}	E_1	E_0^{UM}
8	1.04	0.06	-
9	2.08	0.84	1.19
10	3.13	0.87	2.22
11	4.22	0.85	2.27
12	6.16	1.62	3.38
13	9.26	2.85	6.14

Last, the geometries of the missing structures were investigated in more detail. As it turns out, almost all of the missing stable LJ clusters can be created from a smaller set of missing clusters by capping some of their triangular

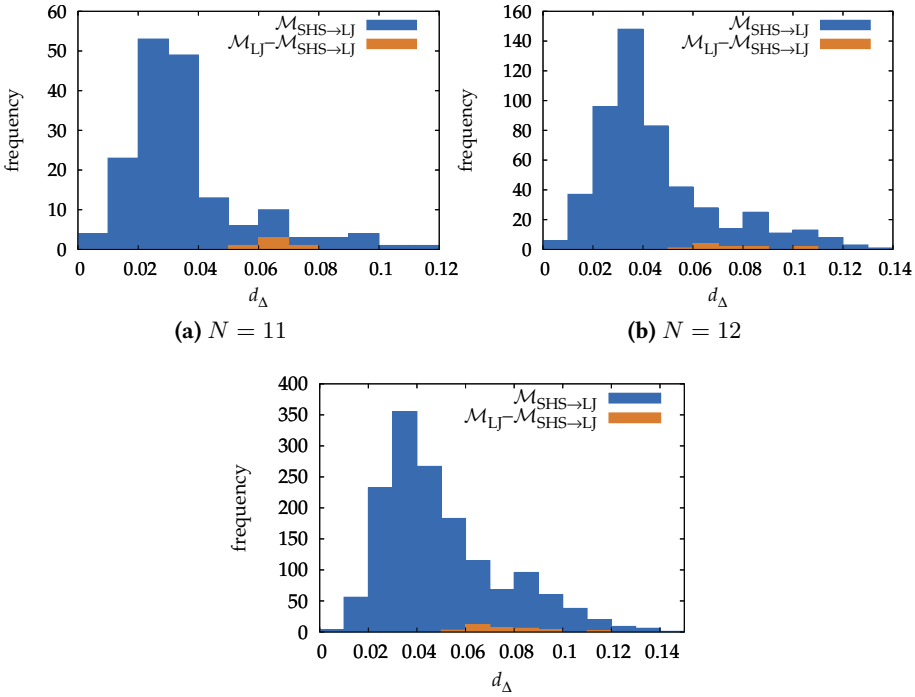

(a) $N = 11$ **(b)** $N = 12$

(c) $N = 13$

Figure 8.6 Histograms of the difference between the longest and shortest bond distances $d_\Delta = d_{\max} - d_{\min}$ for the complete set of distinct LJ minima $\mathcal{M}_{\mathrm{LJ}}(N)$ for $N = \{11, 12, 13\}$. Orange bars give the number of distinct structures not contained in $\mathcal{M}_{\mathrm{LJ}}$ as obtained from the basin-hopping algorithm.

faces. Therefore, these groups of clusters can be referred to as "seeds".[112] The corresponding starting structures of each seed are shown in figure 8.7. None of these structures are stable SHS packings. For example, structure (d) can be described as three octahedra connected via triangular faces sharing one edge. Geometric considerations[112,115] immediately show that this structure cannot be a stable SHS packing; the dihedral angle in an octahedron is approximately $109.5°$, which means three octahedra only fill $328.5°$ of a full circle, leaving a gap between two faces.

Table 8.2 shows the number of missing minima belonging to each seed. Over 60 % of the unmatched structures belong to seeds (a) and (b). From a graph theoretical point of view,[19,112] grouping structures into seeds means that all structures belonging to the same seed contain the graph of the starting structures as a sub-graph in their respective connectivity matrix. This approach simplifies the analysis to a great extent, as the feature that prevents the structures from being found by geometry optimisation is the same for each of the structures arising from a specific seed. The smallest unmatched

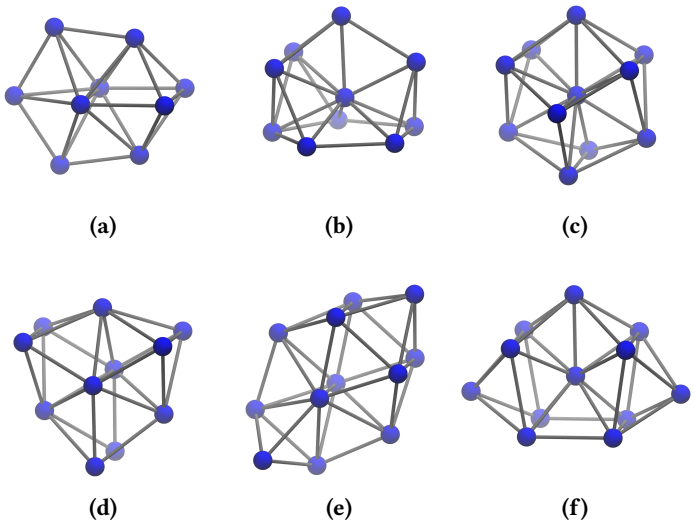

Figure 8.7 Graphical representations of the structures that are starting new seeds, but are not contained in $\mathcal{M}_{\mathrm{SHS}\rightarrow\mathrm{LJ}}$. See table 8.2 and text for more details.

structures that cannot be associated with any of seeds (a)–(f) have $N = 13$; these could be the starting structures for two new seeds.

Finally, it should be noted that the starting SHS minima in the optimisation procedure are not stationary points on the LJ hypersurface, and the optimisations therefore lead to most but not all local and available LJ minima. This observation explains why some high-energy structures were not found by the optimisation procedure. For a smooth change in the topology of the potential energy surface from SHS to LJ type clusters one has to continuously vary the exponents (m, n) in real space, which is computationally too demanding.

8.5 Conclusion

The sets of (m, n)-LJ-potential minima obtained using complete sets of non-isomorphic SHS packings with $8 \leq N \leq 14$[19,112,114–116] as initial states for energy minimisation have been characterised. The number of distinct minima (i.e. excluding permutation-inversion isomers) is far smaller than the number of SHS packings for the standard Lennard-Jones exponents $(m, n) = (6, 12)$, but approaches the SHS limit from below as (m, n) increase. How the number of distinct minima $\mathcal{M}(N)$ increases with cluster size N has been investigated by determining Stillinger's rise rate parameter α (equation (8.7)).[22] The increase of α from ≈ 1.1 for (6,12)-LJ clusters to ≈ 2.2 for SHS clusters is described by a simple functional form (equation (8.8)). All these results

can be understood in terms of a smooth progression of the (m, n)-LJ energy landscape towards the SHS energy landscape as (m, n) increase.

Using a more realistic eLJ potential obtained from coupled cluster calculations for the xenon dimer[106,107] leads to $\mathcal{M}$ values close to those obtained for the (6,12)-LJ potential, but the results indicate that the topology of the energy hypersurface is very sensitive to the model potential applied.

Finally, the optimisation results have been compared to the previously published results for the (6,12)-LJ potential. The mapping from $\mathcal{M}_{\mathrm{SHS}}$ to $\mathcal{M}_{\mathrm{SHS}\rightarrow\mathrm{LJ}}$ is non-injective and non-surjective, however, the number of structures missed by the optimisation procedure is relatively small. The unmatched structures belong to the high energy region of the potential energy hypersurface and possess rather large variations in their bond lengths. An analysis of their geometries revealed that most of the larger structures can be constructed from a smaller cluster by capping some of the triangular faces. This procedure effectively sorts almost all unmatched structures into six seeds for clusters up to $N = 13$.

Further investigations should focus on comparing the presented results with other commonly used interaction potentials like the Morse potential. It would also be interesting to see how three-body interactions would affect the results. However, that would require a considerable amount of programming as the current program was developed with only two-body forces in mind.

9 The Gregory-Newton Clusters[a]

9.1 Introduction

In 1930, Tammes studied the distribution of pores on pollen grains, which required him to find a solution to the problem of packing a number of circles (or spheres) on the surface of a unit sphere, maximising their distance.[242] In graph theoretical terms, in which the centers of all the circles correspond to the vertices of a convex polyhedron, one tries to find the graph representing the polyhedron that maximises the shortest edge lengths, while keeping the distance to the center of the polyhedron fixed. Exact solutions to this problem are available for cluster sizes of $3 \leq N \leq 14$ and $N = 24$.[243,244]

A related problem that goes back to an argument between Newton and Gregory, one of his apprentices, is about the *maximum kissing number* or *Newton number* $N_k(d)$ of three-dimensional unit spheres ($d = 3$) that can simultaneously touch a central sphere of the same size.[245] While Newton believed $N_k(3) = 12$, Gregory thought a 13th sphere could be brought into contact with the central sphere. It turns out that Newton was right, which was first proven in 1953 by Schütte et al.[23] In the following a cluster with $N \geq 13$ and at least 12 spheres in contact with a central sphere will be referred to as a Gregory-Newton cluster (GNC). Figure 9.1 shows the most symmetric icosahedral solution to the Gregory-Newton problem. The Gregory-Newton problem has been solved for dimensions 1–9 and 24 in lattice packings and 1–4, 8 and 25 for non-lattice packings.[246–248] Lower and upper bounds have also been published.[247,249] However, for the problem of cluster nucleation, the three-dimensional problem, as posed by Gregory and Newton, is more relevant and has recently been reviewed by Kusner et al.[250]

There are other problems similar to the Tammes problem like the Thomson problem, that tries to find the optimal solution for charged particles (e.g. electrons) on the surface of a sphere.[251,252] The solutions to this class of problems all show icosahedral symmetry for a size of 12 spheres. When thinking of these problems in terms of nucleation phenomena there is usually not a repulsive force between the surrounding spheres, but an attractive one. For example, such a system could be modelled in a gravitational potential

[a] This chapter is composed of sections previously published in the articles "From Sticky-Hard-Sphere to Lennard-Jones-Type Clusters"[210] and "Gregory-Newton Problem for Kissing Sticky Spheres"[241] and is reprinted with permission from the publisher ©2018 American Physical Society. Some sections have been modified to fit the style of this thesis.

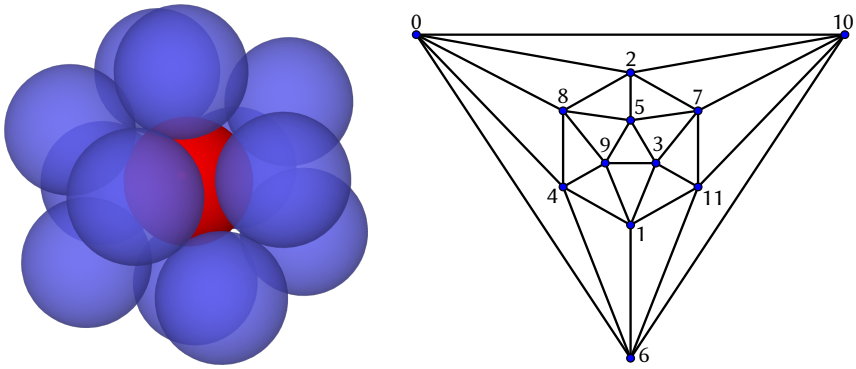

Figure 9.1 Left: Symmetric realization of $N_k(3) = 12$ for unit hard spheres (icosahedral symmetry, I_h). The minimum distance between the outer spheres is $r = \sin^{-1}\left(\frac{2\pi}{5}\right) = 1.05146222\ldots$, hence they do not touch. Right: The corresponding icosahedral graph. Numbering refers to the respective node index.

$V_G = Gm_im_jr_{ij}^{-2}$, where G is the gravitational constant, m_i the mass of sphere i and r_{ij} the distance between spheres i and j. For spheres i and j with radii R_i and R_j a geometry optimisation can be carried out under the constraint $r_{ij} \geq (R_i + R_j)$, which will remove the gaps between the spheres in the icosahedral arrangement. Such problems are often studied for crystallisation and sedimentation phenomena.[253,254]

Two other potentials that enforce theses types of rigidity constraints on the system are the Lennard-Jones (LJ) and sticky-hard-sphere (SHS) potentials already introduced in chapters 5 and 8. Unlike in chapter 8 the exponents (a, b) are now any real positive number instead of integers.

$$V_{a,b}^{\mathrm{LJ}}(r) = \frac{ar^{-b} - br^{-a}}{b-a} \quad (\text{with } r, a, b \in \mathbb{R}^+ \text{ and } b > a). \tag{9.1}$$

The SHS potential is employed unchanged.

$$\lim_{a,b\to\infty} V_{a,b}^{\mathrm{LJ}}(r) \to V_{\mathrm{SHS}}(r) = \begin{cases} \infty & r < 1 \\ -1 \quad \text{for} & r = 1 \\ 0 & r > 1 \end{cases} \tag{9.2}$$

Note that for both potentials both the depth of the energy well and the equilibrium distance have been arbitrarily set to 1.

In the following sections these two potentials will be used to investigate the GNCs. Again, the investigation starts from the SHS clusters derived from the exact enumeration method.[114,116,217] This set of structures is searched for clusters fulfilling the requirements to be GNCs. LJ clusters of this size have an icosahedral global minimum, however, this structure is impossible to realise in the SHS potential. This is due to the fact that in a perfect icosahedron

the distance between the vertices is always larger than the distance of all the vertices to the centre of mass of the cluster. Therefore, as increasing LJ exponents make the potential more SHS-like, there must be a point of symmetry breaking at which the icosahedral structure cannot be supported any more by the LJ potential energy surface.

9.2 Computational Details

Coordinates for GNC structures have been obtained by searching for adjacency matrices of the results for $N = 13$ from Holmes-Cerfon[114] with one row or column containing twelve "1" entries. Sub-graph isomorphism was verified using the *VF2* algorithm[121] as implemented in the *boost graph library*[30] using the program package SPHERES. Structural optimisations with LJ potentials have been carried out using the multidimensional function minimiser from the C++ library *dlib*[118] and an energy convergence criterion of 10^{-15}. Results from the optimisation procedure were analysed based on the Euclidean distance matrix (EDM), which is unique for non-isomorphic structures apart from permutation, translation, rotation and inversion. For this the distances were sorted lexicographically.

9.3 The Gregory-Newton Problem for Soft Potentials

The question of the Newton number in three dimensions has been resolved almost 70 years ago.[23] The proof is valid for hard-sphere short-range potentials, but little is known about the behaviour of such clusters under long-range potentials such as the Kratzer potential.[92] For unequally sized spheres, some simple results are known; for example, 13 hard spheres of radius r_s can touch a central sphere of unit radius only if $r_s \leq 0.9165$.[255] For clusters bound by the aforementioned long-range potentials the situation is far more complicated as it requires to minimise energy rather than distances between neighbouring particles. Nonetheless, it is important to expand our knowledge on these kind of systems as they are crucial to understand real systems such as coordination compounds, which have recently been shown to possess coordination numbers as high as 17[256] or even 20.[257]

The optimisation procedures explained in chapter 6 were used to minimise the energy of a starting structure consisting of 13 spheres surrounding a center sphere with a fixed distance of one. Generating such a starting structure where all surrounding spheres are evenly spaced is impossible since there exists no triangulation of a sphere with 13 vertices, where every vertex has degree five or six.[180] To generate an approximate distribution the Fibonacci sphere algorithm[258,259] was used and the generated structure of size

$N = 14$ was the starting point for optimisations with LJ potentials with small exponents. The difference between the largest and smallest center-to-outer sphere (COS) distance was used as a measure for whether the 13th sphere enters the first coordination shell. A value of zero would be expected for this to be true.

The results for all positive integer combinations of $m \leq 11$ and $n \leq 12$ with $m < n$ are depicted in figure 9.2. Even for the combination of smallest

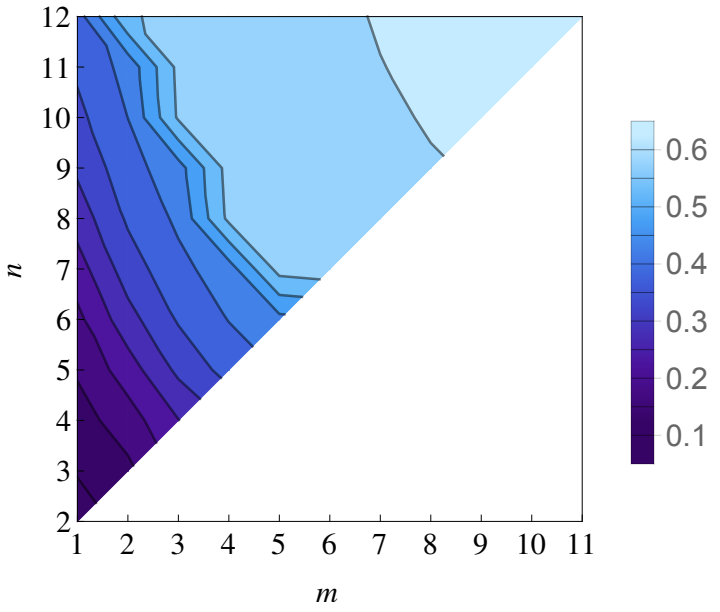

Figure 9.2 Relation of LJ exponents m and n to the difference of largest and smallest COS distances. A value of zero would imply that all surrounding spheres are touching the center sphere.

exponents (1,2) it is clear that the COS distances vary from sphere to sphere. For this potential the largest COS distance is $r_{\text{max}} = 0.882$, while the shortest one is $r_{\text{min}} = 0.804$. While the longest distance only shows up once, the shortest distance appears twice. All other ten distances fall in the range between $r = 0.845$ and $r = 0.861$. The $r_{\text{max}}/r_{\text{min}}$ ratio is 1.097 and much shorter compared to $r_{\text{max}}/r_{\text{min}} = \sqrt{2}$ for the closed packed lattice, or the shortest distance possible for the SHS system which is $r_{14}^{\text{GN}} = 1.347$ (see section 9.6). Hence, the 13th sphere almost touches the center sphere.

Note that all COS distances for the $N = 14$ (1,2)-LJ cluster are significantly shorter than $r = 1$, due to the $N(N-1)/2$ attractive two-body interactions and the softness of the potential. For infinite (e.g. body-centred cubic or close-packed) lattices of particles interacting via $V_{mn}^{\text{LJ}}(r)$ with $n > m > 3$, one can

prove[106] that the nearest neighbour distance is

$$r_{\mathrm{NN}}(m,n) = \left(L_n L_m^{-1}\right)^{\frac{1}{n-m}} . \tag{9.3}$$

Here L_n is the Lennard-Jones-Ingham lattice coefficient for a specific lattice determined from 3D lattice sums. Since $L_n < L_m$ for $n > m$, we see that $r_{\mathrm{NN}} < 1$, and $\lim_{m,n\to\infty} r_{\mathrm{NN}}(m,n) = 1$. The shortest distances found in (6,12)-LJ clusters $r_{\mathrm{min}}(N)$ are: $r_{\mathrm{min}}(8) = 0.986767$, $r_{\mathrm{min}}(9) = 0.964404$, $r_{\mathrm{min}}(10) = 0.964382$, $r_{\mathrm{min}}(11) = 0.956345$, $r_{\mathrm{min}}(12) = 0.947842$, and $r_{\mathrm{min}}(13) = 0.952179$. Surprisingly, $r_{\mathrm{min}}(12)$ is smaller than $r_{\mathrm{NN}}(6,12)$ for typical crystalline lattices; $r_{\mathrm{NN}}(6,12)$ values are 0.95066, 0.95186 and 0.97123 for simple cubic, body-centred cubic and close-packed lattices, respectively. This result shows that stable clusters do not necessarily have longer bonds compared to the solid state.

9.4 Rigid Gregory-Newton Clusters and Corresponding Graphs

The recent results by Holmes-Cerfon contain a putatively complete set of rigid SHS clusters of size $N = 13$ and $N = 14$.[114] The rigid GNCs can easily be identified as a subset of the set of all non-isomorphic rigid SHS clusters, i.e. $\{S_{\mathrm{GN}}\} \subset \{S_{\mathrm{SHS}}\}$; these have adjacency matrices A with exactly one column and row containing twelve "1" entries due to 12 spheres kissing the central sphere. A surprisingly large number of 737 non-isomorphic $N = 13$ GNCs out of 98,540 rigid SHS clusters can be found.[210] There are four different possible contact numbers N_c with $\{724, 10, 1, 2\}$ rigid GNC corresponding to $N_c = \{33, 34, 35, 36\}$;[243] therefore, none of those clusters are hypostatic.

For further analysis and without loss of generality the central sphere was removed and the remaining non-isomorphic shell of spheres[b] was analysed, also called a contact graph according to Schütte et al.[260] This has the advantage that these shells are related to planar connected graphs. In the following the corresponding connected planar graph of such a shell of spheres with the central sphere missing will be referred to as a *GN graph*. The question arises if all 737 non-isomorphic GN graphs are sub-graphs of the icosahedral graph, as shown in figure 9.1. This would make sense as it is impossible to increase the degree of any vertex beyond five in the Gregory-Newton (GN) graph. Note that the icosahedral cluster is completely unjammed and its space of (infinitesimal) deformations has dimension 24.[250]

Employing the *VF2* algorithm[121] as implemented in the *boost graph library*[30] all 737 non-isomorphic GN graphs $G_{\mathrm{GN}}(N, E')$ (vertex count $|N| = 12$, edge count $|E'| < 30$) are found to be (edge-induced) sub-graphs of the

[b] Note that rigidity requires the presence of the central sphere.

icosahedral graph $G_{\text{ico}}(N, E)$ ($|N| = 12$, $|E| = 30$), which implies that their vertices can all be mapped to vertices of the icosahedral graph with certain edges deleted such that the sub-graph remains connected ($N_{\text{GN}} = N_{\text{ico}}$ and $E_{\text{GN}} \subset E_{\text{ico}}$). An extensive list of all sub-graphs is included in the appendix (Tables A.1 and A.2). Note, not all GN graphs are 3-connected and therefore are not strictly polyhedral according to Steinitz's theorem.[261] These are the graphs which have vertices of degree 2, i.e. $|N_2| > 0$, and there are 304 of them, table A.2. As the many non-isomorphic graphs listed in the appendix are obtained from a certain combination of edge deletions under the constraint of maintaining rigidity, it is not surprising at all that the number of non-isomorphic GN graphs is so large.

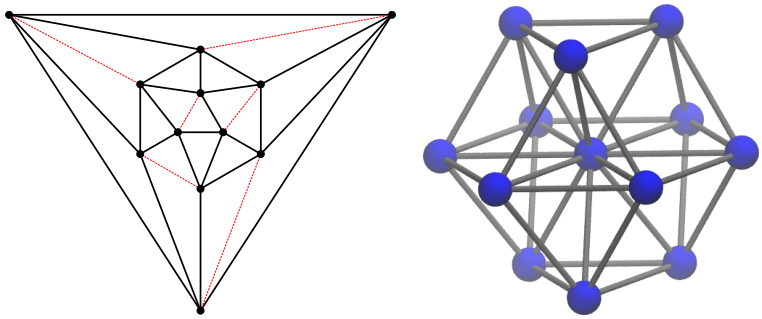

(a) hcp, $|E| = 24, \omega = 1$.

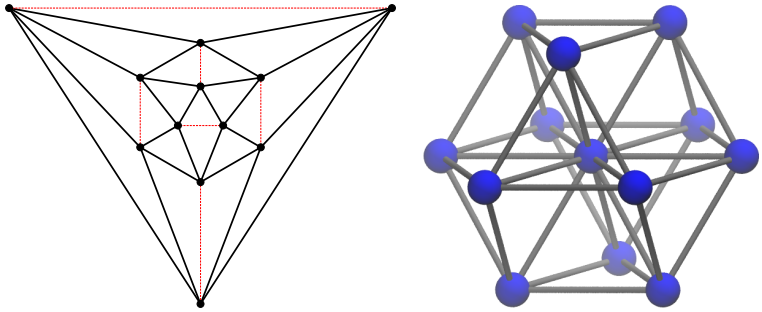

(b) fcc, $|E| = 24, \omega = 2$.

Figure 9.3 GN hcp (triangular orthobicupola) and fcc (cuboctahedron) graphs (central sphere removed) as sub-graphs of the icosahedral graph and corresponding rigid GNCs. Red lines indicate the edges that were removed to create the GN graph. The ordinal numbers ω refer to Table A.1 in the appendix.

The results show, that at least six and up to a maximum of nine edges have to be removed from the icosahedral graph to create a GN graph. Removing six edges from the icosahedral graph results in 24 edges, or $N_c = 36$ if the central sphere is included. For $N = 13$ this is exactly equal to $3N - 3$ which is the maximum contact number observed for this cluster size.[114,116] Consequently, removing nine edges gives $N_c = 33 = 3N - 6$, meaning that rigid

GNCs cannot be hypostatic (i.e. $N_c < 3N - 6$). Interestingly, there are only two graphs with maximum edge count of $|E| = 24$, which are exactly the fragments of the face-centered cubic (fcc) and hexagonal-closed packed (hcp) bulk structures, respectively. These are the result from removing 6 edges in such a way, that exactly one edge is removed from every vertex in the icosahedral graph (thus the degree of every vertex is 4), see figure 9.3. Removing edges in this way implies that the resulting two graphs consist of triangles and rectangles only. The difference between the fcc and hcp clusters is in the way their square faces are connected; in the fcc case the square faces only connect via vertices (cuboctahedron), while in the hcp case the square faces come in pairs sharing one edge (triangular orthobicupola or Johnson solid J_{27}).[250]

The construction of hcp and fcc structures by a continuous deformation of an icosahedron has been described in detail by Kusner et al.[250] and goes back to Conway and Sloane in 1988.[247] hcp and fcc can both be obtained from a rearrangement of the spheres in an icosahedron by forming a (zig-zag) cycle (closed path) through six vertices, and arranging those spheres on the path such that they are in-plane with the central sphere, which becomes part of the hexagonal plane as in the bulk fcc and hcp packing (figure 9.4). Additionally, the plane has to be rotated by $\pi/6$ to create the fcc structure. The

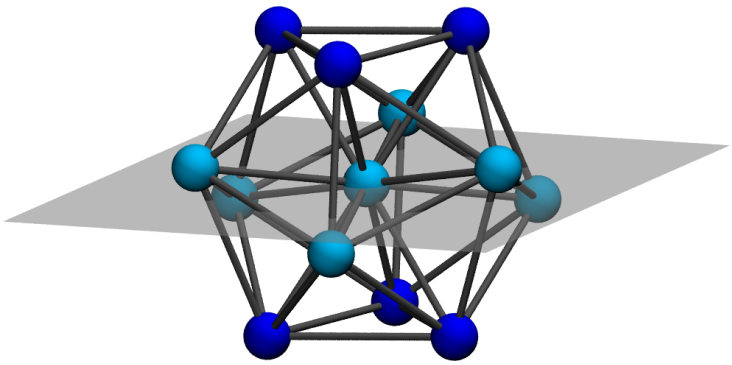

Figure 9.4 Illustration of one zig-zag path (light blue spheres) that needs to be deformed such that it aligns with the triangular plane (shown in grey) of the fcc crystal.

hcp structure can be constructed by also rotating either the top or the bottom plane by the same amount in either direction parallel to the hexagonal plane. Kusner noted that a smooth deformation from the icosahedral configuration to hcp requires 9 moving spheres.[250] This interesting transition path may be the key for the icosahedral to closed-packed rearrangements in larger clusters, which has previously been described in terms of catastrophe theory as a cusp catastrophe.[232]

Even though the rearrangement from the icosahedral to either the fcc or

hcp cluster structure can easily be realised for the GNC, there should be clusters where the icosahedral motif is still clearly visible, i.e. only small rearrangements of the spheres are necessary to break icosahedral symmetry and form a rigid cluster. These are, for example, the ones with maximum count of triangles, i.e. according to table A.2 the GN graphs with $|F_3| = 10$ with edge counts of $|E| = 22$ or 21. Two of these are shown with their corresponding graphs in figure 9.5.

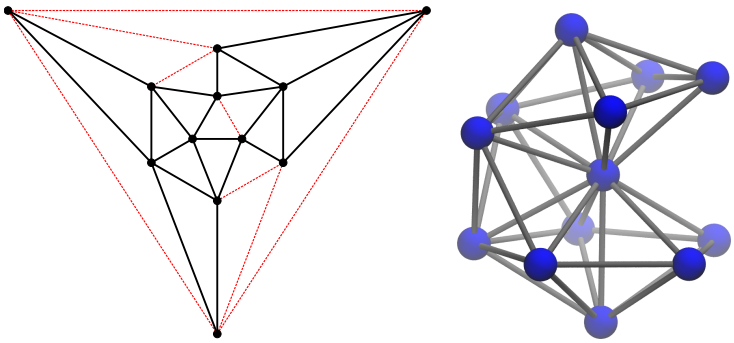

(a) icosahedral motif, $|E| = 22, \omega = 4$.

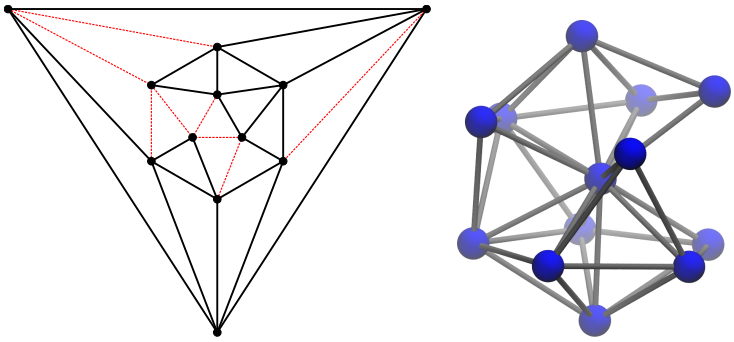

(b) icosahedral motif, $|E| = 22, \omega = 7$.

Figure 9.5 Representative GN graphs (central sphere removed) with $|F_3| = 10$ as sub-graphs of the icosahedral graph and corresponding rigid GNCs. The icosahedral motif in the 3D embedding is clearly visible. Red lines indicate the edges that were removed to create the GN graph. The ordinal numbers ω refer to Table A.1 in the appendix.

Figure 9.6 shows the graph with the next highest edge count after the fcc and hcp packings. The motif of a distorted elongated pentagonal bipyramid (Johnson solid J_{16}) is clearly visible. Note that the Johnson solid can be obtained by deleting five edges and rotating the two opposite pentagonal pyramids by $2\pi/5$. One of the resulting square faces has to be stretched to obey the SHS conditions, which is achieved by removing two additional edges. In the graph this implies that a hexagonal face is formed. Note that this GNC is

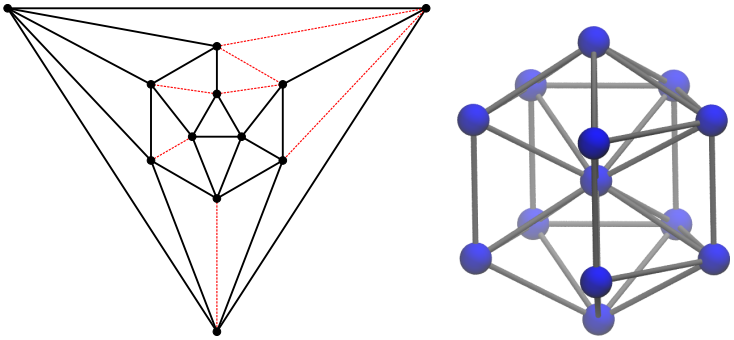

(a) Distorted elongated pentagonal bipyramid (Johnson solid J_{16}), $|E| = 23, \omega = 3$.

Figure 9.6 GN graph (central sphere removed) as sub-graphs of the icosahedral graph and corresponding GN Johnson-like solid (with edges removed). Red lines indicate the edges that were removed from the icosahedral graph to create the GN graph. The ordinal number ω refers to Table A.1 in the appendix.

also the cluster with the largest distance $r_{\max}^{\mathrm{RE}} = 1.47823719$ that corresponds to a removed edge (RE) in the GN graph. Capping this cluster with one more sphere over the distorted square face with $r_{\max}^{\mathrm{RE}}$ leads to the structure with the shortest distance a sphere in the second coordination shell can have to the central sphere ($r^{\mathrm{COS}} = 1.347150628$)[c] out of all 895,478 GN clusters with $N = 14$.[210]

If more edges are removed from the icosahedral graph larger n-gonal faces appear, with the largest face being a 12-gon.

9.5 Symmetry-Broken Lennard-Jones Gregory-Newton Clusters

All 737 non-isomorphic rigid GNCs optimise to the ideal icosahedral symmetry if a (6,12)-LJ potential is applied[210] (however, for larger sized icosahedral structures many more minima appear).[81,262–264] As mentioned in the introduction, for equally sized hard spheres a cluster with icosahedral symmetry leaves gaps between the spheres of the outer shell, i.e. they do not touch, and it is therefore not considered rigid under SHS conditions. Hence, at certain (a, b) combinations a phase transition must occur in the (a, b)-LJ energy landscape where non-icosahedral local minima appear. In order to determine those (a, b) combinations, all 3D cluster geometries were optimised with varying exponents ($6 \leq a \leq 34$ and $7 \leq b \leq 35$) with ($b > a$) and

[c] This will be investigated in detail in section 9.6.

the number of resulting minimum structures was analysed. The results are shown schematically in figure 9.7.

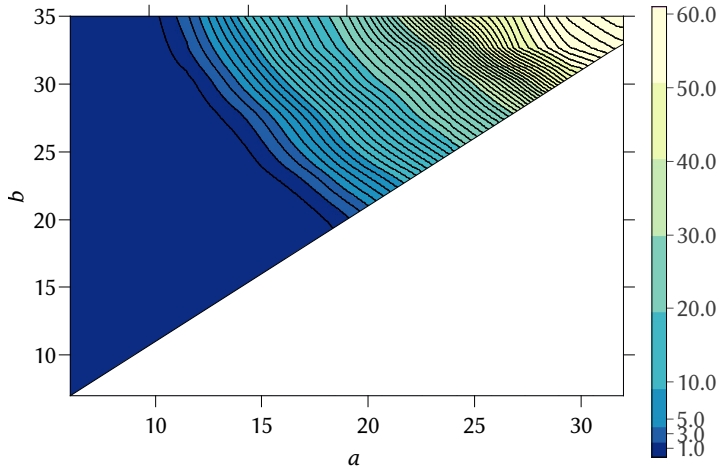

Figure 9.7 Number of unique structures resulting from an optimisation with a (a, b)-LJ potential. The lowest contour line shows the point where more than one structure results from the optimisation and the distance between contour lines is 1.

Another interesting limiting case of the LJ potential with exponents $a \to 0$ and $b \to \infty$, resembling a constant attractive potential with an infinite wall, should be mentioned. In such a potential the kissing spheres can move freely in the available space without change of energy. Indeed, in the region of low a and high b values and increasing number of unique structures is found. For example, values of $a = 0.6$ and $b = 120.0$ result in two distinct structures that are both derived from the icosahedral motif.

Figure 9.8 contains additional information showing three major phase transitions in the topology of the energy landscape going from low to high (a, b) exponents. In the blue shaded area (1), the Mackay icosahedron is the sole minimum in the potential energy landscape. The first transition occurs when this symmetry can be broken, and other local minima are supported by the (a, b)-LJ potential besides the icosahedron. This is indicated in figure 9.8 by the smallest, orange region (2), which still contains the perfect icosahedron as the global minimum. At slightly higher exponents, other structures become energetically more favourable and replace the icosahedron as the global minimum, region (3). However, the icosahedron remains as a local minimum in the potential energy surface. The last transition occurs when the LJ potential becomes SHS-like, and the icosahedral cluster completely disappears from the potential energy surface, region (4). The three transition lines are generally smooth.

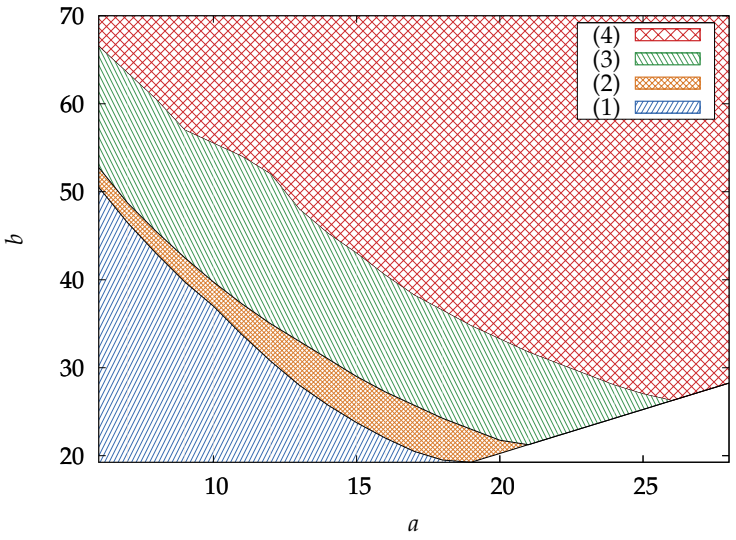

Figure 9.8 Different types of energy landscapes arising from combinations of the (a, b)-LJ exponents. (1) One single (icosahedral) minimum, (2) more than one minimum with the icosahedron as the global minimum, (3) more than one minimum with the icosahedron becoming a local (and not global) minimum, (4) the icosahedral motif disappears completely. The unshaded small area in the bottom right corner corresponds to $a > b$, which is excluded. The resolution for a is 1.0 and for b 0.25.

Figure 9.9 shows representative LJ potentials for combinations of the (a, b) exponents (with low and high a values) on the phase transition lines drawn in figure 9.8. At these phase transition lines, the corresponding LJ potentials show narrow and steep repulsive potentials compared to the $(6, 12)$-LJ potential, which all look very similar in the short range ($r < 1$). However, they differ substantially in the long range ($r > 1$).

The (a, b) parameters can be related to the so-called LJ hard-sphere radius σ (given by the intersection with the abscissa) through equation (8.5),

$$\sigma = \left(\frac{b}{a}\right)^{\frac{1}{a-b}} . \tag{9.4}$$

and only the (a, σ) combinations shown in figure 9.10 along the phase transition lines have to be considered.

The variation of σ along the phase transitions lines for (2)→(3) and (3)→(4) are rather small. However, all three transitions clearly show different ranges for σ and thus can be characterized by the LJ hard-sphere radius. These are also much larger compared to the (6,12)-LJ hard-sphere radius of $\sigma = 0.891$, and close to the ideal hard sphere radius of 1 in the SHS model. This demonstrates that the shape of the LJ potential in the repulsive region has a signif-

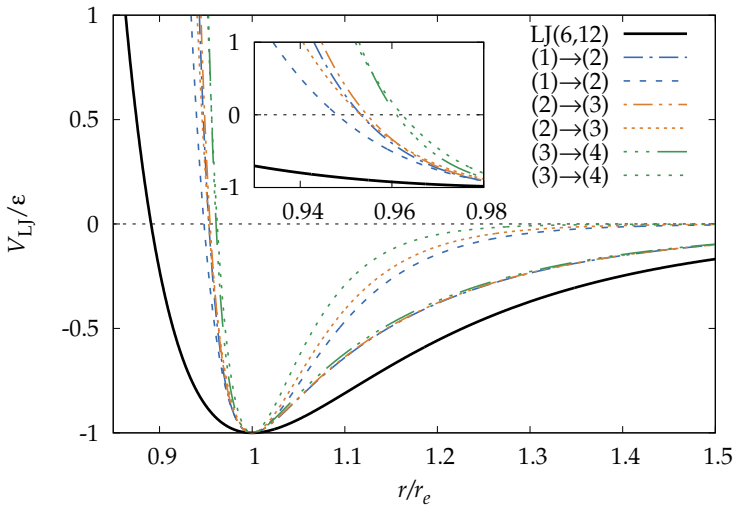

Figure 9.9 Comparison of different shapes of LJ potentials at the phase transition lines shown in figure 9.8 with the traditional (6,12)-LJ potential (black solid line). Dashed lines refer to potentials with low a values (left side of figure 9.8), while solid lines refer to potentials with high a values (right side of figure 9.8).

icant influence on the position of the transition lines, and therefore on the topology of the energy landscape. In contrast, these transitions seem to be far less affected by the shape of the potential in the attractive region. Only for the transition (1)→(2) a larger variation in σ is observed.

Finally, the results show that long-range interactions stabilise the icosahedral cluster. Therefore, the assumption that second-nearest-neighbour interactions may be important seems to come naturally. However, first-nearest neighbour interactions are sufficient for stabilising this structure, i.e. if the GN clusters are optimised with a truncated (6,12)-LJ potential that ignores second-nearest-neighbour interactions by setting the range of interactions to distances below 1.5, it is observed, that the icosahedron is recovered.

9.6 Adding a 14th Sphere

Finally, the set of SHS clusters with $N = 14$ from exact enumeration results[114] has been investigated with respect to the existence of GNCs. The extra sphere in these clusters is required to enter the second coordination shell because of the Newton number. In this case, an even larger number of clusters exists $(14, 529)$, which is $\approx 0.016|\mathcal{M}_{\mathrm{SHS}}(14)|$. All of these structures optimise to just one of two possible (6,12)-LJ minima of GN type. The first is the Mackay icosahedron capped at one of its triangular faces, and the second is an elongated pentagonal bipyramid (belonging to the class of Johnson

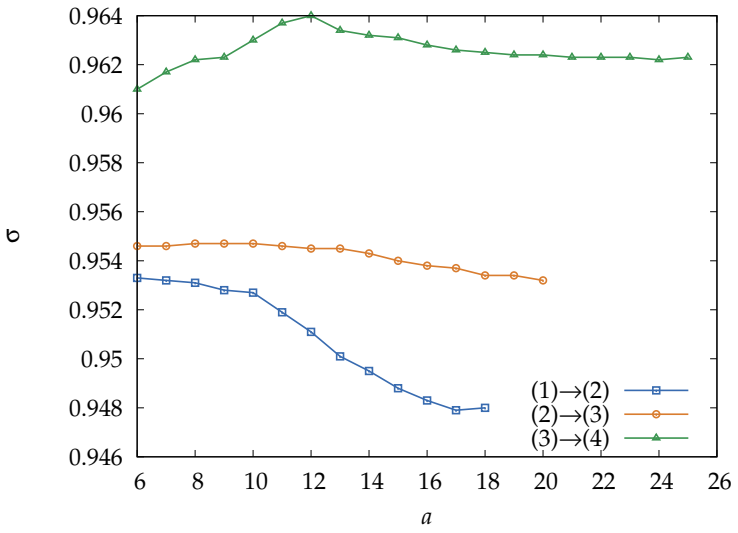

Figure 9.10 Hard-sphere radii σ in reduced units for the (a, b)-LJ potentials on the transition lines shown in figure 9.8.

solids) with the 14th sphere capping a square face.

Most of these $N = 14$ clusters are minimally rigid ($N_c = 3N - 6 = 36$), while only a few are hyperstatic ($N_c > 3N - 6$) and none are hypostatic ($N_c < 3N - 6$). There are $\{14369, 144, 8, 6, 2\}$ such clusters with $N_c = \{36, 37, 38, 39, 40\}$ and $N = 14$. The clusters with $N_c = 40$ are hcp and fcc core-shell structures capped at a square face; these arrangements maximise N_c. Most of the clusters with $N_c = \{38, 39\}$ are deformed versions of the elongated pentagonal bipyramid mentioned above, indicating that this arrangement is a favoured route to these intermediate-energy structures. However, $N_c = 39$ also contains hcp and fcc structures capped at a triangular face. The first example of a cluster derived from a perfect icosahedral symmetry shows up at lower value $N_c = 37$. Representative examples for clusters with high contact numbers are depicted in figure 9.11.

Surprisingly, the $N = 14$ cluster with the closest COS distance $r_{\text{min}}^{\text{COS}}$ was not known. Here, this gap is closed by determining the COS distance for all SHS Gregory-Newton type clusters with $N = 14$. One single cluster with $r_{\text{min}}^{\text{COS}} = 1.3471506281091$ is found. Its structure (figure 9.11a) is similar to the elongated pentagonal bipyramid with one of the square faces stretched to form a regular rectangle. The 14th sphere caps this deformed face, becoming the vertex of a deformed octahedron and allowing the outer sphere to get closer to the central sphere. The next-smallest-r^{COS} cluster ($r^{\text{COS}} = 1.37515$) is shown in figure 9.11b. It does not belong to the category of the clusters derived from the elongated pentagonal bipyramid, but instead can be described as being icosahedral-like. The short distance is achieved by attaching the 14th

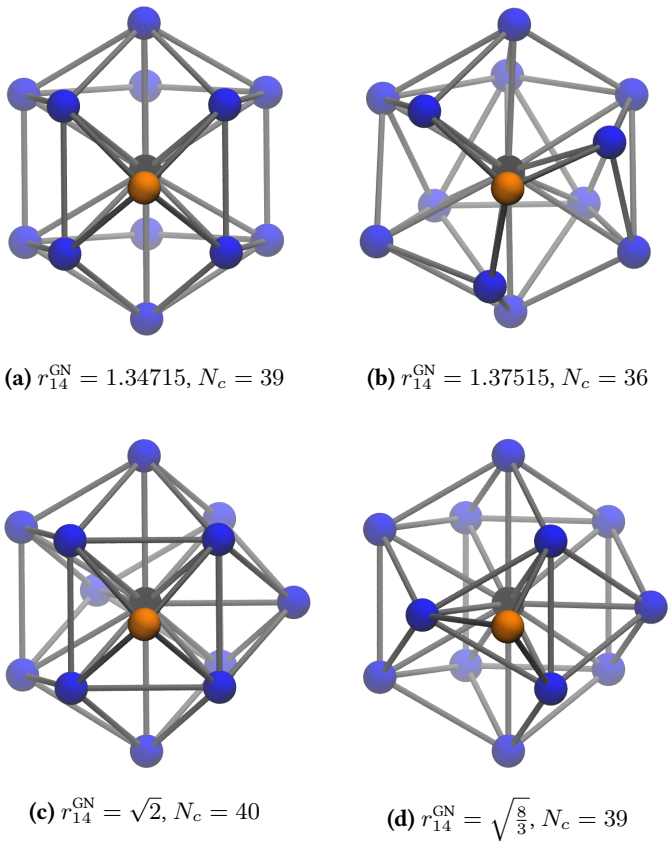

(a) $r_{14}^{\mathrm{GN}} = 1.34715$, $N_c = 39$

(b) $r_{14}^{\mathrm{GN}} = 1.37515$, $N_c = 36$

(c) $r_{14}^{\mathrm{GN}} = \sqrt{2}$, $N_c = 40$

(d) $r_{14}^{\mathrm{GN}} = \sqrt{\frac{8}{3}}$, $N_c = 39$

Figure 9.11 Graphical representations of SHS packings with $N = 14$, where a center sphere is maximally contacting. The orange sphere in each cluster is the 14th outer sphere, not able to touch the center sphere (in black). (a) distorted elongated pentagonal bipyramid (Johnson solid); (b) distorted icosahedron; (c) hcp capped on a square; (d) hcp capped on a triangle.

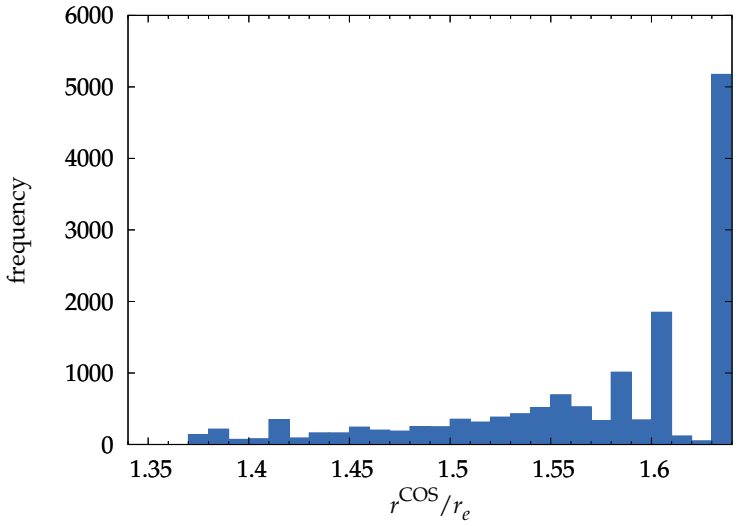

Figure 9.12 Frequency of distances from the cluster center to the most distant sphere for all Gregory-Newton-like clusters with $N = 14$ contained in the structures from Holmes-Cerfon.[114] The width of the bars is $0.01\ r_e$.

sphere to 3 spheres that do not form a face of the cluster (because they are separated by a distance larger than 1.)

The distribution of r^{COS} values for the full set of $N = 14$ GN clusters is shown in figure 9.12. Motifs with larger r^{COS} are far more prevalent. For example, the peak at $r^{\mathrm{COS}} = 1.41$ corresponds to structures where the 14th sphere is touching 4 other spheres that are part of a tetragonal pyramid, therefore forming a regular octahedron with a tip-to-tip distance of $\sqrt{2}$ (figure 9.11c). The maximum r^{COS} value (1.63) corresponds to capping triangular faces, so that the most distant sphere is part of a regular trigonal bipyramid with a height of $\sqrt{8/3}$ (figure 9.11d). The structures corresponding to the bars at $1.60, 1.58$ and 1.55 are derived from the regular trigonal bipyramid and result from breaking its axial bonds. In these structures, the more bonds are broken, or the further the axial spheres are separated, the shorter the COS distance becomes.

9.7 Conclusion

Rigid GNCs have been analysed by graph theoretical means. All 737 non-isomorphic GN graphs are sub-graphs of the icosahedral graph obtained by deleting a minimum of 6 and a maximum of 9 edges. There are only two structures with maximum edge count of 24 corresponding to the sphere packings of the fcc and hcp structures, which can be obtained from the icosahedral structure by a smooth rearrangement moving the six spheres along a closed

zig-zag path into the (hexagonal) plane. The common (6,12)-LJ potential has only one minimum structure corresponding to the ideal icosahedron where the 12 outer spheres do not touch each other. Symmetry breaking requires a very repulsive short-range LJ potential. The (a, b)-line in the (a, b)-LJ potential where the icosahedron completely disappears has also been determined. While the results shown here depend on the functional form chosen (the Lennard-Jones potential), similar results are expected for other well known potentials such as the Morse potential.

It was also shown that for softer potentials, it is still unfavourable for a 13th outer sphere to touch the center sphere. The Gregory-Newton argument still holds true for even the softest (1,2)-LJ potential.

The sphere kissing problem in higher dimensions is a well known problem[247] (in two dimensions there is only 1 non-isomorphic GNC). How many non-isomorphic rigid GNCs there are in greater than three dimensions is currently unknown. Moreover, the rigid kissing sphere problem can be extended to other (convex or not) topologies instead of a central sphere, e.g. kissing spheres on an ellipsoid. Those would all be very interesting questions to investigate.

Part IV

Appendix

A List of Gregory-Newton Contact Graphs

Table A.1 List of all GN polyhedral graphs. The ordinal numbers ω in the first column can be used to identify the individual polyhedral graphs. $|E|$ is the number of edges, and the pairs of numbers refer to edges deleted incident vertices (k, l) as defined in the icosahedral graph as shown in figure 9.1 (page 112). Note that $|E| + |\{(k, l)\}| = 30$.

ω	$\lvert E\rvert$	deleted edges (k, l)
1	24	(0,8) (1,4) (2,10) (3,7) (5,9) (6,11)
2	24	(0,10) (1,6) (2,5) (3,9) (4,8) (7,11)
3	23	(1,6) (2,7) (2,10) (4,9) (5,7) (5,8) (10,11)
4	22	(0,2) (0,6) (0,10) (1,11) (2,8) (3,5) (6,10) (6,11)
5	22	(0,4) (0,6) (0,10) (3,11) (4,8) (5,9) (6,10) (8,9)
6	22	(0,2) (0,6) (0,10) (1,3) (2,8) (2,10) (4,6) (5,7)
7	22	(0,2) (0,8) (1,3) (3,9) (4,8) (5,9) (8,9) (10,11)
8	22	(0,4) (0,6) (0,8) (1,9) (2,10) (3,7) (4,6) (4,8)
9	22	(0,4) (0,6) (0,8) (3,7) (4,6) (4,8) (5,9) (10,11)
10	22	(0,2) (0,8) (0,10) (1,9) (2,10) (3,7) (4,6) (4,8)
11	22	(0,4) (0,6) (0,10) (1,3) (2,5) (2,8) (4,6) (5,7)
12	22	(0,6) (0,8) (0,10) (1,3) (2,8) (2,10) (4,9) (7,11)
13	22	(0,4) (0,6) (1,11) (2,8) (3,5) (3,9) (5,7) (6,10)
14	21	(0,6) (0,10) (1,4) (1,6) (1,9) (2,10) (3,9) (4,6) (4,9)
15	21	(0,2) (0,10) (2,8) (2,10) (4,9) (5,8) (5,9) (7,10) (8,9)
16	21	(0,6) (0,10) (2,5) (2,7) (2,10) (3,5) (5,7) (6,10) (6,11)
17	21	(0,2) (0,8) (1,3) (1,4) (1,9) (3,11) (4,8) (4,9) (8,9)
18	21	(0,6) (0,10) (1,4) (1,9) (2,10) (3,9) (4,6) (4,9) (6,10)
19	21	(0,4) (0,8) (2,5) (2,7) (2,8) (3,5) (3,7) (3,9) (5,7)
20	21	(0,6) (0,10) (2,5) (2,7) (2,10) (3,5) (3,11) (5,7) (7,10)
21	21	(0,6) (0,10) (2,5) (2,7) (2,10) (3,5) (5,7) (6,11) (7,10)
22	21	(0,6) (0,8) (1,3) (1,4) (1,9) (3,5) (3,9) (4,8) (4,9)
23	21	(0,6) (0,8) (1,4) (1,6) (1,9) (2,5) (4,8) (4,9) (8,9)
24	21	(0,8) (0,10) (2,5) (2,7) (2,10) (3,5) (3,11) (5,7) (7,10)
25	21	(0,2) (0,4) (1,3) (2,5) (4,8) (4,9) (5,8) (5,9) (8,9)
26	21	(1,3) (1,6) (3,7) (5,9) (6,10) (6,11) (7,10) (7,11) (10,11)
27	21	(0,6) (2,5) (2,7) (2,8) (5,7) (5,8) (6,11) (7,10) (10,11)
28	21	(0,6) (2,5) (2,7) (2,8) (5,8) (6,11) (7,10) (7,11) (10,11)
29	21	(0,10) (2,5) (2,7) (2,10) (3,7) (3,9) (5,7) (5,8) (8,9)
30	21	(0,4) (0,6) (0,10) (1,9) (2,8) (2,10) (4,8) (4,9) (6,10)
31	21	(0,2) (0,6) (0,10) (1,9) (2,8) (2,10) (4,8) (4,9) (6,10)
32	21	(0,4) (2,5) (2,7) (2,8) (3,5) (3,7) (4,9) (5,7) (8,9)

Table A.1 – continued from previous page

ω	$\lvert E\rvert$	deleted edges (k, l)
33	21	(0,6) (1,4) (1,6) (1,9) (3,5) (3,9) (4,8) (4,9) (5,8)
34	21	(0,4) (2,7) (2,8) (3,5) (3,7) (4,9) (5,7) (5,9) (8,9)
35	21	(0,10) (1,3) (1,9) (2,5) (2,7) (2,10) (3,5) (3,9) (5,7)
36	21	(0,10) (1,3) (1,9) (2,7) (2,10) (3,5) (3,9) (5,7) (5,9)
37	21	(0,4) (2,5) (2,7) (3,5) (3,7) (4,8) (4,9) (5,7) (8,9)
38	21	(0,2) (0,8) (0,10) (2,5) (2,8) (3,5) (3,11) (7,10) (7,11)
39	21	(1,3) (1,9) (1,11) (2,5) (2,8) (3,9) (5,7) (5,8) (7,11)
40	21	(0,2) (0,8) (1,4) (1,9) (2,7) (2,10) (4,8) (4,9) (7,10)
41	21	(0,4) (0,6) (0,10) (1,6) (1,11) (4,8) (4,9) (8,9) (10,11)
42	21	(0,4) (0,6) (0,8) (1,4) (1,11) (2,8) (2,10) (6,10) (6,11)
43	21	(0,6) (0,10) (2,5) (2,7) (2,10) (4,9) (5,7) (5,8) (7,10)
44	21	(0,4) (0,10) (1,3) (1,6) (1,11) (6,10) (6,11) (8,9) (10,11)
45	21	(0,8) (0,10) (2,5) (2,7) (2,8) (3,7) (4,6) (5,7) (5,8)
46	21	(0,6) (0,10) (1,4) (1,6) (1,9) (3,11) (4,6) (4,9) (8,9)
47	21	(0,4) (0,10) (1,4) (1,6) (1,11) (3,11) (4,6) (6,11) (8,9)
48	21	(1,4) (2,7) (3,5) (3,7) (3,9) (4,6) (5,7) (5,9) (8,9)
49	21	(0,4) (0,8) (1,6) (4,6) (4,8) (6,11) (7,11) (8,9) (10,11)
50	21	(0,6) (0,10) (1,3) (1,4) (1,9) (3,9) (3,11) (4,8) (4,9)
51	21	(0,2) (1,3) (1,9) (3,7) (3,11) (6,10) (7,10) (7,11) (10,11)
52	21	(0,6) (0,10) (2,5) (2,7) (2,10) (4,6) (5,8) (5,9) (6,10)
53	21	(0,2) (0,4) (0,8) (1,3) (2,5) (4,8) (4,9) (5,7) (8,9)
54	21	(0,4) (0,6) (0,8) (1,4) (1,6) (2,7) (4,6) (7,11) (10,11)
55	21	(0,4) (0,6) (0,8) (2,8) (3,5) (3,7) (4,9) (5,8) (5,9)
56	21	(0,4) (0,6) (0,10) (1,4) (2,7) (2,10) (5,7) (6,10) (6,11)
57	21	(0,4) (0,6) (0,8) (1,6) (1,11) (2,5) (4,8) (4,9) (8,9)
58	21	(0,4) (0,8) (1,4) (1,6) (1,11) (3,9) (6,10) (6,11) (10,11)
59	21	(0,4) (0,6) (0,8) (1,6) (2,5) (4,8) (4,9) (5,7) (8,9)
60	21	(0,4) (0,10) (1,4) (1,6) (1,9) (2,10) (4,6) (6,11) (8,9)
61	21	(0,4) (0,6) (0,10) (1,4) (1,9) (2,10) (6,10) (6,11) (8,9)
62	21	(0,4) (0,6) (0,8) (2,5) (4,6) (4,8) (5,7) (7,10) (8,9)
63	21	(0,4) (0,6) (0,8) (1,4) (1,6) (2,5) (4,6) (5,7) (8,9)
64	21	(0,4) (0,6) (0,8) (1,6) (1,9) (2,5) (3,9) (4,8) (4,9)
65	21	(0,2) (0,8) (0,10) (2,8) (3,5) (4,9) (5,8) (5,9) (7,10)
66	21	(0,4) (0,6) (0,8) (1,6) (1,9) (2,8) (3,5) (4,8) (4,9)
67	21	(0,4) (0,6) (0,8) (1,6) (1,9) (2,8) (3,5) (4,6) (5,8)
68	21	(0,2) (0,6) (0,10) (1,4) (1,11) (3,9) (3,11) (6,10) (6,11)
69	21	(0,4) (0,6) (0,8) (1,6) (2,8) (3,5) (4,9) (5,8) (5,9)
70	21	(0,4) (0,6) (0,8) (1,3) (2,5) (4,6) (4,8) (5,9) (8,9)
71	21	(0,4) (0,6) (0,8) (1,3) (1,4) (1,9) (2,10) (4,6) (8,9)
72	21	(0,4) (0,6) (0,8) (1,3) (1,4) (1,9) (2,5) (4,6) (8,9)
73	21	(0,4) (0,6) (0,8) (2,5) (4,6) (4,8) (5,9) (7,10) (8,9)
74	21	(0,4) (0,6) (0,8) (2,5) (3,7) (4,6) (4,8) (5,9) (8,9)
75	21	(0,4) (0,6) (0,10) (1,4) (1,11) (2,10) (6,10) (6,11) (8,9)
76	21	(0,4) (0,6) (0,8) (1,3) (1,9) (2,8) (3,5) (4,8) (4,9)
77	21	(0,4) (0,6) (0,8) (1,3) (1,4) (1,9) (2,8) (3,5) (4,6)
78	21	(0,4) (0,6) (0,10) (1,6) (1,11) (3,5) (3,7) (3,11) (4,6)
79	21	(0,4) (0,6) (1,4) (2,8) (4,6) (6,10) (7,10) (7,11) (10,11)
80	21	(0,2) (0,6) (0,10) (1,4) (1,6) (1,11) (3,9) (3,11) (4,6)
81	21	(0,4) (0,6) (0,10) (1,4) (1,9) (2,10) (4,6) (7,10) (8,9)
82	21	(0,4) (0,6) (0,8) (1,3) (1,4) (1,9) (2,5) (3,9) (4,6)

Table A.1 – continued from previous page

ω	$\lvert E\rvert$	deleted edges (k, l)
83	21	(0,4) (0,6) (0,8) (1,6) (2,8) (3,5) (3,9) (5,8) (5,9)
84	21	(0,4) (0,6) (0,10) (1,3) (1,6) (1,11) (2,8) (3,11) (4,6)
85	21	(0,2) (0,4) (0,8) (2,8) (2,10) (4,6) (5,8) (5,9) (7,10)
86	21	(0,4) (0,6) (0,8) (1,3) (2,5) (3,9) (4,8) (5,9) (8,9)
87	21	(0,4) (0,6) (0,10) (1,3) (1,9) (1,11) (3,5) (3,9) (4,6)
88	21	(0,4) (0,6) (0,10) (1,3) (1,11) (3,9) (3,11) (6,10) (7,11)
89	21	(0,4) (0,6) (0,10) (1,3) (1,6) (1,11) (2,7) (2,10) (4,6)
90	21	(1,4) (1,9) (2,5) (3,5) (3,7) (3,11) (4,6) (5,7) (7,11)
91	21	(0,4) (0,6) (0,8) (1,6) (1,11) (2,8) (3,11) (4,8) (4,9)
92	21	(0,4) (0,6) (0,8) (2,5) (3,7) (4,6) (4,8) (5,7) (8,9)
93	21	(0,4) (0,6) (0,10) (1,4) (1,11) (2,10) (3,9) (6,10) (6,11)
94	21	(0,4) (0,6) (0,10) (1,6) (1,9) (2,8) (4,6) (4,8) (10,11)
95	21	(0,4) (0,6) (0,10) (1,3) (1,11) (2,10) (3,9) (6,10) (6,11)
96	21	(0,4) (0,6) (0,10) (1,3) (1,11) (2,7) (2,10) (6,10) (6,11)
97	21	(0,4) (0,6) (0,8) (1,4) (1,6) (2,8) (3,5) (4,6) (5,9)
98	21	(0,2) (0,8) (0,10) (2,7) (2,10) (3,11) (4,8) (6,10) (7,11)
99	21	(0,4) (0,6) (0,10) (1,4) (1,6) (2,10) (4,6) (5,9) (8,9)
100	21	(0,4) (0,6) (0,8) (2,5) (3,9) (4,8) (5,9) (6,10) (8,9)
101	21	(0,4) (0,6) (0,8) (1,6) (1,11) (3,5) (3,7) (3,11) (4,6)
102	21	(1,4) (1,6) (2,5) (2,7) (2,10) (4,9) (5,8) (5,9) (8,9)
103	21	(0,4) (0,6) (0,10) (1,3) (1,11) (3,5) (3,9) (4,6) (6,10)
104	21	(0,2) (0,8) (0,10) (2,7) (2,10) (3,7) (3,11) (4,8) (5,7)
105	21	(0,2) (0,8) (1,3) (1,11) (2,7) (2,10) (3,7) (3,11) (5,7)
106	21	(0,4) (0,6) (0,10) (1,3) (1,9) (4,6) (4,8) (8,9) (10,11)
107	21	(0,4) (0,6) (0,10) (1,4) (1,11) (3,5) (3,9) (6,10) (6,11)
108	21	(0,2) (0,6) (0,10) (2,8) (2,10) (3,7) (3,9) (5,7) (5,8)
109	21	(0,4) (0,6) (0,8) (1,9) (2,8) (2,10) (4,9) (5,8) (6,10)
110	21	(0,2) (0,8) (0,10) (1,6) (2,7) (2,10) (4,6) (5,7) (5,8)
111	21	(0,4) (0,6) (0,10) (2,10) (4,8) (6,11) (7,10) (7,11) (8,9)
112	21	(0,2) (0,4) (0,8) (1,4) (1,6) (2,5) (4,6) (5,7) (8,9)
113	21	(0,4) (0,6) (0,10) (1,3) (1,6) (2,10) (3,7) (4,6) (7,11)
114	21	(0,2) (0,6) (0,10) (1,3) (1,6) (2,10) (3,7) (4,6) (7,11)
115	21	(0,2) (0,8) (0,10) (2,8) (3,5) (4,9) (5,7) (5,9) (7,10)
116	21	(0,2) (0,8) (0,10) (1,4) (1,6) (1,11) (2,7) (4,6) (10,11)
117	21	(0,4) (0,6) (0,8) (2,5) (3,7) (3,9) (4,8) (5,7) (8,9)
118	21	(0,4) (0,6) (0,10) (1,3) (1,11) (2,10) (3,7) (6,11) (7,10)
119	21	(0,4) (0,6) (0,10) (1,4) (2,10) (3,7) (3,11) (6,10) (7,11)
120	21	(0,4) (0,6) (0,10) (1,3) (1,11) (2,7) (3,11) (4,6) (6,10)
121	21	(0,4) (0,6) (0,10) (1,3) (1,11) (2,8) (3,11) (4,6) (6,10)
122	21	(0,4) (0,6) (0,10) (1,3) (1,9) (2,10) (3,9) (4,6) (4,8)
123	21	(0,4) (0,6) (0,8) (1,3) (1,11) (3,9) (4,6) (6,10) (10,11)
124	21	(0,4) (0,6) (0,8) (1,4) (1,9) (3,9) (6,10) (6,11) (10,11)
125	21	(0,2) (0,8) (0,10) (1,3) (2,5) (2,8) (3,11) (7,10) (7,11)
126	21	(0,4) (0,6) (0,8) (2,8) (3,5) (3,7) (4,6) (5,7) (5,9)
127	21	(0,4) (0,6) (0,8) (3,5) (3,7) (4,6) (6,10) (7,11) (10,11)
128	21	(0,4) (0,6) (0,8) (1,3) (3,7) (4,6) (6,10) (7,11) (10,11)
129	21	(0,4) (0,6) (0,8) (1,4) (3,7) (3,11) (6,10) (7,11) (10,11)
130	21	(0,4) (0,6) (0,8) (1,6) (1,11) (3,5) (3,9) (4,8) (4,9)
131	21	(0,2) (0,6) (0,10) (2,8) (2,10) (3,7) (4,6) (5,7) (5,8)
132	21	(0,4) (0,6) (0,10) (1,11) (3,11) (4,8) (4,9) (6,10) (8,9)

Table A.1 – continued from previous page

ω	$\lvert E\rvert$	deleted edges (k, l)
133	21	(0,4) (0,6) (0,8) (1,4) (1,9) (2,8) (6,10) (6,11) (10,11)
134	21	(0,4) (0,6) (0,10) (1,3) (1,6) (2,7) (4,6) (7,11) (10,11)
135	21	(0,2) (0,8) (0,10) (2,7) (4,6) (5,7) (5,8) (6,10) (10,11)
136	21	(0,4) (0,6) (0,10) (1,4) (1,11) (2,10) (3,7) (6,11) (7,10)
137	21	(0,4) (0,6) (0,10) (1,3) (1,11) (2,7) (3,11) (6,10) (7,11)
138	21	(0,4) (0,6) (0,8) (2,8) (3,5) (3,7) (4,9) (5,7) (5,9)
139	21	(0,4) (0,6) (0,10) (1,3) (1,9) (1,11) (2,10) (3,9) (4,6)
140	21	(0,2) (0,6) (0,10) (2,8) (3,11) (5,7) (5,8) (6,10) (10,11)
141	21	(0,4) (0,6) (0,8) (1,4) (1,11) (2,10) (6,10) (6,11) (8,9)
142	21	(0,4) (0,6) (0,8) (1,6) (1,11) (3,9) (3,11) (4,8) (5,9)
143	21	(0,4) (0,6) (0,8) (1,3) (1,11) (3,11) (4,6) (5,9) (8,9)
144	21	(0,4) (0,6) (0,8) (1,11) (2,7) (2,10) (4,8) (6,11) (7,10)
145	21	(0,4) (0,6) (0,10) (1,6) (1,9) (2,8) (2,10) (4,9) (5,8)
146	21	(0,4) (0,6) (0,8) (2,7) (2,10) (3,11) (4,8) (6,10) (7,11)
147	21	(0,4) (0,6) (0,8) (1,4) (1,11) (2,7) (2,10) (6,11) (7,10)
148	21	(0,4) (0,6) (0,8) (2,10) (3,7) (3,11) (4,8) (6,10) (7,11)
149	21	(0,4) (0,6) (0,8) (1,4) (2,8) (2,10) (6,11) (7,10) (7,11)
150	21	(1,4) (1,6) (3,5) (3,9) (4,9) (5,7) (6,10) (7,11) (10,11)
151	21	(1,4) (1,9) (3,5) (3,7) (4,9) (5,7) (6,10) (6,11) (10,11)
152	21	(0,8) (1,3) (2,10) (3,7) (3,11) (5,9) (7,10) (7,11) (10,11)
153	21	(1,3) (1,4) (1,9) (3,5) (3,9) (5,8) (5,9) (6,10) (7,11)
154	21	(1,9) (2,7) (3,5) (3,7) (3,9) (4,8) (5,7) (5,9) (10,11)
155	21	(1,4) (1,6) (1,11) (2,5) (2,7) (2,8) (3,11) (7,10) (7,11)
156	21	(0,4) (0,6) (1,4) (1,6) (1,11) (2,8) (3,11) (4,6) (7,10)
157	21	(0,6) (0,8) (1,4) (3,11) (4,6) (4,9) (5,9) (6,10) (8,9)
158	21	(0,4) (0,6) (1,11) (3,9) (4,6) (4,8) (6,10) (7,10) (10,11)
159	21	(0,4) (0,10) (1,3) (1,4) (1,9) (3,5) (3,9) (4,6) (7,11)
160	21	(0,6) (0,8) (1,3) (1,11) (3,7) (3,11) (4,9) (6,10) (6,11)
161	21	(0,4) (0,6) (1,4) (1,6) (1,9) (3,9) (4,6) (5,7) (10,11)
162	21	(0,8) (0,10) (2,7) (2,10) (3,5) (4,6) (5,7) (5,9) (7,10)
163	21	(0,6) (2,5) (2,7) (2,8) (3,9) (5,7) (5,8) (7,10) (10,11)
164	21	(0,6) (0,8) (1,3) (1,9) (1,11) (2,5) (4,8) (4,9) (8,9)
165	21	(0,2) (0,6) (1,11) (2,8) (3,5) (6,10) (6,11) (7,10) (10,11)
166	21	(0,6) (0,10) (2,5) (2,8) (3,5) (3,7) (3,9) (5,7) (7,11)
167	21	(0,6) (0,10) (1,11) (2,5) (3,7) (5,8) (6,10) (6,11) (10,11)
168	21	(0,6) (0,10) (2,7) (2,8) (3,5) (3,7) (3,11) (5,7) (5,9)
169	21	(0,2) (0,10) (1,6) (2,7) (2,10) (4,8) (5,7) (6,11) (7,10)
170	21	(0,4) (0,6) (1,4) (1,6) (1,11) (3,5) (3,9) (4,6) (7,10)
171	21	(0,2) (0,10) (2,5) (2,8) (3,11) (5,7) (5,8) (6,10) (8,9)
172	21	(0,2) (0,10) (2,5) (2,8) (3,7) (5,7) (5,8) (6,11) (8,9)
173	21	(0,4) (0,8) (1,9) (3,5) (3,7) (3,9) (4,8) (4,9) (6,11)
174	21	(0,4) (0,8) (1,4) (1,6) (3,9) (4,6) (6,11) (7,11) (10,11)
175	21	(0,6) (0,10) (1,4) (1,6) (1,11) (3,5) (4,6) (4,9) (8,9)
176	21	(0,4) (0,6) (1,3) (1,11) (3,9) (3,11) (5,7) (6,10) (6,11)
177	21	(0,4) (0,10) (1,3) (1,6) (6,10) (6,11) (7,11) (8,9) (10,11)
178	21	(0,6) (0,8) (1,4) (1,6) (1,11) (3,7) (4,6) (4,9) (10,11)
179	21	(0,4) (0,6) (1,4) (1,6) (1,9) (3,11) (4,6) (5,7) (8,9)
180	21	(0,4) (0,6) (1,4) (1,6) (1,9) (3,11) (4,6) (7,10) (8,9)
181	21	(0,6) (0,10) (2,7) (2,10) (3,5) (5,8) (5,9) (6,10) (6,11)
182	21	(0,6) (0,10) (2,7) (2,10) (3,5) (4,6) (5,8) (5,9) (6,10)

Table A.1 – continued from previous page

ω	$\lvert E\rvert$	deleted edges (k, l)
183	21	(0,4) (0,6) (1,4) (3,5) (4,6) (5,7) (5,9) (6,10) (8,9)
184	21	(0,4) (0,8) (2,5) (2,7) (4,6) (4,8) (7,10) (7,11) (8,9)
185	21	(0,4) (0,6) (1,3) (1,9) (3,9) (3,11) (4,8) (4,9) (7,10)
186	21	(0,4) (0,6) (1,6) (4,6) (4,8) (5,8) (7,11) (8,9) (10,11)
187	21	(0,4) (0,6) (1,9) (3,9) (4,6) (4,8) (6,10) (7,10) (10,11)
188	21	(0,4) (0,6) (1,9) (3,9) (4,8) (4,9) (6,10) (7,10) (10,11)
189	21	(0,2) (1,3) (1,6) (1,11) (2,5) (2,8) (3,11) (6,11) (7,10)
190	21	(0,4) (0,6) (1,4) (1,6) (1,11) (3,5) (4,6) (5,7) (8,9)
191	21	(0,4) (0,6) (0,8) (1,3) (4,6) (6,10) (7,11) (8,9) (10,11)
192	21	(0,4) (0,6) (0,10) (2,7) (2,10) (3,7) (5,7) (5,8) (6,11)
193	21	(0,10) (1,4) (1,6) (1,9) (3,7) (4,8) (4,9) (6,11) (10,11)
194	21	(0,4) (0,6) (0,10) (1,6) (2,7) (2,10) (4,8) (4,9) (5,9)
195	21	(0,4) (0,6) (0,8) (1,9) (3,7) (4,8) (6,10) (6,11) (10,11)
196	21	(0,4) (0,6) (0,10) (1,6) (2,7) (2,10) (4,8) (4,9) (7,11)
197	21	(0,4) (0,6) (0,8) (1,4) (3,9) (3,11) (6,10) (7,11) (10,11)
198	21	(0,4) (0,6) (0,8) (1,4) (3,11) (6,10) (7,11) (8,9) (10,11)
199	21	(0,4) (0,6) (0,8) (1,11) (3,7) (4,8) (4,9) (6,10) (10,11)
200	21	(0,6) (1,4) (1,9) (2,5) (2,8) (3,7) (3,9) (5,8) (5,9)
201	21	(0,2) (0,6) (0,10) (1,6) (1,11) (2,7) (3,5) (3,11) (4,6)
202	21	(0,2) (0,6) (0,10) (1,6) (1,11) (2,10) (3,9) (4,6) (4,8)
203	21	(0,4) (0,6) (0,8) (3,7) (4,8) (5,9) (6,10) (6,11) (10,11)
204	21	(0,4) (0,6) (0,10) (1,11) (2,7) (2,10) (4,6) (5,8) (7,10)
205	21	(0,4) (0,6) (0,10) (1,3) (1,6) (4,6) (7,11) (8,9) (10,11)
206	21	(0,4) (0,6) (0,8) (1,3) (1,6) (4,6) (7,11) (8,9) (10,11)
207	21	(0,2) (0,8) (0,10) (1,4) (1,11) (2,10) (4,6) (7,10) (8,9)
208	21	(0,4) (0,6) (0,10) (1,3) (1,9) (3,7) (4,6) (4,8) (10,11)
209	21	(0,4) (0,6) (0,10) (2,8) (2,10) (3,5) (3,11) (6,10) (7,11)
210	21	(0,4) (0,6) (0,8) (2,8) (2,10) (3,7) (3,9) (5,7) (5,8)
211	21	(0,4) (0,6) (0,8) (1,6) (1,11) (3,7) (4,8) (4,9) (10,11)
212	21	(0,2) (0,6) (0,10) (2,10) (3,7) (3,9) (5,8) (6,10) (7,11)
213	21	(0,4) (0,6) (0,10) (1,6) (3,9) (4,8) (4,9) (7,11) (10,11)
214	21	(0,4) (0,6) (0,8) (1,6) (2,7) (2,10) (4,8) (4,9) (5,9)
215	21	(0,2) (0,4) (1,6) (2,10) (4,8) (4,9) (5,7) (5,8) (8,9)
216	21	(0,8) (0,10) (1,4) (2,5) (2,7) (2,10) (4,6) (5,9) (7,10)
217	21	(0,4) (0,6) (0,8) (1,3) (1,6) (2,8) (4,6) (7,11) (10,11)
218	21	(0,6) (0,8) (1,3) (1,4) (2,8) (3,11) (4,8) (4,9) (5,9)
219	21	(0,4) (0,6) (0,8) (1,6) (1,11) (2,7) (4,8) (4,9) (10,11)
220	21	(0,2) (0,4) (0,8) (1,11) (3,9) (4,8) (4,9) (6,10) (10,11)
221	21	(0,4) (0,6) (0,10) (1,6) (1,11) (3,7) (4,8) (4,9) (10,11)
222	21	(0,4) (0,6) (0,10) (1,4) (1,11) (2,10) (6,11) (7,10) (8,9)
223	21	(0,2) (0,4) (0,8) (1,11) (3,9) (3,11) (4,6) (4,8) (6,10)
224	21	(0,4) (0,6) (0,8) (1,3) (1,6) (2,10) (3,7) (4,6) (7,11)
225	21	(0,4) (0,6) (0,8) (2,7) (2,10) (3,7) (5,7) (5,8) (6,11)
226	21	(0,4) (0,6) (0,8) (1,4) (1,11) (3,9) (3,11) (6,10) (7,11)
227	21	(0,2) (0,6) (0,10) (2,7) (3,9) (5,8) (5,9) (6,10) (10,11)
228	21	(0,4) (0,6) (0,8) (1,3) (1,9) (1,11) (3,7) (4,6) (10,11)
229	21	(0,2) (0,6) (1,11) (2,7) (2,10) (3,11) (4,8) (6,11) (7,10)
230	21	(0,4) (0,6) (0,8) (1,4) (1,11) (3,11) (6,10) (7,11) (8,9)
231	21	(0,4) (0,6) (0,10) (1,3) (1,9) (1,11) (2,8) (4,6) (10,11)
232	21	(0,4) (0,6) (0,10) (2,8) (3,5) (4,6) (5,7) (5,9) (7,10)

Table A.1 – continued from previous page

ω	$\lvert E\rvert$	deleted edges (k, l)
233	21	(0,2) (0,6) (0,10) (2,8) (2,10) (3,5) (3,7) (4,9) (5,7)
234	21	(0,4) (0,6) (0,10) (1,11) (3,9) (3,11) (4,8) (6,10) (7,11)
235	21	(0,4) (0,6) (0,10) (1,3) (1,9) (1,11) (2,10) (4,6) (8,9)
236	21	(0,4) (0,6) (0,8) (1,3) (1,9) (1,11) (2,8) (2,10) (4,6)
237	21	(0,4) (0,6) (0,10) (1,3) (1,11) (2,8) (2,10) (6,11) (7,10)
238	21	(0,4) (0,6) (0,8) (2,7) (2,10) (3,5) (3,7) (5,7) (6,11)
239	21	(0,4) (0,6) (0,8) (2,7) (2,10) (3,7) (3,11) (5,7) (5,8)
240	21	(0,4) (0,6) (1,9) (3,5) (3,7) (3,11) (4,8) (5,8) (5,9)
241	21	(0,6) (1,4) (3,9) (4,8) (4,9) (6,10) (7,10) (7,11) (10,11)
242	21	(0,4) (0,6) (0,8) (1,6) (2,7) (2,10) (4,8) (4,9) (5,7)
243	21	(0,6) (0,8) (1,4) (2,5) (2,8) (4,8) (4,9) (5,9) (7,10)
244	21	(0,4) (0,6) (0,8) (1,3) (1,9) (3,7) (4,8) (4,9) (10,11)
245	21	(0,4) (0,6) (0,8) (1,6) (1,9) (3,7) (4,8) (4,9) (10,11)
246	21	(0,4) (0,6) (0,10) (2,7) (2,10) (4,9) (5,8) (6,10) (7,11)
247	21	(0,4) (0,6) (0,8) (1,6) (1,11) (2,7) (4,6) (5,8) (10,11)
248	21	(1,3) (1,11) (2,5) (3,7) (3,11) (6,10) (6,11) (7,10) (8,9)
249	21	(0,2) (0,8) (0,10) (2,7) (3,9) (5,8) (6,10) (7,11) (10,11)
250	21	(0,4) (0,6) (0,10) (1,6) (1,9) (2,7) (4,8) (4,9) (10,11)
251	21	(0,4) (0,6) (0,10) (1,3) (2,8) (2,10) (6,11) (7,10) (7,11)
252	21	(0,4) (0,6) (0,8) (1,4) (1,9) (3,7) (6,10) (6,11) (10,11)
253	21	(0,4) (0,6) (0,10) (2,7) (2,10) (3,11) (5,8) (6,10) (7,11)
254	21	(1,4) (1,6) (2,5) (3,11) (4,6) (4,9) (5,7) (6,11) (8,9)
255	21	(0,4) (1,3) (1,9) (1,11) (3,7) (5,7) (6,10) (6,11) (10,11)
256	21	(0,4) (0,6) (0,10) (1,6) (2,7) (2,10) (4,8) (4,9) (5,7)
257	21	(1,4) (3,5) (3,7) (4,9) (5,8) (5,9) (6,10) (6,11) (8,9)
258	21	(0,2) (1,3) (1,9) (1,11) (2,8) (3,11) (6,10) (6,11) (7,10)
259	21	(0,4) (0,6) (0,10) (1,9) (3,7) (3,11) (4,8) (6,10) (6,11)
260	21	(0,2) (0,8) (0,10) (1,6) (1,11) (2,5) (4,8) (4,9) (8,9)
261	21	(0,8) (1,9) (1,11) (3,5) (3,7) (3,11) (4,8) (5,9) (6,11)
262	21	(0,4) (0,6) (0,10) (1,6) (1,11) (2,10) (3,9) (4,8) (4,9)
263	21	(0,2) (1,4) (1,9) (2,7) (2,10) (3,5) (3,11) (7,10) (7,11)
264	21	(0,4) (0,6) (0,8) (1,9) (3,7) (3,11) (4,8) (6,10) (6,11)
265	21	(1,3) (1,6) (1,11) (2,5) (2,8) (3,5) (3,9) (7,10) (7,11)
266	21	(0,2) (0,6) (0,10) (1,4) (1,9) (3,7) (3,11) (6,10) (6,11)
267	21	(0,2) (0,4) (0,8) (2,5) (4,8) (5,7) (6,10) (6,11) (8,9)
268	21	(0,4) (0,6) (0,8) (1,3) (1,9) (2,7) (2,10) (4,6) (4,8)
269	21	(0,4) (0,6) (0,8) (1,4) (1,9) (2,7) (2,10) (6,10) (6,11)
270	21	(0,6) (0,10) (1,11) (2,5) (2,7) (2,10) (4,6) (5,8) (7,10)
271	21	(0,4) (0,6) (0,8) (1,9) (3,7) (4,8) (4,9) (6,10) (10,11)
272	21	(0,4) (0,6) (0,10) (2,7) (2,10) (3,7) (3,11) (5,7) (5,8)
273	21	(0,4) (0,6) (0,10) (1,3) (1,11) (3,11) (6,10) (7,11) (8,9)
274	21	(0,2) (0,4) (0,8) (2,10) (3,5) (3,7) (5,7) (6,11) (7,11)
275	21	(0,4) (0,6) (0,10) (2,8) (2,10) (3,5) (3,7) (3,9) (5,7)
276	21	(0,4) (0,6) (0,8) (2,8) (2,10) (3,5) (3,7) (3,9) (5,7)
277	21	(0,4) (0,6) (0,8) (1,3) (1,11) (3,11) (6,10) (7,11) (8,9)
278	21	(0,2) (0,8) (0,10) (2,10) (3,5) (3,7) (4,6) (5,7) (7,11)
279	21	(0,4) (0,6) (0,10) (2,8) (3,5) (3,9) (5,7) (5,9) (6,10)
280	21	(0,2) (0,6) (0,10) (2,8) (3,5) (3,9) (5,7) (6,10) (10,11)
281	21	(0,4) (0,6) (0,10) (1,11) (3,7) (3,11) (4,8) (4,9) (6,10)
282	21	(0,4) (0,8) (1,6) (2,5) (2,8) (3,5) (4,6) (5,7) (6,11)

Table A.1 – continued from previous page

ω	$\lvert E\rvert$	deleted edges (k, l)
283	21	(0,6) (2,5) (2,7) (2,8) (4,6) (5,8) (5,9) (7,10) (10,11)
284	21	(0,4) (0,6) (0,10) (1,3) (1,9) (2,7) (2,10) (4,6) (4,8)
285	21	(0,2) (1,4) (1,6) (1,11) (2,8) (3,11) (4,6) (7,10) (7,11)
286	21	(0,4) (0,6) (0,10) (1,6) (1,11) (2,7) (2,10) (4,8) (4,9)
287	21	(0,2) (0,8) (0,10) (1,11) (3,7) (3,11) (5,8) (6,10) (6,11)
288	21	(0,4) (0,6) (0,10) (1,3) (1,11) (2,10) (3,9) (6,11) (7,10)
289	21	(0,4) (0,6) (0,10) (1,4) (3,5) (3,7) (4,6) (5,9) (8,9)
290	21	(0,6) (0,10) (1,6) (1,11) (2,5) (2,7) (2,8) (4,6) (5,8)
291	21	(0,4) (0,6) (0,10) (2,7) (2,10) (3,7) (3,11) (4,8) (5,7)
292	21	(0,4) (0,6) (0,10) (1,3) (1,9) (2,7) (2,10) (4,8) (4,9)
293	21	(0,2) (0,6) (0,10) (1,6) (1,9) (2,5) (3,9) (4,8) (5,9)
294	21	(0,4) (0,6) (0,10) (1,11) (3,11) (4,8) (6,10) (7,11) (8,9)
295	21	(0,4) (0,6) (0,8) (1,6) (2,8) (2,10) (4,9) (5,7) (5,8)
296	21	(0,4) (0,6) (0,10) (1,3) (1,9) (4,6) (7,11) (8,9) (10,11)
297	21	(0,4) (0,6) (0,8) (1,3) (1,9) (4,6) (7,11) (8,9) (10,11)
298	21	(0,10) (1,3) (1,6) (2,5) (2,10) (3,9) (3,11) (5,7) (7,11)
299	21	(0,4) (0,6) (0,10) (2,5) (2,8) (3,5) (3,11) (6,10) (7,11)
300	21	(0,4) (0,6) (0,10) (2,5) (4,8) (6,11) (7,10) (7,11) (8,9)
301	21	(0,4) (0,6) (0,8) (1,4) (1,9) (2,8) (2,10) (6,11) (7,10)
302	21	(0,10) (1,3) (1,6) (2,10) (3,7) (3,11) (4,6) (4,9) (7,11)
303	21	(0,4) (0,6) (0,8) (1,4) (1,9) (3,11) (6,10) (7,11) (8,9)
304	21	(0,2) (0,6) (0,10) (1,6) (2,8) (3,5) (4,8) (4,9) (5,9)
305	21	(0,2) (0,6) (0,10) (1,3) (1,9) (3,5) (4,6) (4,8) (8,9)
306	21	(0,4) (0,6) (0,8) (1,11) (2,10) (3,7) (4,8) (6,11) (7,10)
307	21	(0,4) (0,6) (0,8) (1,4) (2,10) (3,7) (3,11) (6,10) (7,11)
308	21	(0,8) (0,10) (1,4) (1,6) (2,5) (2,7) (2,8) (4,6) (7,11)
309	21	(0,4) (0,6) (0,8) (2,8) (2,10) (3,5) (6,11) (7,10) (7,11)
310	21	(0,4) (0,6) (0,8) (1,9) (2,7) (2,10) (4,8) (6,11) (7,10)
311	21	(1,3) (1,4) (2,5) (2,8) (3,5) (4,9) (5,7) (6,11) (8,9)
312	21	(0,4) (0,6) (0,8) (2,7) (2,10) (4,8) (5,9) (6,11) (7,10)
313	21	(0,2) (0,4) (0,8) (2,10) (3,7) (3,11) (4,8) (5,9) (7,11)
314	21	(0,2) (0,8) (1,4) (2,5) (3,7) (3,11) (4,8) (5,7) (8,9)
315	21	(0,4) (0,6) (0,10) (1,9) (3,5) (3,7) (4,6) (7,11) (10,11)
316	21	(0,4) (0,6) (1,11) (3,7) (3,11) (4,8) (4,9) (6,10) (7,10)
317	21	(0,8) (0,10) (1,4) (1,11) (2,5) (2,7) (2,8) (6,10) (6,11)
318	21	(0,4) (0,6) (0,8) (1,4) (1,9) (3,9) (3,11) (6,10) (7,11)
319	21	(0,2) (0,6) (0,10) (2,10) (3,7) (3,11) (5,8) (5,9) (7,11)
320	21	(0,4) (0,6) (0,8) (1,3) (1,11) (2,7) (2,10) (4,6) (7,10)
321	21	(0,4) (0,6) (0,8) (1,3) (2,7) (2,10) (3,11) (6,10) (7,11)
322	21	(0,4) (0,6) (0,8) (1,3) (1,11) (2,8) (2,10) (6,11) (7,10)
323	21	(0,4) (0,6) (0,10) (1,9) (1,11) (3,5) (3,7) (4,6) (10,11)
324	21	(0,4) (0,6) (0,8) (2,7) (2,10) (4,9) (5,8) (6,10) (7,11)
325	21	(0,4) (0,6) (0,10) (2,8) (2,10) (3,7) (3,9) (4,8) (5,7)
326	21	(0,4) (0,6) (0,8) (2,7) (3,11) (5,7) (5,8) (6,10) (10,11)
327	21	(0,4) (0,6) (0,10) (2,5) (4,8) (5,7) (6,11) (7,10) (8,9)
328	21	(0,10) (1,3) (1,6) (2,10) (3,9) (3,11) (5,7) (5,9) (7,11)
329	21	(0,4) (0,6) (0,8) (2,7) (4,9) (5,8) (6,10) (7,11) (10,11)
330	21	(0,4) (0,6) (0,8) (1,3) (1,9) (3,7) (4,6) (7,11) (10,11)
331	21	(0,4) (0,6) (0,8) (1,11) (2,7) (2,10) (5,8) (6,11) (7,10)
332	21	(0,4) (0,6) (0,8) (1,3) (1,11) (2,10) (3,7) (6,11) (7,10)

Table A.1 – continued from previous page

ω	$\lvert E\rvert$	deleted edges (k, l)
333	21	(0,2) (0,8) (0,10) (1,3) (1,11) (2,7) (3,11) (5,7) (6,10)
334	21	(0,4) (0,6) (0,8) (1,4) (1,9) (2,7) (2,10) (6,11) (7,10)
335	21	(0,8) (0,10) (1,3) (2,5) (2,7) (2,10) (3,9) (4,8) (5,7)
336	21	(0,4) (0,6) (0,10) (1,9) (3,9) (3,11) (4,8) (6,10) (7,11)
337	21	(0,4) (0,6) (0,8) (1,9) (3,9) (3,11) (4,8) (6,10) (7,11)
338	21	(0,4) (0,6) (0,8) (1,4) (1,9) (2,10) (6,11) (7,10) (8,9)
339	21	(0,6) (1,4) (1,11) (3,9) (3,11) (4,8) (4,9) (6,10) (7,10)
340	21	(0,4) (0,6) (0,8) (1,4) (1,11) (2,10) (6,11) (7,10) (8,9)
341	21	(0,4) (0,6) (0,8) (1,3) (2,8) (2,10) (4,6) (7,10) (7,11)
342	21	(0,6) (1,3) (1,4) (3,9) (4,6) (5,8) (5,9) (8,9) (10,11)
343	21	(0,4) (0,6) (0,8) (1,3) (2,8) (2,10) (3,11) (6,10) (7,11)
344	21	(0,4) (0,8) (1,3) (1,9) (3,9) (3,11) (4,8) (6,10) (7,11)
345	21	(0,4) (0,6) (0,10) (1,9) (3,11) (4,8) (6,10) (7,11) (8,9)
346	21	(0,4) (0,6) (0,8) (2,7) (3,11) (4,8) (5,7) (6,10) (10,11)
347	21	(0,4) (0,6) (0,10) (2,10) (3,7) (3,9) (4,8) (5,7) (8,9)
348	21	(0,4) (0,8) (1,6) (1,9) (3,5) (3,9) (4,8) (6,10) (6,11)
349	21	(0,2) (0,6) (0,10) (3,5) (3,7) (4,6) (4,8) (5,9) (8,9)
350	21	(0,4) (0,6) (0,8) (1,4) (2,10) (6,11) (7,10) (7,11) (8,9)
351	21	(0,4) (0,6) (0,8) (3,5) (3,7) (4,9) (6,10) (7,11) (10,11)
352	21	(0,6) (1,4) (1,9) (2,10) (3,7) (3,11) (4,9) (6,11) (7,10)
353	21	(0,8) (2,5) (2,10) (3,7) (3,9) (4,8) (5,9) (7,11) (10,11)
354	21	(0,4) (0,8) (1,6) (1,11) (2,5) (3,9) (4,8) (5,9) (6,11)
355	21	(0,6) (1,4) (1,11) (2,5) (2,10) (3,7) (3,11) (4,6) (7,10)
356	21	(0,6) (1,4) (1,11) (3,5) (3,9) (4,9) (6,10) (7,10) (7,11)
357	21	(0,2) (1,6) (1,11) (2,8) (3,9) (5,8) (5,9) (6,10) (10,11)
358	21	(0,4) (3,5) (3,7) (4,6) (5,8) (6,10) (7,11) (8,9) (10,11)
359	21	(0,8) (1,3) (1,11) (2,10) (3,9) (5,8) (5,9) (6,10) (6,11)
360	21	(0,6) (1,3) (1,11) (3,9) (4,8) (5,8) (5,9) (6,10) (10,11)
361	21	(0,4) (1,6) (1,9) (3,11) (4,8) (6,10) (7,10) (7,11) (8,9)
362	21	(0,6) (1,3) (1,6) (4,8) (4,9) (7,10) (7,11) (8,9) (10,11)
363	21	(0,6) (1,4) (1,9) (3,5) (3,7) (4,6) (5,9) (7,10) (10,11)
364	21	(0,6) (0,10) (2,5) (2,7) (2,10) (3,9) (4,8) (7,10) (7,11)
365	21	(0,2) (0,8) (1,9) (2,8) (2,10) (4,6) (5,8) (7,10) (10,11)
366	21	(0,8) (0,10) (1,3) (2,5) (2,7) (2,10) (4,6) (7,10) (7,11)
367	21	(0,4) (0,6) (1,4) (1,6) (1,9) (2,8) (3,11) (4,6) (7,10)
368	21	(0,4) (0,6) (1,4) (1,6) (1,11) (3,5) (4,6) (7,10) (8,9)
369	21	(0,4) (0,6) (1,6) (2,7) (3,7) (4,6) (4,8) (5,7) (10,11)
370	21	(0,6) (1,3) (2,7) (4,6) (5,7) (5,9) (6,10) (7,10) (10,11)
371	21	(0,6) (0,10) (1,3) (1,6) (1,11) (2,5) (2,7) (2,8) (4,6)
372	21	(1,4) (1,6) (2,5) (2,7) (2,8) (3,9) (5,7) (5,8) (10,11)
373	21	(0,6) (2,5) (2,7) (2,10) (3,7) (4,8) (4,9) (5,7) (10,11)
374	21	(1,3) (1,9) (1,11) (2,5) (2,7) (4,9) (5,8) (6,10) (8,9)
375	21	(1,11) (2,5) (2,7) (3,11) (4,6) (5,7) (5,8) (7,10) (8,9)
376	21	(0,2) (0,4) (3,5) (4,8) (5,8) (5,9) (6,11) (7,10) (8,9)
377	21	(1,3) (1,6) (1,11) (2,7) (2,10) (3,7) (3,11) (4,9) (5,8)
378	21	(0,8) (1,4) (1,6) (1,11) (2,10) (3,9) (5,9) (6,10) (6,11)
379	21	(1,11) (2,5) (2,10) (3,7) (4,9) (5,8) (5,9) (6,11) (8,9)
380	21	(1,3) (1,4) (1,9) (2,8) (3,9) (5,7) (5,9) (6,11) (10,11)
381	21	(1,11) (2,5) (2,7) (3,5) (3,7) (4,9) (5,7) (6,10) (8,9)
382	21	(1,9) (1,11) (2,8) (3,5) (3,7) (3,9) (4,9) (6,11) (7,10)

Table A.1 – continued from previous page

ω	$\lvert E\rvert$	deleted edges (k, l)
383	21	(1,9) (2,5) (2,7) (3,7) (3,9) (4,6) (5,7) (5,8) (10,11)
384	21	(1,4) (2,5) (2,7) (3,5) (3,11) (4,6) (5,7) (7,10) (8,9)
385	21	(1,6) (2,5) (3,7) (4,9) (5,8) (6,10) (6,11) (7,11) (10,11)
386	21	(1,3) (1,6) (1,11) (2,7) (2,10) (3,5) (3,9) (4,9) (5,8)
387	21	(1,4) (1,6) (2,5) (2,7) (2,8) (3,11) (5,7) (7,10) (8,9)
388	21	(1,11) (2,5) (2,7) (3,5) (4,6) (4,9) (5,7) (7,10) (8,9)
389	21	(1,3) (2,5) (3,5) (3,9) (4,6) (5,7) (7,11) (8,9) (10,11)
390	21	(1,3) (1,9) (2,7) (3,9) (3,11) (4,6) (5,8) (5,9) (10,11)
391	21	(1,3) (1,6) (1,11) (2,10) (3,5) (3,9) (4,9) (5,8) (7,11)
392	21	(1,6) (2,7) (3,5) (3,7) (3,11) (4,8) (5,8) (5,9) (10,11)
393	21	(1,6) (2,5) (2,7) (3,7) (3,9) (4,8) (5,7) (5,8) (10,11)
394	21	(1,3) (1,9) (2,7) (3,5) (3,9) (4,6) (4,9) (5,8) (10,11)
395	21	(1,6) (2,7) (2,8) (3,5) (3,7) (3,9) (4,9) (5,7) (10,11)
396	21	(1,3) (1,6) (2,7) (3,11) (4,8) (5,9) (7,10) (7,11) (10,11)
397	21	(1,3) (2,5) (2,7) (3,7) (3,11) (4,6) (5,7) (8,9) (10,11)
398	21	(1,6) (1,11) (2,7) (2,8) (3,5) (3,11) (4,9) (7,10) (7,11)
399	21	(1,4) (2,5) (2,10) (3,7) (4,9) (5,8) (5,9) (6,11) (8,9)
400	21	(1,3) (1,4) (2,5) (2,7) (3,7) (3,11) (5,7) (6,10) (8,9)
401	21	(0,2) (0,10) (1,9) (2,7) (3,11) (5,8) (6,10) (7,11) (10,11)
402	21	(1,3) (1,4) (1,9) (2,5) (2,10) (3,9) (5,7) (5,8) (6,11)
403	21	(1,4) (1,6) (1,11) (2,5) (2,10) (3,9) (5,8) (5,9) (7,11)
404	21	(1,3) (1,6) (1,11) (2,7) (3,11) (4,8) (5,7) (5,9) (7,10)
405	21	(1,9) (1,11) (2,7) (3,5) (4,6) (4,9) (5,7) (7,10) (8,9)
406	21	(1,4) (1,6) (1,11) (2,7) (2,8) (3,11) (4,9) (5,7) (7,10)
407	21	(1,6) (2,5) (2,7) (2,8) (3,7) (4,9) (5,8) (7,11) (10,11)
408	21	(1,11) (2,5) (3,7) (4,6) (5,8) (5,9) (6,11) (8,9) (10,11)
409	21	(1,4) (1,6) (2,5) (2,7) (2,10) (3,7) (3,11) (5,7) (8,9)
410	21	(1,4) (1,6) (1,11) (2,10) (3,7) (3,11) (5,8) (5,9) (7,11)
411	21	(1,4) (1,6) (1,9) (2,10) (3,9) (3,11) (5,8) (5,9) (7,11)
412	21	(1,4) (1,6) (1,9) (2,7) (2,10) (3,9) (3,11) (5,8) (5,9)
413	21	(1,4) (1,6) (2,5) (2,7) (2,8) (3,11) (7,10) (7,11) (8,9)
414	21	(1,4) (2,5) (2,7) (3,11) (4,6) (5,7) (5,8) (7,10) (8,9)
415	21	(1,4) (2,5) (2,7) (3,7) (3,11) (5,7) (5,8) (6,10) (8,9)
416	21	(1,4) (1,9) (2,5) (2,7) (3,7) (3,11) (5,7) (5,8) (6,10)
417	21	(1,4) (1,6) (1,11) (2,10) (3,9) (3,11) (5,8) (5,9) (7,11)
418	21	(1,4) (2,5) (3,5) (3,7) (4,9) (5,7) (6,10) (7,11) (8,9)
419	21	(1,4) (1,9) (2,5) (2,7) (3,11) (4,6) (5,7) (5,8) (7,10)
420	21	(1,3) (1,11) (2,5) (2,7) (3,11) (4,6) (7,10) (7,11) (8,9)
421	21	(1,11) (2,5) (2,7) (3,7) (4,9) (5,7) (5,8) (6,10) (8,9)
422	21	(1,4) (1,6) (1,9) (2,7) (2,8) (3,11) (5,7) (5,9) (7,10)
423	21	(1,4) (1,6) (1,11) (2,7) (2,10) (3,5) (3,9) (5,8) (5,9)
424	21	(1,4) (1,6) (2,8) (3,11) (4,9) (5,8) (7,11) (8,9) (10,11)
425	21	(0,6) (1,11) (2,5) (3,7) (3,9) (5,8) (5,9) (6,10) (6,11)
426	21	(1,3) (1,4) (1,9) (2,5) (2,7) (2,8) (3,11) (6,11) (7,10)
427	21	(0,4) (0,6) (0,8) (1,3) (4,6) (5,9) (7,11) (8,9) (10,11)
428	21	(0,4) (0,6) (0,10) (1,9) (2,8) (2,10) (3,7) (4,9) (5,8)
429	21	(0,4) (0,6) (0,8) (1,3) (1,9) (2,7) (2,10) (4,6) (5,8)
430	21	(0,4) (0,6) (0,8) (1,6) (3,9) (4,8) (5,9) (7,11) (10,11)
431	21	(0,2) (0,8) (0,10) (1,9) (2,5) (3,9) (4,8) (7,10) (7,11)
432	21	(0,4) (0,6) (0,8) (2,8) (3,5) (5,9) (6,11) (7,10) (7,11)

Table A.1 – continued from previous page

ω	$\lvert E\rvert$	deleted edges (k, l)
433	21	(0,4) (0,6) (0,10) (1,4) (1,9) (2,8) (3,11) (6,10) (7,11)
434	21	(0,4) (0,6) (0,8) (1,6) (2,7) (2,10) (3,9) (4,8) (5,9)
435	21	(0,4) (0,6) (0,8) (1,3) (2,7) (2,10) (4,6) (5,8) (5,9)
436	21	(0,2) (0,8) (0,10) (1,11) (3,5) (3,9) (4,8) (4,9) (6,10)
437	21	(0,4) (0,6) (0,8) (1,3) (1,9) (2,7) (2,10) (4,6) (7,11)
438	21	(0,4) (0,6) (0,8) (1,9) (2,10) (3,7) (3,9) (4,8) (5,7)
439	21	(0,4) (0,6) (0,10) (1,3) (2,8) (2,10) (3,9) (5,7) (5,8)
440	21	(0,2) (0,6) (0,10) (1,11) (3,9) (3,11) (4,8) (5,9) (6,10)
441	21	(0,4) (0,6) (0,8) (1,11) (2,10) (3,7) (4,8) (5,7) (6,11)
442	21	(0,2) (0,6) (0,10) (1,11) (3,5) (3,9) (4,8) (4,9) (6,10)
443	21	(0,4) (1,4) (1,6) (1,9) (2,10) (3,7) (3,11) (5,7) (6,11)
444	21	(0,4) (0,6) (0,10) (1,6) (1,11) (3,7) (3,11) (4,8) (5,9)
445	21	(0,4) (0,6) (0,10) (2,5) (2,8) (3,9) (5,8) (6,10) (7,11)
446	21	(0,4) (0,6) (0,8) (1,6) (2,7) (2,10) (3,9) (4,8) (5,7)
447	21	(0,6) (0,8) (0,10) (1,4) (2,5) (2,8) (3,7) (4,6) (5,9)
448	21	(0,4) (0,6) (0,8) (1,3) (2,7) (2,10) (3,5) (4,9) (5,7)
449	21	(0,6) (0,8) (0,10) (1,3) (2,7) (2,10) (3,5) (4,9) (5,7)
450	21	(0,4) (0,6) (0,8) (1,9) (3,5) (3,9) (4,8) (6,10) (7,11)
451	21	(0,4) (0,6) (0,8) (1,6) (2,8) (2,10) (3,5) (3,9) (5,7)
452	21	(0,4) (0,6) (0,8) (1,3) (1,9) (2,10) (3,9) (4,6) (7,11)
453	21	(0,4) (0,6) (0,10) (1,6) (2,8) (2,10) (3,5) (3,9) (5,7)
454	21	(0,6) (1,4) (3,7) (5,8) (5,9) (6,10) (6,11) (8,9) (10,11)
455	21	(0,4) (0,6) (0,10) (2,7) (2,10) (3,7) (5,8) (5,9) (6,11)
456	21	(0,2) (0,8) (1,4) (2,7) (2,10) (3,11) (5,8) (5,9) (7,10)
457	21	(0,4) (0,6) (0,10) (1,6) (1,11) (2,7) (2,10) (4,9) (5,8)
458	21	(0,4) (0,6) (0,10) (1,3) (1,9) (2,10) (4,6) (7,11) (8,9)
459	21	(0,2) (0,8) (0,10) (1,6) (3,9) (4,8) (4,9) (7,11) (10,11)
460	21	(0,4) (0,6) (0,8) (1,9) (2,7) (3,11) (4,8) (6,10) (7,11)
461	21	(0,2) (1,6) (2,5) (2,8) (3,7) (3,11) (4,8) (5,7) (10,11)
462	21	(0,4) (0,6) (0,8) (1,3) (1,9) (2,8) (2,10) (4,6) (7,11)
463	21	(0,4) (0,6) (0,10) (1,3) (1,9) (2,8) (2,10) (4,6) (7,11)
464	21	(0,4) (0,6) (0,8) (2,8) (3,5) (4,9) (5,9) (6,10) (7,11)
465	21	(0,4) (0,6) (0,8) (1,11) (3,5) (3,9) (4,8) (6,10) (7,11)
466	21	(0,4) (0,6) (0,10) (1,3) (2,7) (2,10) (4,9) (5,7) (5,8)
467	21	(0,4) (0,6) (0,10) (1,3) (2,8) (2,10) (3,9) (4,8) (5,7)
468	21	(0,2) (0,6) (0,10) (1,11) (2,8) (3,5) (3,9) (6,10) (7,11)
469	21	(0,6) (0,8) (0,10) (1,3) (1,9) (2,7) (4,8) (4,9) (10,11)
470	21	(0,4) (0,6) (0,8) (1,9) (3,9) (3,11) (4,8) (5,7) (6,10)
471	21	(0,4) (0,6) (0,8) (1,11) (3,9) (3,11) (4,8) (5,7) (6,10)
472	21	(0,4) (0,6) (0,8) (1,4) (1,9) (2,7) (3,11) (6,10) (7,11)
473	21	(0,4) (0,6) (0,8) (1,3) (1,9) (2,7) (4,6) (7,11) (10,11)
474	21	(0,4) (0,6) (0,8) (2,7) (2,10) (3,7) (3,11) (5,8) (5,9)
475	21	(0,2) (0,8) (0,10) (1,4) (1,9) (2,7) (3,11) (6,10) (7,11)
476	21	(0,8) (1,4) (1,9) (3,5) (3,7) (3,11) (4,9) (6,10) (6,11)
477	21	(0,2) (0,8) (0,10) (1,4) (3,5) (4,6) (5,9) (7,10) (8,9)
478	21	(0,4) (0,6) (0,8) (2,10) (3,7) (3,9) (5,8) (5,9) (7,11)
479	21	(0,2) (0,10) (1,3) (2,10) (3,9) (3,11) (4,8) (5,7) (8,9)
480	21	(0,4) (0,6) (0,8) (1,3) (2,7) (2,10) (3,9) (5,7) (5,8)
481	21	(0,4) (0,6) (0,8) (1,3) (1,9) (2,7) (2,10) (4,9) (5,8)
482	21	(0,4) (0,6) (0,10) (1,9) (2,5) (2,8) (5,8) (6,11) (7,10)

Table A.1 – continued from previous page

ω	$\lvert E\rvert$	deleted edges (k, l)
483	21	(0,2) (0,8) (0,10) (1,4) (1,6) (4,6) (5,7) (8,9) (10,11)
484	21	(0,4) (0,6) (0,8) (1,6) (2,7) (2,10) (3,9) (5,7) (5,8)
485	21	(0,4) (0,6) (0,8) (1,3) (2,7) (2,10) (4,9) (5,7) (5,8)
486	21	(0,4) (0,6) (0,8) (1,6) (2,7) (2,10) (4,9) (5,8) (7,11)
487	21	(0,4) (0,6) (0,10) (1,9) (2,5) (2,8) (4,8) (6,11) (7,10)
488	21	(0,4) (0,6) (0,10) (1,6) (2,8) (2,10) (3,9) (5,7) (5,8)
489	21	(0,4) (0,6) (0,10) (1,6) (1,9) (3,7) (3,11) (4,8) (5,9)
490	21	(0,8) (0,10) (1,11) (2,5) (3,5) (3,7) (3,9) (6,10) (7,11)
491	21	(0,4) (0,6) (0,8) (2,7) (2,10) (3,7) (4,8) (5,9) (6,11)
492	21	(0,2) (0,8) (0,10) (1,6) (1,9) (3,7) (4,6) (4,8) (10,11)
493	21	(0,4) (0,6) (0,10) (1,11) (2,8) (3,5) (4,9) (5,8) (6,10)
494	21	(0,4) (0,6) (0,10) (1,9) (1,11) (3,5) (3,7) (4,6) (8,9)
495	21	(0,4) (0,6) (0,8) (1,6) (2,8) (2,10) (3,5) (4,9) (5,7)
496	21	(0,4) (0,8) (1,6) (2,7) (2,10) (3,5) (4,9) (5,7) (5,8)
497	21	(0,2) (0,8) (0,10) (1,11) (2,10) (3,7) (4,6) (5,7) (5,8)
498	21	(0,4) (0,6) (0,10) (1,3) (2,8) (2,10) (3,5) (4,9) (5,7)
499	21	(0,4) (0,6) (0,10) (1,6) (2,8) (2,10) (3,5) (4,9) (5,7)
500	21	(0,4) (0,6) (0,8) (2,10) (3,7) (4,8) (5,9) (6,11) (7,11)
501	21	(0,4) (0,6) (0,8) (1,11) (2,5) (2,10) (3,7) (4,6) (5,8)
502	21	(0,6) (0,8) (0,10) (1,11) (2,5) (2,10) (3,7) (4,6) (5,8)
503	21	(0,4) (0,6) (0,10) (1,6) (2,7) (2,10) (4,9) (5,8) (7,11)
504	21	(0,4) (0,6) (0,10) (1,6) (2,8) (2,10) (3,9) (4,8) (5,7)
505	21	(0,4) (0,6) (0,10) (2,7) (2,10) (3,7) (4,8) (5,9) (6,11)
506	21	(0,4) (0,6) (0,10) (1,6) (2,7) (2,10) (3,9) (4,8) (5,7)
507	21	(0,6) (0,8) (0,10) (1,3) (1,4) (2,7) (2,10) (4,6) (5,9)
508	21	(0,4) (0,6) (0,10) (1,9) (2,7) (2,10) (3,7) (4,6) (5,8)
509	21	(0,2) (0,4) (0,10) (1,6) (2,8) (3,9) (5,8) (5,9) (10,11)
510	21	(0,4) (0,6) (0,10) (1,6) (3,7) (3,11) (4,8) (5,9) (8,9)
511	21	(0,4) (0,6) (0,10) (1,3) (1,9) (2,7) (2,10) (4,6) (5,8)
512	21	(0,4) (0,6) (0,10) (1,6) (2,7) (2,10) (3,9) (4,8) (5,9)
513	21	(0,2) (0,8) (0,10) (1,6) (1,11) (2,10) (3,7) (4,8) (4,9)
514	21	(0,2) (0,8) (0,10) (1,11) (3,5) (3,9) (4,8) (6,10) (6,11)
515	21	(0,4) (0,6) (0,10) (1,3) (2,7) (2,10) (3,9) (5,7) (5,8)
516	21	(0,4) (0,6) (0,8) (2,7) (2,10) (3,7) (5,8) (5,9) (6,11)
517	21	(0,4) (0,6) (0,8) (2,10) (3,7) (5,8) (5,9) (6,11) (7,11)
518	21	(0,2) (0,6) (0,10) (1,6) (1,11) (3,9) (4,8) (5,9) (10,11)
519	21	(0,4) (0,6) (0,8) (1,9) (2,7) (2,10) (3,7) (4,9) (5,8)
520	21	(0,4) (0,6) (0,8) (1,6) (1,11) (2,7) (2,10) (4,9) (5,8)
521	21	(0,2) (0,6) (0,10) (1,6) (1,11) (3,7) (4,8) (4,9) (10,11)
522	21	(0,6) (1,3) (1,11) (3,5) (4,9) (5,7) (6,10) (6,11) (8,9)
523	21	(0,2) (0,8) (0,10) (1,11) (2,10) (3,7) (4,8) (5,7) (6,11)
524	21	(0,4) (0,6) (0,10) (1,9) (2,5) (3,9) (4,8) (5,7) (6,10)
525	21	(0,2) (0,8) (0,10) (1,11) (2,7) (3,11) (4,8) (5,7) (6,10)
526	21	(0,4) (0,6) (0,8) (1,11) (2,8) (3,5) (3,11) (5,7) (6,10)
527	21	(0,4) (0,6) (0,10) (1,11) (3,5) (3,7) (4,6) (5,9) (8,9)
528	21	(0,4) (0,6) (0,10) (1,6) (2,7) (2,10) (3,9) (5,8) (5,9)
529	21	(0,2) (0,8) (0,10) (2,8) (3,5) (3,7) (4,6) (5,9) (7,11)
530	21	(0,6) (0,8) (0,10) (2,10) (3,5) (3,7) (4,6) (5,9) (7,11)
531	21	(0,4) (0,6) (0,8) (1,11) (2,7) (3,5) (3,11) (5,7) (6,10)
532	21	(0,4) (0,6) (0,10) (2,8) (2,10) (3,7) (3,11) (5,8) (5,9)

Table A.1 – continued from previous page

ω	$\lvert E\rvert$	deleted edges (k, l)
533	21	(0,10) (1,9) (2,7) (3,5) (4,8) (4,9) (5,7) (6,10) (8,9)
534	21	(0,2) (1,4) (2,10) (3,9) (4,6) (5,8) (5,9) (7,10) (8,9)
535	21	(0,4) (0,6) (0,8) (1,3) (2,7) (2,10) (3,9) (5,8) (5,9)
536	21	(0,2) (0,8) (1,11) (2,7) (2,10) (3,7) (3,11) (4,8) (5,9)
537	21	(0,4) (0,8) (0,10) (1,3) (1,9) (2,8) (3,11) (6,10) (7,11)
538	21	(0,4) (0,6) (0,10) (1,3) (1,9) (2,5) (3,9) (4,8) (5,7)
539	21	(0,4) (0,6) (0,8) (1,11) (3,7) (3,11) (4,8) (5,9) (6,10)
540	21	(0,8) (1,4) (1,9) (2,5) (2,7) (2,8) (4,9) (6,11) (7,10)
541	21	(0,6) (0,10) (1,4) (1,9) (2,5) (3,5) (3,7) (3,11) (4,6)
542	21	(0,2) (0,8) (0,10) (1,6) (1,11) (3,7) (3,11) (4,8) (4,9)
543	21	(0,4) (0,6) (0,10) (1,3) (2,7) (2,10) (3,9) (4,8) (5,9)
544	21	(1,9) (2,7) (3,5) (3,7) (4,9) (5,8) (6,10) (6,11) (10,11)
545	21	(1,4) (1,6) (2,7) (3,9) (3,11) (5,8) (5,9) (6,10) (10,11)
546	21	(1,4) (1,6) (2,7) (3,11) (5,8) (5,9) (6,10) (7,10) (8,9)
547	21	(1,4) (1,6) (2,7) (3,7) (3,11) (5,8) (5,9) (6,10) (8,9)
548	21	(0,2) (0,6) (1,11) (2,10) (3,7) (3,9) (5,8) (5,9) (6,11)
549	21	(1,4) (1,9) (2,5) (3,7) (5,8) (6,10) (6,11) (7,10) (8,9)
550	21	(0,2) (0,6) (1,3) (2,7) (3,9) (5,7) (5,8) (6,10) (10,11)
551	21	(1,3) (1,4) (2,5) (3,9) (5,8) (6,10) (7,10) (7,11) (8,9)
552	21	(1,3) (1,6) (2,7) (2,10) (4,9) (5,8) (7,11) (8,9) (10,11)
553	21	(1,6) (1,11) (2,7) (3,5) (4,9) (5,8) (6,10) (8,9) (10,11)
554	21	(1,4) (1,9) (2,5) (3,7) (3,9) (5,8) (6,10) (6,11) (7,10)
555	21	(0,4) (0,8) (2,5) (3,5) (3,7) (6,10) (6,11) (7,11) (8,9)
556	21	(1,3) (1,11) (2,5) (3,5) (4,8) (4,9) (6,11) (7,10) (8,9)
557	21	(1,4) (1,6) (2,7) (3,11) (4,6) (5,8) (5,9) (7,10) (10,11)
558	21	(1,6) (1,11) (2,10) (3,5) (3,7) (4,9) (5,8) (7,11) (8,9)
559	21	(1,4) (1,6) (2,5) (3,9) (4,6) (5,8) (7,10) (7,11) (10,11)
560	21	(1,4) (1,9) (2,5) (3,7) (4,6) (5,8) (6,11) (7,10) (10,11)
561	21	(1,3) (2,5) (3,9) (4,6) (5,8) (7,10) (7,11) (8,9) (10,11)
562	21	(1,4) (1,6) (2,8) (3,5) (3,9) (5,9) (7,10) (7,11) (10,11)
563	21	(1,6) (1,11) (2,5) (3,7) (3,9) (4,8) (5,8) (6,11) (7,10)
564	21	(0,2) (0,6) (1,3) (2,8) (5,7) (5,9) (6,11) (7,10) (10,11)
565	21	(1,3) (1,4) (2,5) (3,5) (4,9) (6,10) (7,10) (7,11) (8,9)
566	21	(1,6) (2,5) (3,7) (3,9) (4,9) (5,8) (6,10) (7,11) (10,11)
567	21	(1,4) (1,6) (2,10) (3,11) (4,9) (5,7) (6,10) (7,11) (8,9)
568	21	(1,9) (2,7) (3,5) (4,6) (4,9) (5,8) (6,11) (7,10) (10,11)
569	21	(1,3) (1,11) (2,5) (2,10) (4,9) (5,8) (6,10) (7,11) (8,9)
570	21	(1,3) (1,6) (2,5) (3,9) (4,6) (5,8) (7,10) (7,11) (10,11)
571	21	(0,10) (1,6) (2,7) (2,10) (3,5) (3,11) (4,6) (5,9) (7,11)
572	21	(1,4) (1,6) (2,5) (3,5) (3,9) (6,10) (7,10) (7,11) (8,9)
573	21	(1,3) (1,6) (2,8) (3,5) (4,9) (5,7) (7,11) (8,9) (10,11)
574	21	(1,6) (1,11) (2,7) (3,5) (3,9) (4,9) (5,8) (6,10) (10,11)
575	21	(1,3) (1,4) (2,8) (3,7) (5,7) (5,9) (6,11) (8,9) (10,11)
576	21	(1,3) (1,6) (2,7) (3,9) (4,9) (5,7) (5,8) (6,10) (10,11)
577	21	(1,3) (2,7) (4,6) (5,8) (5,9) (6,11) (7,10) (8,9) (10,11)
578	21	(1,4) (2,8) (3,5) (3,7) (5,9) (6,11) (7,10) (8,9) (10,11)
579	21	(1,4) (2,7) (2,8) (3,5) (5,9) (6,11) (7,10) (8,9) (10,11)
580	21	(0,6) (1,4) (1,9) (2,5) (2,10) (3,7) (4,6) (5,7) (10,11)
581	21	(1,3) (1,9) (2,7) (4,6) (5,8) (5,9) (6,11) (7,10) (10,11)
582	21	(1,4) (1,6) (2,5) (3,9) (4,8) (5,7) (6,11) (8,9) (10,11)

Table A.1 – continued from previous page

ω	$\lvert E\rvert$	deleted edges (k, l)
583	21	(1,4) (1,6) (2,7) (3,7) (3,11) (5,8) (5,9) (6,10) (10,11)
584	21	(1,4) (1,9) (2,5) (3,7) (3,11) (5,8) (6,10) (6,11) (7,10)
585	21	(1,6) (2,5) (3,7) (4,9) (5,8) (6,10) (7,11) (8,9) (10,11)
586	21	(0,4) (2,5) (3,7) (4,6) (5,8) (6,10) (7,11) (8,9) (10,11)
587	21	(1,4) (1,6) (2,7) (3,5) (4,8) (5,9) (6,11) (7,10) (10,11)
588	21	(1,11) (2,5) (2,7) (3,11) (4,9) (5,8) (6,10) (7,10) (8,9)
589	21	(1,3) (1,6) (2,7) (4,8) (5,8) (5,9) (6,11) (7,10) (10,11)
590	21	(1,4) (1,6) (2,8) (3,9) (5,7) (5,9) (6,11) (7,10) (10,11)
591	21	(0,2) (0,8) (0,10) (1,4) (2,10) (3,9) (5,8) (6,10) (7,11)
592	21	(0,4) (1,3) (1,6) (1,11) (2,8) (3,11) (5,9) (7,10) (7,11)
593	21	(0,4) (0,6) (0,8) (1,11) (2,10) (3,7) (4,6) (4,8) (5,9)
594	21	(0,4) (0,6) (0,8) (1,11) (2,10) (3,7) (4,8) (4,9) (5,7)
595	21	(0,4) (0,6) (0,10) (1,11) (2,10) (3,9) (4,8) (5,9) (7,10)
596	21	(0,4) (0,6) (0,8) (1,6) (2,8) (3,11) (5,8) (5,9) (7,10)
597	21	(0,2) (0,8) (0,10) (1,4) (1,9) (3,5) (3,7) (3,11) (4,6)
598	21	(0,6) (0,8) (0,10) (1,3) (2,10) (4,9) (5,8) (7,11) (8,9)
599	21	(0,4) (0,6) (0,10) (1,3) (2,8) (2,10) (3,9) (3,11) (5,7)
600	21	(0,4) (0,6) (0,10) (1,6) (1,11) (2,5) (3,9) (4,8) (5,7)
601	21	(0,2) (0,10) (1,6) (3,11) (4,8) (4,9) (5,9) (7,11) (8,9)
602	21	(0,4) (0,6) (0,10) (1,3) (2,5) (2,8) (3,11) (4,9) (5,7)
603	21	(0,2) (0,8) (0,10) (1,4) (1,9) (2,5) (3,7) (3,11) (4,6)
604	21	(0,6) (1,4) (1,11) (2,5) (3,5) (4,8) (4,9) (7,10) (8,9)
605	21	(0,4) (0,6) (0,10) (1,3) (2,8) (2,10) (4,9) (5,7) (6,11)
606	21	(0,4) (0,6) (0,10) (1,3) (2,8) (4,6) (5,7) (5,9) (10,11)
607	21	(0,2) (0,8) (0,10) (1,6) (2,10) (3,9) (4,8) (5,7) (7,11)
608	21	(0,6) (0,8) (0,10) (1,3) (2,7) (2,10) (4,6) (5,9) (7,11)
609	21	(0,6) (0,8) (0,10) (1,3) (2,7) (2,10) (4,9) (5,7) (6,11)
610	21	(0,4) (0,6) (0,10) (1,3) (2,8) (2,10) (4,6) (5,9) (7,11)
611	21	(0,2) (0,8) (0,10) (1,11) (2,5) (3,9) (4,8) (6,10) (7,11)
612	21	(0,4) (0,6) (0,8) (1,11) (2,5) (3,9) (4,8) (6,10) (7,11)
613	21	(0,4) (0,6) (0,10) (1,4) (2,8) (3,5) (5,9) (6,11) (7,10)
614	21	(0,8) (0,10) (1,3) (1,9) (1,11) (2,5) (2,7) (4,6) (10,11)
615	21	(0,2) (0,8) (0,10) (1,4) (1,9) (2,5) (3,7) (4,6) (10,11)
616	21	(0,4) (0,6) (0,10) (1,3) (2,8) (2,10) (3,9) (5,7) (6,11)
617	21	(0,4) (0,6) (0,10) (1,3) (2,5) (2,8) (4,6) (5,9) (7,11)
618	21	(0,4) (0,6) (0,8) (1,6) (2,10) (3,9) (4,8) (5,9) (7,11)
619	21	(0,4) (0,6) (0,8) (1,9) (2,10) (3,7) (4,8) (5,7) (6,11)
620	21	(0,2) (0,6) (0,10) (1,3) (1,11) (2,5) (4,6) (7,10) (8,9)
621	21	(0,4) (0,6) (0,8) (1,6) (2,7) (3,9) (4,8) (5,9) (10,11)
622	21	(0,4) (0,6) (0,8) (1,4) (2,5) (3,11) (6,10) (7,11) (8,9)
623	21	(0,4) (0,6) (0,8) (1,6) (1,11) (2,10) (3,9) (4,8) (5,7)
624	21	(0,4) (0,6) (0,8) (1,9) (2,5) (3,9) (4,8) (6,11) (7,10)
625	21	(0,2) (0,6) (0,10) (1,11) (2,5) (3,9) (4,8) (5,7) (6,10)
626	21	(0,4) (0,6) (0,10) (1,3) (2,8) (2,10) (3,11) (4,9) (5,7)
627	21	(0,10) (1,9) (2,5) (2,7) (2,10) (3,7) (3,11) (4,6) (5,8)
628	21	(0,2) (0,8) (0,10) (1,9) (1,11) (2,10) (3,5) (3,7) (4,6)
629	21	(0,2) (0,8) (0,10) (1,3) (2,10) (3,9) (4,6) (5,7) (7,11)
630	21	(0,4) (0,6) (0,10) (1,3) (1,9) (2,8) (3,5) (4,6) (7,11)
631	21	(0,4) (0,6) (0,10) (1,3) (2,8) (3,5) (4,6) (5,9) (7,11)
632	21	(0,4) (0,6) (0,10) (1,6) (2,10) (3,9) (4,8) (5,9) (7,11)

Table A.1 – continued from previous page

ω	$\lvert E\rvert$	deleted edges (k, l)
633	21	(0,4) (0,6) (0,8) (1,11) (2,8) (3,5) (4,6) (5,9) (7,10)
634	21	(0,4) (0,6) (0,10) (1,3) (2,10) (4,6) (5,9) (7,11) (8,9)
635	21	(0,4) (0,6) (0,10) (1,11) (2,7) (3,11) (4,8) (5,9) (6,10)
636	21	(0,4) (0,6) (0,8) (1,9) (2,7) (3,11) (4,8) (5,7) (6,10)
637	21	(0,6) (0,8) (0,10) (1,3) (1,11) (2,7) (2,10) (4,6) (5,9)
638	21	(0,6) (0,8) (0,10) (1,3) (2,7) (2,10) (3,11) (4,9) (5,7)
639	21	(0,2) (1,9) (2,10) (3,9) (4,8) (5,8) (6,11) (7,10) (10,11)
640	21	(0,4) (1,3) (2,5) (4,8) (5,8) (6,10) (6,11) (7,11) (8,9)
641	21	(0,4) (0,6) (0,8) (1,11) (2,10) (3,7) (5,8) (5,9) (6,11)
642	21	(0,4) (0,6) (0,10) (1,6) (1,11) (2,8) (3,5) (4,9) (5,7)
643	21	(0,4) (0,6) (0,10) (1,9) (2,5) (3,7) (3,11) (4,8) (5,9)
644	21	(0,4) (0,6) (0,8) (1,11) (2,8) (3,5) (5,9) (6,11) (7,10)
645	21	(0,4) (0,6) (0,10) (1,3) (1,9) (2,5) (2,8) (4,6) (7,11)
646	21	(0,4) (0,6) (0,10) (1,3) (1,9) (2,8) (3,11) (4,9) (5,7)
647	21	(0,4) (0,6) (0,10) (1,3) (1,9) (2,8) (3,11) (4,6) (5,7)
648	21	(0,4) (0,6) (0,10) (1,11) (2,10) (3,7) (3,11) (4,8) (5,9)
649	21	(0,4) (1,4) (1,6) (2,7) (2,10) (3,11) (4,9) (5,7) (8,9)
650	21	(0,4) (0,6) (0,10) (1,9) (2,8) (3,5) (3,7) (4,6) (7,11)
651	21	(0,10) (1,3) (1,6) (1,11) (2,7) (2,10) (3,11) (4,9) (5,8)
652	21	(0,4) (1,6) (2,8) (3,5) (5,8) (5,9) (6,11) (7,10) (10,11)
653	21	(0,8) (1,4) (1,11) (2,7) (3,5) (3,9) (4,6) (5,9) (6,10)
654	21	(0,6) (0,10) (1,11) (2,7) (2,8) (3,5) (4,8) (4,9) (6,10)
655	21	(0,4) (0,6) (1,9) (1,11) (2,7) (3,5) (4,6) (7,10) (8,9)
656	21	(0,2) (0,8) (1,6) (2,7) (3,7) (4,6) (4,8) (5,9) (10,11)
657	21	(0,2) (1,6) (1,11) (3,7) (3,9) (4,8) (5,8) (5,9) (10,11)
658	21	(0,2) (0,10) (1,9) (3,5) (4,6) (4,8) (6,10) (7,11) (8,9)
659	21	(0,4) (0,10) (1,6) (2,7) (2,8) (3,11) (5,8) (5,9) (6,10)
660	21	(0,6) (0,10) (1,3) (1,6) (2,5) (2,8) (4,9) (5,8) (7,11)
661	21	(0,4) (0,6) (1,3) (2,8) (2,10) (3,9) (4,8) (5,7) (10,11)
662	21	(0,6) (0,10) (1,3) (2,5) (2,8) (4,6) (4,9) (5,9) (7,11)
663	21	(0,6) (0,8) (1,11) (2,5) (2,10) (3,7) (4,8) (4,9) (6,10)
664	21	(0,4) (0,8) (1,3) (2,8) (2,10) (5,7) (5,9) (6,10) (6,11)
665	21	(0,8) (0,10) (1,3) (2,7) (2,8) (3,11) (4,6) (5,9) (7,11)
666	21	(0,4) (0,10) (1,3) (1,9) (2,8) (2,10) (3,9) (5,7) (6,11)
667	21	(0,2) (0,10) (1,9) (3,5) (3,9) (4,6) (4,8) (6,11) (7,10)
668	21	(0,6) (0,8) (1,11) (2,7) (2,10) (3,5) (4,8) (4,9) (7,10)
669	21	(0,8) (0,10) (1,6) (2,7) (2,10) (3,5) (4,8) (4,9) (7,11)
670	21	(0,4) (0,8) (1,11) (2,5) (2,7) (3,9) (4,6) (5,8) (6,10)
671	21	(0,2) (0,8) (1,6) (1,11) (2,8) (3,5) (4,9) (6,11) (7,10)
672	21	(0,4) (0,8) (1,6) (2,7) (2,10) (3,11) (4,8) (5,9) (7,10)
673	21	(0,6) (0,10) (1,3) (2,5) (2,8) (4,9) (5,8) (6,10) (7,11)
674	21	(0,2) (0,10) (1,4) (1,11) (3,5) (4,9) (6,10) (7,11) (8,9)
675	21	(0,4) (0,6) (1,11) (2,5) (2,8) (3,9) (5,8) (6,10) (7,11)
676	21	(0,4) (0,8) (1,3) (1,9) (2,8) (2,10) (3,9) (5,7) (6,11)
677	21	(0,6) (0,10) (1,3) (2,5) (2,8) (4,6) (4,9) (5,7) (7,11)
678	21	(0,2) (1,4) (1,11) (3,5) (3,9) (5,7) (6,10) (6,11) (8,9)
679	21	(0,6) (0,10) (1,11) (2,7) (3,5) (3,9) (4,8) (5,9) (6,10)
680	21	(0,6) (0,10) (1,4) (2,8) (2,10) (3,7) (4,8) (5,9) (6,11)
681	21	(0,6) (0,10) (1,4) (2,7) (2,8) (3,11) (4,8) (5,9) (6,10)
682	21	(0,6) (0,10) (1,11) (2,10) (3,5) (3,7) (4,6) (4,8) (5,9)

Table A.1 – continued from previous page

ω	$\lvert E\rvert$	deleted edges (k, l)
683	21	(0,6) (0,10) (1,3) (2,8) (2,10) (4,6) (4,9) (5,9) (7,11)
684	21	(0,6) (0,10) (1,4) (2,7) (2,10) (3,7) (4,8) (5,9) (6,11)
685	21	(0,6) (0,8) (1,4) (2,8) (2,10) (3,5) (4,9) (7,10) (7,11)
686	21	(0,4) (0,8) (1,4) (1,9) (2,5) (2,7) (3,11) (5,7) (6,10)
687	21	(0,4) (0,8) (1,3) (1,9) (2,7) (2,10) (5,8) (6,11) (7,10)
688	21	(0,4) (0,8) (1,6) (1,9) (2,10) (3,9) (4,8) (5,7) (6,11)
689	21	(0,6) (0,8) (1,4) (2,7) (2,10) (3,7) (3,11) (4,6) (5,9)
690	21	(0,6) (0,10) (1,9) (2,5) (2,7) (3,7) (3,11) (4,6) (4,8)
691	21	(0,8) (0,10) (1,3) (1,9) (2,5) (2,7) (3,11) (4,6) (4,8)
692	21	(0,6) (0,10) (1,9) (2,5) (2,8) (3,7) (4,6) (4,8) (7,11)
693	21	(0,8) (0,10) (1,3) (2,7) (2,10) (3,11) (4,6) (4,8) (5,9)
694	21	(0,2) (0,10) (1,3) (1,6) (2,10) (4,6) (5,8) (7,11) (8,9)
695	21	(0,6) (0,10) (1,6) (1,11) (2,5) (2,8) (3,7) (4,9) (5,8)
696	21	(0,4) (1,6) (2,7) (2,10) (3,5) (4,6) (5,8) (7,11) (8,9)
697	21	(0,4) (0,6) (1,11) (2,8) (2,10) (3,9) (5,8) (7,10) (7,11)
698	21	(0,4) (0,10) (1,6) (2,7) (2,10) (3,7) (5,8) (5,9) (6,11)
699	21	(0,4) (0,8) (1,3) (1,11) (2,5) (2,7) (4,6) (6,10) (8,9)
700	21	(0,8) (0,10) (1,4) (1,9) (2,5) (2,7) (3,7) (3,11) (4,6)
701	21	(0,6) (0,8) (1,3) (1,11) (2,5) (2,10) (3,9) (4,6) (5,7)
702	21	(0,4) (0,8) (1,11) (2,7) (2,8) (3,5) (4,6) (5,9) (6,10)
703	21	(0,6) (0,10) (1,4) (2,7) (2,10) (3,7) (3,11) (4,8) (5,9)
704	21	(0,8) (1,3) (1,4) (2,8) (3,9) (5,9) (6,11) (7,10) (10,11)
705	21	(0,6) (0,8) (1,4) (2,5) (2,8) (3,11) (4,9) (7,10) (7,11)
706	21	(0,6) (0,10) (1,4) (2,8) (2,10) (3,7) (3,11) (5,8) (5,9)
707	21	(0,6) (0,10) (1,3) (1,11) (2,5) (2,8) (4,9) (5,7) (6,11)
708	21	(0,4) (0,8) (1,3) (1,9) (2,7) (2,10) (3,9) (5,7) (6,11)
709	21	(0,4) (0,8) (1,11) (2,7) (2,10) (3,5) (4,6) (5,9) (7,10)
710	21	(0,6) (0,10) (1,9) (2,5) (2,7) (3,11) (4,8) (4,9) (7,10)
711	21	(0,6) (0,10) (1,6) (2,5) (2,8) (3,7) (4,8) (4,9) (7,11)
712	21	(0,6) (0,10) (1,6) (1,11) (2,5) (2,7) (3,9) (4,8) (5,9)
713	21	(0,4) (0,8) (1,3) (2,7) (2,10) (5,8) (5,9) (6,10) (6,11)
714	21	(0,6) (0,10) (1,3) (1,4) (2,5) (2,8) (3,11) (4,9) (5,7)
715	21	(0,8) (0,10) (1,9) (2,5) (2,7) (3,9) (4,8) (6,10) (6,11)
716	21	(0,2) (0,10) (1,6) (1,11) (3,5) (4,8) (4,9) (5,7) (8,9)
717	21	(0,6) (0,10) (1,4) (2,8) (2,10) (3,7) (3,11) (4,6) (5,9)
718	21	(0,6) (0,10) (1,3) (1,11) (2,7) (2,10) (4,6) (4,8) (5,9)
719	21	(0,8) (0,10) (1,3) (1,6) (2,8) (2,10) (3,5) (4,9) (7,11)
720	21	(0,6) (0,10) (1,3) (2,7) (2,8) (4,8) (4,9) (5,9) (10,11)
721	21	(0,8) (0,10) (1,3) (2,5) (2,10) (4,6) (4,9) (7,11) (8,9)
722	21	(0,4) (0,6) (1,4) (1,6) (2,8) (2,10) (3,9) (3,11) (5,7)
723	21	(0,6) (0,10) (1,3) (2,5) (2,8) (4,9) (5,9) (6,11) (7,11)
724	21	(0,6) (0,8) (1,3) (1,11) (2,5) (2,10) (3,7) (4,6) (5,9)
725	21	(0,4) (0,8) (1,6) (2,7) (2,10) (3,11) (5,8) (5,9) (6,10)
726	21	(0,6) (0,8) (1,4) (2,8) (2,10) (3,11) (4,9) (5,7) (7,10)
727	21	(0,4) (0,6) (1,3) (2,8) (2,10) (3,9) (5,7) (5,8) (10,11)
728	21	(0,4) (0,8) (1,3) (2,5) (2,10) (3,9) (5,8) (6,10) (7,11)
729	21	(0,8) (1,6) (1,11) (2,5) (2,10) (3,7) (4,9) (5,8) (7,11)
730	21	(0,6) (0,8) (1,4) (2,7) (2,10) (3,7) (3,11) (4,8) (5,9)
731	21	(0,8) (1,4) (1,6) (2,10) (3,9) (3,11) (5,7) (5,9) (7,11)
732	21	(0,6) (0,10) (1,3) (1,11) (2,5) (2,8) (3,9) (4,6) (5,7)

Table A.1 – continued from previous page

ω	$\lvert E\rvert$	deleted edges (k, l)
733	21	(0,6) (0,10) (1,4) (1,11) (2,8) (2,10) (3,7) (4,6) (5,9)
734	21	(0,8) (1,3) (1,11) (2,5) (3,9) (4,8) (5,7) (6,10) (6,11)
735	21	(0,6) (0,10) (1,4) (1,9) (2,5) (2,8) (3,7) (3,11) (4,6)
736	21	(0,4) (0,6) (1,11) (2,8) (2,10) (3,9) (5,8) (5,9) (7,10)
737	21	(0,6) (0,10) (1,3) (1,9) (2,7) (2,10) (3,11) (4,9) (5,8)

Table A.2 GN polyhedron grouped by vertex and face degrees. $|N_n|$ is the number of vertices of degree n, $|F_n|$ the number of n-gonal faces. The ordinal numbers ω in the last column identify the polyhedral graphs shown in table A.1.

$\lvert E\rvert$	$\lvert N_5\rvert$	$\lvert N_4\rvert$	$\lvert N_3\rvert$	$\lvert N_2\rvert$	$\lvert F_3\rvert$	$\lvert F_4\rvert$	$\lvert F_5\rvert$	$\lvert F_6\rvert$	$\lvert F_7\rvert$	$\lvert F_8\rvert$	$\lvert F_9\rvert$	$\lvert F_{10}\rvert$	$\lvert F_{11}\rvert$	$\lvert F_{12}\rvert$	ω
24	0	12	0	0	8	6	0	0	0	0	0	0	0	0	1–2
23	2	6	4	0	8	4	0	1	0	0	0	0	0	0	3
22	3	4	3	2	10	1	0	0	0	0	0	1	0	0	4
22	3	3	5	1	10	1	0	0	0	0	0	1	0	0	5
22	2	6	2	2	9	2	0	0	0	0	1	0	0	0	6
22	2	6	2	2	10	1	0	0	0	0	0	1	0	0	7
22	2	6	2	2	8	3	0	0	0	1	0	0	0	0	8–9
22	2	5	4	1	8	3	0	0	0	1	0	0	0	0	10
22	2	5	4	1	9	1	0	1	1	0	0	0	0	0	11
22	1	7	3	1	7	3	1	1	0	0	0	0	0	0	12
22	0	8	4	0	8	2	0	2	0	0	0	0	0	0	13
21	4	2	2	4	10	0	0	0	0	0	0	0	0	1	14–16
21	4	2	2	4	9	0	0	1	0	0	1	0	0	0	17–19
21	4	2	2	4	9	1	0	0	0	0	0	0	1	0	20–22
21	4	2	2	4	8	2	0	0	0	0	0	1	0	0	23–26
21	4	1	4	3	9	1	0	0	0	0	0	0	1	0	27–30
21	4	1	4	3	9	0	0	1	0	0	1	0	0	0	31
21	4	1	4	3	8	1	1	0	0	0	1	0	0	0	32
21	4	1	4	3	8	2	0	0	0	0	0	1	0	0	33–34
21	4	1	4	3	9	0	0	0	1	1	0	0	0	0	35
21	4	1	4	3	10	0	0	0	0	0	0	0	0	1	36
21	4	1	4	3	8	1	0	0	2	0	0	0	0	0	37
21	4	0	6	2	8	1	0	1	0	1	0	0	0	0	38
21	4	0	6	2	8	1	0	0	2	0	0	0	0	0	39
21	4	0	6	2	8	0	1	1	1	0	0	0	0	0	40
21	4	0	6	2	8	1	1	0	0	0	1	0	0	0	41
21	4	0	6	2	8	2	0	0	0	0	0	1	0	0	42
21	3	4	1	4	8	2	0	0	0	0	0	1	0	0	43–47
21	3	4	1	4	9	0	1	0	0	0	0	1	0	0	48–50
21	3	4	1	4	9	1	0	0	0	0	0	0	1	0	51
21	3	4	1	4	7	3	0	0	0	0	1	0	0	0	52
21	3	3	3	3	8	1	1	0	0	0	1	0	0	0	53–63
21	3	3	3	3	8	2	0	0	0	0	0	1	0	0	64–75
21	3	3	3	3	9	1	0	0	0	0	0	0	1	0	76–85
21	3	3	3	3	8	1	0	1	0	1	0	0	0	0	86–89

Table A.2 – continued from previous page

$\|E\|$	$\|N_5\|$	$\|N_4\|$	$\|N_3\|$	$\|N_2\|$	$\|F_3\|$	$\|F_4\|$	$\|F_5\|$	$\|F_6\|$	$\|F_7\|$	$\|F_8\|$	$\|F_9\|$	$\|F_{10}\|$	$\|F_{11}\|$	$\|F_{12}\|$	ω
21	3	3	3	3	9	0	0	1	0	0	1	0	0	0	90–92
21	3	3	3	3	7	3	0	0	0	0	1	0	0	0	93–94
21	3	3	3	3	10	0	0	0	0	0	0	0	0	1	95–96
21	3	3	3	3	9	0	1	0	0	0	0	1	0	0	97–99
21	3	3	3	3	8	1	0	0	2	0	0	0	0	0	100–101
21	3	3	3	3	9	0	0	0	1	1	0	0	0	0	102–104
21	3	3	3	3	8	0	2	0	0	1	0	0	0	0	105
21	3	2	5	2	8	1	1	0	0	0	1	0	0	0	106–114
21	3	2	5	2	7	2	0	1	1	0	0	0	0	0	115–116
21	3	2	5	2	8	1	0	1	0	1	0	0	0	0	117–121
21	3	2	5	2	9	0	0	1	0	0	1	0	0	0	122–124
21	3	2	5	2	9	0	0	0	1	1	0	0	0	0	125–126
21	3	2	5	2	8	0	1	1	1	0	0	0	0	0	127
21	3	2	5	2	9	1	0	0	0	0	0	0	1	0	128–129
21	3	2	5	2	8	0	2	0	0	1	0	0	0	0	130
21	3	2	5	2	9	0	1	0	0	0	0	1	0	0	131–133
21	3	2	5	2	7	2	1	0	0	1	0	0	0	0	134–136
21	3	2	5	2	8	1	0	0	2	0	0	0	0	0	137–139
21	3	2	5	2	8	2	0	0	0	0	0	1	0	0	140
21	3	2	5	2	7	3	0	0	0	0	1	0	0	0	141
21	3	1	7	1	8	0	1	1	1	0	0	0	0	0	142–144
21	3	1	7	1	7	1	2	0	1	0	0	0	0	0	145
21	3	1	7	1	8	0	2	0	0	1	0	0	0	0	146
21	3	1	7	1	7	1	1	2	0	0	0	0	0	0	147
21	3	1	7	1	8	1	0	1	0	1	0	0	0	0	148
21	3	1	7	1	7	2	0	1	1	0	0	0	0	0	149
21	3	0	9	0	8	0	0	3	0	0	0	0	0	0	150–151
21	2	6	0	4	8	2	0	0	0	0	0	1	0	0	152–154
21	2	6	0	4	9	0	0	0	1	1	0	0	0	0	155
21	2	5	2	3	8	2	0	0	0	0	0	1	0	0	156–164
21	2	5	2	3	8	1	1	0	0	0	1	0	0	0	165–170
21	2	5	2	3	9	1	0	0	0	0	0	0	1	0	171–176
21	2	5	2	3	7	3	0	0	0	0	1	0	0	0	177–180
21	2	5	2	3	9	0	0	1	0	0	1	0	0	0	181–182
21	2	5	2	3	9	0	0	0	1	1	0	0	0	0	183–185
21	2	5	2	3	9	0	1	0	0	0	0	1	0	0	186–187
21	2	5	2	3	8	1	0	1	0	1	0	0	0	0	188–189
21	2	5	2	3	7	2	1	0	0	1	0	0	0	0	190
21	2	4	4	2	8	2	0	0	0	0	0	1	0	0	191–204
21	2	4	4	2	7	2	1	0	0	1	0	0	0	0	205–224
21	2	4	4	2	7	2	0	1	1	0	0	0	0	0	225–232
21	2	4	4	2	8	1	0	1	0	1	0	0	0	0	233–242
21	2	4	4	2	7	3	0	0	0	0	1	0	0	0	243–251
21	2	4	4	2	8	1	1	0	0	0	1	0	0	0	252–264
21	2	4	4	2	8	0	2	0	0	1	0	0	0	0	265–269
21	2	4	4	2	9	1	0	0	0	0	0	0	1	0	270–271
21	2	4	4	2	8	1	0	0	2	0	0	0	0	0	272–279
21	2	4	4	2	9	0	0	1	0	0	1	0	0	0	280–282
21	2	4	4	2	9	0	1	0	0	0	0	1	0	0	283–286
21	2	4	4	2	9	0	0	0	1	1	0	0	0	0	287–292

Table A.2 – continued from previous page

$\|E\|$	$\|N_5\|$	$\|N_4\|$	$\|N_3\|$	$\|N_2\|$	$\|F_3\|$	$\|F_4\|$	$\|F_5\|$	$\|F_6\|$	$\|F_7\|$	$\|F_8\|$	$\|F_9\|$	$\|F_{10}\|$	$\|F_{11}\|$	$\|F_{12}\|$	ω
21	2	4	4	2	6	3	0	2	0	0	0	0	0	0	293
21	2	4	4	2	8	0	1	1	1	0	0	0	0	0	294
21	2	4	4	2	6	4	0	0	0	1	0	0	0	0	295
21	2	3	6	1	7	1	2	0	1	0	0	0	0	0	296–306
21	2	3	6	1	7	2	0	1	1	0	0	0	0	0	307–313
21	2	3	6	1	8	1	0	0	2	0	0	0	0	0	314–317
21	2	3	6	1	8	0	1	1	1	0	0	0	0	0	318–322
21	2	3	6	1	6	3	1	0	1	0	0	0	0	0	323–324
21	2	3	6	1	7	2	1	0	0	1	0	0	0	0	325–329
21	2	3	6	1	7	1	1	2	0	0	0	0	0	0	330–334
21	2	3	6	1	8	0	2	0	0	1	0	0	0	0	335–337
21	2	3	6	1	6	2	2	1	0	0	0	0	0	0	338–340
21	2	3	6	1	8	1	0	1	0	1	0	0	0	0	341–344
21	2	3	6	1	8	1	1	0	0	0	1	0	0	0	345–347
21	2	3	6	1	8	0	0	3	0	0	0	0	0	0	348
21	2	3	6	1	9	0	0	0	1	1	0	0	0	0	349
21	2	3	6	1	6	3	0	2	0	0	0	0	0	0	350
21	2	3	6	1	9	1	0	0	0	0	0	0	1	0	351
21	2	2	8	0	6	2	2	1	0	0	0	0	0	0	352–353
21	2	2	8	0	7	1	1	2	0	0	0	0	0	0	354–355
21	2	2	8	0	6	1	4	0	0	0	0	0	0	0	356
21	2	2	8	0	8	0	2	0	0	1	0	0	0	0	357–358
21	2	2	8	0	8	2	0	0	0	0	0	1	0	0	359
21	2	2	8	0	8	1	0	1	0	1	0	0	0	0	360
21	2	2	8	0	6	3	0	2	0	0	0	0	0	0	361–362
21	2	2	8	0	8	0	1	1	1	0	0	0	0	0	363
21	1	7	1	3	8	1	1	0	0	0	1	0	0	0	364–365
21	1	7	1	3	7	3	0	0	0	0	1	0	0	0	366–367
21	1	7	1	3	7	2	1	0	0	1	0	0	0	0	368
21	1	7	1	3	7	2	0	1	1	0	0	0	0	0	369
21	1	7	1	3	8	2	0	0	0	0	0	1	0	0	370
21	1	7	1	3	8	1	0	1	0	1	0	0	0	0	371
21	1	6	3	2	7	2	1	0	0	1	0	0	0	0	372–390
21	1	6	3	2	6	4	0	0	0	1	0	0	0	0	391–395
21	1	6	3	2	7	3	0	0	0	0	1	0	0	0	396–401
21	1	6	3	2	7	2	0	1	1	0	0	0	0	0	402–408
21	1	6	3	2	8	1	1	0	0	0	1	0	0	0	409–414
21	1	6	3	2	8	1	0	1	0	1	0	0	0	0	415–419
21	1	6	3	2	8	2	0	0	0	0	0	1	0	0	420–421
21	1	6	3	2	6	3	0	2	0	0	0	0	0	0	422
21	1	6	3	2	8	0	1	1	1	0	0	0	0	0	423
21	1	6	3	2	9	0	0	1	0	0	1	0	0	0	424
21	1	6	3	2	8	1	0	0	2	0	0	0	0	0	425–426
21	1	5	5	1	7	1	2	0	1	0	0	0	0	0	427–442
21	1	5	5	1	7	2	0	1	1	0	0	0	0	0	443–454
21	1	5	5	1	7	2	1	0	0	1	0	0	0	0	455–471
21	1	5	5	1	7	0	3	1	0	0	0	0	0	0	472–474
21	1	5	5	1	7	1	1	2	0	0	0	0	0	0	475–481
21	1	5	5	1	6	3	0	2	0	0	0	0	0	0	482–485
21	1	5	5	1	5	4	1	1	0	0	0	0	0	0	486

Table A.2 – continued from previous page

$\lvert E\rvert$	$\lvert N_5\rvert$	$\lvert N_4\rvert$	$\lvert N_3\rvert$	$\lvert N_2\rvert$	$\lvert F_3\rvert$	$\lvert F_4\rvert$	$\lvert F_5\rvert$	$\lvert F_6\rvert$	$\lvert F_7\rvert$	$\lvert F_8\rvert$	$\lvert F_9\rvert$	$\lvert F_{10}\rvert$	$\lvert F_{11}\rvert$	$\lvert F_{12}\rvert$	ω
21	1	5	5	1	6	3	1	0	1	0	0	0	0	0	487–502
21	1	5	5	1	6	4	0	0	0	1	0	0	0	0	503–506
21	1	5	5	1	7	3	0	0	0	0	1	0	0	0	507–509
21	1	5	5	1	8	1	1	0	0	0	1	0	0	0	510–515
21	1	5	5	1	6	2	2	1	0	0	0	0	0	0	516–521
21	1	5	5	1	8	0	2	0	0	1	0	0	0	0	522–526
21	1	5	5	1	8	1	0	0	2	0	0	0	0	0	527–530
21	1	5	5	1	8	0	1	1	1	0	0	0	0	0	531–537
21	1	5	5	1	8	0	0	3	0	0	0	0	0	0	538
21	1	5	5	1	8	1	0	1	0	1	0	0	0	0	539–541
21	1	5	5	1	9	0	0	0	1	1	0	0	0	0	542
21	1	5	5	1	9	0	0	1	0	0	1	0	0	0	543
21	1	4	7	0	6	2	2	1	0	0	0	0	0	0	544–555
21	1	4	7	0	6	3	0	2	0	0	0	0	0	0	556
21	1	4	7	0	7	1	1	2	0	0	0	0	0	0	557–562
21	1	4	7	0	5	4	1	1	0	0	0	0	0	0	563–565
21	1	4	7	0	6	3	1	0	1	0	0	0	0	0	566–569
21	1	4	7	0	7	0	3	1	0	0	0	0	0	0	570–571
21	1	4	7	0	5	3	3	0	0	0	0	0	0	0	572–576
21	1	4	7	0	7	2	0	1	1	0	0	0	0	0	577–580
21	1	4	7	0	7	1	2	0	1	0	0	0	0	0	581–582
21	1	4	7	0	6	1	4	0	0	0	0	0	0	0	583–584
21	1	4	7	0	8	1	0	0	2	0	0	0	0	0	585
21	1	4	7	0	8	0	1	1	1	0	0	0	0	0	586
21	1	4	7	0	8	1	1	0	0	0	1	0	0	0	587–588
21	1	4	7	0	7	2	1	0	0	1	0	0	0	0	589–590
21	0	8	2	2	6	3	1	0	1	0	0	0	0	0	591
21	0	8	2	2	6	4	0	0	0	1	0	0	0	0	592–593
21	0	8	2	2	7	2	1	0	0	1	0	0	0	0	594–595
21	0	8	2	2	7	3	0	0	0	0	1	0	0	0	596
21	0	8	2	2	8	0	0	3	0	0	0	0	0	0	597
21	0	8	2	2	6	3	0	2	0	0	0	0	0	0	598
21	0	8	2	2	7	2	0	1	1	0	0	0	0	0	599
21	0	7	4	1	7	1	1	2	0	0	0	0	0	0	600–603
21	0	7	4	1	5	5	0	0	1	0	0	0	0	0	604–606
21	0	7	4	1	6	4	0	0	0	1	0	0	0	0	607–612
21	0	7	4	1	5	4	1	1	0	0	0	0	0	0	613–614
21	0	7	4	1	6	3	0	2	0	0	0	0	0	0	615
21	0	7	4	1	6	3	1	0	1	0	0	0	0	0	616–631
21	0	7	4	1	7	2	1	0	0	1	0	0	0	0	632–640
21	0	7	4	1	6	2	2	1	0	0	0	0	0	0	641–643
21	0	7	4	1	7	1	2	0	1	0	0	0	0	0	644–645
21	0	7	4	1	7	2	0	1	1	0	0	0	0	0	646–651
21	0	7	4	1	8	1	0	1	0	1	0	0	0	0	652
21	0	6	6	0	5	4	1	1	0	0	0	0	0	0	653–667
21	0	6	6	0	6	3	0	2	0	0	0	0	0	0	668–679
21	0	6	6	0	4	6	0	1	0	0	0	0	0	0	680–681
21	0	6	6	0	7	2	0	1	1	0	0	0	0	0	682
21	0	6	6	0	5	5	0	0	1	0	0	0	0	0	683–684
21	0	6	6	0	6	2	2	1	0	0	0	0	0	0	685–701

Table A.2 – continued from previous page

$\|E\|$	$\|N_5\|$	$\|N_4\|$	$\|N_3\|$	$\|N_2\|$	$\|F_3\|$	$\|F_4\|$	$\|F_5\|$	$\|F_6\|$	$\|F_7\|$	$\|F_8\|$	$\|F_9\|$	$\|F_{10}\|$	$\|F_{11}\|$	$\|F_{12}\|$	ω
21	0	6	6	0	6	3	1	0	1	0	0	0	0	0	702–703
21	0	6	6	0	7	1	1	2	0	0	0	0	0	0	704–710
21	0	6	6	0	6	1	4	0	0	0	0	0	0	0	711–713
21	0	6	6	0	7	0	3	1	0	0	0	0	0	0	714–716
21	0	6	6	0	7	2	1	0	0	1	0	0	0	0	717–718
21	0	6	6	0	4	5	2	0	0	0	0	0	0	0	719–724
21	0	6	6	0	5	3	3	0	0	0	0	0	0	0	725–731
21	0	6	6	0	8	0	0	3	0	0	0	0	0	0	732
21	0	6	6	0	6	4	0	0	0	1	0	0	0	0	733
21	0	6	6	0	8	0	2	0	0	1	0	0	0	0	734–735
21	0	6	6	0	7	1	2	0	1	0	0	0	0	0	736
21	0	6	6	0	8	1	0	0	2	0	0	0	0	0	737

Bibliography

[1] R. P. Feynman, Engineering and Science **23**, 22 (1960).

[2] G. Binnig and H. Rohrer, IBM Journal of Research and Development **30**, 355 (1986).

[3] D. M. Eigler and E. K. Schweizer, Nature **344**, 524 (1990).

[4] G. Binnig, C. F. Quate, and C. Gerber, Physical Review Letters **56**, 930 (1986).

[5] H. W. Kroto, J. R. Heath, S. C. O'Brien, R. F. Curl, and R. E. Smalley, Nature **318**, 162 (1985).

[6] S. Iijima, Nature **354**, 56 (1991).

[7] T. Kudernac, N. Ruangsupapichat, M. Parschau, B. Maciá, N. Katsonis, S. R. Harutyunyan, K.-H. Ernst, and B. L. Feringa, Nature **479**, 208 (2011).

[8] Y. Wu, Y.-m. Lin, A. A. Bol, K. A. Jenkins, F. Xia, D. B. Farmer, Y. Zhu, and P. Avouris, Nature **472**, 74 (2011).

[9] M. E. Vance, T. Kuiken, E. P. Vejerano, S. P. McGinnis, M. F. H. Jr, D. Rejeski, and M. S. Hull, Beilstein Journal of Nanotechnology **6**, 1769 (2015).

[10] F. A. Cotton, Inorganic Chemistry **3**, 1217 (1964).

[11] R. L. Johnston, *Atomic and molecular clusters*, Masters Series in Physics and Astronomy (Taylor & Francis, London, New York, 2002).

[12] D. J. Wales, *Energy Landscapes*, Cambridge Molecular Science (Cambridge University Press, Cambridge, 2003).

[13] K. Liu, J. D. Cruzan, and R. J. Saykally, Science **271**, 929 (1996).

[14] T. A. Beu and U. Buck, The Journal of Chemical Physics **114**, 7848 (2001).

[15] H. Takeuchi, The Journal of Physical Chemistry A **112**, 7492 (2008).

[16] X. Zhu and X. C. Zeng, The Journal of Chemical Physics **118**, 3558 (2003).

[17] G. Pacchioni and J. Koutecký, The Journal of Chemical Physics **84**, 3301 (1986).

[18] C. P. Massen and J. P. K. Doye, Physical Review E **75**, 037101 (2007).

[19] N. Arkus, V. N. Manoharan, and M. P. Brenner, Physical Review Letters **103**, 118303 (2009).

[20] C. J. Tsai and K. D. Jordan, The Journal of Physical Chemistry **97**, 11227 (1993).

[21] F. H. Stillinger and T. A. Weber, Science **225**, 983 (1984).

[22] F. Stillinger, Physical Review E **59**, 48 (1999).

[23] K. Schütte and B. L. van der Waerden, Mathematische Annalen **125**, 325 (1953).

[24] D. B. West, *Introduction to graph theory*, 2nd ed. (Prentice Hall, Upper Saddle River, 2001).

[25] V. K. Balakrishnan, *Schaum's outline of theory and problems of graph theory*, Schaum's Outline Series (McGraw-Hill, New York, 1997).

[26] L. Euler, Commentarii academiae scientiarum Petropolitanae **8**, 128 (1741).

[27] E. M. Patterson, "Some Aspects of Euler's Theorem", 1977.

[28] L. P. Cordella, P. Foggia, C. Sansone, and M. Vento, in Graph Based Representations in Pattern Recognition, edited by J.-M. Jolion and W. G. Kropatsch, Computing Supplement (1998), pp. 43–52.

[29] L. P. Cordella, P. Foggia, C. Sansone, and M. Vento, in 3rd IAPR-TC15 Workshop on Graph-based Representations in Pattern Recognition (2001), pp. 149–159.

[30] J. Siek, L.-Q. Lee, and A. Lumsdaine, *The Boost Graph Library: User Guide and Reference Manual* (Addison-Wesley Longman Publishing Co., Boston, 2002).

[31] F. Jensen, *Introduction to Computational Chemistry*, 2nd ed. (Wiley, Chichester, 2007).

[32] A. Szabo and N. S. Ostlund, *Modern Quantum Chemistry: Introduction to Advanced Electronic Structure Theory*, Dover Books on Chemistry Series (Dover Publications, Dover, 1996).

[33] W. Koch and M. C. Holthausen, *A Chemist's Guide to Density Functional Theory*, 2nd ed. (Wiley, Weinheim, 2001).

[34] M. Planck, Annalen der Physik **309**, 553 (1901).

[35] L. De Broglie, Annales de Physique **10**, 22 (1925).

[36] E. Schrödinger, Annalen der Physik **384**, 361 (1926).

[37] M. Born, Zeitschrift für Physik **37**, 863 (1926).

[38] M. Born, Zeitschrift für Physik **40**, 167 (1927).

[39] M. Born and R. Oppenheimer, Annalen der Physik **389**, 457 (1927).

[40] J. C. Slater, Physical Review **34**, 1293 (1929).

[41] V. Fock, Zeitschrift für Physik **61**, 126 (1930).

[42] C. C. J. Roothaan, Reviews of Modern Physics **23**, 69 (1951).

[43] G. G. Hall, Proceedings of the Royal Society A **205**, 541 (1951).

[44] P.-O. Löwdin, in *Advances in Chemical Physics*, Vol. 2, edited by I. Prigogine (John Wiley & Sons, New York, 1958), pp. 207–322.

[45] P. Hohenberg and W. Kohn, Physical Review **136**, B864 (1964).

[46] W. Kohn and L. J. Sham, Physical Review **140**, A1133 (1965).

[47] J. P. Perdew, K. Burke, and M. Ernzerhof, Physical Review Letters **77**, 3865 (1996).

[48] J. P. Perdew, K. Burke, and M. Ernzerhof, Physical Review Letters **78**, 1396 (1997).

[49] S. Grimme, J. Antony, S. Ehrlich, and H. Krieg, The Journal of Chemical Physics **132**, 154104 (2010).

[50] S. Grimme, S. Ehrlich, and L. Goerigk, Journal of Computational Chemistry **32**, 1456 (2011).

[51] D. Figgen, G. Rauhut, M. Dolg, and H. Stoll, Chemical Physics **311**, 227 (2005).

[52] P. E. Blöchl, Physical Review B **50**, 17953 (1994).

[53] R. Fletcher, *Practical methods of optimization*, 2nd ed. (Wiley, Chichester, New York, 1987).

[54] A. A. Goldstein and J. F. Price, Numerische Mathematik **10**, 184 (1967).

[55] K. Levenberg, Quarterly of Applied Mathematics **2**, 164 (1944).

[56] D. W. Marquardt, Journal of the Society for Industrial and Applied Mathematics **11**, 431 (1963).

[57] S. M. Goldfeld, R. E. Quandt, and H. F. Trotter, Econometrica **34**, 541 (1966).

[58] W. A. Murray, in *Numerical methods for unconstrained optimization*, edited by W. A. Murray (Academic Press, London, New York, 1972).

[59] M. D. Hebden, *An algorithm for minimization using exact second derivatives*, TP515 (Theoretical Physics Division, U.K.A.E.A. Research Group, Atomic Energy Research Establishment, Harwell, 1973).

[60] A. Fiacco and G. McCormick, *Nonlinear Programming*, Classics in Applied Mathematics (Society for Industrial and Applied Mathematics, Washington, 1990).

[61] C. G. Broyden, Mathematics of Computation **21**, 368 (1967).

[62] W. C. Davidon, The Computer Journal **10**, 406 (1968).

[63] W. Davidon, SIAM Journal on Optimization **1**, 1 (1991).

[64] R. Fletcher and M. J. D. Powell, The Computer Journal **6**, 163 (1963).

[65] C. G. Broyden, IMA Journal of Applied Mathematics **6**, 76 (1970).

[66] C. G. Broyden, IMA Journal of Applied Mathematics **6**, 222 (1970).

[67] R. Fletcher, The Computer Journal **13**, 317 (1970).

[68] D. Goldfarb, Mathematics of Computation **24**, 23 (1970).

[69] D. F. Shanno, Mathematics of Computation **24**, 647 (1970).

[70] P. Pulay, G. Fogarasi, F. Pang, and J. E. Boggs, Journal of the American Chemical Society **101**, 2550 (1979).

[71] P. Pulay and G. Fogarasi, The Journal of Chemical Physics **96**, 2856 (1992).

[72] G. Fogarasi, X. Zhou, P. W. Taylor, and P. Pulay, Journal of the American Chemical Society **114**, 8191 (1992).

[73] C. Peng, P. Y. Ayala, H. B. Schlegel, and M. J. Frisch, Journal of Computational Chemistry **17**, 49 (1996).

[74] R. Fletcher and C. M. Reeves, The Computer Journal **7**, 149 (1964).

[75] E. Polak, *Computational Methods in Optimization: A Unified Approach* (Academic Press, New York, London, 1971).

[76] C. J. Cerjan and W. H. Miller, The Journal of Chemical Physics **75**, 2800 (1981).

[77] D. J. Wales, J. P. K. Doye, M. A. Miller, P. N. Mortenson, and T. R. Walsh, in *Advances in Chemical Physics*, edited by I. Prigogine and S. A. Rice (John Wiley & Sons, Inc., 2000), pp. 1–111.

[78] S. Kirkpatrick, C. D. Gelatt, and M. P. Vecchi, Science **220**, 671 (1983).

[79] N. Metropolis, A. W. Rosenbluth, M. N. Rosenbluth, A. H. Teller, and E. Teller, The Journal of Chemical Physics **21**, 1087 (1953).

[80] D. J. Wales and J. P. K. Doye, The Journal of Physical Chemistry A **101**, 5111 (1997).

[81] J. P. K. Doye and D. J. Wales, Journal of the Chemical Society, Faraday Transactions **93**, 4233 (1997).

[82] J. P. K. Doye, D. J. Wales, W. Branz, and F. Calvo, Physical Review B **64**, 235409 (2001).

[83] Z. Li and H. A. Scheraga, Proceedings of the National Academy of Sciences of the United States of America **84**, 6611 (1987).

[84] D. E. Goldberg, *Genetic Algorithms in Search, Optimization and Machine Learning*, 1st (Addison-Wesley Longman Publishing, Boston, 1989).

[85] B. Hartke, The Journal of Physical Chemistry **97**, 9973 (1993).

[86] J. O. Hirschfelder, C. F. Curtiss, and R. B. Bird, *Molecular theory of gases and liquids*, Corr. print. with notes added, Structure of Matter Series (Wiley, New York, 1964).

[87] H. Kamerlingh Onnes, in *Proceedings of the section of sciences*, Vol. 4 (Johannes Müller, Amsterdam, 1902).

[88] H. D. Ursell, Mathematical Proceedings of the Cambridge Philosophical Society **23**, 685 (1927).

[89] B. M. Axilrod and E. Teller, The Journal of Chemical Physics **11**, 299 (1943).

[90] J. E. Jones, Proceedings of the Royal Society A **106**, 463 (1924).

[91] F. Simon and C. von Simson, Zeitschrift für Physik **25**, 160 (1924).

[92] A. Kratzer, Zeitschrift für Physik **3**, 289 (1920).

[93] G. Mie, Annalen der Physik **316**, 657 (1903).

[94] J. E. Jones and A. E. Ingham, Proceedings of the Royal Society A **107**, 636 (1925).

[95] S. C. Wang, Physikalische Zeitschrift **28**, 663 (1927).

[96] R. Eisenschitz and F. London, Zeitschrift für Physik **60**, 491 (1930).

[97] J. E. Lennard-Jones, Proceedings of the Royal Society A **129**, 598 (1930).

[98] H. R. Hassé, Mathematical Proceedings of the Cambridge Philosophical Society **27**, 66 (1931).

[99] J. C. Slater and J. G. Kirkwood, Physical Review **37**, 682 (1931).

[100] F. London, Zeitschrift für Physik **63**, 245 (1930).

[101] J. E. Jones, Proceedings of the Royal Society A **107**, 157 (1925).

[102] J. E. Lennard-Jones and P. A. Taylor, Proceedings of the Royal Society A **109**, 476 (1925).

[103] J. E. Lennard-Jones and W. R. Cook, Proceedings of the Royal Society A **112**, 214 (1926).

[104] J. E. Lennard-Jones and W. R. Cook, Proceedings of the Royal Society A **115**, 334 (1927).

[105] J. E. Lennard-Jones, Proceedings of the Physical Society **43**, 461 (1931).

[106] P. Schwerdtfeger, N. Gaston, R. P. Krawczyk, R. Tonner, and G. E. Moyano, Physical Review B **73**, 064112 (2006).

[107] P. Jerabek, O. Smits, E. Pahl, and P. Schwerdtfeger, Molecular Physics **116**, 1 (2017).

[108] S. Kakar, O. Björneholm, J. Weigelt, A. R. B. de Castro, L. Tröger, R. Frahm, T. Möller, A. Knop, and E. Rühl, Physical Review Letters **78**, 1675 (1997).

[109] K. D. Ball and R. S. Berry, The Journal of Chemical Physics **111**, 2060 (1999).

[110] J. P. K. Doye and D. J. Wales, Journal of Chemical Physics **116**, 3777 (2002).

[111] R. J. Baxter, The Journal of Chemical Physics **49**, 2770 (1968).

[112] N. Arkus, V. Manoharan, and M. Brenner, SIAM Journal on Discrete Mathematics **25**, 1860 (2011).

[113] J. C. Maxwell, The London, Edinburgh, and Dublin Philosophical Magazine and Journal of Science **27**, 294 (1864).

[114] M. Holmes-Cerfon, SIAM Review **58**, 229 (2016).

[115] R. S. Hoy, J. Harwayne-Gidansky, and C. S. O'Hern, Physical Review E **85**, 051403 (2012).

[116] R. S. Hoy, Physical Review E **91**, 012303 (2015).

[117] M. Lindner, *Libconfig, A Library For Processing Structured Configuration Files*, `https://github.com/hyperrealm/libconfig`.

[118] D. E. King, Journal of Machine Learning Research **10**, 1755 (2009).

[119] B. Stroustrup, *The C++ programming language*, Special ed. (Addison-Wesley, Reading, Mass, 2000).

[120] I. Dokmanic, R. Parhizkar, J. Ranieri, and M. Vetterli, IEEE Signal Processing Magazine **32**, 12 (2015).

[121] L. P. Cordella, P. Foggia, C. Sansone, and M. Vento, IEEE Transactions on Pattern Analysis and Machine Intelligence **26**, 1367 (2004).

[122] P. Schwerdtfeger, L. Wirz, and J. Avery, Journal of Computational Chemistry **34**, 1508 (2013).

[123] L. Trombach, S. Rampino, L.-S. Wang, and P. Schwerdtfeger, Chemistry–A European Journal **22**, 8823 (2016).

[124] M. Haruta, T. Kobayashi, H. Sano, and N. Yamada, Chemistry Letters **16**, 405 (1987).

[125] M. Haruta, The Chemical Record **3**, 75 (2003).

[126] T. Ishida and M. Haruta, Angewandte Chemie International Edition **46**, 7154 (2007).

[127] M. Haruta, ChemPhysChem **8**, 1911 (2007).

[128] P. Schwerdtfeger, Angewandte Chemie International Edition **42**, 1892 (2003).

[129] H. Häkkinen, Chemical Society Reviews **37**, 1847 (2008).

[130] P. Maity, S. Xie, M. Yamauchi, and T. Tsukuda, Nanoscale **4**, 4027 (2012).

[131] Y. Zhang, X. Cui, F. Shi, and Y. Deng, Chemical Reviews **112**, 2467 (2012).

[132] J. Gong, Chemical Reviews **112**, 2987 (2012).

[133] M.-S. Miao, J. A. Kurzman, N. Mammen, S. Narasimhan, and R. Seshadri, Inorganic Chemistry **51**, 7569 (2012).

[134] K. Park, L. F. Drummy, R. C. Wadams, H. Koerner, D. Nepal, L. Fabris, and R. A. Vaia, Chemistry of Materials **25**, 555 (2013).

[135] Y. Chen, C. Zeng, C. Liu, K. Kirschbaum, C. Gayathri, R. R. Gil, N. L. Rosi, and R. Jin, Journal of the American Chemical Society **137**, 10076 (2015).

[136] G. Bravo-Pérez, I. L. Garzón, and O. Novaro, Journal of Molecular Structure: THEOCHEM **493**, 225 (1999).

[137] H. Häkkinen and U. Landman, Physical Review B **62**, 2287 (2000).

[138] H. Häkkinen, M. Moseler, and U. Landman, Physical Review Letters **89**, 033401 (2002).

[139] P. Pyykkö, Chemical Reviews **88**, 563 (1988).

[140] P. Schwerdtfeger, Heteroatom Chemistry **13**, 578 (2002).

[141] P. Pyykkö, Angewandte Chemie International Edition **43**, 4412 (2004).

[142] P. Pyykkö, Nature Nanotechnolgy **2**, 273 (2007).

[143] W. Huang, M. Ji, C.-D. Dong, X. Gu, L.-M. Wang, X. G. Gong, and L.-S. Wang, ACS Nano **2**, 897 (2008).

[144] P. Schwerdtfeger and M. Lein, in *Gold Chemistry* (Wiley-VCH, Weinheim, 2009), pp. 183–247.

[145] P. Pyykkö, Annual Review of Physical Chemistry **63**, 45 (2012).

[146] H.-Y. Zhao, H. Ning, J. Wang, X.-J. Su, X.-G. Guo, and Y. Liu, Physics Letters A **374**, 1033 (2010).

[147] A. S. Barnard, Reports on Progress in Physics **73**, 086502 (2010).

[148] D. Tian, J. Li, Y. Zhao, J. Zhao, and X. Guo, Computational Materials Science **50**, 2359 (2011).

[149] M. P. Johansson, A. Lechtken, D. Schooss, M. M. Kappes, and F. Furche, Physical Review A **77**, 1 (2008).

[150] W. Fa, C. Luo, and J. Dong, Physical Review B **72**, 205428 (2005).

[151] B. Assadollahzadeh and P. Schwerdtfeger, The Journal of Chemical Physics **131**, 064306 (2009).

[152] L.-M. Wang, R. Pal, W. Huang, X. C. Zeng, and L.-S. Wang, The Journal of Chemical Physics **132**, 114306, 114306 (2010).

[153] B. Wang, M. Liu, Y. Wang, and X. Chen, The Journal of Physical Chemistry C **115**, 11374 (2011).

[154] A. S. Barnard, Accounts of Chemical Research **45**, 1688 (2012).

[155] D. A. Götz, R. Schäfer, and P. Schwerdtfeger, Journal of Computational Chemistry **34**, 1975 (2013).

[156] A. Kinaci, B. Narayanan, F. G. Sen, M. J. Davis, S. K. Gray, S. K. R. S. Sankaranarayanan, and M. K. Y. Chan, Scientific Reports **6**, 34974 (2016).

[157] M. P. Johansson, D. Sundholm, and J. Vaara, Angewandte Chemie International Edition **43**, 2678 (2004).

[158] A. J. Karttunen, M. Linnolahti, T. A. Pakkanen, and P. Pyykkö, Chemical Communications, 465 (2008).

[159] E. M. Fernández, M. B. Torres, and L. C. Balbás, in Recent Advances in the Theory of Chemical and Physical Systems, edited by J.-P. Julien, J. Maruani, D. Mayou, S. Wilson, and G. Delgado-Barrio (2006), pp. 407–432.

[160] X. Gu, M. Ji, S. H. Wei, and X. G. Gong, Physical Review B **70**, 205401 (2004).

[161] E. M. Fernández, J. M. Soler, and L. C. Balbás, Physical Review B **73**, 235433 (2006).

[162] W. Fa and J. Dong, The Journal of Chemical Physics **124**, 114310, 114310 (2006).

[163] W. Fa, J. Zhou, C. Luo, and J. Dong, Physical Review B **73**, 085405 (2006).

[164] G. Chen, Q. Wang, Q. Sun, Y. Kawazoe, and P. Jena, The Journal of Chemical Physics **132**, 194306 (2010).

[165] H. S. De, S. Krishnamurty, and S. Pal, Catalysis Today **198**, Special Issue dedicated to Paul Ratnasamy on the occasion of his 70th birthday, 106 (2012).

[166] H. Ning, J. Wang, Q.-M. Ma, H.-Y. Han, and Y. Liu, Journal of Physics and Chemistry of Solids **75**, 696 (2014).

[167] K. Joshi and S. Krishnamurty, Molecular Physics **113**, 2980 (2015).

[168] J. Autschbach, B. A. Hess, M. P. Johansson, J. Neugebauer, M. Patzschke, P. Pyykkö, M. Reiher, and D. Sundholm, Physical Chemistry Chemical Physics **6**, 11 (2004).

[169] H.-J. Zhai, J. Li, and L.-S. Wang, The Journal of Chemical Physics **121**, 8369 (2004).

[170] Y. Gao, S. Bulusu, and X. C. Zeng, Journal of the American Chemical Society **127**, 15680 (2005).

[171] L.-M. Wang, S. Bulusu, W. Huang, R. Pal, L.-S. Wang, and X. C. Zeng, Journal of the American Chemical Society **129**, 15136 (2007).

[172] L.-M. Wang, S. Bulusu, H.-J. Zhai, X.-C. Zeng, and L.-S. Wang, Angewandte Chemie International Edition **46**, 2915 (2007).

[173] W. Fa and J. Dong, The Journal of Chemical Physics **128**, 144307 (2008).

[174] A. Muñoz-Castro, The Journal of Physical Chemistry Letters **4**, 3363 (2013).

[175] D. Manna, T. Jayasekharan, and T. K. Ghanty, The Journal of Physical Chemistry C **117**, 18777 (2013).

[176] C. Tang, W. Zhu, A. Zhang, K. Zhang, and M. Liu, Computational and Theoretical Chemistry **1018**, 1 (2013).

[177] M. Ji, X. Gu, X. Li, X. Gong, J. Li, and L.-S. Wang, Angewandte Chemie International Edition **44**, 7119 (2005).

[178] S. Bulusu, X. Li, L.-S. Wang, and X. C. Zeng, Proceedings of the National Academy of Sciences of the United States of America **103**, 8326 (2006).

[179] F. Cataldo, A. Graovac, and O. Ori, *The mathematics and topology of fullerenes* (Springer, Berlin, 2011).

[180] P. Schwerdtfeger, L. N. Wirz, and J. Avery, Wiley Interdisciplinary Reviews: Computational Molecular Science **5**, 96 (2015).

[181] P. W. Fowler and D. E. Manolopoulos, *An Atlas of Fullerenes*, 2nd ed. (Dover Publications, Mineolal, New York, 2006).

[182] M. Goldberg, Tohoku Mathematical Journal, First Series **43**, 104 (1937).

[183] H. S. M. Coxeter, in *A Spectrum of mathematics - Essays Presented to H. G. Forder*, edited by J. C. Butcher (Oxford University Press, Oxford, 1971), pp. 98–107.

[184] Y. Kondo and K. Takayanagi, Science **289**, 606 (2000).

[185] M. Fujita, R. Saito, G. Dresselhaus, and M. S. Dresselhaus, Physical Review B **45**, 13834 (1992).

[186] B. Grünbaum and T. S. Motzkin, Canadian Journal of Mathematics **15**, 744 (1963).

[187] W. P. Thurston, Geometry and Topology Monographs **1**, 511 (1998).

[188] L. N. Wirz, R. Tonner, J. Avery, and P. Schwerdtfeger, Journal of Chemical Information and Modeling **54**, 121 (2014).

[189] H. W. Kroto, Nature **329**, 529 (1987).

[190] M. Dutour and M. Deza, The Electronic Journal of Combinatorics **11**, 20 (2004).

[191] H.-S. Nam, N. M. Hwang, B. D. Yu, and J.-K. Yoon, Physical Review Letters **89**, 275502 (2002).

[192] A. L. Mackay, Acta Crystallographica **15**, 916 (1962).

[193] K. H. Kuo, Structural Chemistry **13**, 221 (2002).

[194] L. N. Wirz, P. Schwerdtfeger, and J. E. Avery, Fullerenes, Nanotubes and Carbon Nanostructures **26**, 607 (2018).

[195] L. N. Wirz, R. Tonner, A. Hermann, R. Sure, and P. Schwerdtfeger, Journal of Computational Chemistry **37**, 10 (2015).

[196] G. Brinkmann, K. Coolsaet, J. Goedgebeur, and H. Mélot, Discrete Applied Mathematics **161**, 311 (2013).

[197] W. R. Wadt and P. J. Hay, The Journal of Chemical Physics **82**, 284 (1985).

[198] L. A. Mancera and D. M. Benoit, Computational and Theoretical Chemistry **1067**, 24 (2015).

[199] K. A. Peterson and C. Puzzarini, Theoretical Chemistry Accounts **114**, 283 (2005).

[200] D. Schooss, P. Weis, O. Hampe, and M. M. Kappes, Philosophical Transactions of the Royal Society A **368**, 1211 (2010).

[201] A. Lechtken, C. Neiss, M. M. Kappes, and D. Schooss, Physical Chemistry Chemical Physics **11**, 4344 (2009).

[202] F. Weigend and R. Ahlrichs, Physical Chemistry Chemical Physics **7**, 3297 (2005).

[203] *TURBOMOLE V7.0 2015*, a development of University of Karlsruhe and Forschungszentrum Karlsruhe GmbH, 1989-2007, TURBOMOLE GmbH, since 2007, `http://www.turbomole.com`.

[204] G. Kresse and J. Furthmüller, Computational Materials Science **6**, 15 (1996).

[205] G. Kresse and D. Joubert, Physical Review B **59**, 1758 (1999).

[206] P. Pyykkö and N. Runeberg, Angewandte Chemie International Edition **41**, 2174 (2002).

[207] M. Laupp and J. Strähle, Angewandte Chemie International Edition **33**, 207 (1994).

[208] A. F. Jalbout, F. F. Contreras-Torres, L. A. Pérez, and I. L. Garzón, The Journal of Physical Chemistry A **112**, 353 (2008).

[209] N. Takeuchi, C. T. Chan, and K. M. Ho, Physical Review B **40**, 1565 (1989).

[210] L. Trombach, R. S. Hoy, D. J. Wales, and P. Schwerdtfeger, Physical Review E **97**, 043309 (2018).

[211] T. Martin, Physics Reports **273**, 199 (1996).

[212] J. P. K. Doye and D. J. Wales, Science **271**, 484 (1996).

[213] E. Vlieg, M. Deij, D. Kaminski, H. Meekes, and W. van Enckevort, Faraday Discussions **136**, 57 (2007).

[214] G. Meng, N. Arkus, M. P. Brenner, and V. N. Manoharan, Science **327**, 560 (2010).

[215] C. R. A. Catlow, S. T. Bromley, S. Hamad, M. Mora-Fonz, A. A. Sokol, and S. M. Woodley, Physical Chemistry Chemical Physics **12**, 786 (2010).

[216] S. Karthika, T. K. Radhakrishnan, and P. Kalaichelvi, Crystal Growth & Design **16**, 6663 (2016).

[217] M. Holmes-Cerfon, Annual Review of Condensed Matter Physics **8**, 77 (2017).

[218] P. R. Rowland, Discussions of the Faraday Society **5**, 364 (1949).

[219] A. R. Oganov and C. W. Glass, The Journal of Chemical Physics **124**, 244704 (2006).

[220] D. J. Wales, ChemPhysChem **11**, 2491 (2010).

[221] A. R. Oganov, A. O. Lyakhov, and M. Valle, Accounts of Chemical Research **44**, 227 (2011).

[222] F. Calvo, J. P. K. Doye, and D. J. Wales, Nanoscale **4**, 1085 (2012).

[223] D. J. Wales, The Journal of Chemical Physics **142**, 130901 (2015).

[224] N. V. Krainyukova, R. E. Boltnev, E. P. Bernard, V. V. Khmelenko, D. M. Lee, and V. Kiryukhin, Physical Review Letters **109**, 245505 (2012).

[225] N. V. Krainyukova, The European Physical Journal D **43**, 45 (2007).

[226] K. Bezdek and S. Reid, Journal of Geometry **104**, 57 (2013).

[227] P. Erdős, American Mathematical Monthly **53**, 248 (1946).

[228] Y. Forman and M. Cameron, Journal of Statistical Physics **168**, 408 (2017).

[229] S. Heiles and R. L. Johnston, International Journal of Quantum Chemistry **113**, 2091 (2013).

[230] J. P. K. Doye, M. A. Miller, and D. J. Wales, The Journal of Chemical Physics **111**, 8417 (1999).

[231] P. A. Braier, R. S. Berry, and D. J. Wales, The Journal of Chemical Physics **93**, 8745 (1990).

[232] D. J. Wales, Science **293**, 2067 (2001).

[233] *Pele: Python energy landscape explorer*, pele-python, 2017, `https://github.com/pele-python/pele`.

[234] D. J. Wales and H. A. Scheraga, Science **285**, 1368 (1999).

[235] D. C. Wallace, Physical Review E **56**, 4179 (1997).

[236] F. Sciortino, W. Kob, and P. Tartaglia, Physical Review Letters **83**, 3214 (1999).

[237] M. R. Hoare and P. Pal, Advances in Physics **24**, 645 (1975).

[238] M. R. Hoare and J. McInnes, Faraday Discussions of the Chemical Society **61**, 12 (1976).

[239] M. R. Hoare, in *Advances in Chemical Physics*, Vol. 40 (John Wiley & Sons, New York, Chichester, Brisbane, Toronto, 2007), pp. 49–135.

[240] P. Schwerdtfeger, R. Tonner, G. E. Moyano, and E. Pahl, Angewandte Chemie International Edition **55**, 12200 (2016).

[241] L. Trombach and P. Schwerdtfeger, Physical Review E **98**, 033311 (2018).

[242] P. M. L. Tammes, "On the origin of number and arrangement of the places of exit on the surface of pollen-grains" (Groningen, 1930).

[243] R. M. Robinson, Mathematische Annalen **144**, 17 (1961).

[244] O. R. Musin and A. S. Tarasov, Experimental Mathematics **24**, 460 (2015).

[245] F. Pfender and G. M. Ziegler, Notices of the AMS **51**, 873 (2004).

[246] O. Musin, Annals of Mathematics **168**, 1 (2008).

[247] J. H. Conway and N. J. A. Sloane, *Sphere Packings, Lattices and Groups*, red. by S. S. Chern, B. Eckmann, P. de la Harpe, H. Hironaka, F. Hirzebruch, N. Hitchin, L. Hörmander, M.-A. Knus, A. Kupiainen, J. Lannes, G. Lebeau, M. Ratner, D. Serre, Y. G. Sinai, N. J. A. Sloane, J. Tits, M. Waldschmidt, S. Watanabe, M. Berger, J. Coates, and S. R. S. Varadhan, Vol. 290, Grundlehren Der Mathematischen Wissenschaften (Springer New York, New York, 1999).

[248] O. R. Musin, Acta Mathematica Hungarica **155**, 184 (2018).

[249] H. D. Mittelmann and F. Vallentin, Experimental Mathematics **19**, 175 (2010).

[250] R. Kusner, W. Kusner, J. C. Lagarias, and S. Shlosman, in *New Trends in Intuitive Geometry*, edited by G. Ambrus, I. Bárány, K. J. Böröczky, G. Fejes Tóth, and J. Pach, Bolyai Society Mathematical Studies (Springer Berlin Heidelberg, Berlin, Heidelberg, 2018), pp. 219–277.

[251] D. J. Wales and S. Ulker, Physical Review B **74**, 212101 (2006).

[252] D. J. Wales, H. McKay, and E. L. Altschuler, Physical Review B **79**, 224115 (2009).

[253] Y. Levin, Physica A: Statistical Mechanics and its Applications **287**, 100 (2000).

[254] P. N. Pusey, E. Zaccarelli, C. Valeriani, E. Sanz, W. C. K. Poon, and M. E. Cates, Philosophical Transactions of the Royal Society of London A: Mathematical, Physical and Engineering Sciences **367**, 4993 (2009).

[255] C. Phillips, A. Jankowski, M. Marval, and S. Glotzer, Physical Review E **86**, 041124 (2012).

[256] N. Kaltsoyannis, Angewandte Chemie International Edition **56**, 7066 (2017).

[257] T. D. Della and C. H. Suresh, Physical Chemistry Chemical Physics **18**, 14588 (2016).

[258] Á. González, Mathematical Geosciences **42**, 49 (2010).

[259] B. Keinert, M. Innmann, M. Sänger, and M. Stamminger, ACM Transactions on Graphics **34**, 193:1 (2015).

[260] K. Schütte and B. L. van der Waerden, Mathematische Annalen **123**, 96 (1951).

[261] E. Steinitz, in *Encyklopädie der mathematischen Wissenschaften mit Einschluss ihrer Anwendungen*, Vol. 3 (Teubner, Leipzig, 1916), pp. 1–101.

[262] J. P. K. Doye, D. J. Wales, and R. S. Berry, The Journal of Chemical Physics **103**, 4234 (1995).

[263] D. J. Wales and J. P. K. Doye, in *Large Clusters of Atoms and Molecules* (Springer Netherlands, Dordrecht, 1996), pp. 241–279.

[264] J. P. K. Doye and D. J. Wales, Journal of Physics B: Atomic, Molecular and Optical Physics **29**, 4859 (1996).

MASSEY UNIVERSITY
GRADUATE RESEARCH SCHOOL

STATEMENT OF CONTRIBUTION TO DOCTORAL THESIS CONTAINING PUBLICATIONS

(To appear at the end of each thesis chapter/section/appendix submitted as an article/paper or collected as an appendix at the end of the thesis)

We, the candidate and the candidate's Principal Supervisor, certify that all co-authors have consented to their work being included in the thesis and they have accepted the candidate's contribution as indicated below in the *Statement of Originality*.

Name of Candidate: Lukas Trombach

Name/Title of Principal Supervisor: Prof. Dr. Peter Schwerdtfeger

Name of Published Research Output and full reference:

L. Trombach, S. Rampino, L.-S. Wang, P. Schwerdtfeger, "Hollow Gold Cages and Their Topological Relationship to Dual Fullerenes", Chemistry - A European Journal 22, 8823 (2016)

In which Chapter is the Published Work: 7

Please indicate either:

- The percentage of the Published Work that was contributed by the candidate 80%

  and / or
- Describe the contribution that the candidate has made to the Published Work:

Lukas Trombach Digitally signed by Lukas Trombach Date: 2019.01.08 10:31:50 +13'00'

Candidate's Signature

08/01/2019

Date

PeterSchwerdtfeger Digitally signed by PeterSchwerdtfeger Date: 2019.01.08 10:57:55 +13'00'

Principal Supervisor's signature

08/01/2019

Date

MASSEY UNIVERSITY
GRADUATE RESEARCH SCHOOL

STATEMENT OF CONTRIBUTION TO DOCTORAL THESIS CONTAINING PUBLICATIONS

(To appear at the end of each thesis chapter/section/appendix submitted as an article/paper or collected as an appendix at the end of the thesis)

We, the candidate and the candidate's Principal Supervisor, certify that all co-authors have consented to their work being included in the thesis and they have accepted the candidate's contribution as indicated below in the *Statement of Originality*.

Name of Candidate: Lukas Trombach

Name/Title of Principal Supervisor: Prof. Dr. Peter Schwerdtfeger

Name of Published Research Output and full reference:

L. Trombach, R. S. Hoy, D. J. Wales, P. Schwerdtfeger, "From sticky-hard-sphere to Lennard-Jones-type clusters", Physical Review E 97, 043309 (2018)

In which Chapter is the Published Work: 8,9

Please indicate either:

- The percentage of the Published Work that was contributed by the candidate 80%
  and / or
- Describe the contribution that the candidate has made to the Published Work:

Lukas Trombach Digitally signed by Lukas Trombach Date: 2019.01.08 10:36:09 +13'00'

Candidate's Signature

08/01/2019

Date

PeterSchwerdtfeger Digitally signed by PeterSchwerdtfeger Date: 2019.01.08 10:58:52 +13'00'

Principal Supervisor's signature

08/01/2019

Date

MASSEY UNIVERSITY
GRADUATE RESEARCH SCHOOL

STATEMENT OF CONTRIBUTION TO DOCTORAL THESIS CONTAINING PUBLICATIONS

(To appear at the end of each thesis chapter/section/appendix submitted as an article/paper or collected as an appendix at the end of the thesis)

We, the candidate and the candidate's Principal Supervisor, certify that all co-authors have consented to their work being included in the thesis and they have accepted the candidate's contribution as indicated below in the *Statement of Originality*.

Name of Candidate: Lukas Trombach

Name/Title of Principal Supervisor: Prof. Dr. Peter Schwerdtfeger

Name of Published Research Output and full reference:

L. Trombach, P. Schwerdtfeger, "Gregory-Newton problem for kissing sticky spheres", Physical Review E 98, 033311 (2018)

In which Chapter is the Published Work: 9

Please indicate either:

- The percentage of the Published Work that was contributed by the candidate 80%
  and / or
- Describe the contribution that the candidate has made to the Published Work:

Lukas Trombach Digitally signed by Lukas Trombach Date: 2019.01.08 10:38:41 +13'00'

Candidate's Signature

08/01/2019

Date

PeterSchwerdtfeger Digitally signed by PeterSchwerdtfeger Date: 2019.01.08 10:59:20 +13'00'

Principal Supervisor's signature

08/01/2019

Date